Stem Cells International

Stem Cells in Large Animal Models of Retinal and Neurological Disease

Guest Editors: Henry Klassen, Budd A. Tucker, Chee G. Liew, Morten La Cour, and Heuy-Ching Wang

Stem Cells in Large Animal Models of Retinal and Neurological Disease

Stem Cells International

Stem Cells in Large Animal Models of Retinal and Neurological Disease

Guest Editors: Henry Klassen, Budd A. Tucker,
Chee G. Liew, Morten la Cour, and Heuy-Ching Wang

Editorial Board

Contents

Hindawi Publishing Corporation
Stem Cells International
Volume 2012, Article ID 460504, 2 pages
doi:10.1155/2012/460504

Editorial

Stem Cells in Large Animal Models of Retinal and Neurological Disease

Henry Klassen,[1] Budd A. Tucker,[2] Chee G. Liew,[3] Morten La Cour,[4] and Heuy-Ching Wang[5]

[1] *Gavin Herbert Eye Institute and Stem Cell Research Center, University of California-Irvine, Irvine, CA 92697, USA*
[2] *Department of Ophthalmology and Visual Science, University of Iowa, Iowa City, IA 52242, USA*
[3] *Stem Cell Core, University of California-Riverside, Riverside, CA 92521, USA*
[4] *Department of Ophthalmology, Glostrup Hospital, University of Copenhagen, 2600 Glostrup, Denmark*
[5] *Ocular Trauma Division, U.S. Army Institute of Surgical Research, Fort Sam Houston, TX 78234, USA*

Correspondence should be addressed to Henry Klassen, hklassen@uci.edu

Received 13 February 2012; Accepted 13 February 2012

The mammalian central nervous system (CNS) is notable in terms of complexity and sophistication, but also for a very limited regenerative ability in the face of injury and disease. While it is not uncommon to find remarkable regenerative capabilities in the CNS tissues of fish and amphibian species, similar findings are much more limited in reptiles and quite difficult to replicate in mammals. One method used to circumvent this inherent limitation has been the use of fetal tissue transplantation which has resulted in evidence of graft survival, integration and functional repair in a number of rat [1, 2] and also mouse models. Nevertheless, the use of fetal tissue grafts is generally impractical as a source of donor material and of relatively limited utility in the adult human eye [3]. Stem cell transplantation has more recently emerged as a potential treatment modality that offers even greater potential for tissue integration, while also being more scalable for widespread therapeutic use.

Much progress has been made in the development of stem cell transplantation in rodent models of retinal disease [4–6]; however, limitations to rodent-based research include nonhuman features such as small eyes, rod-dominated vision, the absence of a macula or visual streak, and short life span. As stem cell research moves toward clinical application in ophthalmology, the value of modeling and refining transplantation procedures in larger mammals becomes increasingly evident.

This special issue includes 10 papers that focus on stem and progenitor cells from the central nervous system (both brain and retina) of nonrodent mammals, or cells modified to resemble such cells (e.g., iPS cells), together with the development of useful allogeneic donors and recipients. Although any species is of potential interest, here there is a particular emphasis on pig and cat following on from previous work conducted in these species.

The reports included in this special issue represent an interesting range of animals, including a nonhuman primate, as well as experimental approaches, including genetic modification and tissue engineering. Collectively, they serve to extend both the scope and horizon of stem cell research in nonrodent mammalian species. Despite the challenges of such work, it can be hoped that further efforts will be made to harness the potential of this area for translation of basic research findings into the clinical domain, not only as preclinical models for human treatment, but also as bone fide veterinary applications.

Henry Klassen
Budd A. Tucker
Chee G. Liew
Morten La Cour
Heuy-Ching Wang

References

[1] S. B. Dunnett, A. Björklund, U. Stenevi, and S. D. Iversen, "CNS transplantation: structural and functional recovery from brain damage," *Progress in Brain Research*, vol. 55, pp. 431–443, 1982.
[2] H. Klassen and R. Lund, "Retinal transplants can drive a pupillary reflex in host rat brains," *Proceedings of the National*

Academy of Sciences of the United States of America, vol. 84, no. 19, pp. 6958–6960, 1987.

[3] N. D. Radtke, R. B. Aramant, H. M. Petry, P. T. Green, D. J. Pidwell, and M. J. Seiler, "Vision improvement in retinal degeneration patients by implantation of retina together with retinal pigment epithelium," *American Journal of Ophthalmology*, vol. 146, no. 2, pp. 172–182, 2008.

[4] M. Young, J. Ray, S. Whiteley, H. Klassen, and F. Gage, "Neuronal differentiation and morphological integration of hippocampal progenitor cells transplanted to the retina of immature and mature dystrophic rats," *Molecular and Cellular Neurosciences*, vol. 16, no. 3, pp. 197–205, 2000.

[5] H. Klassen, T.-F. Ng, Y. Kurimoto et al., "Multipotent retinal progenitors express developmental markers, differentiate into retinal neurons, and preserve light-mediated behavior," *Investigative Ophthalmology and Visual Science*, vol. 45, no. 11, pp. 4167–4173, 2004.

[6] H. Klassen, D. Sakaguchi, and M. Young, "Stem cells and retinal repair," *Progress in Retinal and Eye Research*, vol. 23, no. 2, pp. 149–181, 2004.

Hindawi Publishing Corporation
Stem Cells International
Volume 2012, Article ID 108340, 10 pages
doi:10.1155/2012/108340

Research Article

Feline Neural Progenitor Cells I: Long-Term Expansion under Defined Culture Conditions

Jing Yang,[1] Jinmei Wang,[1] Ping Gu,[1,2] X. Joann You,[1] and Henry Klassen[1]

[1] *Department of Ophthalmology, Ophthalmology Research Laboratories, The Gavin Herbert Eye Institute, University of California, Irvine, CA 92697, USA*
[2] *Department of Ophthalmology, Shanghai Ninth People's Hospital, School of Medicine, Shanghai Jiaotong University, Shanghai 200011, China*

Correspondence should be addressed to Henry Klassen, hklassen@uci.edu

Received 30 September 2011; Accepted 3 February 2012

Academic Editor: Heuy-Ching Hetty Wang

Neural progenitor cells (NPCs) of feline origin (cNPCs) have demonstrated utility in transplantation experiments, yet are difficult to grow in culture beyond the 1 month time frame. Here we use an enriched, serum-free base medium (Ultraculture) and report the successful long-term propagation of these cells. Primary cultures were derived from fetal brain tissue and passaged in DMEM/F12-based or Ultraculture-based proliferation media, both in the presence of EGF + bFGF. Cells in standard DMEM/F12-based medium ceased to proliferate by 1-month, whereas the cells in the Ultraculture-based medium continued to grow for at least 5 months (end of study) with no evidence of senescence. The Ultraculture-based cultures expressed lower levels of progenitor and lineage-associated markers under proliferation conditions but retained multipotency as evidenced by the ability to differentiate into neurons and glia following growth factor removal in the presence of FBS. Importantly, later passage cNPCs did not develop chromosomal aberrations.

1. Introduction

The mammalian central nervous system (CNS) has a restricted capacity for self-repair and regeneration and, as a consequence, the extent of clinical recovery from CNS injury or disease is generally limited. Because of this unmet clinical need, much work has been devoted to exploring potential ways of enhancing clinical outcomes in the setting of debilitating neurological conditions. One particularly interesting approach is the transplantation of allogeneic neural progenitor cells (NPCs). These multipotent cells are derived from the developing nervous system and, under defined serum-free conditions, are capable of at least limited expansion in culture, followed by differentiation into mature neurons and glia, either following cessation of mitogenic stimulation in vitro or transplantation to the diseased CNS [1, 2].

There are a number of characteristics of NPCs that recommend them for application to neural repair strategies. From a practical standpoint, the proliferative capability of the cells mentioned above allows for the generation of cell banks [3], thereby decreasing the need for continued derivation from donor tissue. From a biological standpoint, the ability of NPCs to exhibit directed migration to areas of disease and integrate into the local cytoarchitecture represents a major breakthrough compared to previous work, for example, with fetal tissue transplantation [4, 5]. From a clinical standpoint, the immune tolerance-afforded allogeneic NPCs in animal studies [6–8] would appear to obviate the need for mandatory immune suppression in many cases, hopefully including allografts in humans. If this is the case, it would substantially decrease the therapeutic risk to patients. In addition, it would appear that progenitor cells of this type convey a substantially decreased risk of tumor formation, particularly when compared to analogous cells derived from pluripotent cell types [9].

In addition to their potential role in cell replacement, NPCs also represent an attractive method for gene delivery, particularly with respect to neuroprotective cytokines. These molecules are gene products that are rapidly degraded in vivo by endogenous proteases and notably include trophic factors

such as glial cell line-derived neurotrophic factor (GDNF). It has been demonstrated that NPCs can be genetically modified to express these types of factors ex vivo, expanded in number, and subsequently transplanted for study [10, 11]. Given that these cells are typically well tolerated immunologically, genetically modified NPCs could provide a method of sustained drug delivery to local sites within the brain, retina, and spinal cord. This option is of interest in species, where NPCs can be successfully isolated, and where models of CNS disease are available.

Progenitor or precursor cells have now been isolated and grown from viable brain tissue in a broad range of mammalian species, including mouse, rat, cat, pig, sheep, dog, monkey, and human [12]. The cat represents a model of interest for neural repair strategies because of the potential for detailed electrophysiological and behavioral studies. In previous work, we and another group have reported the isolation of feline neural progenitor-like cells, combined with successful transplantation to the dystrophic retina [13] and the normal brain [14] of allorecipients. Nevertheless, it has proven difficult to grow these cells for extended periods in culture using conventional protocols. This lack of in vitro expansion hampers further research by restricting the number of studies that can be performed from a given isolation. Here, we identify a modified culture method that allows for sustained, abundant growth of feline neural progenitor cells sufficient for banking. We provide additional characterization of these cells, including examination of karyotype and analysis of gene expression at multiple time points in culture.

2. Materials and Methods

2.1. Isolation and Culture of NPCs from the Cat (cNPCs). The isolation of cNPCs followed a protocol similar to that described previously [13], but in this case the donor was a 47-day timed-pregnant domestic cat (E47). Fetuses were removed under terminal anesthesia at an academic veterinary facility and shipped on ice to the site of cell isolation and culture. Upon arrival, brains were removed by dissection and the forebrain separated from the cerebellum and brainstem. Forebrain tissue was relocated to a petridish containing cold DMEM (Invitrogen, Carlsbad, CA, USA). The tissue was minced using 2 scalpels and then enzymatically digested using 0.05% TrypLE Express (Invitrogen). The resulting cell suspension was washed repeatedly and dissociated by repeated, gentle aspiration using a flame-polished glass pipette. The resulting cells were then divided and seeded into 1 of 2 different complete culture media, namely, standard medium (SM) or Ultraculture-based medium (UM). SM consisted of Advanced DMEM/F12 (Invitrogen), 1% by volume N2 neural supplement (Invitrogen), 1% GlutaMax (Invitrogen), 50 U/mL penicillin-streptomycin (Invitrogen), 20 ng/mL epidermal growth factor (recombinant human EGF, Invitrogen) and 20 ng/mL basic fibroblast growth factor (recombinant human bFGF; Invitrogen). To promote adherence, 5% FBS (Sigma) was also included at the time of initial plating. The following day all medium in cultures was completely replaced with serum-free SM. The remaining half of the primary cells were seeded in an alternate proliferation medium, henceforth designated UltraCulture-based medium (UM), containing Ultraculture (Lonza), 1% GlutaMax, 50 U/mL penicillin-streptomycin, 20 ng/mL epidermal growth factor, and 20 ng/mL basic fibroblast growth factor. The plating density was 0.5×10^6 cells/mL for both conditions. Subsequently, cells were fed by medium exchange every 2 to 3 days and passaged at confluence using TrypLE Express and gentle trituration through a flame-polished glass pipette. At each passage, cell number was counted using a hemocytometer.

2.2. Cytogenetic Analysis (Chromosome Counting and Karyotyping). Confluent cNPCs generated in UM were harvested at culture passages 8 and 14 and prepared for analysis, as follows. Cells were plated onto a T-25 flask, and the media were changed 24 hours before harvesting the culture to stimulate cell division and maximize the mitotic index. The cells were then mitotically arrested with colcemid (KaryoMax Colcemid solution, Invitrogen) at a final working concentration of 0.12 μg/mL at 37°C for 20 minutes. Isolated cNPCs were harvested for hypotonic treatment in 0.075 M KCl solution at room temperature for 25 minutes. The cells were pelleted by centrifugation at 1000 rpm for 8 minutes and fixed in ice-cold fixative (3 : 1 methanol: glacial acetic acid) for 10 min. After a second wash in fixative, the cells were resuspended in 2 mL fixative. Slides were prepared by dropping the cell suspension onto dry microscope slides prewashed with fixative. G-banded karyotyping was performed by Cell Line Genetics LLC (Madison, WI, USA).

2.3. RNA Isolation and cDNA Synthesis. Total RNA was extracted from passage 8 cNPCs using the RNeasy Mini Kit (Qiagen, Valencia, CA, USA) according to the manufacturer's protocol. DNase I was used to digest and eliminate any contaminating genomic DNA. Two micrograms of total RNA in a 20 μL reaction were reverse-transcribed using an Omniscript cDNA Synthesis Kit (Qiagen, Valencia, CA, USA).

2.4. Quantitative PCR (qPCR). qPCR was performed on an Applied Biosystems 7500 Fast Real-Time PCR Detection System (Applied Biosystems, Foster, CA, USA) following protocols previously described [15]. Briefly, 20 μL total reaction was made up of 10 μL 2x Power SYBR Green PCR Master Mix (Applied Biosystems, Foster, CA, USA), 100 ng cDNA, and gene specific primers (Table 1) at a concentration of 300 μM. Samples were initially denatured at 95°C for 10 min, followed by 40 cycles of PCR amplification (15 seconds at 95°C and 1 minute at 60°C). To normalize template input, β-actin (endogenous control) transcript level was measured for each sample. Melting curves were determined to confirm amplification of the expected fragment. Fold change and heat map were generated using JMP 4.1 and DataAssist 2.0 software.

2.5. Induction of cNPC Differentiation. The cNPCs were cultured in UM or UM-FBS that contained 10%FBS but no added growth factors with the same cell density, 0.3×10^6 cells/mL. Culture media was exchanged every 2 days.

Table 1: Cat-specific primers for real-time PCR.

Genes	Description	Forward (5′–3′)	Reverse (5′–3′)	Annealing temperature (°C)	Product size (base pairs)
Nestin	Intermediate filament, Progenitor	CTGGAGCAGGAGAAGGAGAG	GAAGCTGAGGGAAGCCTTG	60	180
Sox-2	Transcription factor, progenitor	ACCAGCTCGCAGACCTACAT	TGGAGTGGGAGGAAGAGGTA	60	154
Vimentin	Intermediate filament, progenitor	ATCCAGGAGCTACAGGCTCA	GGACCTGTCTCCGGTACTCA	60	247
Pax 6	Transcription factor, progenitor	AGGAGGGGGAGAGAATACCA	CTTTCTCGGGCAAACACATC	60	183
Notch1	Surface receptor, progenitor	CAGTGTCTGCAGGGCTACAC	CTCGCACAGAAACTCGTTGA	60	231
CD133	Progenitor	AGGAAGTGCTTTGCGGTCT	TGCCAGTTTCCGAGTCTTTT	60	120
Cyclin D2	Cell cycle protein	CAAGATCACCAACACGGATG	ATATCCCGCACGTCTGTAGG	60	162
Ki-67	Cell cycle protein, proliferation	TCGTCTGAAGCCGGAGTTAT	TCTTCTTTTCCCGATGGTTG	60	150
CD81	Tetraspaniin	CCACAGACCACCAACCTTCT	CAGGCACTGGGACTCCTG	60	156
EGFR	EGF receptor, surface marker	AACTGTGAGGTGGTCCTTGG	CGCAGTCCGGTTTTATTTGT	60	231
FABP7	fatty acid binding protein	TGGAGGCTTTCTGTGCTACC	TGCTTTGTGTCCTGATCACC	60	165
β3-tubulin	Microtubule protein, neural precursor	CATTCTCGTGGACCTTGAGC	GCAGTCGCAATTCTCACATT	60	199
Map2	Microtubule-associated, neuron	ACCTAAGCCATGTGACATCCA	CTCCAGGTACATGGTGAGCA	60	152
GFAP	Intermediate filament, glia	CGGTTTTTGAGGAAGATCCA	TTGGACCGATACCACTCCTC	60	188
AQP4	water channel protein	TACACTGGTGCCAGCATGA	CACCAGCGAGGACAGCTC	60	118
SDF 1	stromal-cell-derived factor-1	ACAGATGTCCTTGCCGATTC	CCACTTCAATTTCGGGTCAA	60	152
CXCR4	fusin	TCTGTGGCAGACCTCCTCTT	TTTCAGCCAACAGCTTCCTT	60	220
Dcx	Doublecortin, neuroblast marker	GGCTGACCTGACTCGATCTC	GCTTTCATATTGGCGGATGT	60	222
Lhx2	Homeobox transcription factor	GATCTGGCGGCCTACAAC	AGGACCCGTTTGGTGAGG	60	224
NCAM (CD56)	Adhesion molecule, surface marker	AGAACAAGGCTGGAGAGCAG	TTTCGGGTAGAAGTCCTCCA	60	172
NogoA	Reticulon 4, surface protein	TTTGCAGTGTTGATGTGGGTA	TAACAGGAACGCTGAAGAGTGA	60	100
nucleostemin	Nucleolar protein	CAGTGGTGTTCAGAGCCTCA	CCGAATGGCTTTGCTGTAA	60	165
Pbx 1	Transcription factor	CTCCGATTACAGAGCCAAGC	GCTGACCATACGCTCGATCT	60	166
β-actin	Housekeeping gene	GCCGTCTTCCCTTCCATC	CTTCTCCATGTCGTCCCAGT	60	168

The morphology of cells was monitored every day, and the cells were photographed on days 1, 3, 5, and 7.

2.6. Immunocytochemistry. After 4 months in culture, cNPCs were plated on four-well chamber slides in either UM or UM-FBS medium and fed every two days. On day 5, cells were fixed with freshly prepared 4% paraformaldehyde (Invitrogen) in 0.1 M phosphate-buffered saline (PBS) for 20 minutes at room temperature. Fixed cells were washed with PBS, then they were incubated for 1 hour at room temperature in antibody blocking buffer containing the following: PBS containing 10% (v/v) normal donkey serum (Sigma), 0.3% Triton X-100, and 0.1% NaN3 (Sigma-Aldrich, Saint Louis, MO, USA). Slides were then incubated in primary antibodies (Table 2) at 4°C overnight. After washing, slides were incubated for 1 hour at room temperature in fluorescent-conjugated secondary antibody, 1 : 400 Alexa Fluor^{546} goat anti-mouse, followed by washings. Cell nuclei were counterstained with 1.5 μg/mL 4′,6-diamidino-2-phenylindole (DAPI;

Table 2: Primary antibodies for immunocytochemistry.

Antigen	Host species and reactivity in retina	Dilution	Source
Nestin	Mouse monoclonal; progenitors, reactive glia	1 : 200	BD, 611658
Vimentin	Mouse monoclonal; progenitors, reactive glia	1 : 200	Sigma, V6630
βIII-tubulin	Mouse monoclonal; immature neurons	1 : 200	Chemicon, MAB1637
Ki-67	Mouse monoclonal; proliferating cells	1 : 200	BD, 556003
GFAP	Mouse monoclonal; Astrocyte, reactive glia	1 : 200	Chemicon, MAB3402

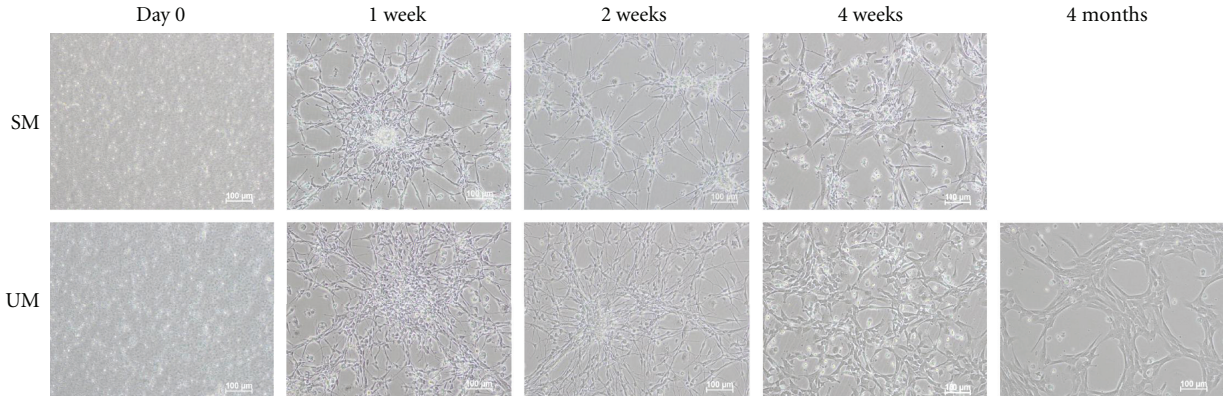

Figure 1: Morphology of cNPCs in different proliferation media at serial time points. Upper panel shows cNPCs cultured in SM and the lower panel cells of the same age in UM. Cultures are shown on day 0, after 1, 2, and 4 weeks as well as 4 months (UM only). In both media the cells exhibited morphologic features consistent with primitive neural cells throughout the period examined. In both cases, the adherent cells extended processes and expanded greatly during the initial week. The cells in SM ceased expanding during the first month and were not evaluated beyond the 3-month time point, whereas those in UM continued to expand throughout the course of the study. Scale bar: 100 μm.

Invitrogen, Molecular Probes, Eugene, OR, USA) in Vectashield Hard Set Mounting Medium (Vector Laboratories, Burlingame, CA, USA) for 15 min at room temperature. Negative controls for immunolabeling were performed in parallel using the same protocol but with omission of the primary antibody. Fluorescent labeling was judged as positive only with reference to the negative controls. Immunoreactive cells were visualized and images recorded using a Nikon fluorescent microscope (Eclipse E600; Nikon, Melville, NY, USA).

3. Results

3.1. Comparison of cNPCs Grown in Different Proliferation Media. Proliferative cultures were obtained from forebrain-derived feline NPCs seeded and maintained in both types of media (SM and UM); however, only those seeded in UM continued to expand throughout the duration of the study (5 months). The cells in both types of media exhibited morphologic features consistent with primitive neuroectodermal cells throughout their growth period (Figure 1). In both cultures, the majority of cells were adherent to the surface of the flask and continued to proliferate, forming a pattern of random networks and nodal clusters as is typical of mammalian neural progenitors when not grown as suspended neurospheres.

The morphology of cNPCs cultured in the two different growth media was also examined. In both conditions, the initially dissociated cells divided and formed small clusters over the first week in culture. During this period, cellular processes had started to form by day 3 and were greatly elaborated by the end of the first week. Cells cultured in SM showed little evidence of proliferation beyond week 3, but continued to survive up to 3 months. In contrast, cells cultured in UM established stably expanding populations. The cNPCs continued to expand vigorously, while maintaining progenitor morphology, although a tendency of the cells to enlarge and flatten was observed (Figure 1).

3.2. Long-Term Expansion of cNPC Cells Is Possible in UM. The growth characteristics of cNPCs are plotted in Figure 2. Initial growth of cells was observed in either medium, but sustained expansion was only achieved using UM. The number of cells in SM medium increased initially and peaked shortly after day 20. After that, the total cell count began to drop, and no further passaging or counting was performed although the cells continued to survive up to at least 3 months. In contrast, the cNPCs in UM continued to increase steadily, without indications of senescence, throughout the 5-month duration of this study.

3.3. Cytogenetics of cNPCs during Extended Culture. Because increased rates of cellular proliferation can be the result of chromosomal abnormalities arising during extended periods of cell culture, the karyotypic stability of cNPCs cultures in UM was evaluated by chromosome counting and G-banded karyotyping. Cytogenetic analysis was performed on twenty

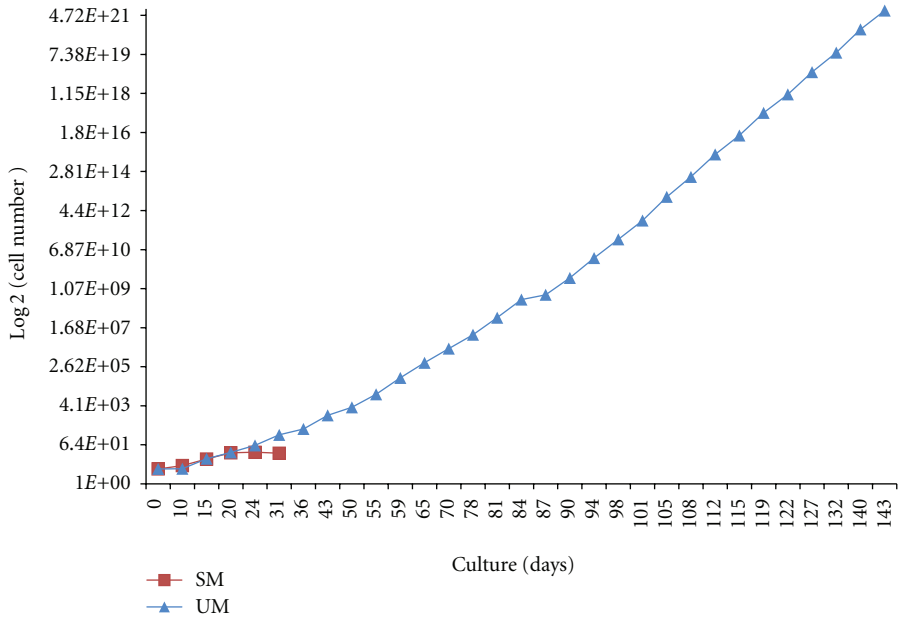

Figure 2: Expansion capacity of cNPC cells in long-term culture. Cells were cultured in 1 of 2 proliferation media of differing composition and counted at each passage using a hemocytometer. The number of cells in SM medium (red) increased initially, then began to drop shortly after day 20, with no measurable proliferation beyond 1 month. In contrast, cultures grown in UM (blue) exhibited sustained growth throughout the course of the study (143 days), with no evidence of senescence. The rate of expansion did not diminish with passage number. Numbers on x-axis represent days in culture at each passage, the y-axis shows cell number as total estimated yield.

G-banded metaphase cells from passage 8 (day 50) and from passage 14 (day 87) time points that roughly corresponded to possible upward inflections in the growth curve. The results showed that the cells from both time points possessed normal feline 38XX karyotypes (Figure 3), indicating that the increased proliferation rate seen was not the result of a culture-induced chromosomal abnormality.

3.4. Quantitative Evaluation of the Effect of Different Culture Media on cNPC Gene Expression. Having determined that UM effectively sustains the proliferation of NPCs of feline origin, whereas the conventional media formation did not, it was of interest to compare the phenotype of the cells grown using these methods. In order to look for differences related to the alternate proliferation conditions used, we compared gene expression profiles for cNPCs grown in SM versus UM at the 1 month time point using quantitative RT-PCR (Figures 4(a) and 4(b)).

Both sampled populations expressed the neural progenitor-associated genes nestin, sox-2, vimentin, and notch1 as well as the proliferation markers cyclinD2 and Ki-67 (Figure 4(a)). Expression of the markers CD81 and FABP7, which are also known to be expressed by NPCs [16–18], was detected as well. Low expression of the early neuronal marker β-III tubulin was seen, as reported previously [13]. The mature neuronal and astroglial markers Map2 and GFAP were detectable, the latter more prominently than the former. Overall, these results were consistent with the maintenance of markers associated with neural progenitor populations by cNPCs when grown in UM, including the modest but detectable tendency for ongoing, spontaneous differentiation along the neuronal lineage, as previously reported in analogous cells from various mammalian species.

Looked at more closely, there were similarities and differences in the level of expression for particular markers (Figure 4(b)). Less than 2 fold variance between conditions was observed for expression of the majority of markers including AQP4, β3-tubulin, CD9, CD81, CyclinD2, EGFR, GFAP, Lhx2, NCAM, nestin, nogoA, notch1, Pax6, Sox2, and vimentin. Growth in UM was associated with greater than 2 fold increased expression in the neuroblast marker DCX, the neuronal marker Map2, the transcription factor Pbx1, and the migration-associated marker SDF1. Markers that were greater than 2 fold lower in UM were CXCR4, FABP7 and Ki-67. Of note, the most upregulated marker (SDF1) is a receptor for the migration factor CXCR4, which was downregulated.

3.5. Sequential Analysis of cNPC Gene Profile with Time in Culture. To examine the phenotypic stability of cRPCs during extended culture in UM, we employed qPCR, in this case to compare the expression profile obtained at 2 weeks to that present at 1, 2, 3, and 5 months (Figure 5). A preponderance of the markers examined showed a tendency to decrease with time in culture. This trend included progenitor-associated and neurodevelopmental markers as well as some markers associated with further lineage restriction. Both heat map and cluster analysis indicated an overall drop in marker expression between the 1- and 2-month time points (Figure 5(a)). Interestingly, this is the same time frame in

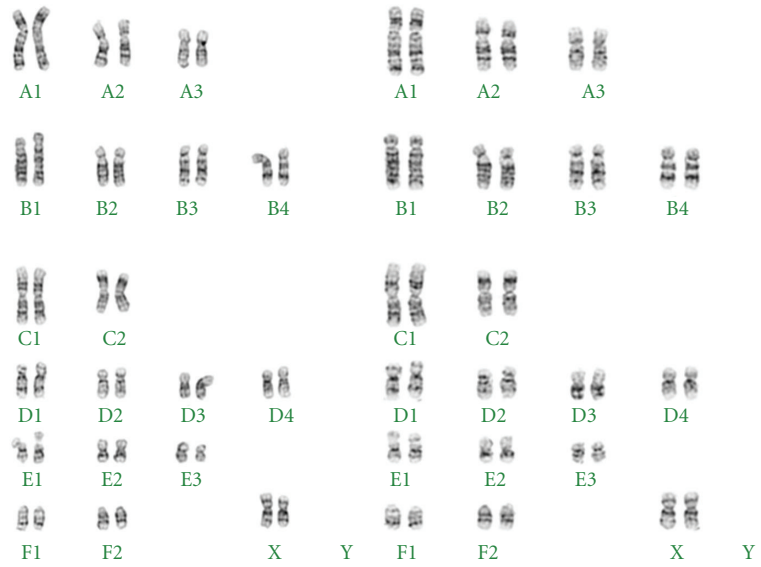

Figure 3: G-banded karyotyping of cNPCs at early and later passage. Cytogenetic G-banded karyotyping results based on analysis of 20 metaphase cNPCs. (a) passage 8 (day 50); (b) passage 14 (day 87). The cells from both time points exhibited a normal 38XX feline karyotype.

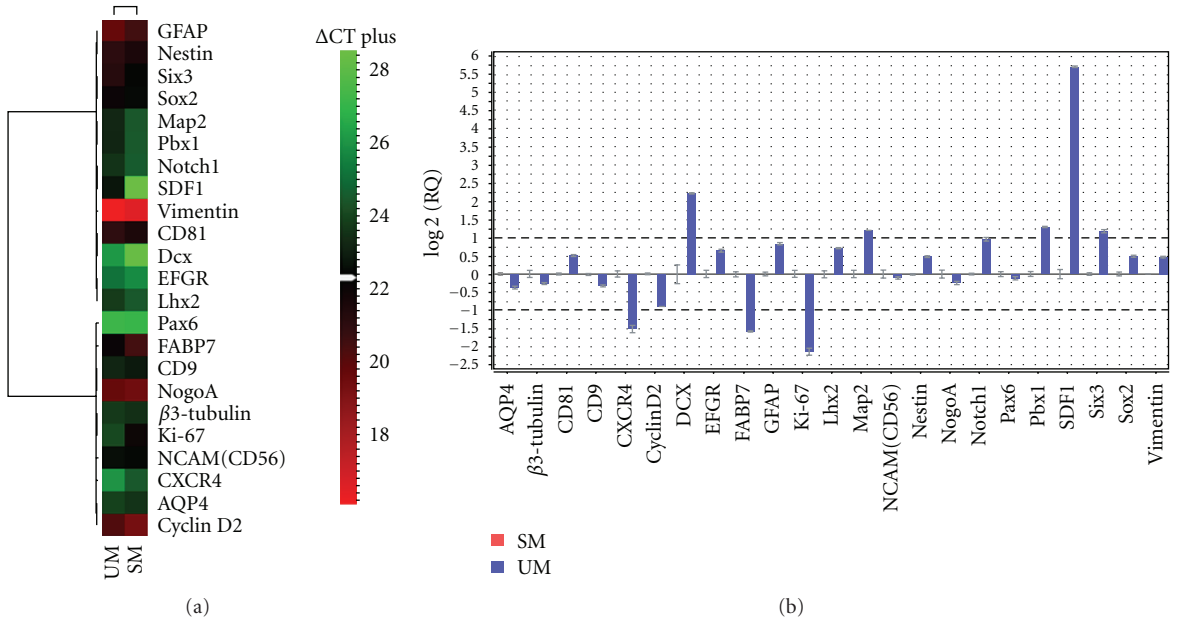

Figure 4: Comparison by qPCR of gene expression profile for cNPCs in different culture media. The cNPCs were cultured in either SM or UM for 1 month prior to testing. (a) heat map display showing relative expression levels of 23 genes expressed by NPCs or related progeny of neural lineage. The scale to the right shows that moderate expression level (as determined by CT value) is shown as black, while lower expression appears increasingly green, and higher expression increasingly red. Viewed in this way, the general similarity of the 2 conditions is evident in that the color of a particular gene tends to be conserved across conditions, even if the intensity often varies. (b) fold change, with SM used as calibrator. Note that expression is represented on a log2 scale, such that 1.00 corresponds to a 2 fold change. Viewed in this way, differences in expression are highlighted. The majority of genes showed less than 2 fold change (between 1.00 to −1.00, on log2 scale), again confirming the general similarity between conditions; however, a number of individual genes fell outside this range. The error bars-show standard deviation.

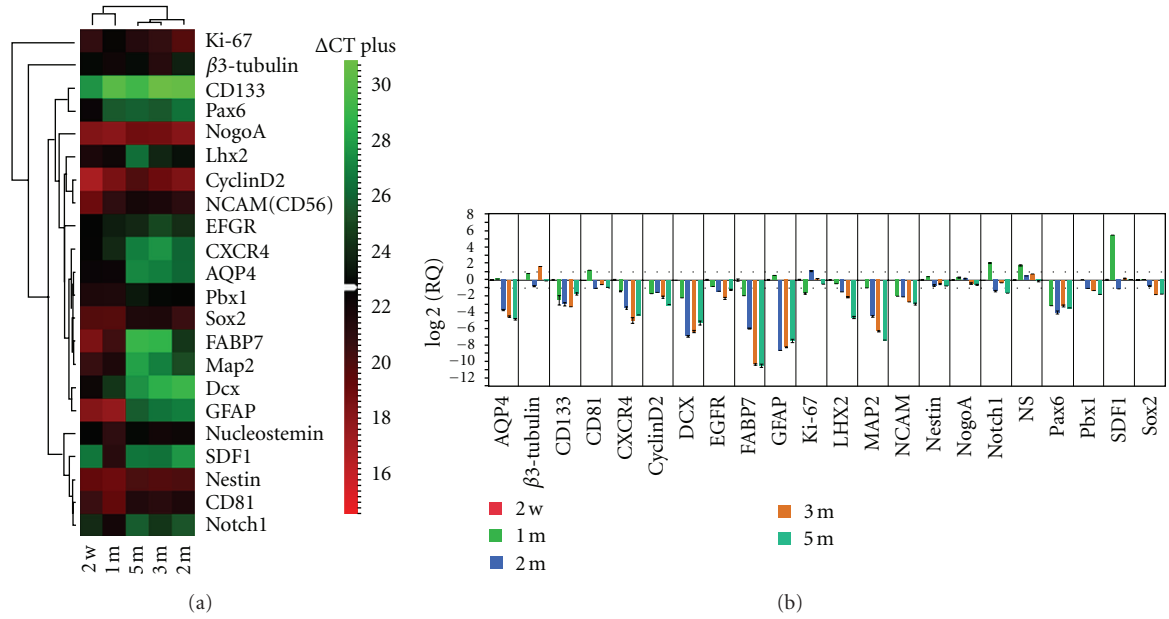

Figure 5: Comparison of gene expression from cNPCs at different time points in UM via qPCR. A 22-gene profile was assayed at each time point. The initial time point for comparison was 2 weeks (calibrator), followed by 1, 2, 3 and 5 months. (a) viewed as a heat map, there was an apparent overall drop in marker expression (shift from red towards green end of spectrum), and this was most evident between the 1- and 2-month time points, both visually and by cluster analysis (dendrogram at top). (b) data viewed as RQ (fold change) confirms the prevalent downward trend with time as well as highlighting the quantitative differences in fold change between markers. Error bars show standard deviation.

which the cells in UM diverged in growth characteristics from those in SM, as seen above in Figure 2. Viewed as a histogram, the qPCR data showed a sequential downward trend, although expression levels appeared to be leveling off at the latter time points (Figure 5(b)). Again, this is concomitant to the robust proliferation seen beyond 1 month in the UM condition.

3.6. Differentiation. Having determined that cNPCs can be grown beyond the 1-month time point using UM, it was important to confirm whether cNPCS grown in this medium retain the potential to differentiate into both neuronal and glial cell types. As a first step, cNPCs (4 months, P26) were dissociated into single cells and induced to differentiate by culture in UM without growth factors, but containing 10% serum (UM-FBS), for 7 days. The cells cultured in UM-FBS appeared similar but exhibited a more flattened morphology than undifferentiated controls (Figure 6). Interestingly, the cultures in UM-FBS reached confluence more rapidly than those in UM. The next step was to examine the expression of relevant markers.

3.7. Effect of UM-FBS on Marker Expression of cNPCs, Evaluated by Immunocytochemistry. Immunocytochemical analysis (Figure 7) at the same time point (4 months, P26) confirmed that feline cells cultured in UM expressed a numbers of markers associated with neural precursor cells. These included strong expression of the intermediate filaments nestin and vimentin as well as the proliferation marker Ki-67. There was also trace labeling for the lineage markers β3-tubulin and GFAP, both of which are cytoskeletal proteins. β3-tubulin is a marker of neurons, and GFAP is strongly expressed by astrocytes. These data are suggestive of a small but detectable level of spontaneous differentiation in the cultures under proliferation conditions, as is expected with cells of this type.

At 5 days after induction of differentiation in UM-FBS, very few cells remained nestin positive, the signal for vimentin persisted at a diminished level, and expression of Ki-67 had decreased notably. In contrast, many more cells were positive for β3-tubulin and a subset of cells GFAP was strongly positive for GFAP, consistent with differentiation along neuronal as well as glial lineages (Table 3).

4. Discussion

Since their initial isolation, neural progenitor cells have been viewed as a powerful research tool for experimental investigation of novel approaches to cell replacement throughout the central nervous system (CNS). The recognized potential of NPC transplantation-based regenerative therapy for CNS diseases has generated considerable enthusiasm among many investigators and resulted in rapid growth of the field. The scientific understanding of NPCs has increased accordingly, although transplantation of these cells has yet to achieve accepted clinical use. One challenge has been growing sufficient quantities of the cells, and this is, therefore, a fundamental area deserving of additional attention. Refinement and the optimization of culture conditions is an obvious initial approach to further sustaining the proliferation of NPCs *in vitro*. It is also important to consider that the culture

Table 3: Estimated percentage and intensity of labeling of cultured cNPCs for specific markers after 5-day exposure to differentiation conditions (UM-FBS). +: weak expression; ++: moderate expression; +++: strong expression.

	Nestin	Vimentin	β3-tubulin	Ki-67	GFAP
UM	100/++	100/+++	60/+	85/++	5/+
UM-FBS	2/+	100/++	85/++	60/+	35/+++

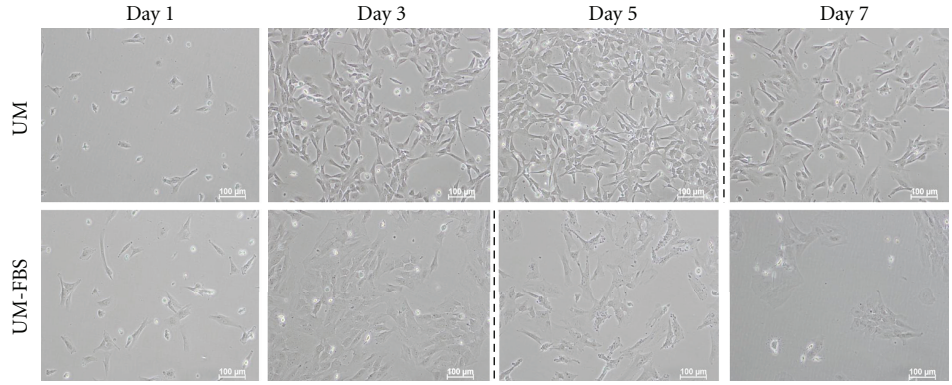

Figure 6: Morphology of cNPCs grown under proliferation versus differentiation conditions. Cultured cNPCs grown under proliferation conditions (UM), beginning at P26 (4 months), maintained the appearance of neural progenitors, while those grown under differentiation conditions (UM-FBS) appeared similar but exhibited a more flattened morphology. Dotted vertical lines represent passaging/reseeding, thereby accounting for the decreased cell density in images to the right of those points. Cells in the UM-FBS condition reached confluence more quickly.

requirements of progenitor cells may differ between species. Research has shown that extended culture of neural progenitors is often associated with loss of multipotency, particularly a reduced potential to generate neurons, together with loss of self-renewal, as reflected in a marked propensity towards early senescence [19, 20]. A pertinent issue is the extent to which changes in culture conditions might enhance the expansion of functionally multipotent NPCs.

Feline NPCs can be difficult to propagate using conventional serum-free conditions. Here, we directly compared two variations on serum-free proliferation media, SM and UM, which differed in base medium but contained the same growth factors. Both formulations were used to examine their ability to sustain the proliferation and development of cNPCs derived from E47 brain tissue. In the more conventional SM medium, cNPCs stopped dividing and began to senesce by 1-month in culture. In UM, the cells continued to exhibit vigorous growth for up to 5 months, the latest time point examined, thereby allowing the banking of considerable numbers of mitotically active cNPCs. Although cNPCs grown in SM and UM appear similar in terms of certain key genes expressed, quantitative analysis of expression level did reveal differences between the conditions at the 1 month point. Interestingly, the expression level of the majority of genes, including progenitor and lineage markers, was downregulated in UM versus SM. Furthermore, this tendency toward downregulation in UM was even more pronounced beyond the 1-month time point, although the possible trend toward a new, lower set point in expression was noted. The reason for this is not clear, but might relate to a state of continuous, rapid cell division. What is clear is that UM is strongly permissive of feline NPCs survival and proliferation *in vitro*, whereas use of conventional SM medium rapidly leads to a failure to propagate.

One possible explanation for the facile growth exhibited by cNPCs in UM could be spontaneous immortalization. The cells in UM displayed repeated upward inflections in growth rate with time in culture that might reflect dysregulation of the cell cycle. It is known that immortalization of NPCs can occur with extended time in culture, and that such events are frequently associated with abnormalities in karyotype. To examine this, we evaluated whether karyotypic alterations were present in our cells, and the results showed that despite 14 passages in UM, the karyotype remained stable. Therefore, the improved growth seen in UM cannot be attributed to changes in karyotype.

Because altered gene expression might be associated with a loss of multipotency, it was important to confirm whether NPCs grown in UM maintain their ability to differentiate into cells of neural lineage. Comparing various progenitor markers and differentiation markers in UM versus UM-FBS conditions, we found that expression levels of progenitor markers decreased while neuronal and glial markers increased. These data indicate that cNPCs cultured in UM retain multipotency and the capacity to differentiate.

The source of the improvement in growth of cBPCs seen in UM thus appears to reside in the beneficial effects of the media constituents rather than aberrations of cellular proliferation. There is no question that Ultraculture is a much richer base medium, containing approximately 6 fold greater total protein than SM. While it is tempting to speculate that certain serum proteins or peptides may be critical to

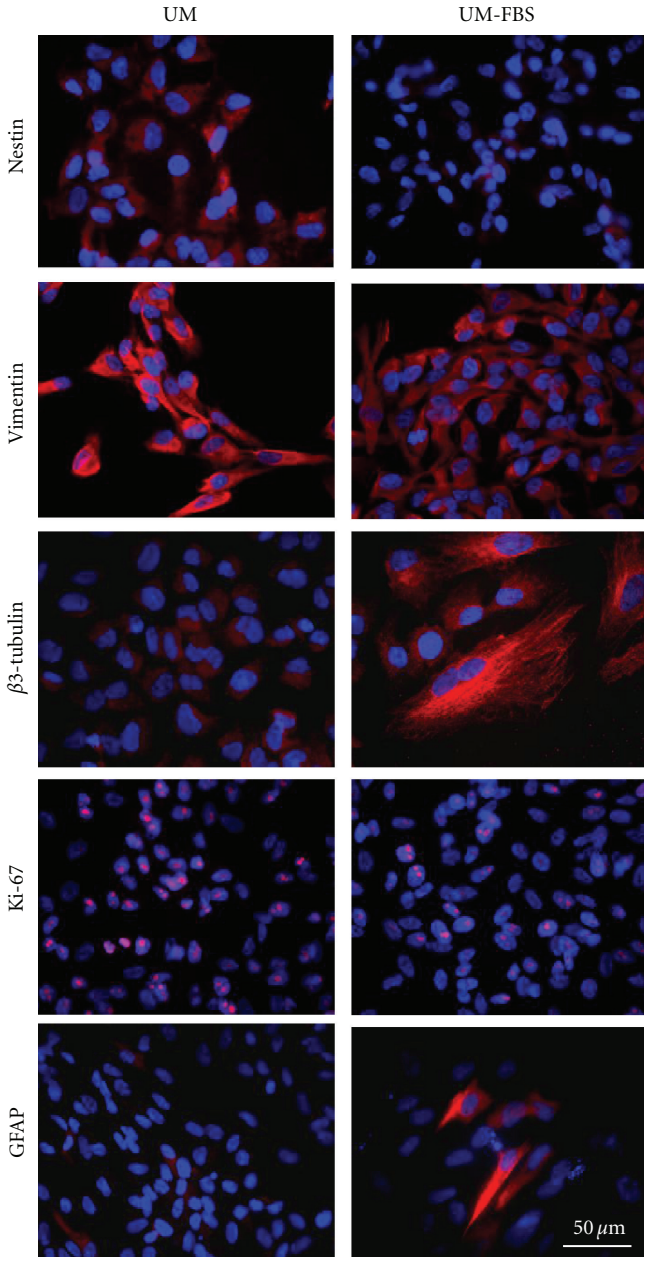

Figure 7: Effect of differentiation conditions on expression of markers by immunocytochemistry. To examine the lineage potential of cNPCs, P26 (4 month) cultures were grown in UM or UM-FBS for 5 days and immunolabeled with antibodies (red) against nestin, vimentin, β3-tubulin, Ki-67, and GFAP. Cell nuclei were labeled with DAPI (blue). Scale bars represent 50 μm.

the growth of feline progenitors, further work is needed to define which particular components are responsible for the dramatic improvements seen in the current study.

In summary, we have shown that the use of a highly enriched, serum-free medium allows the long-term propagation of feline neural progenitor cells, something that standard serum-free conditions does poorly, if at all. The resulting cells retain multipotency and the ability to differentiate, as well as a normal karyotype. This does not rule out the possibility that the cells may have taken a significant, but less obvious, step towards spontaneous immortalization, and that the growth-promoting influence of UM might be causative. Fortunately, the resulting ability to generate and bank large numbers of cNPCs should greatly facilitate additional examination of these cells, including both safety concerns and the potential for therapeutic benefits following transplantation.

Abbreviations

AQP4: Aquaporin 4
FABP7: Fatty acid binding protein 7
GFAP: Glial fibrillary acidic protein
NCAM: Neural cell adhesion molecule
SDF1: Stromal cell-derived factor 1
RT-PCR: Reverse transcriptase-polymerase chain reaction.

Acknowledgments

The authors are grateful to Victor David for providing the cat-specific primer sequences used in this study and to Kristina Narfstrom for her longstanding involvement in cat models of retinal dystrophy as well as the provenance of fetal feline tissue used for our original derivation of feline neural progenitor cells. In addition, the authors thank the Lincy Foundation, the Discovery Eye Foundation, the Andrei Olenicoff Memorial Foundation, and the Polly and Michael Smith Foundation for their generous financial support of this paper.

References

[1] F. H. Gage, "Mammalian neural stem cells," *Science*, vol. 287, no. 5457, pp. 1433–1438, 2000.
[2] D. van der Kooy and S. Weiss, "Why stem cells?" *Science*, vol. 287, no. 5457, pp. 1439–1441, 2000.
[3] R. J. Thomas, A. D. Hope, P. Hourd et al., "Automated, serum-free production of ctx0e03: a therapeutic clinical grade human neural stem cell line," *Biotechnology Letters*, vol. 31, no. 8, pp. 1167–1172, 2009.
[4] C. Lundberg, A. Martínez-Serrano, E. Cattaneo, R. D. G. McKay, and A. Björklund, "Survival, integration, and differentiation of neural stem cell lines after transplantation to the adult rat striatum," *Experimental Neurology*, vol. 145, no. 2, pp. 342–360, 1997.
[5] M. Olsson, "Incorporation of mouse neural progenitors transplanted into the rat embryonic forebrain is developmentally regulated and dependent on regional and adhesive properties," *European Journal of Neuroscience*, vol. 10, no. 1, pp. 71–85, 1998.
[6] J. Hori, T. F. Ng, M. Shatos, H. Klassen, J. W. Streilein, and M. J. Young, "Neural progenitor cells lack immunogenicity and resist destruction as allografts," *Stem Cells*, vol. 21, no. 4, pp. 405–416, 2003.
[7] H. Klassen, K. Warfvinge, P. H. Schwartz et al., "Isolation of progenitor cells from gfp-transgenic pigs and transplantation to the retina of allorecipients," *Cloning and Stem Cells*, vol. 10, no. 3, pp. 391–402, 2008.
[8] S. J. Van Hoffelen, M. J. Young, M. A. Shatos, and D. S. Sakaguchi, "Incorporation of murine brain progenitor cells

into the developing mammalian retina," *Investigative Ophthalmology and Visual Science*, vol. 44, no. 1, pp. 426–434, 2003.

[9] P. G. Hess, "Risk of tumorigenesis in first-in-human trials of embryonic stem cell neural derivatives: ethics in the face of long-term uncertainty," *Accountability in Research*, vol. 16, no. 4, pp. 175–198, 2009.

[10] S. Behrstock, A. D. Ebert, S. Klein, M. Schmitt, J. M. Moore, and C. N. Svendsen, "Lesion-induced increase in survival and migration of human neural progenitor cells releasing gdnf," *Cell Transplantation*, vol. 17, no. 7, pp. 753–762, 2008.

[11] A. D. Ebert, E. L. McMillan, and C. N. Svendsen, "Isolating, expanding, and infecting human and rodent fetal neural progenitor cells," *Current Protocols in Stem Cell Biology*, no. 6, pp. 2D.2.1–2D.2.16, 2008.

[12] H. Klassen, "Transplantation of cultured progenitor cells to the mammalian retina," *Expert Opinion on Biological Therapy*, vol. 6, no. 5, pp. 443–451, 2006.

[13] H. Klassen, P. H. Schwartz, B. Ziaeian et al., "Neural precursors isolated from the developing cat brain show retinal integration following transplantation to the retina of the dystrophic cat," *Veterinary Ophthalmology*, vol. 10, no. 4, pp. 245–253, 2007.

[14] L. Wang, D. R. Martin, H. J. Baker et al., "Neural progenitor cell transplantation and imaging in a large animal model," *Neuroscience Research*, vol. 59, no. 3, pp. 327–340, 2007.

[15] M. W. Pfaffl, "A new mathematical model for relative quantification in real-time rt-pcr," *Nucleic Acids Research*, vol. 29, no. 9, article e45, 2001.

[16] H. Klassen, M. R. Schwartz, A. H. Bailey, and M. J. Young, "Surface markers expressed by multipotent human and mouse neural progenitor cells include tetraspanins and non-protein epitopes," *Neuroscience Letters*, vol. 312, no. 3, pp. 180–182, 2001.

[17] P. H. Schwartz, P. J. Bryant, T. J. Fuja, H. Su, D. K. O'Dowd, and H. Klassen, "Isolation and characterization of neural progenitor cells from post-mortem human cortex," *Journal of Neuroscience Research*, vol. 74, no. 6, pp. 838–851, 2003.

[18] P. H. Schwartz, H. Nethercott, I. I. Kirov, B. Ziaeian, M. J. Young, and H. Klassen, "Expression of neurodevelopmental markers by cultured porcine neural precursor cells," *Stem Cells*, vol. 23, no. 9, pp. 1286–1294, 2005.

[19] L. Anderson, R. M. Burnstein, X. He et al., "Gene expression changes in long term expanded human neural progenitor cells passaged by chopping lead to loss of neurogenic potential *in vivo*," *Experimental Neurology*, vol. 204, no. 2, pp. 512–524, 2007.

[20] L. S. Wright, K. R. Prowse, K. Wallace, M. H. K. Linskens, and C. N. Svendsen, "Human progenitor cells isolated from the developing cortex undergo decreased neurogenesis and eventual senescence following expansion in vitro," *Experimental Cell Research*, vol. 312, no. 11, pp. 2107–2120, 2006.

Hindawi Publishing Corporation
Stem Cells International
Volume 2012, Article ID 939801, 9 pages
doi:10.1155/2012/939801

Research Article

Photoreceptor Differentiation following Transplantation of Allogeneic Retinal Progenitor Cells to the Dystrophic Rhodopsin Pro347Leu Transgenic Pig

H. Klassen,[1] J. F. Kiilgaard,[2] K. Warfvinge,[3] M. S. Samuel,[4] R. S. Prather,[4] F. Wong,[5] R. M. Petters,[6] M. la Cour,[2] and M. J. Young[7]

[1] *Gavin Herbert Eye Institute, Ophthalmology Research, University of California-Irvine, Irvine, CA 92697-4390, USA*
[2] *Department of Ophthalmology, Glostrup Hospital, SUND, University of Copenhagen, 2600 Copenhagen, Denmark*
[3] *Warfvinge Science Support and Department of Ophthalmology, Lund University, SE, 221 84 Lund, Sweden*
[4] *Division of Animal Sciences, University of Missouri-Columbia, Columbia, MO 65211, USA*
[5] *Duke Eye Center, Duke University, Durham, NC 27710, USA*
[6] *Department of Animal Science, North Carolina State University, Raleigh, NC 27695, USA*
[7] *Minda de Gunzburg Center for Ocular Regeneration, Schepens Eye Research Institute, Boston, MA 02114, USA*

Correspondence should be addressed to H. Klassen, hklassen@uci.edu

Received 15 August 2011; Accepted 26 January 2012

Academic Editor: Chee Gee Liew

Purpose. Transplantation of stem, progenitor, or precursor cells has resulted in photoreceptor replacement and evidence of functional efficacy in rodent models of retinal degeneration. Ongoing work has been directed toward the replication of these results in a large animal model, namely, the pig. *Methods.* Retinal progenitor cells were derived from the neural retina of GFP-transgenic pigs and transplanted to the subretinal space of rhodopsin Pro347Leu-transgenic allorecipients, in the early stage of the degeneration and the absence of immune suppression. *Results.* Results confirm the survival of allogeneic porcine RPCs without immune suppression in the setting of photoreceptor dystrophy. The expression of multiple photoreceptor markers by grafted cells included the rod outer segment-specific marker ROM-1. Further evidence of photoreceptor differentiation included the presence of numerous photoreceptor rosettes within GFP-positive grafts, indicative of the development of cellular polarity and self-assembly into rudiments of outer retinal tissue. *Conclusion.* Together, these data support the tolerance of RPCs as allografts and demonstrate the high level of rod photoreceptor development that can be obtained from cultured RPCs following transplantation. Strategies for further progress in this area, together with possible functional implications, are discussed.

1. Introduction

As a group, degenerative diseases of the retina constitute a significant source of visual disability, particularly in the developed world, and yet current therapeutic options are quite limited. For instance, the loss of photoreceptor cells, as seen in the later stages of retinitis pigmentosa and macular degeneration, results in permanent visual deficits for which no restorative treatment is available. Nevertheless, the notion that photoreceptor cells might be replaceable in the therapeutic setting has been given recent support by experimental work in animal models.

Work in the rat first showed that transplanted neural progenitor cells could migrate into the host retina, take up residence within the cellular laminae of this tissue, and exhibit morphological signs of integration into the local cytoarchitecture [1–3]. Subsequent studies reported that similar cells could be derived from the developing neural retina of both rats [4] and mice [5, 6] and that these retinal progenitor cells (RPCs) could express photoreceptor markers, including recoverin and rhodopsin, and rescue light sensitivity following engraftment in the host retina.

More recent work has shown that many of the results obtained using progenitor cell transplantation in rodents

also apply to other mammalian species, including the Brazilian opossum [7], the pig [8–10], and the cat [9, 10]. In some of this work, particularly following the use of brain-derived progenitors as donor cells, the evidence for retinal integration was substantial and yet the evidence of photoreceptor differentiation was limited [7, 9–13].

Prior work in the pig has shown profuse expression of photoreceptor markers by grafted retinal progenitor cells, yet the full extent of donor cell differentiation was difficult to determine, in part due to limited visualization of donor cell morphology [9, 10]. In addition, previous work in the pig made use of retinal injury models, whereas a model of photoreceptor degeneration has also been generated in the pig [14–16]. Here we investigate the fate of RPCs derived from GFP-transgenic pigs following transplantation to the subretinal space of transgenic rhodopsin Pro347Leu allorecipients.

2. Methods

2.1. Donor Animals and Cells. Two timed-pregnant NT5 GFP-transgenic sows [17] were sacrificed at 45 days gestation, on separate occasions, to provide fetal tissue as the starting point for the derivation of GFP-transgenic porcine retinal progenitor cells (gpRPCs). Details of the tissue harvest and cell derivation procedures were otherwise similar to those previously described [9, 10]. Briefly, the immature neural retina was dissected free from each fetal eye (excluding the optic nerve head and ciliary margin), the retinal tissue was pooled and subjected to repeated cycles of enzymatic digestion followed by seeding into tissue culture flasks in neurobasal media supplemented with B-27 and 20 ng/mL EGF and bFGF. FBS (10%) was included overnight, but then removed with all subsequent feedings being serum-free. These cells of retinal origin were then expanded under serum-free culture conditions thereby selectively enriching for proliferating progenitors.

The resulting cultures were defined as RPCs and these cells have been further characterized, as previously reported [9, 10, 18]. Like brain-derived porcine neural progenitors [19], these cells are nestin-, sox2-, and Ki-67-positive, and small subpopulations express neuronal markers and the glial marker GFAP. Unlike brain-derived neural progenitors, proliferating RPC cultures contain subpopulations of recoverin-positive profiles [5, 6], whereas rhodopsin expression is rare and ROM-1 undetectable. Differentiating RPCs give rise to rod photoreceptor cells but not oligodendrocytes.

Cells were passaged for approximately 4–6 weeks prior to transplantation. The cells were grown as monolayers and dissociated with each passage, but prior to transplantation were allowed to form nascent spherical aggregates, and the smaller aggregates were preferentially collected for use as donor material. The reason for adopting this last approach is that fully dissociated RPCs exhibit poor survival rates following transplantation, whereas large spherical aggregates can be associated with glial differentiation within the sphere core [19].

2.2. Recipient Animals. Recipient animals used in the present experiments were 15 transgenic rhodopsin Pro347Leu transgenic swine (from 2 litters: age 6 and 9 weeks) with a known retinal dystrophic phenotype [15] as well as 1 nontransgenic littermate (age: 6 weeks), which served as a normal control.

2.3. Transplant Surgery. The transplantation technique was similar to that previously described in pigs [8–10, 18]. Briefly, recipient animals underwent preanesthesia, endotracheal intubation, and general anesthesia. The left pupil was dilated. A standard three port pars plana vitrectomy was performed. The posterior hyaloids were detached and the central vitreous removed in all cases. A retinal bleb was elevated in the area centralis by the subretinal injection of 0.25–0.5 mL BSS through a 41-gauge cannula (ref. 1270; DORC International BV, Zuidland, the Netherlands). A small retinotomy was made by gentle endodiathermy of the detached retina. GFP+ cells (approximately $5–10 \times 10^6$ cells) were injected either as spheres or as single cell suspension through the retinotomy and into the retinal bleb using a 27-gauge silicon-tipped needle. Immediate reflux of some cells into the vitreous cavity was observed in some animals. A small air bubble was placed in the subretinal bleb under the retinotomy to prevent further reflux of cells after withdrawal of the needle. Sclerotomies and conjunctiva were sutured with 7–0 vicryl. Lateral canthal incisions were sutured with 6–0 vicryl. The pigs were examined by ophthalmoscopy 1-2 days after surgery.

The research protocol used was previously reviewed and approved by the Danish Animal Experiment Inspectorate, the North Carolina State University IACUC, and completed in accordance with the ARVO statement for the Use of Animals in Ophthalmic and Vision Research.

2.4. Tissue Processing. Eyes were enucleated following euthanasia by overdose of intravenous pentobarbital at the termination of the experiment. The survival time for the first litter (6 dystrophic animals, 1 normal control) was 5 weeks posttransplantation (age 11 weeks), while that of the second litter (9 animals) was 9 weeks (age 18 weeks). Globes were placed in 4% paraformaldehyde (PFA) for 10–20 minutes. The anterior segment and the lens were then removed and the posterior segment was postfixed for 2 hours in 4% PFA, with subsequent rinsing in rising concentrations of sucrose containing Sörensen's phosphate buffer. A horizontal cut was made which extended from the temporal retinal margin to 2-3 mm nasal to the optic disc, thus comprising the temporal ciliary margin, the area centralis, and the optic disc. The tissues were embedded in a gelatin medium and serially sectioned at 12 μm on a cryostat. During the sectioning process, every fifteenth section was examined by epifluorescence microscopy for GFP+ cells, and every tenth slide was stained with Hematoxylin-Eosin (Htx-Eosin).

2.5. Immunohistochemistry. The retinal sections were exposed to primary anti-sera (see Table 1) in a moist chamber for 16–18 hours, 4°C, followed by rinsing in 0.1 M phosphate-buffered saline (PBS) with 0.25% Triton-X-100. Sections were then incubated with secondary Alexa 409 (recoverin; 1 : 400, Invitrogen, La Jolla, CA) or Texas Red-conjugated antibodies (ROM-1 and rhodopsin, 1 : 200, Jackson Immunoresearch, West Grove, PA) for 1-2 hrs at room

Table 1: Primary antibodies used for immunohistochemistry.

Name	Host	Dilution	Detects	Supplier
Recoverin	Rabbit	1 : 10.000	Rods, cones, some bipolar cells	Kind gift of Dr. A Dizhoor, Detroit, MI
Rho4D2	Mouse	1 : 100	Rods	Kind gift of Dr. RS Molday, Vancouver, Canada
ROM-1	Mouse	1 : 10	Rod outer segments	Kind gift of Dr. RS Molday, Vancouver, Canada
GFP	Chicken	1 : 5000	Green fluorescent protein	Chemicon, Temecula, CA

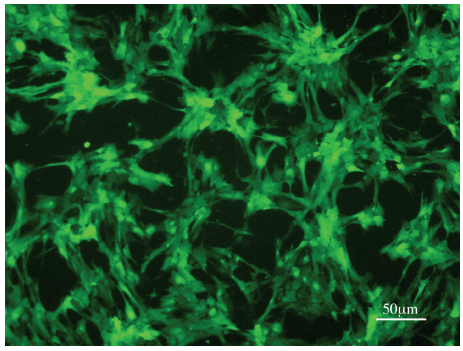

Figure 1: Donor porcine retinal progenitor cells (RPCs). RPCs isolated from GFP-transgenic donors at 45d gestational age and expanded in culture in the presence of EGF and bFGF. The cells grew as a monolayer and strongly expressed the GFP reporter gene. No tendency toward rosette formation is seen.

temperature in the dark. Normal eyes, processed in parallel, were used as controls. In addition, negative controls with omission of the primary anti-sera were performed. The specimens were examined with an epifluorescence microscope. Colocalization of Texas Red-labeled primary antibodies and GFP+ cells was assessed by superimposition of separate digital images of each fluorochrome.

Sections were frequently stained with chicken anti-GFP (with FITC secondary antibody, 1 : 200, Jackson Immunoresearch, West Grove, PA), either in order to examine the quality of the GFP expression or to reveal possible downregulated grafted cells. The endogenous GFP expression was always high and enhancing with anti-GFP resulted in blurring of the cell boundaries. The GFP staining did not appear to reveal more surviving cells.

3. Results

Progenitor cells from the fetal porcine retina proliferated rapidly in culture, as previously described [9, 10, 18]. Cultured GFP-transgenic pRPCs maintained extensive reporter gene-associated fluorescence and did not show evidence of rosette formation under proliferation conditions (Figure 1).

Following transplantation to nonimmunosuppressed juvenile rhodopsin Pro347Leu transgenic pigs, GFP+ donor cells could be readily identified at the site of transplantation (Figure 2). Strong nuclear staining and classical rosettes were apparent within the cellular aggregate of the graft. There were also a few pigmented profiles present within the subretinal graft and host outer nuclear layer (ONL; Figure 2(a)).

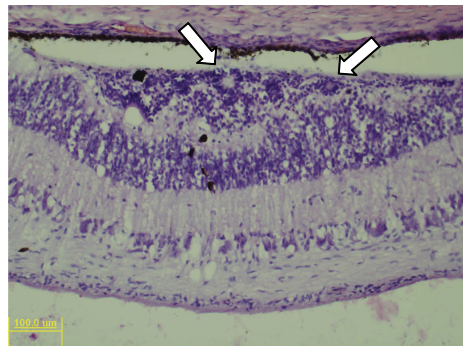

(a)

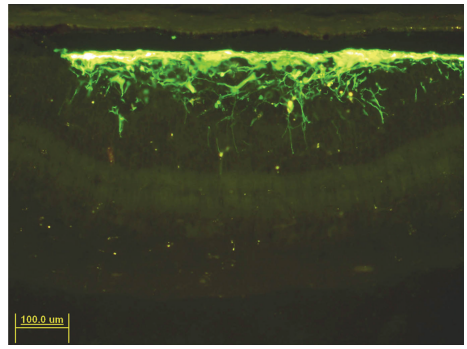

(b)

Figure 2: Engraftment of RPCs in rhodopsin Pro347Leu recipient. Recipient was 6 weeks of age at time of transplantation. (a) H&E stained section through the graft site 5 weeks after transplantation shows a cellular mass in the subretinal space of presumptive donor origin. Artifactual detachment of the retina reveals the cellular mass to be adherent to the outer surface of the retina, in preference to the adjacent RPE layer. A number of photoreceptor rosettes are present within the cellular mass (arrows), as well as some focal pigment profiles, some of which are also found within the adjacent host neural retina. (b) Fluorescence imaging shows intense GFP-associated immunoreactivity in the subretinal space, corresponding to the cellular mass noted with H&E, above, thereby confirming the identity and location of the graft. A presumptive rosette is visible within the center of the graft, in a location similar to that seen in the H&E section. The majority of GFP+ cells remain in the subretinal mass; however, a number of donor cells are visible within the host retina and these have processes that exhibit a high degree of radial orientation.

Despite a few limited indications of prior surgical intervention, there was no clinical or histological evidence of inflammatory or immune responses in recipient eyes.

Donor cells were predominantly located in the subretinal space directly adjacent to the RPE layer, while a subset of

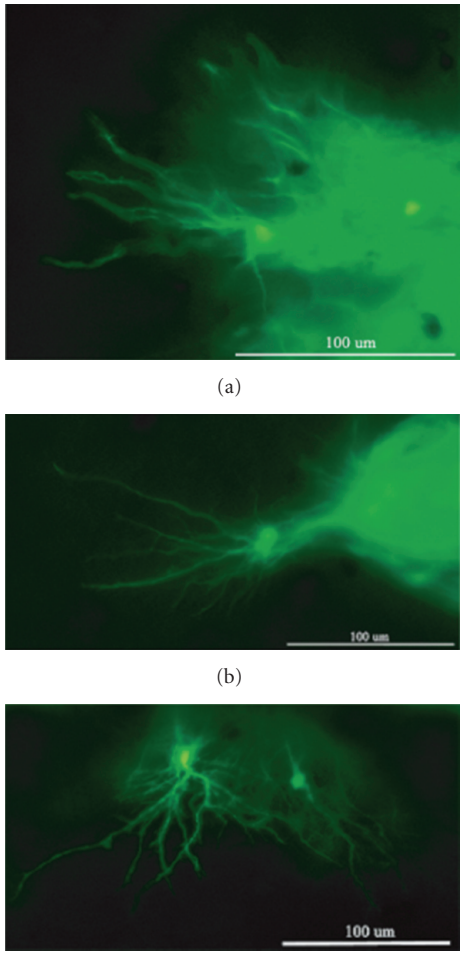

(a)

(b)

(c)

Figure 3: Arborization of grafted cells in dystrophic recipient retina. Recipient was 9 weeks of age at time of transplantation and experiment terminated 9 weeks later. Photomicrograph of a retinal wholemount viewed *en face* using fluorescence microscopy. Image reveals GFP+ profiles within the retina of rhodopsin Pro347Leu recipient. Inspection of regions near the edge of the graft allows visualization of individual donor-derived cells and reveals extension of elaborate processes in the plane of focus.

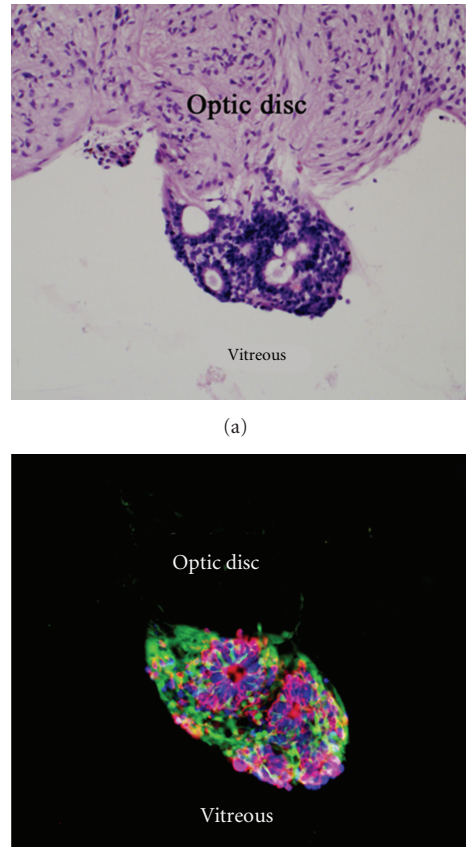

(a)

(b)

Figure 4: Grafted cells form rosettes and express photoreceptor markers. Recipient was 6 weeks of age at time of transplantation and experiment terminated 5 weeks later. The H&E section (a) shows a cluster of grafted cells adhering to vitreal surface of the host optic nerve head, likely a result of reflux around the time of surgery. This cluster contains multiple rosettes of the type formed by photoreceptor cells, with darkly staining nuclei densely packed in a peripheral rim and lighter staining material in the rosette's core. Fluorescence imaging (b) confirms the cluster to be GFP+ and therefore of donor origin. Immunolabeling for rhodopsin (red) and recoverin (blue) demonstrates photoreceptor marker expression by a subset of grafted cells. Cells expressing photoreceptor markers are predominantly found within rosettes.

GFP+ profiles migrated or extended processes into the host ONL. Cells in the subretinal space frequently extended processes perpendicular to the retina or with random orientations, whereas GFP+ processes within the host ONL exhibited predominantly radial orientations (Figure 2(b)). Donor profiles within the neural retina at a distance from the graft site showed extensive horizontal branching, as visualized in retinal wholemounts (Figure 3). In one case, a cluster of donor cells was identified on the vitreal surface of the optic nerve head, presumably as a result of reflux through the retinotomy at the time of subretinal injection (Figure 4). These cells had formed a rudiment of retinal tissue that appeared to be fused to the optic nerve tissue, as seen in work with embryonic retinal tissue grafts [20].

There was evidence of widespread differentiation of donor RPCs along the photoreceptor lineage following transplantation to the eye of dystrophic allorecipients. This data included both morphological considerations and marker expression. In H&E stained sections, cells within the graft predominantly exhibited small, densely packed nuclei which closely resembled adjacent photoreceptors of the host ONL (Figure 2(a)). In addition, there were numerous rosettes consisting of a dense ring of nuclei surrounding a pale central core. These were of the type known to be formed by photoreceptor cells under a variety of circumstances following disruption and spontaneous reorganization of the ONL [20]. In addition, the cells could be identified as being of donor origin

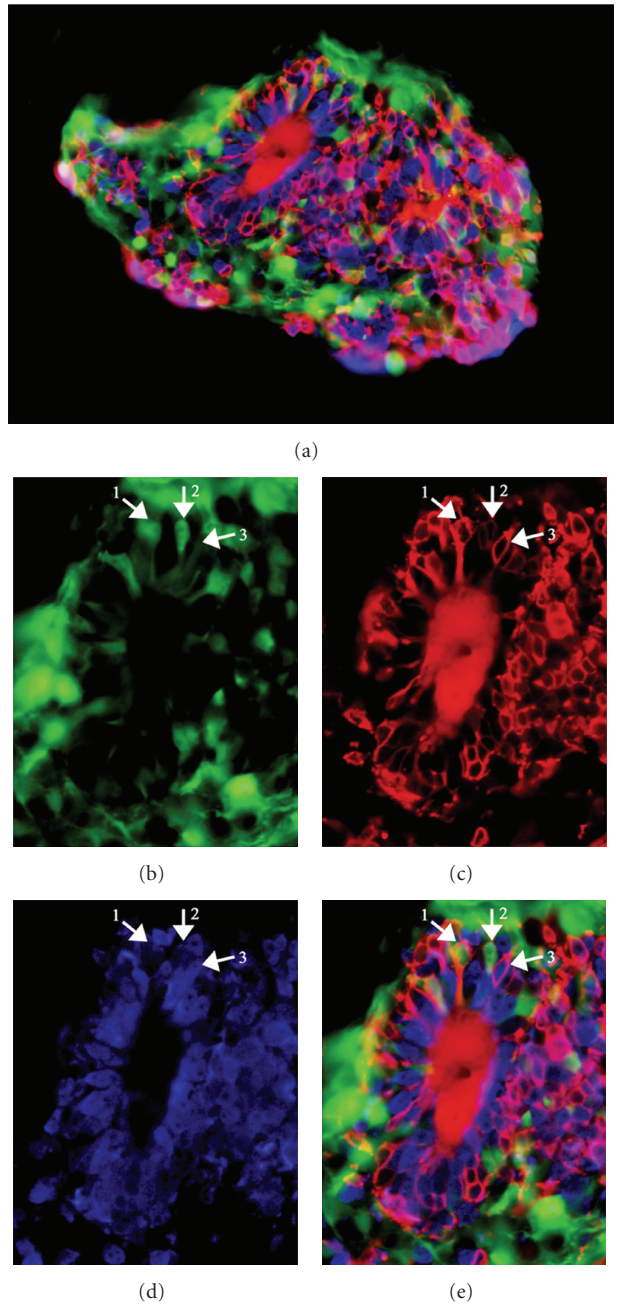

Figure 5: Photoreceptor marker expression within a rosette of donor origin. Recipient was 6 weeks of age at time of transplantation and experiment terminated 5 weeks later. (a) Immunohistochemical labeling of the same RPC graft was shown in previous figure. Endogenous GFP fluorescence (green) was present in many cells of the graft, but less so within the rosettes. The largest, most well formed of the rosettes was selected for more detailed evaluation of individual marker expression patterns. (b) GFP labeling was most notable around the periphery of the rosette; however, GFP+ profiles were also integrated into this structure, with small peripheral soma and straight process oriented towards the core of the rosette (arrow 1). An adjacent region (arrow 2) shows a similar cell with a less clearly defined process. A third cell (arrow 3), does not express GFP. (c) Rhodopsin labeling (red) is strongest in the central core of the rosette. In addition, multiple profiles exhibiting rod photoreceptor morphology can be seen to contribute to the rim of the rosette, and these have cell bodies located around the periphery and processes directed inward where they merge with the central core. The arrows point to the same profiles as before, in this case showing strong rhodopsin labeling (arrow 1), no rhodopsin (arrow 2), and moderate rhodopsin (arrow 3). (d) Recoverin (blue) labeling was dense in areas populated by rhodopsin-positive cells and revealed a dense ring of recoverin-positive cells central to the rhodopsin-positive somata, although this labeling did not extend into the core of the rosette despite some marginal overlap at the interface. (e) The merged image reveals that much of the rhodopsin colabels recoverin-positive cells, whereas many recoverin-positive cells do not appear to colabel with rhodopsin. The core is exclusively positive for rhodopsin, as previously noted.

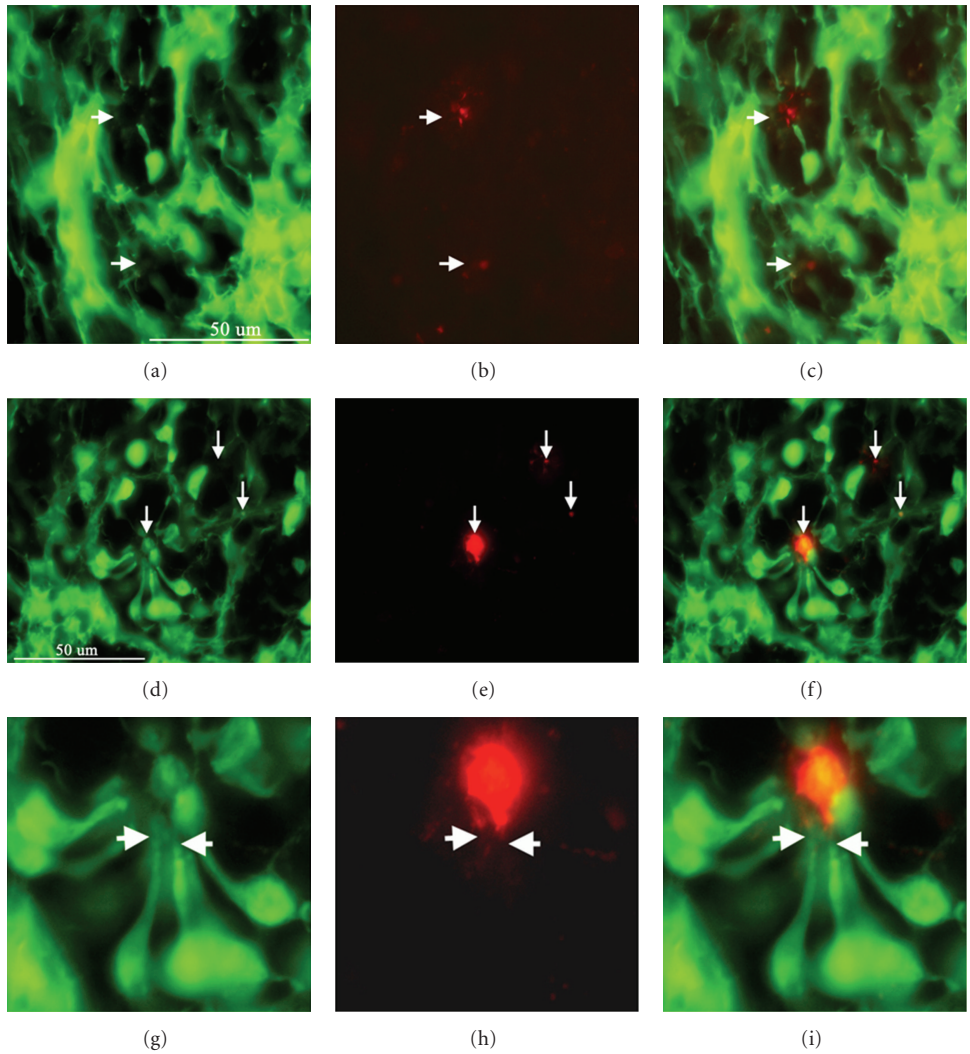

Figure 6: Expression of ROM-1 within rosettes of the graft. Recipient was 6 weeks of age at time of transplantation and experiment terminated 5 weeks later. Immunohistochemical labeling for rod outer segment marker-1. Panels in the left column of Figures (a, d, g) show endogenous GFP transgene expression (green) of donor cells, panels in the central column (b, e, h) show ROM-1 expression (red), and panels in the right column (c, f, i) show the merged images comprised of the 2 preceding panels of the same row. (a) The widespread GFP expression within the graft is periodically interrupted by rounded lacunae (arrows), where (b) ROM-1 labeling can be found. Merged image (c) shows that regions of ROM-1 labeling are encircled by inwardly directed straight processes, thereby indicating that ROM-1 corresponds to the core region of the rosettes, which is the predicted location for rod outer segments in this type of structure. These findings are corroborated by examination of another rosette (d) in which there is a greater number of GFP+ cells with photoreceptor morphology, the processes of which are directed inward toward a small central core. (e) ROM-1 labeling (arrows) predominantly localizes to the core region of the rosette. (g–i) Examination of the same rosette at higher power allows visualization of the limit of GFP expression (arrows) within some of the processes of donor-derived photoreceptor-like cells, in juxtaposition to the adjacent localization of ROM-1 labeling.

based on graft location (subretinal space, vitreous cavity) and comparison to GFP expression patterns (Figures 2(b) and 4).

Further support for photoreceptor differentiation was obtained by analysis of marker expression. Grafted cells showed immunohistochemical evidence for expression of multiple photoreceptor-associated markers. Cells of the grafts, including cells within rosettes, showed expression of recoverin and rhodopsin, with a notable degree of double-labeling for these markers (Figures 4 and 5). These markers were expressed by donor cells within grafts, regardless of location within either the subretinal space or vitreal surface of the optic nerve. The rod photoreceptor outer segment-specific marker ROM-1 was also expressed by rosette-forming grafted cells (Figure 6).

In terms of marker expression patterns, GFP was evident in many grafted cells but was somewhat less expressed within rosettes and was excluded from the central core of these structures (Figures 4 and 5), as might be expected based on differential protein trafficking. Conversely, rhodopsin expression was more predominant within rosettes and was notable for being highly concentrated in the central core. Recoverin was also more highly expressed within the rosettes,

albeit with a different pattern than rhodopsin. Recoverin appeared to be excluded from all but the periphery of the rosette central core (Figure 5). ROM-1, a marker specifically associated with rod outer segment disc membranes, was exclusively expressed in the rosette central core (Figure 6).

4. Discussion

A major challenge faced during the development of therapeutic applications for stem cells is the requirement for reliable tissue-specific differentiation of grafted cells. This is particularly true in the setting of the retina, owing both to the need for molecular transduction of photic stimuli as well as the requirement for a highly organized and optically transparent tissue. Here we show that cultured RPCs are capable of attaining a high level of photoreceptor development following transplantation to the retina of a large mammal. In this model, grafted RPCs differentiated into photoreceptor-like profiles in sufficient quantities and with sufficient structural polarity and cytological affinity to self-organize into rosettes. Marker expression closely followed normal patterns, supporting the conclusion that these donor cells had differentiated into morphological photoreceptors.

Previous work with stem [21], progenitor [5, 6], and precursor [22] cell transplantation has shown that various degrees of morphological photoreceptor development can be achieved by way of this approach in rodents. Moreover, these same studies have provided evidence of functional improvements in host vision, relative to controls. Although rodent recipients are frequently used, these types of cells have been derived from human sources [5, 6, 21, 23–26]. The question, therefore, arises as to whether allogeneic RPC transplantation represents a viable method for treatment of human retinal conditions. One way to approach this question prior to human trials is the use of large animal models for replication of the rodent data under conditions more equivalent to those faced clinically. One such model that is gaining in popularity is the pig. In terms of retinal degeneration, the pig model is enhanced by the availability of swine transgenic for the reporter gene GFP for use as donors [17, 18] and retinal degenerative swine for use as recipients [14–16]. We have previously shown that progenitor cells can be isolated from the porcine brain [19] and retina [9, 10], including from GFP-transgenic donors [18], and that porcine RPCs are capable of expressing photoreceptor markers, both in vitro and after transplantation to the subretinal space [9, 10]. Here we provide additional evidence that grafted RPCs undergo a high level of photoreceptor differentiation after transplantation to the dystrophic pig eye.

We found that porcine RPCs expressed photoreceptor markers after transplantation to the subretinal space, yet photoreceptor differentiation was also observed in a grafted cluster of cells that adhered ectopically to the optic nerve head. The unintended location of this cluster is likely a consequence of the misdirection of grafted neurospheres, at or near the time of surgery, presumably due to reflux from the subretinal space through the retinotomy, as is known to occur. In this instance, the potential for confusion with host cells was eliminated by endogenous GFP reporter gene expression. Interestingly, this data supports the concept that RPCs are capable of spontaneously differentiating into photoreceptors at relatively high yield without the need for microenvironmental cues such as might be obtained from engraftment in the host retina. In addition, the photoreceptor cells generated within the graft exhibited sufficient polarity to self-organize into rosettes. This particular cluster contained multiple rosettes of the type typical of those formed by photoreceptor cells after various perturbations of the retina, wherein the nuclei are densely packed around the periphery and the inner and outer segments are oriented inward to form the rosette's core. These types of highly organized rosettes can be viewed as focal tissue rudiments, each attempting to recapitulate the structure of the outer nuclear layer (ONL), albeit in a manner lacking global continuity. Rosettes of this type are to be distinguished from the more primitive Flexner Wintersteiner rosettes seen in a number of neoplastic conditions.

The functional capabilities of the grafted cells were not assessed; however, prior work with embryonic retinal transplants in rodents has demonstrated that rosettes of similar morphology are capable of detecting light and providing limited light-mediated behaviors, even in the absence of an RPE layer [20, 27–29]. That said, the abnormal topography of a rosette obviously limits the potential for spatial vision. The point to be made is that although rosette formation poses a limit to spatial vision, it does not rule out the potential for functionality at the level of the graft-derived photoreceptors. Photoreceptors in the cluster attached to the optic nerve would not be expected to integrate with the host visual pathways; however, cells transplanted to the subretinal space may have done so although this possibility was not demonstrated in the current study. It could be that such integration did not occur, or it may have occurred but been obscured by the tendency of donor cells to downregulate GFP expression as they differentiated into rhodopsin- and recoverin-expressing photoreceptors. This latter tendency is attributable to the CMV promoter used to drive GFP expression in the transgenic donor pigs. Use of an alternate promoter could provide a solution to this problem [30].

Appropriately localized expression of the rod-specific marker ROM-1 seen in the current study provides additional evidence of the high level of photoreceptor differentiation obtainable from cultured RPCs. The presence of ROM-1 in the core of rosettes is consistent with the development of rod outer segments (ROS) by the donor-derived photoreceptors. The survival of the grafted cells seen in the current study, in the absence of immune suppression, provides additional confirmation for the high level of tolerance shown to allogeneic RPCs following introduction to both the vitreous cavity and subretinal space of a retinal dystrophic large mammal. Less certain is the contribution of the transgenic rhodopsin Pro347Leu background to the integration of donor cells. RPCs, like many other types of neural progenitor and precursor cells, are known to display an evident tropism for areas of degeneration, trauma, or disease. It was anticipated that the use of dystrophic hosts would result in enhanced intraretinal integration by grafted RPCs. GFP+ profiles did

exhibit radially oriented integration into the host ONL and extension of elaborater processes in the orthogonal plane; however, the identity of the integrated cells remains to be determined, as does the question of graft-host connectivity.

The pig has emerged a preferred species for modeling of surgical procedures, including ocular applications. The increasing availability of transgenic swine and recent sequencing of the porcine genome provide additional advantages to the use of this model. The current study illustrates the value of the porcine model in the translational development of regenerative strategies and, in particular, intraocular stem cell transplantation.

Acknowledgments

The authors wish to dedicate this work to the memory of Richard D. Siegal, who generously supported this and other work directed towards retinal and optic nerve repair. They also wish to thank Donna Hardin for excellent technical assistance during surgery, Dr. Jill Barnes for generously providing cell culture facilities, and Dr. Jinmei Wang for assistance with the paper and acknowledge financial support from the Richard D. and Gail Siegal Foundation (M. J. Young, K. Warfvinge), the Lincy and Discovery Eye Foundations (H. Klassen, M. J. Young), the Crown Princess Margareta's Committee for the Blind (K. Warfvinge), and the Swedish Science Council (K. Warfvinge).

References

[1] M. Takahashi, T. D. Palmer, J. Takahashi, and F. H. Gage, "Widespread integration and survival of adult-derived neural progenitor cells in the developing optic retina," *Molecular and Cellular Neurosciences*, vol. 12, no. 6, pp. 340–348, 1998.

[2] M. J. Young, J. Ray, S. J. O. Whiteley, H. Klassen, and F. H. Gage, "Neuronal differentiation and morphological integration of hippocampal progenitor cells transplanted to the retina of immature and mature dystrophic rats," *Molecular and Cellular Neurosciences*, vol. 16, no. 3, pp. 197–205, 2000.

[3] K. Warfvinge, C. Kamme, U. Englund, and K. Wictorin, "Retinal integration of grafts of brain-derived precursor cell lines implanted subretinally into adult, normal rats," *Experimental Neurology*, vol. 169, no. 1, pp. 1–12, 2001.

[4] D. M. Chacko, J. A. Rogers, J. E. Turner, and I. Ahmad, "Survival and differentiation of cultured retinal progenitors transplanted in the subretinal space of the rat," *Biochemical and Biophysical Research Communications*, vol. 268, no. 3, pp. 842–846, 2000.

[5] H. Klassen, B. Ziaeian, I. I. Kirov, M. J. Young, and P. H. Schwartz, "Isolation of retinal progenitor cells from post-mortem human tissue and comparison with autologous brain progenitors," *Journal of Neuroscience Research*, vol. 77, no. 3, pp. 334–343, 2004.

[6] H. J. Klassen, T. F. Ng, Y. Kurimoto et al., "Multipotent retinal progenitors express developmental markers, differentiate into retinal neurons, and preserve light-mediated behavior," *Investigative Ophthalmology and Visual Science*, vol. 45, no. 11, pp. 4167–4173, 2004.

[7] S. J. Van Hoffelen, M. J. Young, M. A. Shatos, and D. S. Sakaguchi, "Incorporation of murine brain progenitor cells into the developing mammalian retina," *Investigative Ophthalmology and Visual Science*, vol. 44, no. 1, pp. 426–434, 2003.

[8] K. Warfvinge, J. F. Kiilgaard, E. B. Lavik et al., "Retinal progenitor cell xenografts to the pig retina: morphologic integration and cytochemical differentiation," *Archives of Ophthalmology*, vol. 123, no. 10, pp. 1385–1393, 2005.

[9] H. Klassen, J. F. Kiilgaard, T. Zahir et al., "Progenitor cells from the porcine neural retina express photoreceptor markers after transplantation to the subretinal space of allorecipients," *Stem Cells*, vol. 25, no. 5, pp. 1222–1230, 2007.

[10] H. Klassen, P. H. Schwartz, B. Ziaeian et al., "Neural precursors isolated from the developing cat brain show retinal integration following transplantation to the retina of the dystrophic cat," *Veterinary Ophthalmology*, vol. 10, no. 4, pp. 245–253, 2007.

[11] A. B. Wojciechowski, U. Englund, C. Lundberg, and K. Warfvinge, "Long-term survival and glial differentiation of the brain-derived precursor cell line RN33B after subretinal transplantation to adult normal rats," *Stem Cells*, vol. 20, no. 2, pp. 163–173, 2002.

[12] A. B. Wojciechowski, U. Englund, C. Lundberg, and K. Warfvinge, "Migratory capacity of the cell line RN33B and the host glial cell response after subretinal transplantation to normal adult rats," *GLIA*, vol. 47, no. 1, pp. 58–67, 2004.

[13] A. B. Wojciechowski, U. Englund, C. Lundberg, and K. Warfvinge, "Survival and long distance migration of brain-derived precursor cells transplanted to adult rat retina," *Stem Cells*, vol. 22, no. 1, pp. 27–38, 2004.

[14] R. M. Petters, C. A. Alexander, K. D. Wells et al., "Genetically engineered large animal model for studying cone photoreceptor survival and degeneration in retinitis pigmentosa," *Nature Biotechnology*, vol. 15, no. 10, pp. 965–970, 1997.

[15] M. O. M. Tso, W. W. Y. Li, C. Zhang et al., "A pathologic study of degeneration of the rod and cone populations of the rhodopsin Pro347Leu transgenic pigs," *Transactions of the American Ophthalmological Society*, vol. 95, pp. 467–483, 1997.

[16] Z. Y. Li, F. Wong, J. H. Chang et al., "Rhodopsin transgenic pigs as a model for human retinitis pigmentosa," *Investigative Ophthalmology and Visual Science*, vol. 39, no. 5, pp. 808–819, 1998.

[17] K.-W. Park, B. Kühholzer, L. Lai et al., "Development and expression of the green fluorescent protein in porcine embryos derived from nuclear transfer of transgenic granulosa-derived cells," *Animal Reproduction Science*, vol. 68, no. 1-2, pp. 111–120, 2001.

[18] H. Klassen, K. Warfvinge, P. H. Schwartz et al., "Isolation of progenitor cells from GFP-transgenic pigs and transplantation to the retina of allorecipients," *Cloning and Stem Cells*, vol. 10, no. 3, pp. 391–402, 2008.

[19] P. H. Schwartz, H. Nethercott, I. I. Kirov, B. Ziaeian, M. J. Young, and H. Klassen, "Expression of neurodevelopmental markers by cultured porcine neural precursor cells," *Stem Cells*, vol. 23, no. 9, pp. 1286–1294, 2005.

[20] H. Klassen and R. D. Lund, "Retinal graft-mediated pupillary responses in rats: restoration of a reflex function in the mature mammalian brain," *Journal of Neuroscience*, vol. 10, no. 2, pp. 578–587, 1990.

[21] D. A. Lamba, J. Gust, and T. A. Reh, "Transplantation of human embryonic stem cellderived photoreceptors restores some visual function in Crx-deficient mice," *Cell Stem Cell*, vol. 4, no. 1, pp. 73–79, 2009.

[22] R. E. MacLaren, R. A. Pearson, A. MacNeil et al., "Retinal repair by transplantation of photoreceptor precursors," *Nature*, vol. 444, no. 7116, pp. 203–207, 2006.

[23] M. W. Kelley, J. K. Turner, and T. A. Reh, "Regulation of proliferation and photoreceptor differentiation in fetal human retinal cell cultures," *Investigative Ophthalmology and Visual Science*, vol. 36, no. 7, pp. 1280–1289, 1995.

[24] D. A. Lamba, M. O. Karl, C. B. Ware, and T. A. Reh, "Efficient generation of retinal progenitor cells from human embryonic stem cells," *Proceedings of the National Academy of Sciences of the United States of America*, vol. 103, no. 34, pp. 12769–12774, 2006.

[25] F. Osakada, H. Ikeda, M. Mandai et al., "Toward the generation of rod and cone photoreceptors from mouse, monkey and human embryonic stem cells," *Nature Biotechnology*, vol. 26, no. 2, pp. 215–224, 2008.

[26] U. Aftab, C. Jiang, B. Tucker et al., "Growth kinetics and transplantation of human retinal progenitor cells," *Experimental Eye Research*, vol. 89, no. 3, pp. 301–310, 2009.

[27] H. Klassen and R. D. Lund, "Retinal transplants can drive a pupillary reflex in host rat brains," *Proceedings of the National Academy of Sciences of the United States of America*, vol. 84, no. 19, pp. 6958–6960, 1987.

[28] P. J. Coffey, R. D. Lund, and J. N. P. Rawlins, "Retinal transplant-mediated learning in a conditioned suppression task in rats," *Proceedings of the National Academy of Sciences of the United States of America*, vol. 86, no. 18, pp. 7248–7249, 1989.

[29] R. Banerjee and R. D. Lund, "A role for microglia in the maintenance of photoreceptors in retinal transplants lacking pigment epithelium," *Journal of Neurocytology*, vol. 21, no. 4, pp. 235–243, 1992.

[30] K. M. Whitworth, R. Li, L. D. Spate et al., "Method of oocyte activation affects cloning efficiency in pigs," *Molecular Reproduction and Development*, vol. 76, no. 5, pp. 490–500, 2009.

Hindawi Publishing Corporation
Stem Cells International
Volume 2012, Article ID 417865, 9 pages
doi:10.1155/2012/417865

Research Article

Derivation of Neural Progenitors and Retinal Pigment Epithelium from Common Marmoset and Human Pluripotent Stem Cells

Laughing Bear Torrez,[1] Yukie Perez,[1] Jing Yang,[2] Nicole Isolde zur Nieden,[1,3] Henry Klassen,[2] and Chee Gee Liew[1]

[1] *Stem Cell Center, Department of Cell Biology and Neuroscience, University of California, Riverside, Riverside, CA 92521, USA*
[2] *Gavin Herbert Eye Institute, Department of Ophthalmology, School of Medicine, University of California, Irvine, Irvine, CA 92697, USA*
[3] *Deptartment of Cell Therapy, Applied Stem Cell Technology Unit, Fraunhofer Institute for Cell Therapy and Immunology, Perlickstraße 1, 04103 Leipzig, Germany*

Correspondence should be addressed to Chee Gee Liew, duncan@ucr.edu

Received 2 October 2011; Accepted 28 November 2011

Academic Editor: Morten La Cour

Embryonic and induced pluripotent stem cells (IPSCs) derived from mammalian species are valuable tools for modeling human disease, including retinal degenerative eye diseases that result in visual loss. Restoration of vision has focused on transplantation of neural progenitor cells (NPCs) and retinal pigmented epithelium (RPE) to the retina. Here we used transgenic common marmoset (*Callithrix jacchus*) and human pluripotent stem cells carrying the enhanced green fluorescent protein (eGFP) reporter as a model system for retinal differentiation. Using suspension and subsequent adherent differentiation cultures, we observed spontaneous *in vitro* differentiation that included NPCs and cells with pigment granules characteristic of differentiated RPE. Retinal cells derived from human and common marmoset pluripotent stem cells provide potentially unlimited cell sources for testing safety and immune compatibility following autologous or allogeneic transplantation using nonhuman primates in early translational applications.

1. Introduction

Novel applications of stem-cell-based therapies have revolutionized how degenerative diseases are approached. Given the propensity of stem cells to differentiate to neuronal pathways, diseases affecting the nervous system and associated tissues, such as the retina, are of great value. Retinal diseases, such as age-related macular degeneration (AMD), retinitis pigmentosa, and Stargardt disease, that render individuals functionally blind are commonly the result of impaired or complete loss of function of the photoreceptor cells or supporting retinal pigmented epithelium (RPE) [1–3]. To support *in vivo* transplantation, a readily available and efficient protocol for obtaining donor neural retinal and RPE cells is required.

Previous studies have demonstrated the capacity of human embryonic stem cells (HESCs) and human-induced pluripotent stem cells (HIPSCs) to differentiate into cells with RPE morphology, function, and molecular phenotypes [4, 5]. Thus far, HESC-, HIPSC- and fetal-derived RPE have been used to study the extent to which transplantation can correct retinal degenerative diseases [2, 5]. Preclinical studies in dystrophic rats have reported the ability of HESC-derived RPE cells to rescue visual function [1].

Before HESC or HIPSC derivatives can be used in clinical settings, safety and reproducibility of these cells must be vigorously tested in animal models. Although the use of transgenic mice has been of great value in early studies, cross-species differences often hamper efficacy and risk assessment in preclinical studies and are generally inadequate for evaluation of immunological responses. On the other hand, nonhuman primates provide valuable, and infrequently exploited, tools for extension of rodent results in models potentially more relevant to regenerative medicine. Due to

their homology and highly similar physiology with humans, several species of monkeys have been used as preclinical nonhuman primate models. Recently, the common marmoset monkey (*Callithrix jacchus)* has been identified to be a cost-efficient and easily maintained nonhuman primate model of interest in biomedical research [6].

Derivation of Callithrix embryonic stem cells (CESCs) has opened up opportunities to study various aspects of early embryonic development pertinent to humans, as well as use of these cells to derive functional cell types for *in vitro* and *in vivo* studies [7, 8]. However there is a passage limit on long-term cultivation of CESC lines that have been created. It is therefore essential to utilize the lines that have been successfully derived in order to characterize their lineage-specific differentiation and explore their full potential.

Transgenic pluripotent stem cell lines carrying a marker gene are valuable for the study of differentiation potential and migration in host tissue. To test the function of transgenes in genetically modified ESCs, it is important to achieve stable gene expression during different stages of cell differentiation [9]. Here, we demonstrate the derivation of retina, including neural progenitor cells (NPCs) and retinal pigmented epithelium (RPE), from stable transfectants of both human and marmoset pluripotent stem cells carrying the enhanced green fluorescent protein (eGFP) reporter.

2. Materials and Methods

2.1. Derivation of Human Induced Pluripotent Stem Cells (HIPSCs). Foreskin fibroblast cells (ATCC) were propagated in Dulbecco's Modified Eagle Medium (DMEM) supplemented with 10% fetal bovine serum (FBS), 1 mM Glutamax-I, and 1 mM nonessential amino acid (NEAA). 293FT cells were used as a packaging, cell line for generating retroviruses. 293FT were transfected with FuGENE HD with pMXS-OCT4, -SOX2 or -KLF4 plasmid, pHIT60 packaging and pVSV-G envelope construct. Medium-containing retroviruses were collected two days after-transfection. Foreskin fibroblast cells were infected with retroviruses and maintained in a 5% O_2 incubator. Two days later, cells were replated on feeder layers and medium was changed to HIPSC medium (KnockOut DMEM/F12 supplemented with KnockOut Serum Replacement, 1 mM Glutamax-I, 1 mM NEAA, 55 mM 2-mercaptoethanol and 10 ng/mL FGF2). HIPSC colonies were picked using 200 μL pipette tips four weeks after-transduction and maintained on matrigel as feeder-free cultures in StemPro (Invitrogen) or mTESR medium (Stem Cell Technologies). For subcultivation, HIPSCs were treated with accutase (Invitrogen) for 1 min, harvested by centrifugation, and replated onto new matrigel-coated dishes in StemPro medium. All cell lines were maintained in 37°C and 5% CO_2.

2.2. Culture of Human Embryonic and Induced Pluripotent Stem Cells. Riv9 HIPSCs [10] were cultured in mTESR media (Stem Cell Technologies) on Geltrex-coated tissue-culture-treated dishes in 5% CO_2 and 37°C. Cells were subcultivated every 5–7 days upon reaching 80–90% confluency by gently dislodging colonies using accutase and 15 mm glass beads. mTESR media were replenished daily.

2.3. Culture of Callithrix Embryonic Stem Cells (CESCs). Cjes001 Callithrix embryonic stem cells (CESCs) [8] were maintained on irradiated mouse embryonic fibroblast (MEF) feeders in growth medium: knockout high glucose DMEM supplemented with 15% KOSR, 1% nonessential amino acids, 2 mM of Glutamax-I, 0.1 mM b-mercaptoethanol, and 10 ng/mL bFGF. The cells were routinely passaged with 0.25% trypsin/EDTA at a ratio of 1 : 5–1 : 8 every 5–7 days.

2.4. Differentiation of HESCs, HIPSCs, and CESCs. HESC and HIPSC cultures previously maintained in mTeSR were treated with rock inhibitor (RI) for 1 hour prior to dissociation into single cells with 0.25% trypsin/EDTA. Cells were resuspended in STEMPRO media lacking bFGF and replated onto non-tissue-culture-treated Petri dishes. Cjes001 cells were trypsinized, pelleted, and differentiated in CESC media lacking bFGF on non-tissue-culture-treated Petri dishes. The differentiating cells formed aggregates termed embryoid bodies (EBs), consisting of cells representative of three differentiated germ layers.

2.5. Nucleofection of HESC and HIPSCs. Trypsinized single-cell suspension was resuspended in 100 μL of prewarmed human stem cell nucleofector solution 1 (Lonza). The cells in human stem cell Nucleofector solution 1 were then transferred to a cuvette and 4 μg of plasmid DNA was added. The cuvette was gently swirled, tapped twice on the bench, inserted into the cuvette holder of the Lonza Amaxa Nucleofector II Device, and nucleofected using B-16 program. The nucleofected cells were recovered in prewarmed media and incubated at 37°C for 10 minutes prior to replating on feeder cells.

2.6. Flow Cytometry Analysis. Nucleofected cells were dissociated with 0.25% trypsin/EDTA. Cell pellets were then resuspended in 250 μL of wash buffer and subjected to flow cytometry on a SC Quanta flow cytometer (Beckman Coulter).

2.7. Reverse Transcription-Polymerase Chain Reaction (RT-PCR). Total RNA was isolated using the ZR RNA MicroPrep kit (Zymo Research). RNA concentration was measured using a NanoDrop spectrophotometer (Thermo Scientific). First-strand cDNA synthesis was performed using iScript cDNA Synthesis kit (Bio-Rad). Following cDNA synthesis semiquantitative RT-PCR was performed. Each RT-PCR reaction consisted of PCR master mix, 0.3 pM forward primer, and 0.3 pM reverse primer, and cDNA, RT-PCR amplifications were initiated at 95°C for 5 mins followed annealing and extension. The forward/reverse primers and annealing temp used for primate genes were ACTB 5′-ATC TGGCACCACACCTTCTACAATGAGCTGCG-3′z and 3′-CGTCATACTCCTGCTTGCTGATCCACATCTGC-5′, 58°C; LRAT 5′-CTCATCCTGGGCGTTATTGT-3′ and 3′-CCAGCCAT CCAT AGGA AGAA-5′, 49°C; NEUROD1 5′-AAGCCATGAACGCAGAGGAGGACT-3′ and 3′-AGCTGT-

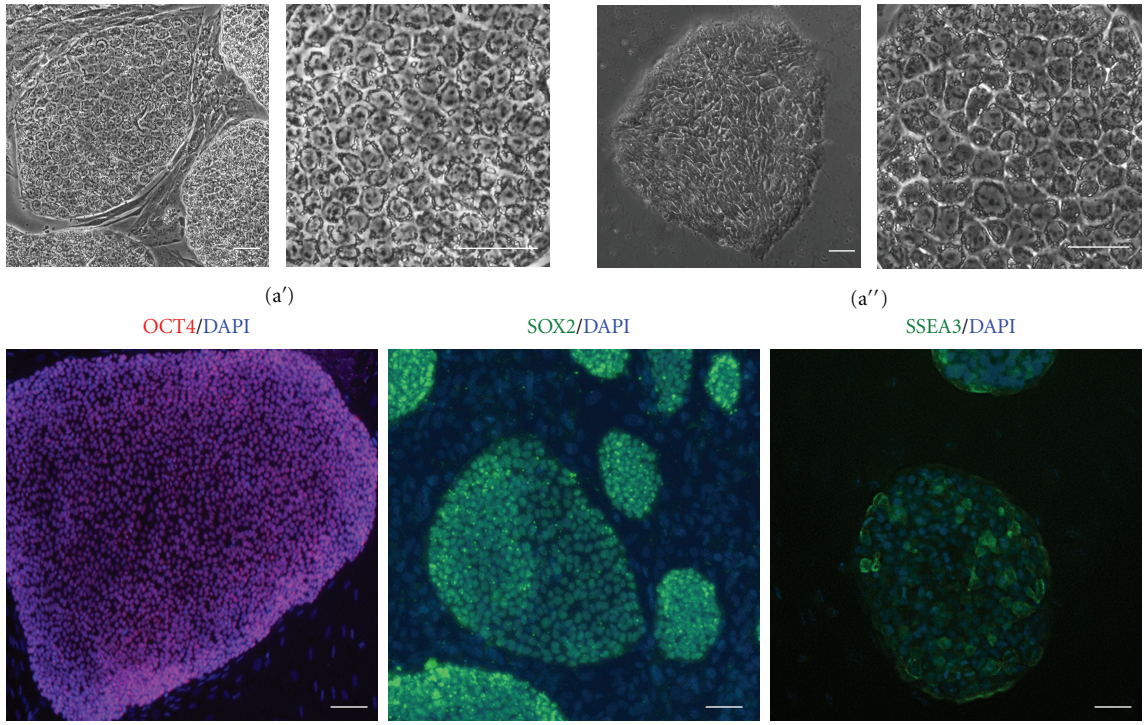

Figure 1: Cjes001 common marmoset embryonic stem cells (CESCs) closely resemble the morphology of human pluripotent stem cells. (a′) Colonies of CESCs grown on irradiated feeder cells (4x magnification, left) and morphology of individual CESCs at 20x magnification (right). (a′′) Morphology of Riv9 HIPSC colony (4x mag, left) and individual cells within the colony (20x, right). (b) Immunocytochemical analysis of CESCs showing nuclear localization of OCT4 (red), SOX2 (green), and stage-specific embryonic antigen-3 (SSEA3, green). Cell nuclei were counterstained with DAPI. Scale bars, 50 μm.

CCATGGTACCGTAA-5′, 55°C. Following RT-PCR amplification products were observed by gel electrophoresis on a flash gel (Lonza).

2.8. Real-Time Quantitative Polymerase Chain Reaction (Q-PCR) Analysis. Q-PCR was performed using the Assay-on-Demand technology (Applied Biosystems). Each reaction consisted of 2.5 μL of 2x TaqMan master mix, 0.25 μL of TaqMan probes, 1.25 μL of water, and 1 μL of cDNAs (100 ng, standardized based on housekeeping gene controls). PCR amplifications were initiated at 95°C for 10 mins followed by 42 cycles of 95°C for 15 seconds and 60°C for 60 seconds. PCR reactions for each sample were performed using 384-well real-time CFX384 thermocycler (BioRad). The Q-PCR data were analyzed using the comparative C_T method. Q-PCR was performed in duplicates from three different cDNA samples.

2.9. Immunocytochemistry. Cells were washed twice with PBS w/o Mg^{2+} and Ca^{2+} and fixed with 4% paraformaldehyde for 10 minutes. The fixed cells were then washed again with PBS w/o Mg^{2+} and Ca^{2+}. Next, fixed cells were blocked for 30 minutes with PBS w/o Mg^{2+}- and Ca^{2+}-based wash buffer containing 1% donkey serum and 0.1% Triton-X. Fixed cells were then incubated overnight at 4°C in primary antibodies: Vimentin, MAP2 (Cell Signaling), OCT4, GFAP (Santa Cruz), SOX2 (R&D Systems), SSEA3 (Millipore), and TUJ1 (Covance). After overnight incubation at 4°C, primary antibody solution was removed. Cells were subsequently washed twice with wash buffer. Secondary antibodies were then added to the stained cells in wash buffer and incubated in the dark at 25°C for 1 hour. Following secondary antibody incubation the cells were washed twice with wash buffer with a 5 min incubation step during each wash. Cells were mounted in DAPI mounting solution (Vectashield) and imaged using the Nikon Ti Eclipse and NIS-elements imaging software.

3. Results

3.1. Derivation of eGFP-Expressing Callithrix and Human Pluripotent Stem Cell Lines. Cjes001 Callithrix embryonic stem cells (CESCs) displayed similar morphology to Riv9 human induced pluripotent stem cells (HIPSCs; Figure 1(a′)). The undifferentiated cjes001 also expressed OCT4 and SOX2 transcription factors and stage-specific embryonic antigen-3 (SSEA3; Figure 1(b)). In these characteristics, marmoset ESCs closely resemble HIPSCs and HESCs [11]. In a pilot study, we compared the efficacy of the CMV and CAG promoters in deriving stable transfectants in cjes001 CESCs

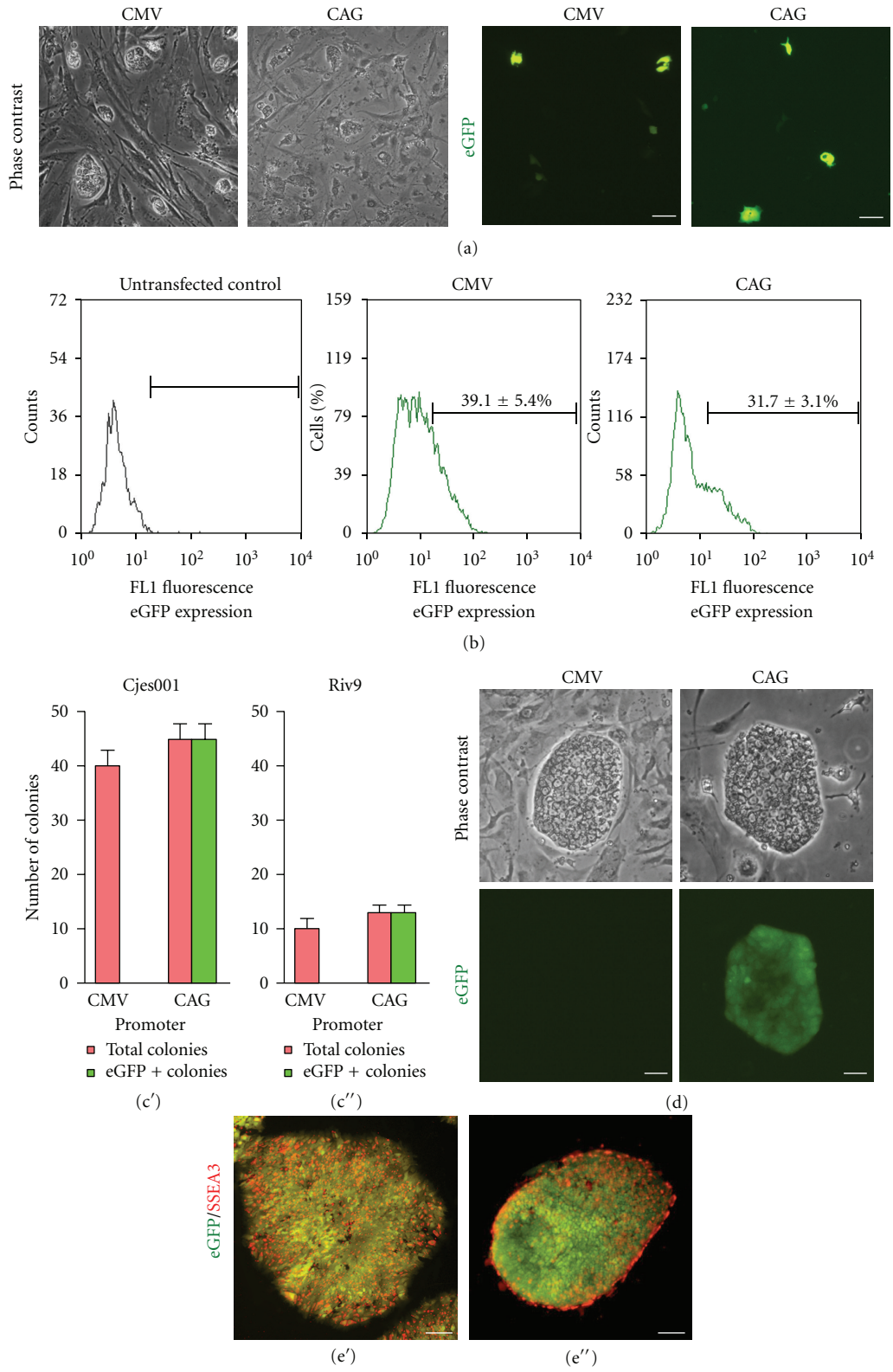

Figure 2: Transfection of cjes001 common marmoset CESCs and Riv9 HIPSCs. Micrographs (a) and FACS histograms (b) enumerating the percentage of eGFP-positive (eGFP +ve) cjes001 CESCs 24 hours after-transfection. (c) Numbers of drug-resistant and eGFP-expressing colonies formed after two weeks were scored for the stable transfection assay. (d) eGFP expression was lost in all pCMV-transfected clones. In contrast, all puromycin-resistant colonies were also eGFP +ve. Cjes001 (e′) and Riv9 clone (e″) retained ubiquitous and constitutive eGFP expression while continuously express undifferentiated stem cell marker SSEA3 (red). Scale bars, 50 μm.

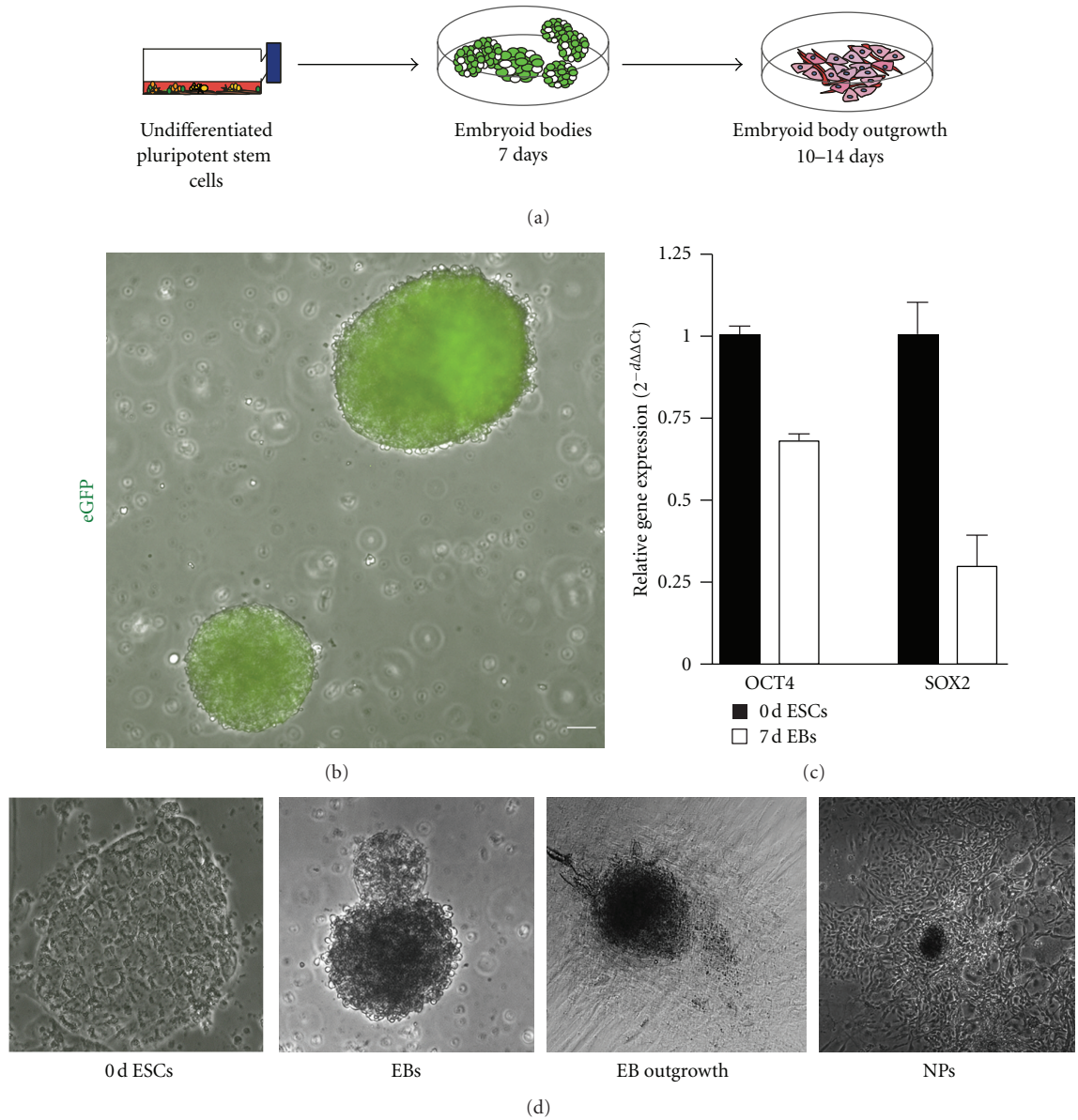

Figure 3: Differentiation of cell progenitors associated with the central nervous system (CNS) and the neural retina. (a) Experimental overview for *in vitro* differentiation of CESCs. (b) Constitutive eGFP expression in differentiated aggregates of cjes001 EBs. (c) Q-PCR analysis of OCT4 and SOX2 pluripotency markers in undifferentiated cjes001 (0-day ESCs) and 7-day EBs. (d) Changes in morphology during *in vitro* differentiation. Arrowheads indicate EB outgrowth observed 1 week after replating. Neurites resembling neural progenitors (NPs) were formed 10–14 days after replating. Scale bars, 50 μm.

and Riv9 HIPSCs. These two promoters were previously described as strong promoters in human embryonic stem cells (HESCs) and HIPSCs [10, 12], but their activities in CESCs were not known. Single-cell suspensions were nucleofected, replated on feeders, and examined for transient transfection efficiency the next day (Figure 2(a)). Flow cytometry analysis demonstrated that 39.1 ± 5.4% and 31.7 ± 3.1% cjes100 cells transfected with pCMV-eGFP and pCAG-eGFP expressed eGFP marker gene, respectively (Figure 2(b)). Thus our data suggests that marmoset ESCs yielded higher transient transfection efficiency compared to HIPSCs [10].

Stable transfectants that survived in the presence of antibiotic selection appeared within two weeks after-nucleofection. The frequency with which stably transfected clones could be recovered during the drug selection process varied among HIPSCs and CESCs. Optimal doses for drug selection were constructed from kill curves with Geneticin (G418) and puromycin. 500 μg/μL of G418 and 1.5 μg/μL puromycin were sufficient to select for transfectants in cjes001, while 200 μg/μL of G418 and 1 μg/μL of puromycin specifically selected for stable integrants in Riv9 with minimal background of nonresistant cells. We observed

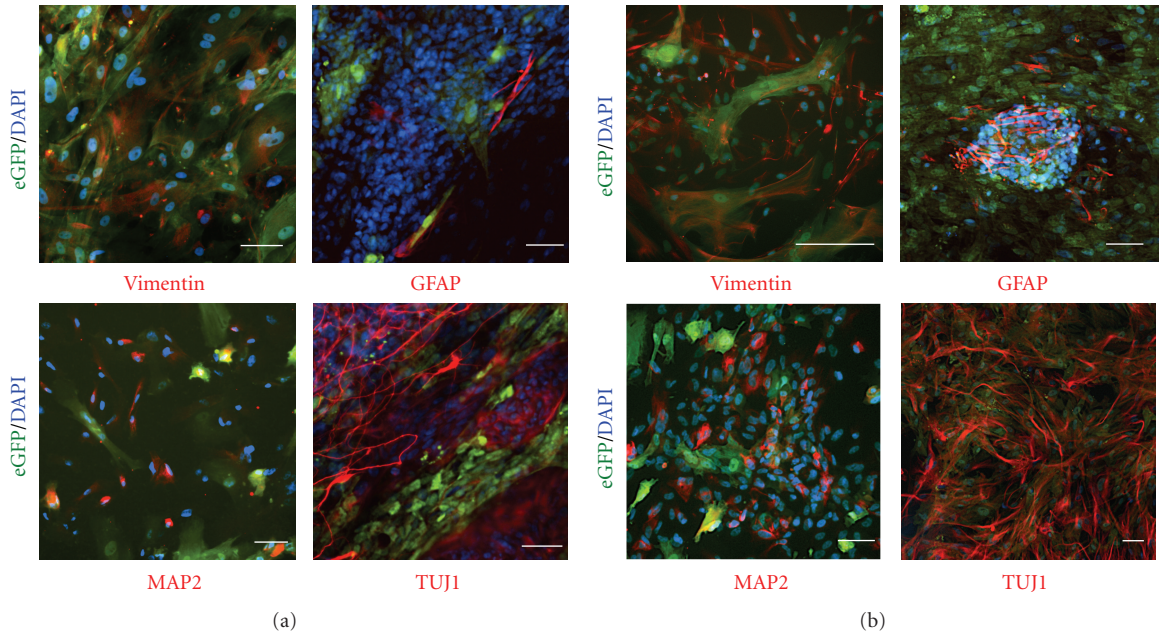

Figure 4: Expression of neural lineage-related cytoskeletal proteins in cjes001 CESCs (a), Riv9 HIPSCs (b). Immunocytochemistry using antibodies specific for neural markers are shown in red. Green fluorescence indicates eGFP expression in pCAG-transfected differentiated derivatives. Scale bars, 50 μm.

the presence of distinct eGFP-expressing colonies in pCAG-transfected Riv9 and cjes001 (Figures 2(c) and 2(d)). In contrast, none of the cells were eGFP positive in clones carrying the CMV promoter, confirming previous reports that CMV promoter is highly silenced in pluripotent stem cells [12]. These transgenic eGFP-expressing pCAG-transfected clones continued to express SSEA3 a month after cultivation (Figure 2(e)). Thus we demonstrated that transgenic HIPSCs and CESCs maintained their pluripotent potential.

3.2. Differentiation of Retinal Cell Precursors. We next sought to characterize the potential of these eGFP-expressing transgenic human and nonhuman primate ESCs to differentiate into cells related to retinal lineage. Cjes001 and Riv9 cells were detached, transferred to non-tissue-culture-treated dishes, and differentiated in media lacking bFGF to facilitate spontaneous differentiation of cells (Figure 3(a)). Suspension cultures prompted the formation of free-floating aggregates termed embryoid bodies (EBs). eGFP expression was retained in these cells during *in vitro* differentiation, indicating stable transgene integration (Figure 3(b)). Q-PCR analysis revealed downregulation of pluripotency markers OCT4 and SOX2 in EBs (Figure 3(c)).

To investigate the effect of transgene expression on central nervous system (CNS) and retinal differentiation, we replated EBs on matrigel for further differentiation in monolayer cultures. Cells spread out, expanded to monolayer as EB outgrowth, and readily underwent further differentiation (Figure 3(d)). Stably transfected eGFP-expressing cjes001 CESCs differentiated to neural progenitor cells (NPCs) following *in vitro* differentiation. Notably, cellular morphologies of cells were similar to those observed in primary or HESC-derived neural progenitor cultures [13, 14]. Immunocytochemistry analysis revealed the expression of markers representative of different stages of neural lineage commitment in EB outgrowth, including the immature neural cell marker Vimentin (Figure 4(a)). Cells from EB outgrowth also showed immunoreactivity for gial fibrillary acidic protein (GFAP), an intermediate filament specific for astrocytes in CNS and Muller cells in retina. Cells immunoreactive for cytoplasmic microtubule-associated protein 2 (MAP2) and β III-tubulin (TUJ1), two markers of committed neural cells, were first observed two weeks after replating.

We compared the propensity of neural and retinal lineage differentiation in marmoset cjes001 CESCs to Riv9 HIPSCs. Reminiscent of spontaneous differentiation in marmoset cells, human pluripotent stem cells gave rise to cells with neuron-like morphologies. Nevertheless, we observed an increase in Vimentin, MAP2, TUJ1, and GFAP protein expression in Riv9 EB outgrowth (Figure 4(b)). Neural clusters possessed long processes and intense filamentous staining for TUJ1, indistinguishable from those of HESCs [15, 16]. In addition, as they emerged, GFAP-expressing cells were self-organized into filamentous aggregates, suggesting a more mature differentiation stage of HIPSC-derived neural cells. Taken together, these results indicate that HESCs and HIPSCs were predisposed to differentiate towards a neural lineage compared to marmoset ESCs.

3.3. Isolation of Retinal Pigment Epithelium. We consistently observed the appearance of pigmented cell colonies during the cell outgrowth from the EB clusters in cjes001 and Riv9. This phenomenon was strikingly similar to previous observation of retinal pigmented epithelium (RPE) present

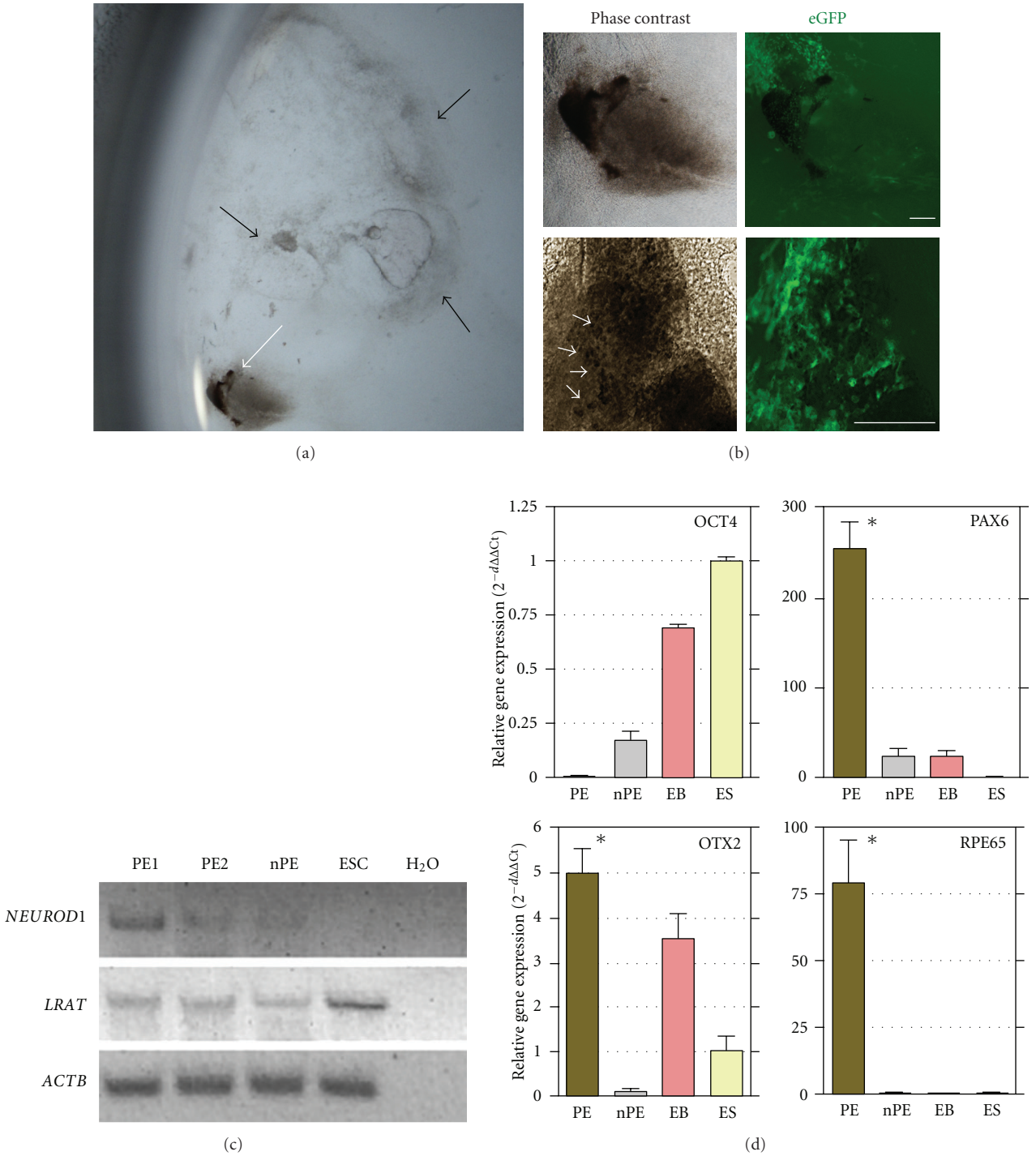

Figure 5: Differentiation of retinal pigmented epithelium (RPE) from Callithrix ESCs. (a) Stereoscopic image of cell outgrowth following EB replating. The white arrows indicate the visible pigmented area derived from an area of EB outgrowth. Black arrows indicate the colonies that did not develop to RPE structures. (b) Phase contrast and green fluorescence of the pigmented epithelium in RPE patch-like structures. The white arrowheads indicate the presence of putative RPE cells with typical pigmented cobblestone-like morphology. Scale bars, 200 μm. (c) Semiquantitative PCR analysis of manually picked clusters of pigmented epithelium (PE1 and PE2), nonpigmented cells (nPE), and undifferentiated ESCs. Water (H_2O) only was included as negative control. (d) Relative expression levels of OCT4, PAX6, OTX2s and RPE65 mRNA in PE, nPE, embryoid bodies (EB), and undifferentiated ES cells (ES). Mean normalized expression of each target gene is relative to ACTB and GAPDH housekeeping genes. Error bars represent standard deviation. Asterisk shows significant difference of PAX6, OTX2, and RPE65 expression in PE clusters, $P < 0.05$.

in confluent cultures derived from various HESCs and HIPSC lines [17, 18]. In our case, the most densely pigmented cells were located in the periphery of the EB clusters (Figure 5(a)). On average, less than 20% of cjes001 EB colonies differentiated to RPE structures. These CESC-derived pigmented cells exhibited cobblestone morphology, confirming the existence of RPE progenitors (Figure 5(b)).

To further examine the identity of these pigmented cells, we hand-picked and isolated the pigmented epithelium (PE) foci using pipette tips and examined the gene expression patterns. Although LRAT mRNA was observed in undifferentiated ESC sample, similar to previous report in HESCs [18], its expression was enriched in manually picked PE in comparison to nonpigmented area (nPE; Figure 5(c)). We also detected the expression of bHLH transcription factor NEUROD1, suggesting the presence of terminally differentiated neurons and thus the formation of an retina niche in the isolated PE cell layers. As revealed by quantitative PCR analysis, isolated RPE acquired expression for transcription factors associated with general neural retina induction (PAX6), eye field specification (OTX2), and retinal pigment epithelium (RPE65; Figure 5(d)). Notably, there was a complete loss of OCT4 mRNA expression in RPE, indicating the absence of residual undifferentiated stem cells.

4. Discussion

A key challenge in early translational research using human stem cells is the availability of a reliable host model to evaluate long-term benefits in clinical applications. Nonhuman primates are good candidates for testing the safety and feasibility of experimental protocols prior to cell replacement therapies in humans. Previous reports, as well as more recent studies, are beginning to reveal that stem cells can ameliorate the consequences of various degenerative diseases in nonhuman primates [19]. While the evidence for human pluripotent stem cell-derived retinal neural and RPE cells is burgeoning, the equivalent differentiation propensity in marmoset ESCs has not been previously explored.

The ability to genetically manipulate nonhuman primate embryonic stem cells is central in our efforts to harness their enormous potential for use in regenerative medicine. Whereas transgenic marmoset offspring have been generated using self-inactivating lentivirus [6], to our knowledge this study is the first to report derivation of transgenic Callithrix embryonic stem cell lines. Although lentiviral infection has proven efficient in generating stable integrants, its application can be hampered by several challenges such as size limitations on inserted DNA and the time-consuming production of vectors. Here we report that the use of a plasmid harboring the CAG promoter resulted in ubiquitous and highly stable eGFP expression in marmoset and human pluripotent stem cells. Our finding also underscores the importance of the choice of promoter in engineering stable cell lines, as the activity of the CMV promoter was completely silenced after several cell divisions.

The present study demonstrates the derivation of retinal neural cells and pigmented epithelium from stable eGFP-expressing transfectants. Our success with deriving transgenic Callithrix embryonic stem cell clones allows the use of these reporter cell lines to follow and track transplanted cells in preclinical studies. Furthermore, targeted gene knockdown could be developed using overexpression or short hairpin RNA interference (shRNAi) vectors [20] to study human diseases involving the loss of function of specific genes in nonhuman primates, including Huntington's disease [21], spinal cord injury [22], and Parkinson's disease [23].

Commitment toward retinal lineage occurs as a stepwise process. RPE, despite its nonneural phenotype, is anatomically and developmentally close to the neural retina [24]. Our results suggest that different types of neural cells in the retina, as well as RPE structures *in vitro*, result from a normal developmental pathway which can be replicated using marmoset and human pluripotent stem cells in suspension cultures. Consistent with Osakada's finding [25], we did not detect any RPE-like pigmented foci in cells directly differentiated from monolayer cultures. Our finding is a necessary prerequisite for therapeutic strategies based on cell enrichment from human and nonhuman primate ESCs as a source of donor retinal cell types.

In order to achieve the long-term goal of utilizing pluripotent stem cells from nonhuman primates, methods for optimizing NPCs and RPE formation from CESCs are required. We found that Riv9 HIPSCs showed a higher incidence of differentiation towards neural lineage, further supporting the notion that human pluripotent stem cells assume a default neural default pathway in the absence of extrinsic factors during *in vitro* differentiation [26]. Another possible explanation of lower neural commitment of cjes001 CESC line includes their readily enhanced differentiation potential into germ cells as previously reported [7]. Hence, early neutralization may increase the yield of neural precursors from cjes001 CESCs.

As ES cell lines are derived from a genetically heterogeneous population, there may be biological variations, heterogeneity, genetic, and epigenetic differences between different ESC lines. Our findings thus underscore the necessity of establishing and screening novel nonhuman primate stem cell lines for lineage-specific differentiation. Moreover, the availability of marmoset IPSCs [27] would accelerate the advance of preclinical studies in regenerative medicine, allowing the assessment of safety and efficacy of allogenic and xenogenic transplantation for various retinal degenerative diseases.

Acknowledgments

The authors are grateful to Jimmy To, Angela Wang, and Holly Eckelhoefer for assistance in cell cultures. This work was made possible by funding from the California Institute for Regenerative Medicine (CIRM) to the UCR Stem Cell Core.

References

[1] A. J. Carr, A. Vugler, J. Lawrence et al., "Molecular characterization and functional analysis of phagocytosis by human embryonic stem cell-derived RPE cells using a novel human retinal assay," *Molecular vision*, vol. 15, pp. 283–295, 2009.

[2] J. S. Meyer, R. L. Shearer, E. E. Capowski et al., "Modeling early retinal development with human embryonic and induced pluripotent stem cells," *Proceedings of the National Academy of Sciences of the United States of America*, vol. 106, no. 39, pp. 16698–16703, 2009.

[3] P. Bovolenta and E. Cisneros, "Retinitis pigmentosa: cone photoreceptors starving to death," *Nature Neuroscience*, vol. 12, no. 1, pp. 5–6, 2009.

[4] D. E. Buchholz, S. T. Hikita, T. J. Rowland et al., "Derivation of functional retinal pigmented epithelium from induced pluripotent stem cells," *Stem Cells*, vol. 27, no. 10, pp. 2427–2434, 2009.

[5] J. L. Liao, J. Yu, K. Huang et al., "Molecular signature of primary retinal pigment epithelium and stem-cell-derived RPE cells," *Human Molecular Genetics*, vol. 19, no. 21, Article ID ddq341, pp. 4229–4238, 2010.

[6] E. Sasaki, H. Suemizu, A. Shimada et al., "Generation of transgenic non-human primates with germline transmission," *Nature*, vol. 459, no. 7246, pp. 523–527, 2009.

[7] T. Müller, G. Fleischmann, K. Eildermann et al., "A novel embryonic stem cell line derived from the common marmoset monkey (Callithrix jacchus) exhibiting germ cell-like characteristics," *Human Reproduction*, vol. 24, no. 6, pp. 1359–1372, 2009.

[8] E. Sasaki, K. Hanazawa, R. Kurita et al., "Establishment of novel embryonic stem cell lines derived from the common marmoset (Callithrix jacchus)," *Stem Cells*, vol. 23, no. 9, pp. 1304–1313, 2005.

[9] S. Shiozawa, K. Kawai, Y. Okada et al., "Gene targeting and subsequent site-specific transgenesis at the β-actin (ACTB) locus in common marmoset embryonic stem cells," *Stem Cells and Development*, vol. 20, no. 9, pp. 1587–1599, 2011.

[10] P. Chatterjee, Y. Cheung, and C. Liew, "Transfecting and nucleofecting human induced pluripotent stem cells," *Journal of Visualized Experiments*, no. 56, article e3110, 2011.

[11] J. S. Draper, C. Pigott, J. A. Thomson, and P. W. Andrews, "Surface antigens of human embryonic stem cells: changes upon differentiation in culture," *Journal of Anatomy*, vol. 200, no. 3, pp. 249–258, 2002.

[12] C. G. Liew, J. S. Draper, J. Walsh, H. Moore, and P. W. Andrews, "Transient and stable transgene expression in human embryonic stem cells," *Stem Cells*, vol. 25, no. 6, pp. 1521–1528, 2007.

[13] H. Klassen, J. F. Kiilgaard, T. Zahir et al., "Progenitor cells from the porcine neural retina express photoreceptor markers after transplantation to the subretinal space of allorecipients," *Stem Cells*, vol. 25, no. 5, pp. 1222–1230, 2007.

[14] B. Y. Hu, J. P. Weick, J. Yu et al., "Neural differentiation of human induced pluripotent stem cells follows developmental principles but with variable potency," *Proceedings of the National Academy of Sciences of the United States of America*, vol. 107, no. 9, pp. 4335–4340, 2010.

[15] S. C. Zhang, M. Wernig, I. D. Duncan, O. Brüstle, and J. A. Thomson, "In vitro differentiation of transplantable neural precursors from human embryonic stem cells," *Nature Biotechnology*, vol. 19, no. 12, pp. 1129–1133, 2001.

[16] H. Liu and S.-C. Zhang, "Specification of neuronal and glial subtypes from human pluripotent stem cells," *Cellular and Molecular Life Sciences*, vol. 68, no. 24, pp. 3995–4008, 2011.

[17] Q. Hu, A. M. Friedrich, L. V. Johnson, and D. O. Clegg, "Memory in induced pluripotent stem cells: reprogrammed human retinal-pigmented epithelial cells show tendency for spontaneous redifferentiation," *Stem Cells*, vol. 28, no. 11, pp. 1981–1991, 2010.

[18] A. Vugler, A. J. Carr, J. Lawrence et al., "Elucidating the phenomenon of HESC-derived RPE: anatomy of cell genesis, expansion and retinal transplantation," *Experimental Neurology*, vol. 214, no. 2, pp. 347–361, 2008.

[19] A. Iwanami, S. Kaneko, M. Nakamura et al., "Transplantation of human neural stem cells for spinal cord injury in primates," *Journal of Neuroscience Research*, vol. 80, no. 2, pp. 182–190, 2005.

[20] G. Zafarana, S. R. Avery, K. Avery, H. D. Moore, and P. W. Andrews, "Specific knockdown of OCT4 in human embryonic stem cells by inducible short hairpin RNA interference," *Stem Cells*, vol. 27, no. 4, pp. 776–782, 2009.

[21] S. H. Yang, P. H. Cheng, H. Banta et al., "Towards a transgenic model of Huntington's disease in a non-human primate," *Nature*, vol. 453, no. 7197, pp. 921–924, 2008.

[22] A. Iwanami, J. Yamane, H. Katoh et al., "Establishment of graded spinal cord injury model in a nonhuman primate: the common marmoset," *Journal of Neuroscience Research*, vol. 80, no. 2, pp. 172–181, 2005.

[23] K. Ando, J. Maeda, M. Inaji et al., "Neurobehavioral protection by single dose l-deprenyl against MPTP-induced parkinsonism in common marmosets," *Psychopharmacology*, vol. 195, no. 4, pp. 509–516, 2008.

[24] L. Liang, R. T. Yan, W. Ma, H. Zhang, and S. Z. Wang, "Exploring RPE as a source of photoreceptors: differentiation and integration of transdifferentiating cells grafted into embryonic chick eyes," *Investigative Ophthalmology and Visual Science*, vol. 47, no. 11, pp. 5066–5074, 2006.

[25] F. Osakada, H. Ikeda, M. Mandai et al., "Toward the generation of rod and cone photoreceptors from mouse, monkey and human embryonic stem cells," *Nature Biotechnology*, vol. 26, no. 2, pp. 215–224, 2008.

[26] D. Kamiya, S. Banno, N. Sasai et al., "Intrinsic transition of embryonic stem-cell differentiation into neural progenitors," *Nature*, vol. 470, no. 7335, pp. 503–509, 2011.

[27] I. Tomioka, T. Maeda, H. Shimada et al., "Generating induced pluripotent stem cells from common marmoset (Callithrix jacchus) fetal liver cells using defined factors, including Lin28," *Genes to Cells*, vol. 15, no. 9, pp. 959–969, 2010.

Hindawi Publishing Corporation
Stem Cells International
Volume 2012, Article ID 604982, 9 pages
doi:10.1155/2012/604982

Research Article

Feline Neural Progenitor Cells II: Use of Novel Plasmid Vector and Hybrid Promoter to Drive Expression of Glial Cell Line-Derived Neurotrophic Factor Transgene

X. Joann You,[1] Jing Yang,[1] Ping Gu,[1,2] Chee Gee Liew,[3] and Henry J. Klassen[1,4]

[1] *The Gavin Herbert Eye Institute, School of Medicine, University of California, Irvine, Hewitt Hall, Rm. 2014, 843 Health Sciences Road, Irvine, CA 92697-1705, USA*
[2] *Department of Ophthalmology, Shanghai Ninth People's Hospital, Shanghai Jiao Tong University, School of Medicine, Shanghai 200011, China*
[3] *Stem Cell Center, Department of Cell Biology and Neuroscience, University of California Riverside, Riverside, CA 92521, USA*
[4] *University of California, Irvine, Hewitt Hall, Rm. 2014, 843 Health Sciences Road, Irvine, CA 92697-1705, USA*

Correspondence should be addressed to Henry J. Klassen, hklassen@uci.edu

Received 14 September 2011; Accepted 8 January 2012

Academic Editor: Morten La Cour

Sustained transgene expression is required for the success of cell transplant-based gene therapy. Most widely used are lentiviral-based vectors which integrate into the host genome and thereby maintain sustained transgene expression. This requires integration into the nuclear genome, and potential risks include activation of oncogenes and inactivation of tumor suppressor genes. Plasmids have been used; however lack of sustained expression presents an additional challenge. Here we used the pCAG-PyF101-eGFP plasmid to deliver the human GDNF gene to cat neural progenitor cells (cNPCs). This vector consists of a CAGG composite promoter linked to the polyoma virus mutant enhancer PyF101. Expression of an episomal eGFP reporter and GDNF transgene were stably maintained by the cells, even following induction of differentiation. These genetically modified cells appear suitable for use in allogeneic models of cell-based delivery of GDNF in the cat and may find veterinary applications should such strategies prove clinically beneficial.

1. Introduction

Transplantation of neural stem or progenitor cells for treatment of neurodegenerative diseases is an approach that has shown considerable promise in a variety of animal models (as reviewed by [1–4]). One region of the central nervous system (CNS) where particular progress has been notable is the retina, where cells of this type have been shown to integrate into immature neonatal [5], as well as mature degenerative [6] host rats, and exhibit morphological profiles suggestive of resident local neurons. Studies of this type have also been extended to nonrodent species, including the immature Brazilian opossum [7] and the dystrophic Abyssinian cat [8]. Throughout this work, transplantation of neural progenitor cells (NPCs) to the retina has been shown to be well tolerated in allogeneic models [9] and even some xenogeneic situations [7]. Survival of NPCs as grafts does not therefore routinely require systemic immune suppression, although exceptions certainly exist, as has been clearly documented [10, 11].

The results of the above work with NPC transplantation to the eye, together with a substantial volume of related studies, have helped to nurture enthusiasm for the translational development of this technology. The goal of these efforts is the treatment of a range of conditions affecting the retina, for which current clinical outcomes frequently leave room for improvement and many of which remain incurable, despite impressive recent pharmacological advances. The abilities of NPCs to be expanded in culture, integrate into retinal tissue, survive without immune suppression, and differentiate in presumptive retinal cell types all represent favorable characteristics for a donor cell type to possess. However, the

apparent inability of NPCs to generate photoreceptor cells [6], at least in sizeable numbers [7], does restrict their use as a means of cell replacement in the retina. This constraint does not mitigate their potential effectiveness in an alternate role, namely, as delivery vehicles for neuroprotective cytokines.

Neurotrophic factors contribute greatly to promoting cell survival of specific neurons in the CNS. Among the most potent for this purpose are glial cell line-derived neurotrophic factor (GDNF), brain-derived neurotrophic factor (BDNF), and ciliary neurotrophic factor (CNTF). Among these, GDNF is known to be antiapoptotic [12] in the brain [13, 14], spinal cord [15], and retina [16–19]. Receptors for GDNF are known to be expressed by cells of the mature retina [16, 19, 20]. Several types of stem and progenitor cells have been genetically modified to overexpress neurotrophic factors, resulting in enhanced levels of growth factor secretion and an enhanced ability to rescue retinal neurons and preserve visual function following transplantation to animal models of retinal injury and disease [21]. Neural progenitor cells derived from the human cerebral cortex that had been genetically modified to overexpress GDNF showed considerable efficiency in delaying neural degeneration [22], and the same strategy has been investigated in the retina [23].

Viral vectors have been widely used for transgene delivery [24] and are currently regarded as the most efficient method. However their use is limited due to safety issues, DNA loading capacity, and difficulties in scale-up for production. An alternate approach that does not require integration of the gene into the genome and therefore avoids the risk of insertional mutagenesis is the use of autonomously replicating plasmids or episomes (as reviewed by [25]). In episomally replicating plasmids, sequences of incorporated DNA (generally viral) enable the plasmid to replicate extrachromosomally. This poses several advantages over integrating systems: (1) the transgene cannot be interrupted or subjected to regulatory constraints that often occur with integration into cellular DNA; (2) higher transfection efficiency can be obtained than with chromosome-integrating plasmids; (3) episomes display a low mutation rate and tend not to rearrange [26]; (4) episomally replicating systems have the ability to transfer larger amounts of DNA [27].

In the present study, we explore the efficiency of nonviral plasmid vector pCAG-PyF101-eGFP mediated gene delivery in NPCs of feline origin. This plasmid consists of the CAGG composite promoter derived from the fusion of the human cytomegalovirus major immediate early enhancer (HCMV-MIE), chicken β-actin promoter, and rabbit globin intron sequence [28] that drives the expression of a transgene linked to a downstream internal ribosomal entry site (IRES) and a drug selection cassette. This plasmid has previously been shown to resist gene silencing in murine and human embryonic stem cells [29, 30]. Importantly, the inclusion of a virus mutant polyoma enhancer sequence, PyF101, ensures continuous transgene expression in the absence of drug selection [29]. To assess whether an efficient transgene delivery and persistence transgene expression can be achieved in neural progenitor cells, we first overexpressed the eGFP reporter gene in cNPCs as a proof of principle. Here we show that eGFP can be efficiently delivered to cNPCs using regular transfection methods. These cells continued to express eGFP for more than 60 days without significant loss of the eGFP expression. We then overexpressed GDNF in cNPCs and showed that transgenic cNPCs produced elevated levels of GDNF in the culture media and retained their identity of neural progenitors.

2. Material and Methods

2.1. Culture of Cat Neural Progenitor Cells (NPCs). Primary cNPCs were derived from the brains of 47-day cat fetuses as previously described [8]. For the present work, a frozen sample of cNPCs at passage 9 (P9) was thawed and cultured in Ultraculture medium (Lonza, Walkersville, MD), supplemented with 2 mM L-glutamine, 20 ng/mL epidermal growth factor (human recombinant EGF; Invitrogen, Carlsbad, CA), and 20 ng/mL basic fibroblast growth factor (human recombinant bFGF; Invitrogen). The complete Ultraculture-based medium is designated UM. Cells were passaged every 3-4 days.

2.2. Transfection of cNPCs with pCAG-PyF101-eGFP. The pCAG-PyF101-eGFP plasmid was purified using a QIAprep spin maxiprep kit (QIAGEN, Valencia, CA). Plasmid transfection was performed using Lipofectamine 2000 reagent (Invitrogen, Carlsbad, CA) following the manufacturers' instructions. Briefly, 2 million cNPCs were seeded into a T25 culture flask and allowed to grow overnight. Separately, 8 mg of plasmid DNA and 20 uL of Lipofectamine 2000 reagent were each individually diluted in 0.5 mL of Ultraculture-based proliferation medium (UM, as described above), mixed, and allowed to stand for 5 min. The diluted DNA and Lipofectamine 2000 were then combined, mixed, and allowed to stand for another 20 min. Meanwhile, the T25 flask containing cNPCs was washed once with fresh UM, which was replaced entirely with another 2 mL of fresh UM. The transfection mixture was added dropwise and mixed. The flask was kept in a cell culture incubator under standard conditions (37°C, 5% CO_2) for 48 h. Cells were subsequently reseeded into two T25 flasks, and selection was performed via the addition of 1.0 ug/mL puromycin to the culture medium for a duration of at least two weeks. The expression of eGFP by transfected cNPCs was monitored by fluorescence microscopy and photographed daily.

2.3. pCAG-PyF101-GDNF Plasmid Construction and Transfection of cNPCs. To construct pCAG-PyF10-GDNF, the original plasmid pCAG-PyF101-eGFP was digested with NotI/XhoI. The digested eGFP fragments were excised and replaced with human GDNF BstbI/NotI fragment from pEX-Z0010-Lv31 (GeneCopoeia, Germantown, Maryland) by blunt ends ligation. pCAG-PyF101-GDNF transfection of cNPCs was performed in the same manner used for pCAG-PyF101-eGFP, as described above.

2.4. Cell Growth Assessment Using IncuCyte Live Cell Monitoring System. The growth properties of pCAG-PyF101-GDNF

Table 1: Primary antibodies used for immunocytochemistry on cNPCs.

Target	Antibody type	Reactivity in retina	Source	Dilutions
Nestin	Mouse monoclonal	Progenitors, reactive glia	BD	1 : 200
Vimentin	Mouse monoclonal	Progenitors, reactive glia	Sigma	1 : 200
Ki-67	Mouse monoclonal	Proliferating cells	BD	1 : 200
GFAP	Mouse monoclonal	Astrocytes, reactive glia	Chemicon	1 : 200
β3-tubulin	Mouse monoclonal	Immature neurons	Chemicon	1 : 200
GDNF	Rabbit polyclonal	Growth factor	SCBT	1 : 200

transfected and nontransfected cNPCs were assessed by culturing cells under proliferation conditions in ultraculture-based medium (UM). Cells of identical passage number (P17) were seeded in a 24-well plate at a density of 40,000 cells/well. Cells were photographed and counted at 24 h intervals, based on 2 distinct measures, namely, nuclear counts and percentage confluency. Both parameters were measured using an IncuCyte (Essen Instruments, Ann Arbor, Michigan) live cell monitoring system installed within the incubator. For nuclear counts, triplet wells were labeled using the nuclear-specific fluorescent dye Vybrant DyeCycle Green Stain (Molecular Probes, Invitrogen), which binds to double-stranded DNA in viable cells. The dye was added to cultures 30 min prior to assessment and nuclear profiles counted using the proprietary IncuCyte program at 24, 48, 72, and 96 h after seeding of cells. Cells were also measured by percentage confluency at the same time points, again using the proprietary IncuCyte program.

2.5. Differentiation of cNPCs In Vitro. To differentiate cNPCs, the cells were cultured in ultraculture-based medium containing 10% FBS but not recombinant growth factors (UM-FBS) for a period of 5–15 days, prior to further analysis via FACS, ICC, or ELISA.

2.6. Fluorescence-Activated Cell Sorting (FACS) Analysis. For FACS analysis, puromycin-selected pCAG-PyF101-eGFP transfected and nontransfected cNPCs were seeded in T25 flasks (0.25 million cells/flask) and cultured for 7 days in either UM or UM-FBS. Cells were then harvested and filtered through cell strainer caps (35-μm mesh) to obtain a single-cell suspension (approximately 10^6 cells/mL). Cells were analyzed in an automated manner using a FACSAria (BD Biosciences, San Diego, CA) and FACSDiva software (BD Biosciences), without need for cell labeling or nuclear dyes. The GFP fluorochrome was excited by this instrument's standard 488 nm laser, while fluorescence was detected using a 510/20 filter.

2.7. ELISA Analysis. Plasmid pCAG-PyF101-GDNF transfected cNPCs were cultured in UM or UM-FBS, and the effects of differentiation on transgene expression were assessed by ELISA. In the case of undifferentiated cNPC controls, cells were seeded in T25 culture flasks in UM and allowed to grow for one or three days. At the end of days 1 and 3, culture media were replaced with 4 mL of fresh UM. Twenty four hours later, conditioned media were collected, and cultured cells were counted and collected at days 2 and 4 for ELISA analysis. For differentiated cNPCs, cells were seeded in T75 culture flask and cultured in UM-FBS for 7 days. Fresh UM-FBS medium was exchanged at day 6, and, 24 h later, conditioned medium was collected for ELISA analysis. Cells were also counted and collected for ELISA.

ELISA analysis was performed using a human GDNF DuoSet ELISA kit and protocol from R and D systems (Minneapolis, MN). Wells of microtiter plates were coated (overnight, room temperature) with 2 μg/mL of GDNF capture antibody in 100 μL of coating buffer (0.05 M Na_2CO_3, 0.05 M $NaHCO_3$, pH 9.6). Blocking was performed with 1% BSA in PBS for 1 h at room temperature. Samples (100 μL) were loaded in triplicates and incubated for 2 h at room temperature, followed by the addition of 100 μL antibody detection antibody (0.1 μg/mL) for additional 2 h at room temperature. HRP-conjugated streptavidin (1 : 200) in blocking buffer was added (20 min, room temperature), and the reaction was visualized by the addition of 100 μL of substrate solution and incubation for 20 min. The reaction was stopped with 50 μL H_2SO_4, and absorbance at 450 nm was measured with reduction at 540 nm using an ELISA plate reader. Plates were washed five times with washing buffer (PBS, pH 7.4, containing 0.1% (v/v) Tween 20) after each step. As a reference for quantification, a standard curve was established by a serial dilution of recombinant GDNF protein (31.25 pg/mL–2.0 ng/mL).

2.8. Immunocytochemistry. Transfected and nontransfected cNPCs were seeded on 4-well chamber slides (Nalge Nunc International, Rochester, NY) and allowed to grow for 3–5 days. Cells were fixed with freshly prepared 4% paraformaldehyde (Invitrogen, Carlsbad, CA) in 0.1 M phosphate-buffered saline (PBS) for 20 min at room temperature and washed with PBS. Cells on slides were incubated in antibody blocking buffer (PBS containing 10% (v/v) normal goat serum (NGS) (BioSource, Camarillo, CA), 0.3% Triton X-100, 0.1% NaN3 (Sigma-Aldrich, Saint Louis, MI)) for 1 h at room temperature. Slides were then incubated with primary antibodies at proper dilutions (Table 1) overnight at 4°C. The next morning, after washing, slides were incubated in fluorescent-conjugated secondary antibody (Alexa Fluor546-goat anti-mouse/rabbit, 1 : 800 in PBS, BD) for 1 h at room temperature. After an additional wash, slides were mounted using DAPI-containing Vectashield Hard Set

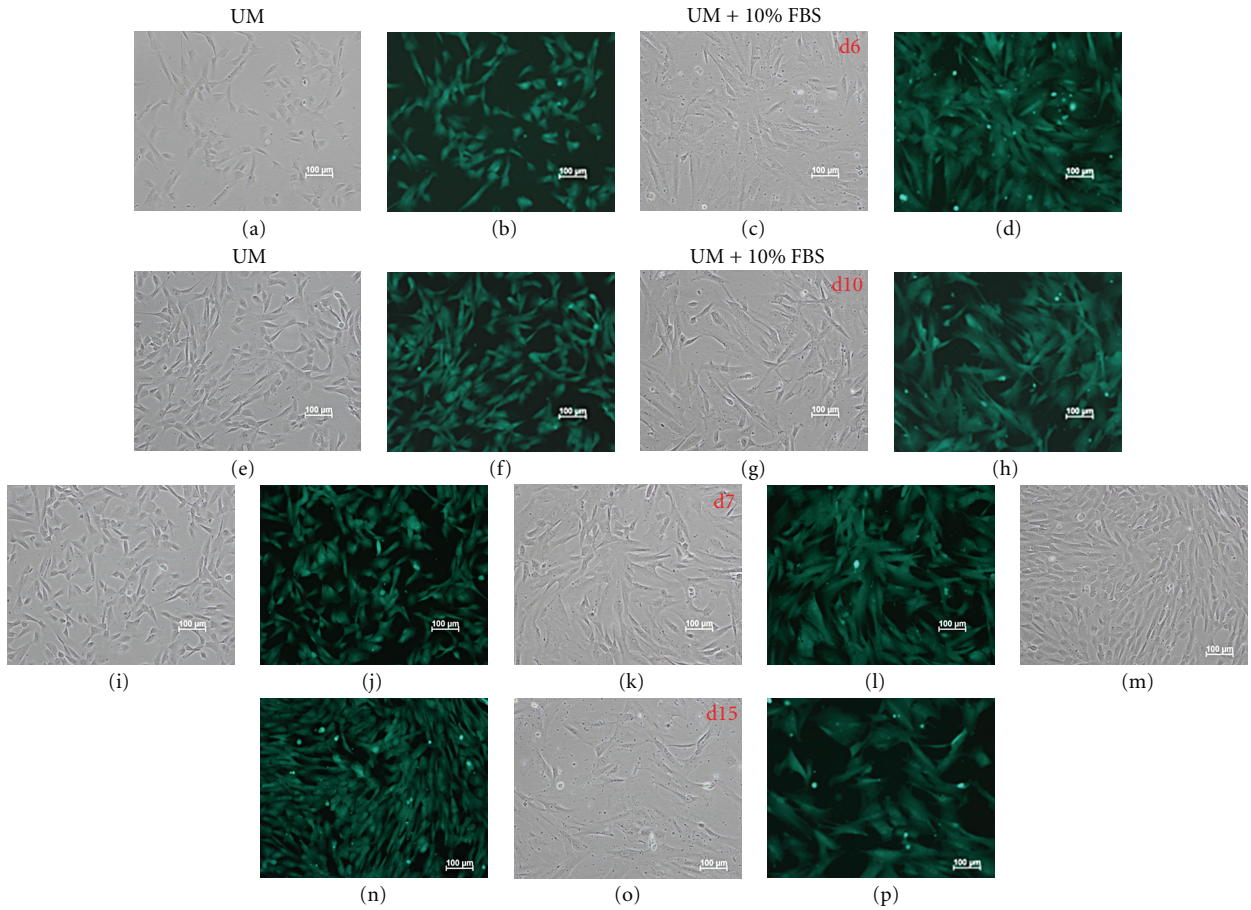

Figure 1: GFP expression in cNPCs transfected with pCAG-PyF101-eGFP plasmid. Transfected cNPC (passage 21) were maintained under proliferation conditions (UM) or switched to growth factor-free differentiation conditions (UM + 10% FBS) to evaluate potential loss of transgene expression. Cultures were photographed at 6, 7, 10, and 15 days. Sustained expression of green fluorescence protein (GFP) was observed for both conditions at all time points. Paired images are shown for each time point and include phase contrast (a, c, e, g, i, k, m, o) and fluorescence (b, d, f, h, j, l, n, p) micrographs of the same areas in culture.

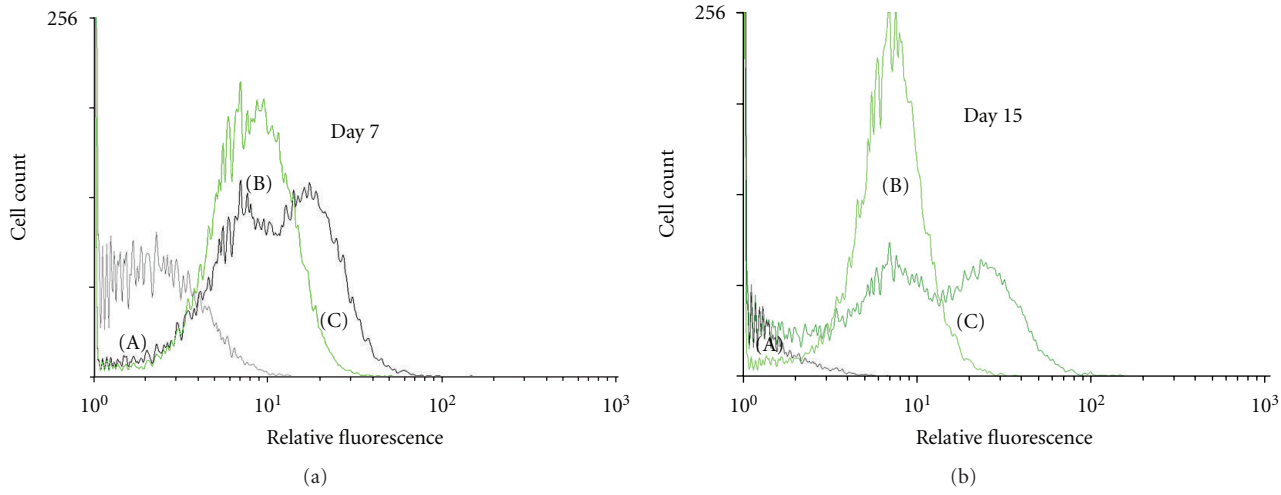

Figure 2: FACS analysis of GFP expression in nontransfected and transfected cNPCs. FACS analysis was performed on nontransfected and transfected cNPCs to show the expression of the GFP reporter gene. The vertical axis shows cell count, and the horizontal axis shows relative fluorescence. (a) Nontransfected cNPCp25 cultured in UM; (b) transfected cNPCp25 cultured in UM; (c) transfected cNPCp25 cultured in UM containing 10% FBS for 7 days (a) and 15 days (b).

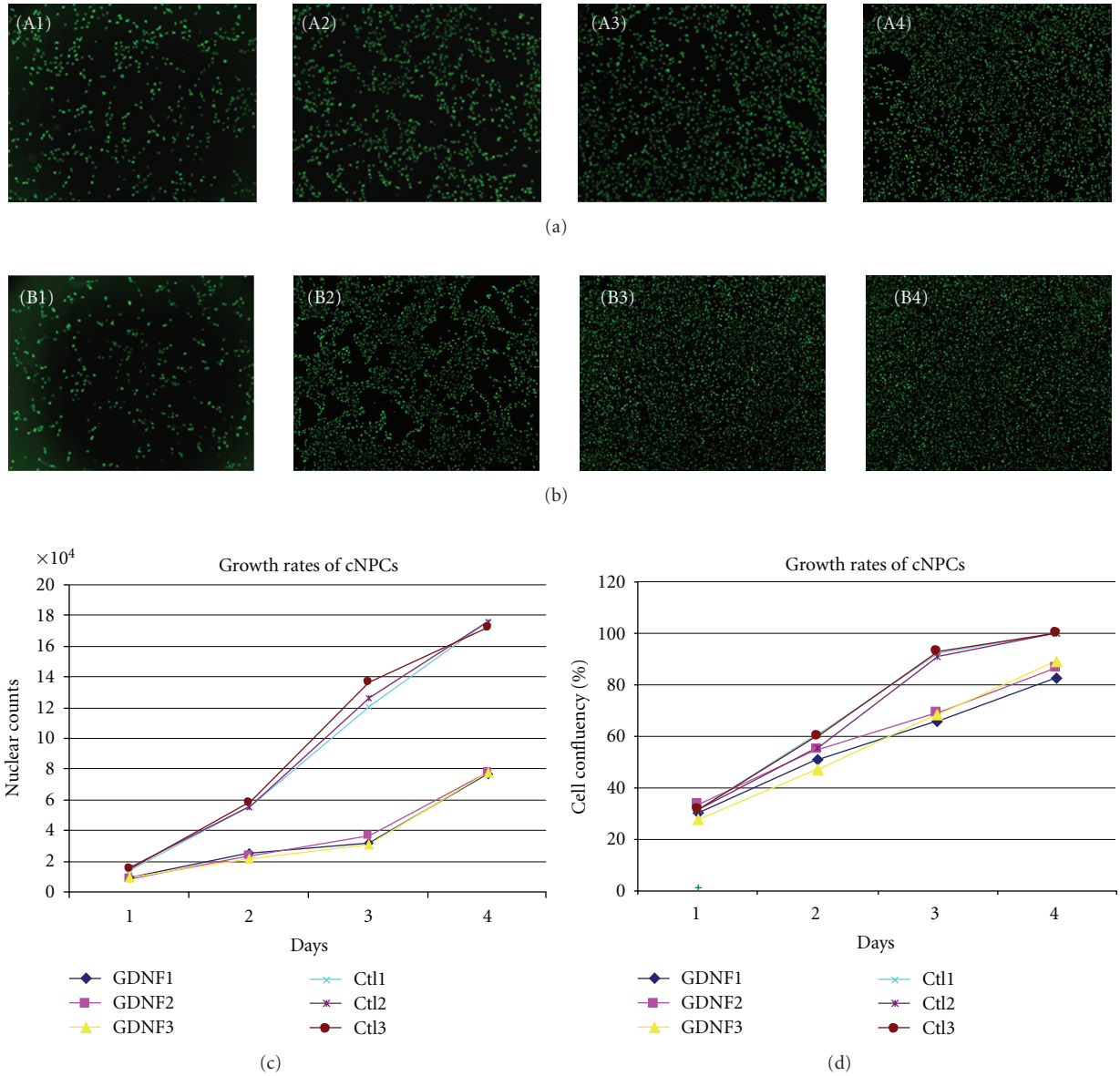

Figure 3: Growth of nontransfected and pCAG-PyF101-eGDNF plasmid transfected cNPCs. The fluorescence stained nuclei of (a) transfected and (b) nontransfected cNPCs. cNPCs were cultured in 24-well plate in UM for 4 days. Cells were labeled with a marker for nuclear DNA, and an IncuCyte live cell monitoring system was used to assess the growth rate of cells on each day. (a) GDNF-transfected cNPCs; A1–4: Day1–4. (b) Nontransfected cNPCs; B1–4: Day1–4. (c, d) Growth curves of GDNF-transfected and nontransfected cNPCs (labeled GDNF and Ctl, resp.) imaged and analyzed using an IncuCyte live cell monitoring system. Cells were stained with Vybrant Dycycle fluorescence nuclear-specific dye daily for 4 consecutive days (c). At the same time, cells in duplicate sets of wells without nuclear stain were measured for percentage cell confluency (d). The tight grouping of control data in (d) makes it difficult to discern Ctl1, which is present in the upper group and reaches confluence rapidly along with the other nontransfected cNPCs. IncuCyte programs were used for both analyses (c, d).

Mounting Medium (Vector laboratories, Burlingame, CA) for 20 min at room temperature. Negative controls for immunolabeling were performed in parallel using the same protocol but without primary antibody. Fluorescent labeling was judged as positive only with reference to the negative controls. Immunoreactive cells were visualized and imaged using a Nikon fluorescent microscope (Nikon, Eclipse E600, Melville, NY).

3. Results

3.1. Ubiquitous and Constitutive Reporter Gene Expression in eGFP-Transfected cNPCs. Expression of eGFP in pCAG-PyF101-eGFP transfected cNPCs was monitored by fluorescence microscopy to assess the transfection efficiency of the plasmid vector. Transfected cells began to exhibit eGFP-related fluorescence at 18 h following-transfection.

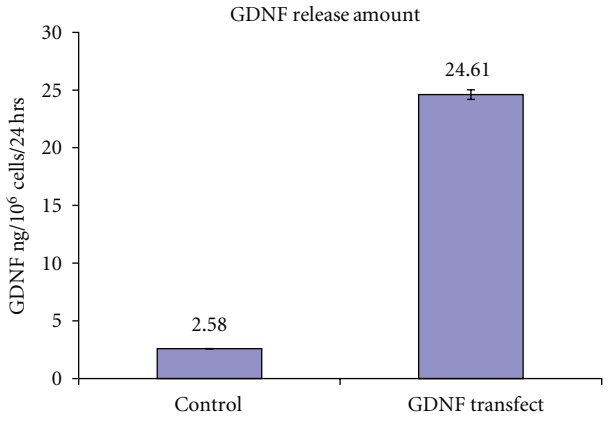

Figure 4: The amount of GDNF produced by nontransfected and transfected cNPCs measured by ELISA. Nontransfected and transfected cNPCs were seeded in UM. Culture media were refreshed 24 hours prior to collection of conditioned media for ELISA. Samples of culture media conditioned by transfected or control cells were analyzed to determine the level of GDNF present. Error bars = SEM.

The percentage of cells expressing eGFP reached approximately 40% by day 3. At the end of day 3, cells were reseeded, and puromycin (1 ug/mL) was added to the culture medium in order to select for stable transfectants. After 2 weeks of drug selection, a preponderance of the surviving cells expressed eGFP (as demonstrated by FACS analysis below). Continued propagation of these cells in UM for more than 60 days showed that eGFP expression was ubiquitously retained in the cells.

3.2. Sustained eGFP Transgene Expression under Differentiation Conditions. To evaluate the influence of cellular differentiation on transgene expression, transfected cNPCs (at P21) were cultured in UM containing 10% FBS for at least two weeks. Fluorescence microscopy detected eGFP expression in almost every cell, indicating that the transfection procedure was efficient and that the pCAG-PyF101-eGFP plasmids were stably maintained and actively transcribed without significant attenuation due to cell division or growth under *in vitro* differentiation conditions (Figure 1).

Flow cytometric analysis was performed to further confirm eGFP expression in transfected cNPCs. Almost all transfected cNPCs cultured in either UM or UM containing 10% FBS (differentiation medium) expressed eGFP (Figure 2). Interestingly, eGFP fluorescence intensity increased in transfected cells cultured in UM containing 10% FBS. We also detected two subpopulations of transfected cells that expressed eGFP at different levels ("high" and "medium high"). This observation may relate to the heterogenous morphology and size distribution of differentiating cells, some of which are larger in size which might serve to dilute the eGFP concentration within the cell.

3.3. Overexpression of GDNF in cNPCs. To further demonstrate the application of the pCAG vector for efficient transgene delivery beyond an eGFP reporter, we next overexpressed human GDNF in cNPCs. The effect of transduction on cellular proliferation was evaluated using an IncuCyte live cell monitoring system, allowing sequential observation of cell number in undisturbed cultures (Figures 3(a) and 3(b)). Both transfected and nontransfected cNPCs were seeded in 24-well plates in UM. Cell numbers were evaluated in terms of nuclear count and assessment of relative confluence (percentage). The resulting data showed that transfected cNPCs continued to proliferate, albeit at a slower rate than that of nontransfected cNPCs (Figures 3(c) and 3(d)). Interestingly, the monolayer cultures of the GDNF-transfected cNPCs appeared to be healthier, with fewer floating cells, less cell clumps, and minimal evidence of cell death.

3.4. Confirmation of Increased GDNF Protein Production by Transfected cNPCs. The levels of GDNF produced by GDNF-transfected cNPCs were measured by ELISA. Cells were cultured in UM or UM containing 10% FBS, and fresh media were added 24 hours prior to collection of conditioned media for ELISA analysis. The data showed that GDNF-expressing cNPCs produced large amount of GDNF, even 60 days after initial transfection. In addition, cells cultured in UM as well as those cultured in UM containing 10% FBS produced similar amounts of GDNF (Figure 4), indicating that GDNF expression was maintained under in vitro differentiation conditions. We also determined the level of GDNF present within transfected cells. ELISA indicated that intracellular GDNF level was low (<10 ng/10^6 cells/day, data not shown) compared to the amount of GDNF present in culture media (227–258 ng/10^6 cells/day). Therefore the majority of GDNF produced was secreted into the culture media.

3.5. Immunocytochemistry Confirms GDNF and Absence of Treatment-Related Changes in cNPCs. Immunocytochemical analysis was performed to confirm elevated GDNF protein expression within treated cNPCs and to evaluate the potential effects of pCAG transduction and GDNF overexpression on the ontogenetic status and lineage potential of the cells. First, an anti-GDNF antibody was used to detect GDNF protein in transfected cNPCs (Figure 5). This showed that GDNF expression was modest in nontransfected cNPCs (Figure 5(a)), but was strongly expressed in the transfected cells (Figure 5(b)). Although GDNF protein was also prominent in FBS-treated cNPCs, the fluorescence level was weaker, implying a more dilute distribution of GDNF, perhaps reflecting the larger size of the differentiating cells (Figure 5(c)).

Immunocytochemical analysis of a range of neural progenitor markers showed that GDNF overexpression did not significantly affect the expression of neural progenitor and proliferation markers (Figure 6). Thus, GDNF-expressing cNPCs retained their identity as neural progenitors.

4. Discussion

Here we report the use of a nonintegrating, plasmid-based vector to effectively transfect neural progenitor cells

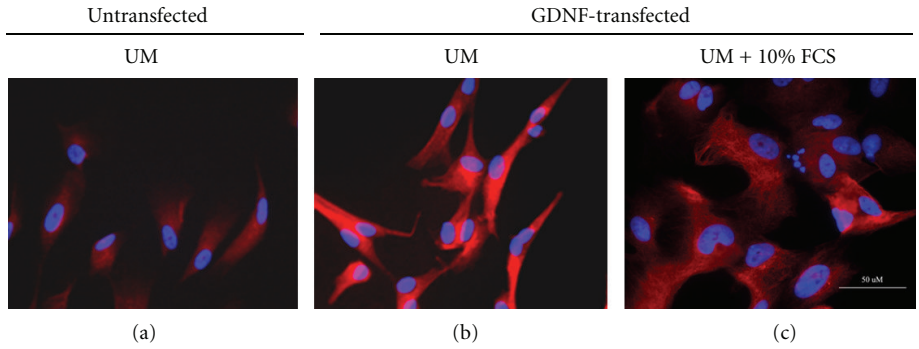

Figure 5: GDNF expression profiles in nontransfected and transfected cNPCp19. GDNF expression profiles were evaluated by immunocytochemistry (ICC) on cNPCs using an anti-human rabbit poly clone antibody. (a) Nontransfected cNPCs in UM; (b) pCAG-PyF101-GDNF plasmid transfected cNPCs in UM; (c) pCAG-PyF101-GDNF plasmid transfected cNPCs in UM containing 10% FBS for 5 days.

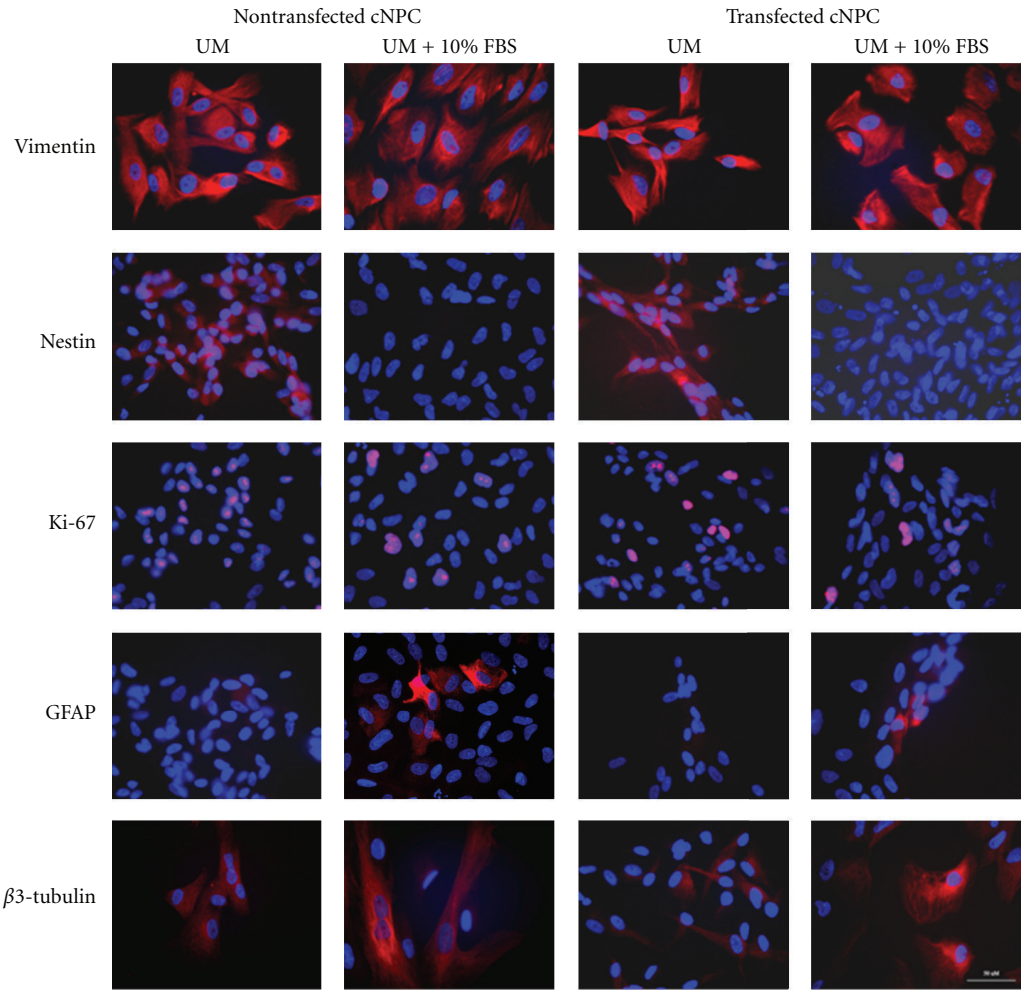

Figure 6: Expression profiles of marker genes in transfected cNPCs by ICC. Gene expression profiles of several neural progenitor, cell proliferation, and differentiation markers were evaluated by immunocytochemistry (ICC). Transfected cNPCs were cultured in UM, or UM containing 10% FBS, for 5 days and then immunolabeled with different epitope-specific antibodies to detect the markers shown.

with an exogenous gene encoding a neuroprotective growth factor. Specifically, this plasmid vector, also containing the CAGG hybrid promoter and polyoma virus mutant enhancer PyF101a, was used to deliver the human GDNF gene to progenitor cells cultured from the fetal cat brain (cNPCs). This is one of the few studies investigating the genetic modification of NPCs derived from nonrodent, nonprimate mammalian species [24] and the first study to demonstrate the applicability of plasmid-based vector technology to feline NPCs.

Gene transfer represents a powerful tool for enhancing the desired characteristics of a therapeutic cell type. Early work exploiting transgenic reporter genes and disease models has been followed by more ambitious strategies, including cytokine delivery, immune modulation, and, more recently, cellular reprogramming [31, 32]. Nevertheless, the enthusiasm surrounding these advances has been tempered by the realization that integration of exogenous transgenes into the recipient genome can result in significant complications, including malignant transformation of cells and death of treated patients. For this reason, the use of a nonintegrating plasmid-based vector is of interest in that it might avoid the potential adverse perturbations of host cell gene regulation associated with uncontrolled alteration of the chromosomal DNA-coding sequence.

One challenge connected with the use of nonintegrating vectors is the transcriptional silencing of nonchromosomal DNA sequences by host cells. Use of the highly transcribed chicken β-actin [33] and its derivative composite promoter CAGG has recently gained popularity as a strategy for countering this phenomenon, providing a robust tool for deriving long-term constitutive transfectants [29, 30, 33, 34]. The findings of the current study demonstrate that, in combination, the plasmid-based vector system and CAGG promoter can effectively transfect feline NPCs. These results suggest that this method could find applicability in the delivery of various other genes of interest to feline NPCs, as well as possibly other feline cells, and immature and differentiated cells from additional mammalian species.

One interesting observation is that the GDNF-transfected cells exhibited a slower growth curve than untransfected controls. The reason for this was not delineated in the current study, but could relate to a number of considerations. One of these is that the cells were genetically manipulated and this could be deleterious in a number of ways. Another is that the cells overexpress the signaling molecule GDNF, which could in turn exert physiological influences on apoptosis or rate of proliferation. In another study with murine retinal progenitor cells [35], we showed that exogenous GDNF was antiapoptotic and did not impede proliferation, suggesting that the slower growth seen in the current study likely results from the genetic modification process or resultant protein overexpression, rather than from subsequent GDNF-induced signaling.

The cells generated and banked during this study provide a uniquely modified cell type with potential scalability. As such, these genetically modified feline NPCs could be of translational interest in the setting of veterinary applications. Further studies involving transplantation will be necessary to explore the safety and therapeutic potential of these cells. In terms of feline retinal degeneration, a suitable recipient exists in the form of the retinal dystrophic Abyssinian cat [8].

Author's Contribution

X. Joann You and J. Yang contributed equally to this work.

Acknowledgments

The authors are grateful to Professor Peter Andrews for developing the pCAG-PyF101-eGFP plasmid and to Steven Menges for assistance with the paper. In addition, the authors would like to thank the Lincy Foundation, the Discovery Eye Foundation, the Andrei Olenicoff Memorial Foundation, and the Polly and Michael Smith Foundation for their generous financial support of this work.

References

[1] F. H. Gage, "Mammalian neural stem cells," *Science*, vol. 287, no. 5457, pp. 1433–1438, 2000.

[2] R. McKay, "Stem cells in the central nervous system," *Science*, vol. 276, no. 5309, pp. 66–71, 1997.

[3] D. van der Kooy and S. Weiss, "Why stem cells?" *Science*, vol. 287, no. 5457, pp. 1439–1441, 2000.

[4] C. N. Svendsen and M. A. Caldwell, "Neural stem cells in the developing central nervous system: implications for cell therapy through transplantation," *Progress in Brain Research*, vol. 127, pp. 13–34, 2000.

[5] M. Takahashi, T. D. Palmer, J. Takahashi, and F. H. Gage, "Widespread integration and survival of adult-derived neural progenitor cells in the developing optic retina," *Molecular and Cellular Neurosciences*, vol. 12, no. 6, pp. 340–348, 1998.

[6] M. J. Young, J. Ray, S. J. Whiteley, H. Klassen, and F. H. Gage, "Neuronal differentiation and morphological integration of hippocampal progenitor cells transplanted to the retina of immature and mature dystrophic rats," *Molecular and Cellular Neurosciences*, vol. 16, no. 3, pp. 197–205, 2000.

[7] S. J. Van Hoffelen, M. J. Young, M. A. Shatos, and D. S. Sakaguchi, "Incorporation of murine brain progenitor cells into the developing mammalian retina," *Investigative Ophthalmology and Visual Science*, vol. 44, no. 1, pp. 426–434, 2003.

[8] H. Klassen, P. H. Schwartz, B. Ziaeian et al., "Neural precursors isolated from the developing cat brain show retinal integration following transplantation to the retina of the dystrophic cat," *Veterinary Ophthalmology*, vol. 10, no. 4, pp. 245–253, 2007.

[9] J. Hori, T. F. Ng, M. Shatos, H. Klassen, J. W. Streilein, and M. J. Young, "Neural progenitor cells lack immunogenicity and resist destruction as allografts," *Stem Cells*, vol. 21, no. 4, pp. 405–416, 2003.

[10] K. Warfvinge, J. F. Kiilgaard, E. B. Lavik et al., "Retinal progenitor cell xenografts to the pig retina: morphologic integration and cytochemical differentiation," *Archives of Ophthalmology*, vol. 123, no. 10, pp. 1385–1393, 2005.

[11] K. Warfvinge, J. F. Kiilgaard, H. Klassen et al., "Retinal progenitor cell xenografts to the pig retina: immunological reactions," *Cell Transplantation*, vol. 15, no. 7, pp. 603–612, 2006.

[12] A. Blesch and M. H. Tuszynski, "GDNF gene delivery to injured adult CNS motor neurons promotes axonal growth,

expression of the trophic neuropeptide CGRP, and cellular protection," *Journal of Comparative Neurology*, vol. 436, no. 4, pp. 399–410, 2001.

[13] A. Björklund, C. Rosenblad, C. Winkler, and D. Kirik, "Studies on neuroprotective and regenerative effects of GDNF in a partial lesion model of Parkinson's disease," *Neurobiology of Disease*, vol. 4, no. 3-4, pp. 186–200, 1997.

[14] S. Behrstock, A. Ebert, J. McHugh et al., "Human neural progenitors deliver glial cell line-derived neurotrophic factor to parkinsonian rodents and aged primates," *Gene Therapy*, vol. 13, no. 5, pp. 379–388, 2006.

[15] S. M. Klein, S. Behrstock, J. Mchugh et al., "GDNF delivery using human neural progenitor cells in a rat model of ALS," *Human Gene Therapy*, vol. 16, no. 4, pp. 509–521, 2005.

[16] M. Frasson, S. Picaud, T. Léveillard et al., "Glial cell line-derived neurotrophic factor induces histologic and functional protection of rod photoreceptors in the rd/rd mouse," *Investigative Ophthalmology and Visual Science*, vol. 40, no. 11, pp. 2724–2734, 1999.

[17] L. H. M. Sanftner, H. Abel, W. W. Hauswirth, and J. G. Flannery, "Glial cell line derived neurotrophic factor delays photoreceptor degeneration in a transgenic rat model of retinitis pigmentosa," *Molecular Therapy*, vol. 4, no. 6, pp. 622–629, 2001.

[18] C. Andrieu-Soler, A. Aubert-Pouëssel, M. Doat et al., "Intravitreous injection of PLGA microspheres encapsulating GDNF promotes the survival of photoreceptors in the rd1/rd1 mouse," *Molecular Vision*, vol. 11, pp. 1002–1011, 2005.

[19] S. M. Hauck, N. Kinkl, C. A. Deeg, M. Swiatek-De Lange, S. Schöffmann, and M. Ueffing, "GDNF family ligands trigger indirect neuroprotective signaling in retinal glial cells," *Molecular and Cellular Biology*, vol. 26, no. 7, pp. 2746–2757, 2006.

[20] A. Kretz, A. M. Jacob, S. Tausch, G. Straten, and S. Isenmann, "Regulation of GDNF and its receptor components GFR-α1, -α2 and Ret during development and in the mature retinocollicular pathway," *Brain Research*, vol. 1090, no. 1, pp. 1–14, 2006.

[21] M. M. Harper, S. D. Grozdanic, B. Blits et al., "Transplantation of BDNF-secreting mesenchymal stem cells provides neuroprotection in chronically hypertensive rat eyes," *Investigative Ophthalmology & Visual Science*, vol. 52, no. 7, pp. 4506–4515, 2011.

[22] T. Ostenfeld, Y. T. Tai, P. Martin, N. Déglon, P. Aebischer, and C. N. Svendsen, "Neurospheres modified to produce glial cell line-derived neurotrophic factor increase the survival of transplanted dopamine neurons," *Journal of Neuroscience Research*, vol. 69, no. 6, pp. 955–965, 2002.

[23] D. M. Gamm, S. Wang, B. Lu et al., "Protection of visual functions by human neural progenitors in a rat model of retinal disease," *Plos ONE*, vol. 2, no. 3, article e338, 2007.

[24] X. J. You, P. Gu, J. Wang et al., "Efficient transduction of feline neural progenitor cells for delivery of glial cell line-derived neurotrophic factor using a feline immunodeficiency virus-based lentiviral construct," *Journal of Ophthalmology*, vol. 2011, Article ID 378965, 11 pages, 2011.

[25] E. V. van Gaal, W. E. Hennink, D. J. A. Crommelin, and E. Mastrobattista, "Plasmid engineering for controlled and sustained gene expression for nonviral gene therapy," *Pharmaceutical Research*, vol. 23, no. 6, pp. 1053–1074, 2006.

[26] J. Black and J. M. Vos, "Establishment of an oriP/EBNA1-based episomal vector transcribing human genomic β-globin in cultured murine fibroblasts," *Gene Therapy*, vol. 9, no. 21, pp. 1447–1454, 2002.

[27] K. Van Craenenbroeck, P. Vanhoenacker, and G. Haegeman, "Episomal vectors for gene expression in mammalian cells," *European Journal of Biochemistry*, vol. 267, no. 18, pp. 5665–5678, 2000.

[28] H. Niwa, K. Yamamura, and J. Miyazaki, "Efficient selection for high-expression transfectants with a novel eukaryotic vector," *Gene*, vol. 108, no. 2, pp. 193–200, 1991.

[29] C. G. Liew, J. S. Draper, J. Walsh, H. Moore, and P. W. Andrews, "Transient and stable transgene expression in human embryonic stem cells," *Stem Cells*, vol. 25, no. 6, pp. 1521–1528, 2007.

[30] A. N. Alexopoulou, J. R. Couchman, and J. R. Whiteford, "The CMV early enhancer/chicken β actin (CAG) promoter can be used to drive transgene expression during the differentiation of murine embryonic stem cells into vascular progenitors," *BMC Cell Biology*, vol. 9, article 2, 2008.

[31] K. Takahashi and S. Yamanaka, "Induction of pluripotent stem cells from mouse embryonic and adult fibroblast cultures by defined factors," *Cell*, vol. 126, no. 4, pp. 663–676, 2006.

[32] J. Yu, K. Hu, K. Smuga-Otto et al., "Human induced pluripotent stem cells free of vector and transgene sequences," *Science*, vol. 324, no. 5928, pp. 797–801, 2009.

[33] S. Chung, T. Andersson, K. C. Sonntag, L. Björklund, O. Isacson, and K. S. Kim, "Analysis of different promoter systems for efficient transgene expression in mouse embryonic stem cell lines," *Stem Cells*, vol. 20, no. 2, pp. 139–145, 2002.

[34] M. Kosuga, S. Enosawa, X. K. Li et al., "Strong, long-term transgene expression in rat liver using chicken β-actin promoter associated with cytomegalovirus immediate-early enhancer (CAG promoter)," *Cell Transplantation*, vol. 9, no. 5, pp. 675–680, 2000.

[35] J. Wang, J. Yang, P. Gu, and H. Klassen, "Effects of glial cell line-derived neurotrophic factor on cultured murine retinal progenitor cells," *Molecular Vision*, vol. 16, pp. 2850–2866, 2010.

Hindawi Publishing Corporation
Stem Cells International
Volume 2012, Article ID 454295, 8 pages
doi:10.1155/2012/454295

Research Article

Subretinal Implantation of Electrospun, Short Nanowire, and Smooth Poly(ε-caprolactone) Scaffolds to the Subretinal Space of Porcine Eyes

A. T. Christiansen,[1] S. L. Tao,[2] M. Smith,[3] G. E. Wnek,[4] J. U. Prause,[5] M. J. Young,[6] H. Klassen,[7] H. J. Kaplan,[8] M. la Cour,[1] and J. F. Kiilgaard[1]

[1] *Department of Ophthalmology, Glostrup Hospital, Copenhagen University Hospital, 2600 Glostrup, Denmark*
[2] *Advanced Development Center, CooperVision, Inc., Pleasanton, CA 94588, USA*
[3] *NuVention Solutions Inc., Valley View, OH 44125, USA*
[4] *Case Western Reserve University, Cleveland, OH 44106, USA*
[5] *Eye Pathology Institute, University of Copenhagen, 2100 Copenhagen, Denmark*
[6] *Department of Ophthalmology, Schepens Eye Research Institute, Harvard Medical School, Boston, MA 02114, USA*
[7] *The Gavin Herbert Eye Institute and Stem Cell Research Center, University of California, Irvine, CA 92697, USA*
[8] *Department of Ophthalmology and Visual Sciences, Kentucky Lions Eye Center, University of Louisville, Louisville, KY 40208, USA*

Correspondence should be addressed to J. F. Kiilgaard, jfkiilgaard@gmail.com

Received 14 September 2011; Accepted 4 January 2012

Academic Editor: Chee Gee Liew

Biodegradable scaffolds play an important adjunct role in transplantation of retinal progenitor cells (RPCs) to the subretinal space. Poly(ε-Caprolactone) (PCL) scaffolds with different modifications were subretinally implanted in 28 porcine eyes and evaluated by multifocal electroretinography (mfERG) and histology after 6 weeks of observation. PCL Short Nanowire, PCL Electrospun, and PCL Smooth scaffolds were well tolerated in the subretinal space in pigs and caused no inflammation and limited tissue disruption. PCL Short Nanowire had an average rate of preserved overlying outer retina 17% higher than PCL Electrospun and 25% higher than PCL Smooth. Furthermore, PCL Short Nanowire was found to have the most suitable degree of stiffness for surgical delivery to the subretinal space. The membrane-induced photoreceptor damage could be shown on mfERG, but the reductions in P1 amplitude were only significant for the PCL Smooth. We conclude that of the tested scaffolds, PCL Short Nanowire is the best candidate for subretinal implantation.

1. Introduction

Subretinally transplanted retinal progenitor cells (RPCs) have in a number of animal models shown the ability to migrate to the outer retina, differentiate to mature photoreceptors, and generate synapses with existing cells [1]. As the mammalian retina does not regenerate [2], this provides a great restorative potential for retinal degenerative diseases. When transplanting cells to the subretinal space, the use of scaffolds has been shown to increase the number of delivered and surviving cells, to enable a more precise and localized delivery [3], and to promote differentiation and organization of grafted RPCs [3–5]. Furthermore, scaffolds can be loaded with regulatory and modulating drugs to further assist differentiation, function, and survival [6–8].

Several materials have been tested as scaffolds for RPC transplantation and found to support adhesion, survival, and migration [3, 9]. One of the more promising scaffold materials is poly(ε-caprolactone) (PCL) as it is mechanically compliant, nontoxic, degrades by slow surface erosion and can be fabricated as very thin membranes [9–11]. Scaffolds of PCL can be fabricated by different methods to produce specific structural and mechanical properties [9, 10, 12, 13]. Such types of PCL membranes are the electrospun (PCL-E),

the Short Nanowire (PCL-SNW), and the Smooth (PCL-S). All three have previously been tested and for the PCL-E and PCL-SNW shown promising abilities for supporting growth, differentiation and migration of RPCs in vitro and in the case of PCL-SNW also in an in vivo study on mice [9, 13]

In this study, we transplanted naked PCL membranes to the subretinal space of pigs to obtain a baseline for the histological and electrophysiological effect of subretinal transplantation as well as long time presence of PCL-E, PCL-SNW, and PCL-S membranes in the eye. The size of the porcine eye enabled the use of surgical techniques and equipment used in the clinic, and thereby this study also evaluates the mechanical properties of the tested membranes in relation to the procedure of subretinal transplantation in humans. Voss Kyhn et al. [14] have shown the surgical steps of gaining access to the subretinal space to have no detectable effect on the multifocal electroretinogram (mfERG) in pigs 6 weeks post-surgically, and we assume that the electrophysiological effects seen arise only from the transplanted membranes. Also the immediate histological shortening of photoreceptor outer segments following bleb formation has been shown to normalized 6 weeks post-surgically [14]. We thereby intended this study to serve as histological and electrophysiological baseline for future RPC-PCL composite studies.

2. Material and Method

All experiments were performed in compliance with the ARVO Statement for the Use of Animals in Ophthalmic and Vision Research. The Danish Animal Experiments Inspectorate granted permission for the use of the animals (permission 2007/561-768). Trained veterinary nurses and technicians carried out all handling of the animals.

A total of 28 female domestic pigs of Danish Landrace/Duroc/Hampshire/Yorkshire breed were used for these experiments (age 3-4 months; weight 23–30 kg). Only left eyes underwent membrane implantation. The animals were premedicated with Tiletamine 1.19 mg/kg, Zolazepam 1.19 mg/kg (Zoletil 50 Vet Virbac SA, Carros, France), Methadone 0.24 mg/kg (Nycomed, Roskilde, Denmark), Ketamine 1.43 mg/kg (Intervet, Skovlunde, Denmark), and Xylazine 1.24 mg/kg (Intervet, Skovlunde, Denmark). Thereafter, anesthesia was maintained with continuous intravenous infusion (i.v.) of propofol 15 mg/kg/h (Fresenius Kabi, Bad Homburg, Germany). The animals were endotracheally intubated and artificially ventilated on 34% O_2. During anesthesia the animals were placed resting on their elbows to minimize the impact on the cardiovascular system [15]. In order to avoid hypothermia, the animals were wrapped in a blanket during anesthesia

2.1. Membrane Fabrication. The PCL-E membrane was fabricated by transferring a solution of 10 weight percent (wt%) PCL in $CHCl_3$ to a 5 mL syringe attached to a blunt tipped 18 gauge (G) stainless steel needle. Electrospinning was then carried out through the application of a 15 kV positive voltage to the polymer solution. The solution was fed via a syringe pump at a constant mass flow rate of 1 mL/hr. Finally fibers were collected on a stainless steel grounded rotating drum until a nonwoven mat was formed.

The PCL-SNW membrane was fabricated by first preparing a polymer casting solution by dissolving PCL in dichloromethane (4 wt%) (Sigma-Aldrich). The PCL solution was then cast onto a nanoporous anodized aluminum oxide template using a spin coater (Specialty Coating Systems, Indianapolis, IN, USA). The solvent was allowed to evaporate at room temperature. Polymer melts were formed at 130°C while in contact with the nanoporous template. Nanowire length was tuned as a function of melt time. A melt time of 5 min was used to form the short nanowires of 2.5 μm in length. Finally the thin-film scaffold of vertically aligned nanowires was released by etching the template in a dilute sodium hydroxide solution and allowed to air dry at room temperature.

The PCL-s membrane was fabricated on an electrochemically polished silicon wafer using a spin-cast/solvent evaporation method.

2.2. Surgical Procedure. Eyes were anesthetized, dilated, disinfected, and a standard three-port core vitrectomy was performed as previously described [16]. In brief, the infusion line was secured inferiorly (Ringer Lactate; SAD, Copenhagen, Denmark), and the vitreous was removed during endoillumination using a 20 G vitrector (Karl Storz GmbH, Tuttlingen, Germany). The posterior hyaloid was meticulous removed in the visual streak and optic disc area. A subretinal bleb in the visual streak area was raised by injection of Ringer Lactate (SAD, Copenhagen, Denmark) through a 41 G cannula (ref. 1270; DORC International BV, Zuidland, the Netherlands). To gain access to the subretinal space, a retinotomy was performed in the temporal aspect of the bleb using endodiathermy (Storz Premiere, Bausch & Lomb; energy set 15%, output range 7.5 Watts nominal at 100 ohms) and automated scissors (Storz Premiere, automatic scissors).

This allowed a large piece of membrane (approx. 12 mm^2) to be inserted in the visual streak area. DORC's combined spatula/peeling forceps was used for this (Ref. 1297, DORC, Netherlands). In order to secure the membrane, a partial fluid-air-exchange with drainage at the retinotomy site was performed after the membrane was placed subretinally. Sclera and conjunctiva were sutured with 7-0 coated vicryl (Ethicon, Norderstedt, Germany). After the procedure, intraocular pressure was evaluated with bimanual palpation, and indirect ophthalmoscopy was performed to ensure correct placement of the membrane and absence of bleeding and retinal detachment. Finally, topical application of chloramphenicol ointment was given, and the eye was patched (Kloramfenikol "DAK"; Nycomed, Roskilde, Denmark). In order to ensure reliable histology and mfERG recordings, animals with any surgical complication, such as bleeding, surgical lens damage, or retinal detachment as well as animals with significant opacities in the media were excluded from the study.

2.3. Follow-Up Procedure. Six weeks past surgery, animals were reanesthetized as previously described [15] with addition of a neuromuscular blocker to avoid eye movement: 2 mg/h i.v. Pancurium Bromide (Oss, Organon, Holland).

Infrared (IR) fundus imaging, mfERG (VERIS Science 5.0.1), and color fundus photos (Zeiss FF450 plus-IR) were obtained just prior to euthanasia. All color fundus photos were taken with an angle of 50 degrees. Animals were euthanized by a lethal injection of 20 mL pentobarbital 200 mg/mL (Royal Veterinary and Agricultural University, Copenhagen, Denmark) and the left membrane-transplanted eye was then enucleated. After an initial fixation for 15 min in formaldehyde 4%, the enucleated eye was divided into two parts by incision posterior to the ora serrata. Subsequently, the formaldehyde fixation was prolonged for 24 hr.

2.4. Histology. The optic nerve and the visual streak were isolated from the formaldehyde fixed eyecup. The obtained specimens were paraffin embedded and sections of 4.5 μm were then stained with haematoxylin and eosin (HE) and evaluated by light microscopy. The proportion of morphologically undisturbed retinal layer overlaying the transplanted membrane was measured on a micrograph. For each retinal layer, a fraction of morphologically undisturbed retina could then be calculated. This semiquantitative scoring of the histological effects on the retina enabled comparison of membranes independently of the placement of the membrane within the eye.

2.5. Multifocal Electroretinogram. Multifocal ERG was recorded on both eyes as previously described [17]. In brief, eyes were dilated and a Burian Allen (VERIS Infrared Illuminating Electrode, EDI, Inc., Red Wood, CA) bipolar contact lens was placed on the cornea. Recordings were conducted using VERIS Science 5.0.1 with visual stimulus displayed on a 1.5-inch cathode ray tube monitor integrated in the stimulus camera. The left membrane-implanted eye was recorded first and always recorded within the first two hours of anesthesia. The two eyes were recorded within a timeframe of 30 min. A stimulus pattern of 241 unscaled white and black hexagons with a frame rate of 75 Hz and 16 samples per frames was used. The m-sequence exponent was 15 and the durations of recordings were 7.17 minutes. Signals were band-passes filtered outside 10–300 Hz. No spatial averaging and only first-order kernels were used.

Multifocal electroretinogram scoring of the membranes was done as previously described [17]. In brief, IR fundus photo of the left eye with the stimulus grid from the VERIS system and the corresponding Zeiss color fundus photo was aligned to identify hexagons covering membrane-supported retina. The corresponding area in the right (control) eye was identified, and the averages of the P1-amplitudes of the mfERGs derived from hexagons of the two areas were calculated and a ratio was found. ANOVA-test was used to test for equality of means between the different membrane types (SigmaPlot 11.0 for Windows, Systat Software Inc., San Jose, California, USA).

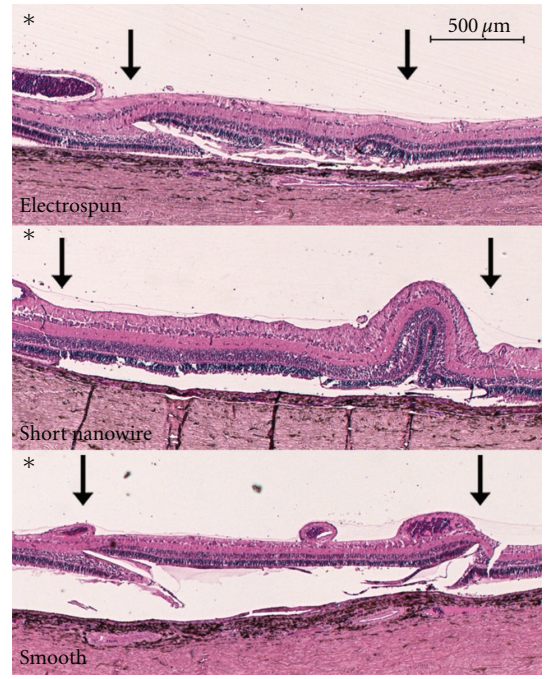

Figure 1: Micrograph of hematoxylin and eosin stained porcine retina after subretinally implanted poly(ε-caprolactone) membranes (marked with arrows). Top: Poly(ε-caprolactone) Electrospun PCL-E) membrane. The left edge of the membrane has penetrated up through the outer retina. Mild choroidal neovascularization is seen under the membrane and a few RPE-cells have transformed to a macrophage morphology on the outer face of the membrane. Very little of the retina from the inner nuclear layer, and outward, is preserved and no photoreceptors are preserved. Middle: Poly(ε-caprolactone) Short Nanowire (PCL-SNW) membrane. A retinal fold is seen over the right end of the membrane taking up approximately 30% of the length of the membrane. All retinal layers left of the fold from neurofiber to outer nuclear layer are well-preserved giving approximately 70% well-preserved retina. Half the photoreceptor outer segments are flattened but still present. Bottom: Poly(ε-caprolactone) Smooth (PCL-S) membrane. Both membrane edges are perforated up through the outer retina. The inner membrane-supported retinal layers are well preserved. From the inner nuclear layer, the outer retina is more disrupted with preserved morphology in only approximately half the length of the membrane. The part of fattened but still present photoreceptor outer segments is even less than the rest of the outer retina. No sign of inflammation is seen in either of the micrographs. ($*$ marks the vitreous body).

2.6. Brightness Analysis. Color fundus photos were used to evaluate the brightness of the subretinally transplanted membranes. Area of interest was marked and measured in Photoshop on a scale ranging from 0 (black point) to 255 (white point) as described by Hubbard et al. [18]. The ratio between the membrane area and the optic disc brightness was used to even out differences in the fundus photo flash intensity. The brightness ratios for the three membranes were plotted using SigmaPlot.

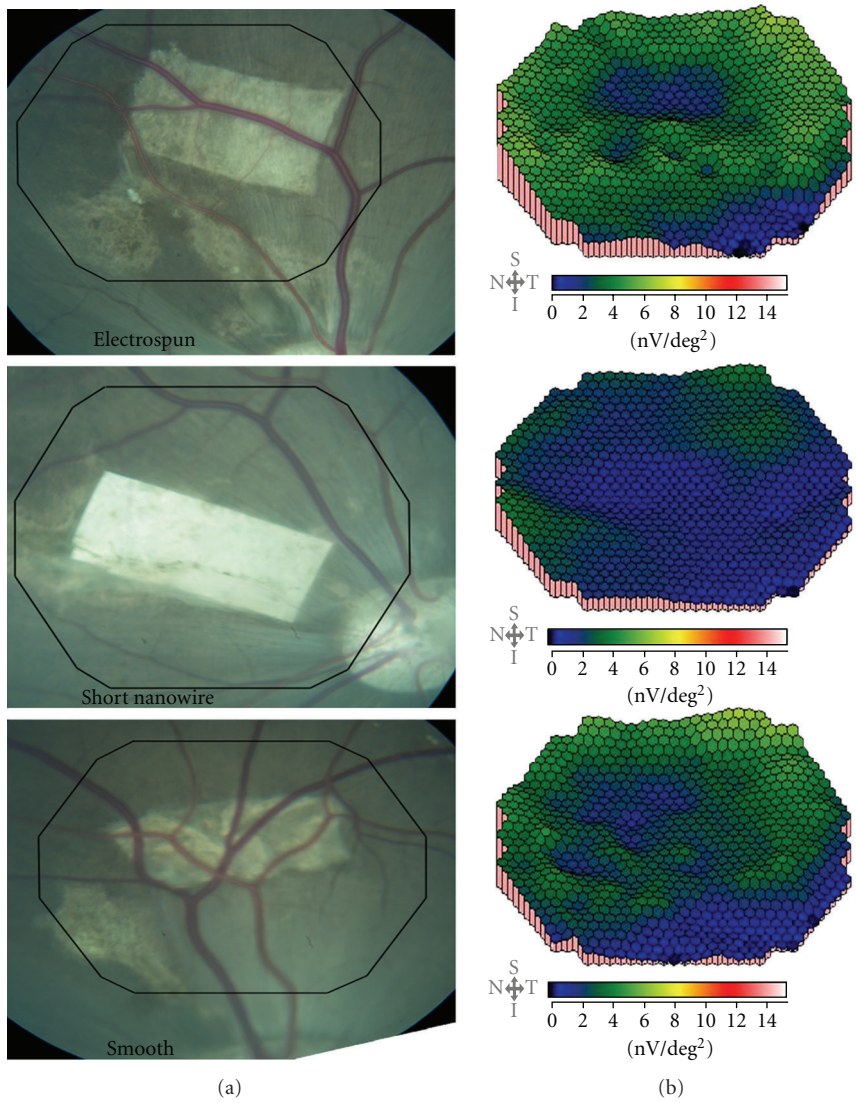

Figure 2: Fundus photos 6 weeks after membrane implantation (a) and corresponding 3D-presentation of amplitudes for the 241 hexagons recorded by multifocal electroretinography (b). Black circle on the fundus photo marks position of the 241-unscaled multifocal electroretinogram-grit. Color scale on the 3D-presentation ranges from 0 to 14 nV/deg^2. Top: Poly(ε-caprolactone) Electrospun PCL-E) membrane. Middle: Poly(ε-caprolactone) Short Nanowire (PCL-SNW) membrane. Bottom: Poly(ε-caprolactone) Smooth (PCL-S) membrane.

3. Results

A total of 28 pigs underwent PCL-membrane implantation surgery, whereof 12 had PCL-S, 10 had PCL-E, and 6 had PCL-SNW membranes implanted.

The implanted membrane could not be found in 7 cases at followup and in 1 pig the membrane was found in the vitreous cavity. Two pigs developed intraocular bleeding that did not resolve, and in 2 pigs the retina did not reattach. One PCL-SNW had mfERG responses, but the retina was lost during histological preparation; in 4 eyes (one PCL-E, one PCL-SNW, and two PCL-S), the membrane moved so far peripherally that detection of the mfERG was not possible, and in one PCL-E the membrane had migrated intraretinally. This gives a total of 10 pigs that were included for both histological scoring and mfERG recordings (Table 1).

The different fabrication methods of PCL membranes irrefutably resulted in different degrees of flexibility. This proved to influence the ease of implantation to the eye. PCL-SNW was the easiest to maneuver to and insert in the subretinal space. The relatively stiff PCL-E gave an impression of distorting the surrounding tissue when inserted subretinally, whereas the high flexibility of the Smooth membrane made it bend and curl up during the implantation.

Histological examination showed all the membranes to be rather well tolerated in the subretinal space with no inflammation in either retina or choroid (Figure 1). In a few cases, RPE cells on the outer face of the membranes

Table 1: Number of implanted, included, and excluded polymer scaffolds, by type.

	No. of eyes (total)	No. of eyes (histology)	No. of eyes (mfERG)	No. of eyes (mfERG and histology)	Exclusions
PCL Electrospun	10	6	5	4*	1 bleeding; 2 retinal detachments; 1 membrane not found at follow up
PCL Short Nanowire	6	4	4	3	1 membrane not found at follow up
PCL Smooth	12	5	3	3	1 bleeding; 1 membrane dislocated to corpus vitreum; 5 membranes not found at follow up

* One membrane migrated intraretinally and was not scored histologically.

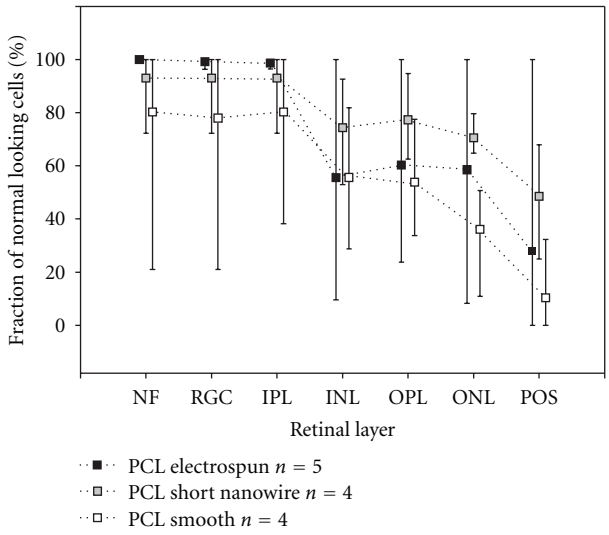

Figure 3: Mean fractions of morphologically intact membrane supported retinal layers for the three membrane types (squares). The lowest and highest scored fractions for each layer are given by the thin bars. Number of pigs included for histological scoring are given as n values in the figure.

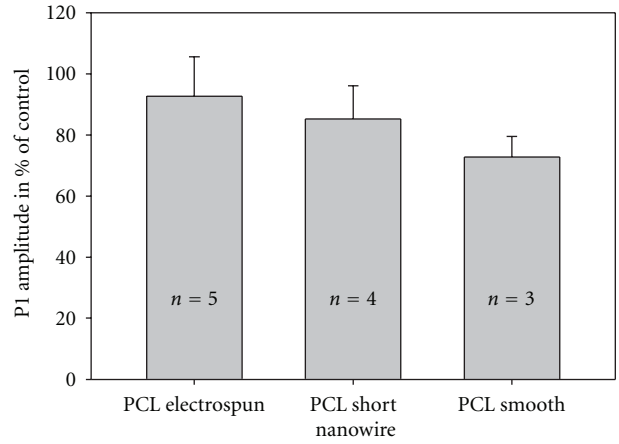

Figure 4: Mean P1 amplitude ratios for the three membrane-types. Ratios are given as the percentage of P1 amplitude for the membrane supported area of retina in the left eye compared to that of the corresponding area in the right untouched eye. Confidence intervals are given by the thin bars. Number of included animals for each membrane are written on the broad bars. No significant differences are seen. Only the P1 amplitude ratio of PCL Smooth is significantly different from 1 ($P = 0.028$).

transformed to a histiocytic morphology creating giant cells (Figure 1(top)). Choroidal neovascularization (CNV) was seen in 67% cases with PCL-E, 75% of cases transplanted with PCL-S, and in 50% of cases with PCL-SNW membranes.

It was possible to score the morphologically intact fraction of all overlying retinal layers of all included eyes. Mean values for each layer and membrane type including lowest and highest fraction are given in Figure 3. The PCL-SNW had the highest average percentage of morphologically well-preserved overlying retina for all evaluated outer retinal layers. The photoreceptor outer segment layer was disrupted over all the membranes, varying from flattened to completely gone. This layer, as the only one, is, therefore, included as preserved if present (Figure 3). All other layers varied from undisturbed to disturbed beyond recognition and only the morphologically undisturbed part of these layer were included as preserved. The inner retina was left almost intact by all membranes but one case of PCL-S (Figure 3). The one PCL-SNW that scored low on outer retinal layers did so because of a retinal fold that was scored as morphologically disturbed (Figure 1). Common for all membranes was a tendency for the edges to penetrate up through the retinal layers and in one case the membrane was found to be located completely intraretinally.

It was possible to obtain good mfERGs with acceptable signal-to-noise ratios in both the left and right eye on all included pigs. The 3D presentations of amplitudes show a general depression over the membranes when compared to adjacent retina (Figure 2). This tendency is also found for the P1-amplitude ratios (Figure 4). The depression in

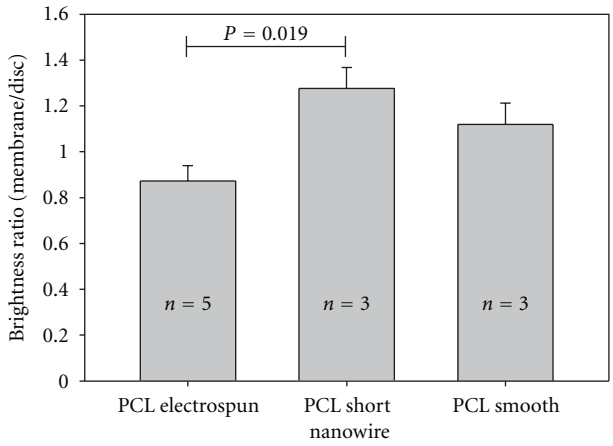

Figure 5: Mean brightness ratios for the three membrane types. Ratios are calculated as brightness of the membrane compared to that of the optic disc. Confidence intervals (thin bars) reveal a significant difference between the poly(ε-caprolactone) (PCL) Electrospun and the PCL Short Nanowire membranes. Numbers of included animals for each membrane type are written on the broad bars.

P1-amplitude ratio is, however, only significantly different from 1 for the PCL-S. Between the three membrane types, no significant difference in mean P1-amplitude ratios was found (Figure 4). The 3D presentation of amplitudes for the membrane adjacent retina of the three membrane types shows the interindividual difference generally seen between the pigs (Figure 2).

Fundus photos of the membranes reveal a difference in brightness of the membranes (Figure 2). This difference in brightness is significant between the PCL-SNW and the PCL-E membranes (Figure 5).

4. Discussion

We demonstrate, in this study, that three different modifications of poly(ε-caprolactone) membranes, Electrospun, Short Nanowire, and Smooth, are well tolerated in the subretinal space in pigs. None of the tested membrane variants caused an inflammatory response, but differences in the retinal damage seen could be related to the physical properties of the different membrane types.

The thickness and biocompatibility of scaffolds has previously been addressed as essential properties of tissue scaffolds for subretinal stem cell transplantation [13, 19, 20]. Firstly, the scaffold must be thin and permeable to nutrients to allow outer retinal survival. The PCL-SNW scaffolds especially fulfill this requirement, as it is one of the thinnest polymer substrates used for subretinal RPC transplantation [13]. Secondly, scaffold material must not be toxic to the surrounding tissue. PCL as a material for scaffold complies well with these requirements, as it is both highly permeable [12] and degrades in a slow manner and is less prone to leave an acidic microenvironment than polymers of higher molecular weight as the PLGA [21, 22]. Finally, to allow surgical delivery to the subretinal space, the scaffold needs to be stiff, but still flexible enough to prevent distortion of the subretinal space. The PCL-E has a very high Young's modulus (stiffness) [9], which prevented the membrane from adapting to the curvature of the eyeball, and likely caused the observed migration up into retina. In contrast, the PCL-S proved too flexible, as it tended to curl up during implantation, and therefore caused a larger surgical trauma. Over all, we find the PCL-SNW to have the best degree of flexibility and the PCL-S to have the worst.

Our histological results also point towards the PCL-SNW as the best scaffold candidate of the three tested as the overlying outer retina (from inner nuclear layer and out) of the PCL-SNW had approximately 17% more preserved morphology than the PCL-E, and 25% more than the PCL-S (Figure 3). Histology showed that the inner retina was mainly left intact in all specimens, except for one smooth membrane. In one specimen with PCL-E we found intact photoreceptor layer, but the overall finding was that photoreceptors were shortened and nowhere was a completely morphologically intact layer observed. Flattening of the outer segments has previously been observed in the porcine retina after detachment but here the morphology of outer segments was restored 6 weeks after detachment and the subsequent reattachment [14]. We, therefore, regard the loss and morphological change of the outer segments to be expected and not specific to these membrane types. Besides the effect of mechanical differences between the membranes, an explanation for the different degrees of preservation could be the ability of membranes to support growing cells [13].

We believe that the tendency to curl up after implantation combined with the smooth surface is the explanation for the high number of PCL-S membranes not found subretinally at followup (Table 1). As the PLC degrades very slowly and is found so well preserved in the other eyes, we do not believe that the membranes not found after 6 weeks had dissolved. They either migrated subretinally so far anteriorly, that they were not visible on neither fundus photo nor histology or, more likely, they were displaced through the retinotomy, as the one seen at the posterior lens capsule, and were, therefore, not seen during the preparation process.

Choroidal neovascularizton often occurs with damage to Bruch's membrane [23] and was in this study found in more than half the included eyes. We do not expect the presence if the electrically inactive CNV to influence the mfERG directly. Indirectly, however, CNV could influence the mfERG via scatter. Again we do not expect this to affect the mfERG of the membrane supported retina as the CNV is located under the implanted membranes.

The intentional use of mfERG as an in vivo measurement of cell survival is compromised in this study. If mfERG is to be used for assessment of survival of transplanted cells, a significant depression in mfERG amplitude ratio in the control situation (the naked membrane) is mandatory. On the 3D presentation of the mfERG, there was a tendency for depression of the mfERG signals over the membranes, but when compared to the control eye only PCL smooth showed a significant decrease in P1 amplitude. Although histology revealed marked differences in the destruction of outer retinal layers covering the different membrane types, we

could not show any significant differences in P1 amplitude ratios. This was further complicated by the observation of significantly higher brightness ratio for PCL-SNW compared to PCL-E and so a correlation between brightness ratio and mfERG P1 amplitude ratios could not be demonstrated, as was previously shown for PLGA membranes [17]. We explain this dissimilarity by the presence of residual functional photoreceptors overlaying the bright membrane, resulting in mfERG amplitudes composed of both signals from functional local retina and from light scatter in various degrees.

5. Conclusion

In conclusion, PCL derivatives are well tolerated in the subretinal space in pigs. Among the three PCL scaffolds tested, PCL short nanowire seems to be the best candidate for future use as a scaffold in RPC transplantation.

Abbreviations

RPC:	Retinal progenitor cell
PCL:	Poly(ε-caprolactone)
PCL-E:	Poly(ε-caprolactone) electrospun,
PCL-SNW:	Poly(ε-caprolactone) short nanowire
PCL-S:	Poly(ε-caprolactone) smooth
mfERG:	Multifocal electroretinogram
i.v.:	Intravenous infusion
G:	Gauge
IR:	Infrared
HE:	Haematoxylin and eosin
CNV:	Choroidal neovascularization.

Conflict of Interests

The authors of this paper have no conflict of interests to disclose.

Acknowledgments

The authors would like to thank The Danish Agency for Science, Technology and Innovation, as well as the Lincy Foundation and the Andrei Olenicoff Memorial Foundation.

References

[1] H. Klassen and B. Reubinoff, "Stem cells in a new light," *Nature Biotechnology*, vol. 26, no. 2, pp. 187–188, 2008.

[2] D. Lamba, M. Karl, and T. Reh, "Neural regeneration and cell replacement: a view from the eye," *Cell Stem Cell*, vol. 2, no. 6, pp. 538–549, 2008.

[3] M. Tomita, E. Lavik, H. Klassen, T. Zahir, R. Langer, and M. J. Young, "Biodegradable polymer composite grafts promote the survival and differentiation of retinal progenitor cells," *Stem Cells*, vol. 23, no. 10, pp. 1579–1588, 2005.

[4] E. B. Lavik, H. Klassen, K. Warfvinge, R. Langer, and M. J. Young, "Fabrication of degradable polymer scaffolds to direct the integration and differentiation of retinal progenitors," *Biomaterials*, vol. 26, no. 16, pp. 3187–3196, 2005.

[5] K. Warfvinge, J. F. Kiilgaard, E. B. Lavik et al., "Retinal progenitor cell xenografts to the pig retina: morphologic integration and cytochemical differentiation," *Archives of Ophthalmology*, vol. 123, no. 10, pp. 1385–1393, 2005.

[6] B. A. Tucker, S. M. Redenti, C. Jiang et al., "The use of progenitor cell/biodegradable MMP2-PLGA polymer constructs to enhance cellular integration and retinal repopulation," *Biomaterials*, vol. 31, no. 1, pp. 9–19, 2010.

[7] J. Yao, B. A. Tucker, X. Zhang, P. Checa-Casalengua, R. Herrero-Vanrell, and M. J. Young, "Robust cell integration from co-transplantation of biodegradable MMP2-PLGA microspheres with retinal progenitor cells," *Biomaterials*, vol. 32, no. 4, pp. 1041–1050, 2011.

[8] A. Silva-Cunha, S. L. Fialho, M. C. Naud, and F. Behar-Cohen, "Poly-ε-caprolactone intravitreous devices: an in vivo study," *Investigative Ophthalmology and Visual Science*, vol. 50, no. 5, pp. 2312–2318, 2009.

[9] S. Cai, M. E. Smith, S. M. Redenti, G. E. Wnek, and M. J. Young, "Mouse retinal progenitor cell dynamics on electrospun poly(ε-caprolactone)," *Journal of Biomaterials Science, Polymer Edition*. In press.

[10] S. Sodha, K. Wall, S. Redenti, H. Klassen, M. J. Young, and S. L. Tao, "Microfabrication of a three-dimensional polycaprolactone thin-film scaffold for retinal progenitor cell encapsulation," *Journal of Biomaterials Science, Polymer Edition*, vol. 22, no. 4–6, pp. 443–456, 2011.

[11] H. Chen, X. Fan, J. Xia et al., "Electrospun chitosan-graft-poly (ε-caprolactone)/poly (ε-caprolactone) nanofibrous scaffolds for retinal tissue engineering," *International journal of nanomedicine*, vol. 6, pp. 453–461, 2011.

[12] S. L. Tao and T. A. Desai, "Aligned arrays of biodegradable poly(ε-caprolactone) nanowires and nanofibers by template synthesis," *Nano Letters*, vol. 7, no. 6, pp. 1463–1468, 2007.

[13] S. Redenti, S. Tao, J. Yang et al., "Retinal tissue engineering using mouse retinal progenitor cells and a novel biodegradable, thin-film poly(ε-caprolactone) nanowire scaffold," *Journal of Ocular Biology, Diseases, and Informatics*, vol. 1, no. 1, pp. 1–11, 2008.

[14] M. Voss Kyhn, J. F. Kiilgaard, A. G. Lopez, E. Scherfig, J. U. Prause, and M. la Cour, "Functional implications of short-term retinal detachment in porcine eyes: study by multifocal electroretinography," *Acta Ophthalmologica Scandinavica*, vol. 86, no. 1, pp. 18–25, 2008.

[15] M. Voss Kyhn, J. F. Kiilgaard, A. G. Lopez, E. Scherfig, J. U. Prause, and M. la Cour, "The multifocal electroretinogram (mfERG) in the pig," *Acta Ophthalmologica Scandinavica*, vol. 85, no. 4, pp. 438–444, 2007.

[16] R. Ejstrup, E. Scherfig, and M. la Cour, "Electrophysiological consequences of experimental branch retinal vein occlusion in pigs and the effect of dorzolamide," *Investigative Ophthalmology and Visual Science*, vol. 52, no. 2, pp. 952–958, 2011.

[17] A. T. Christiansen, J. F. Kiilgaard, M. Smith et al., "The influence of brightness on functional assessment by mfERG: a study on scaffolds used in retinal cell transplantation in pigs," *Stem Cells International*, vol. 2012, Article ID 263264, 7 pages, 2012.

[18] L. D. Hubbard, R. P. Danis, M. W. Neider et al., "Brightness, contrast, and color balance of digital versus film retinal images in the age-related eye disease study 2," *Investigative Ophthalmology and Visual Science*, vol. 49, no. 8, pp. 3269–3282, 2008.

[19] S. R. Hynes and E. B. Lavik, "A tissue-engineered approach towards retinal repair: scaffolds for cell transplantation to the

subretinal space," *Graefe's Archive for Clinical and Experimental Ophthalmology*, vol. 248, no. 6, pp. 763–778, 2010.

[20] C. Sheridan, R. Williams, and I. Grierson, "Basement membranes and artificial substrates in cell transplantation," *Graefe's Archive for Clinical and Experimental Ophthalmology*, vol. 242, no. 1, pp. 68–75, 2004.

[21] L. Lu, M. J. Yaszemski, and A. G. Mikos, "Retinal pigment epithelium engineering using synthetic biodegradable polymers," *Biomaterials*, vol. 22, no. 24, pp. 3345–3355, 2001.

[22] A. C. R. Grayson, G. Voskerician, A. Lynn, J. M. Anderson, M. J. Cima, and R. Langer, "Differential degradation rates in vivo and in vitro of biocompatible poly(lactic acid) and poly(glycolic acid) homo- and co-polymers for polymeric drug-delivery microchip," *Journal of Biomaterials Science, Polymer Edition*, vol. 15, no. 10, pp. 1281–1304, 2004.

[23] J. F. Kiilgaard, M. V. N. Andersen, A. K. Wiencke et al., "A new animal model of choroidal neovascularization," *Acta Ophthalmologica Scandinavica*, vol. 83, no. 6, pp. 697–704, 2005.

Hindawi Publishing Corporation
Stem Cells International
Volume 2012, Article ID 716968, 5 pages
doi:10.1155/2012/716968

Research Article

Transplantation of Amniotic Membrane to the Subretinal Space in Pigs

Jens Folke Kiilgaard,[1,2] Erik Scherfig,[2] Jan Ulrik Prause,[2] and Morten la Cour[1]

[1] *Department of Ophthalmology, Glostrup Hospital, Copenhagen University Hospital, Nordre Ringvej 57, 2600 Glostrup, Denmark*
[2] *Eye Pathology Institute, Teilumbygningen, University of Copenhagen, 2100 Copenhagen, Denmark*

Correspondence should be addressed to Jens Folke Kiilgaard, jfkiilgaard@gmail.com

Received 15 September 2011; Accepted 22 December 2011

Academic Editor: Budd A. Tucker

Purpose. To investigate the effect of transplanted amniotic membrane (AM) on subretinal wound healing. *Methods*. Nine Danish Landrace pigs had surgical removal of retinal pigment epithelium (RPE) and mechanical damage of Bruch's membrane (BM) and served as a control group. 15 pigs additionally had AM transplanted to the subretinal space. *Results*. AM significantly reduces choroidal neovascularisation when complete coverage of the induced defect is obtained (7 pigs) ($P < 0.05$). In cases where AM did not cover the rupture in BM choroidal tissue covered the transplanted membrane (8 pigs). AM is well tolerated in the subretinal space, causes only limited inflammation, and is covered with a monolayer of pigmented cells when in contact with the host RPE. *Conclusions*. AM modifies choroidal neovascularisation after BM damage and may serve as a basement membrane substitute for the RPE.

1. Introduction

During the last decade there has been an immense progress within the field of study of retinal progenitor cells and today several clinical transplantation studies are ongoing (http://clinicaltrials.gov/). While the basic clinical studies often seek to prevent damage in either healthy animal injury models [1] or in models of retinal degeneration [2], the clinical situation often represents the end-stage situation with loss of cells and fibrotic scar formation. In this situation, survival of transplanted cells may be impaired.

A recent study, where retinal pigment epithelial (RPE) was transplanted into the subretinal space after CNV membranectomy, showed that the transplanted RPE was severely impaired by the still underlying active age-related macular degeneration (AMD) [3]. CNV membranes in exudative AMD eyes do not differ histologically from CNV membranes found in eyes with other underlying diseases, indicating that CNV membranes are a nonspecific wound repair to breaks in Bruch's membrane (BM) [4–6]. This may suggest that the entire milieu needs to be altered before transplanted cells can rescue retinal function [7]. Several synthetic materials have been tested as scaffolds for retinal progenitor cell transplantation and have been found to support adhesion, survival, and migration [8, 9].

We have previously shown that amniotic membrane transplanted into the subretinal space in young pigs stimulates the host RPE to cover this basement membrane substitute [10, 11]. The amniotic membrane (AM) is a basement membrane with antiangiogenic and anti-inflammatory properties well known in anterior segment reconstructive surgery. We have previously described a model of CNV in the pig [12, 13]. We wanted to investigate if the AM transplanted to the subretinal space in this model could facilitate regrowth of RPE cells and prevent the formation of a CNV membrane.

2. Material and Methods

Domestic pigs (Danish Landrace), 4 months old and weighing approximately 30 kg, were used as experimental animals. Their treatment followed the ARVO resolution for the use of animals in ophthalmic and vision research, and was supervised by a veterinarian nurse. The Danish Animal

Experiments Inspectorate granted permission for the use of pigs in this study.

2.1. Amnion Membrane Isolation. Porcine amniotic membranes from placenta from full borne pigs (114 days) and from 104-day-old foetuses were used. Placentas from full borne specific pathogen-free (SPF) pigs were obtained from the local supplier of SPF pigs. Placentas from foetuses were obtained by planned Caesarean section on SPF pigs. The amnionchorion-endometrium was identified and isolated. Using microscope and forceps it was possible to separate the AM from the chorion. Epithelial cells were removed from the AM by mechanically scraping with a silicone-coated tip after 15–20 min incubation in 0,1 M NH_4OH followed by repeated freezing and thawing until histopathology confirmed complete removal of epithelial cells.

2.2. Anaesthesia. All animals were preanaesthetised with intramuscular injections of 15 mg midazolam (Dormicum, Roche, Hvidovre, Denmark) and 250 mg ketamine (Ketalar, Parke-Davis, ballerup, Denmark) followed by intravenous administration of 250 mg mebumal (Mebumal, SAD, Copenhagen, Denmark). The pigs were endotracheally intubated, artificially ventilated, and anaesthetised with halothane 1% in combination with 66% NO2 in oxygen.

2.3. Induction of CNV. Mechanical induction of a CNV has previously been described [13]. In short, a three-port localized vitrectomy was used. Access to the subretinal space was obtained with a retinal perforator (Synergetics Inc, st Charles, MO, USA). Retina was then carefully lifted off by injecting isotonic NaCl through a 30G needle (BSS injection needle, straight 1270, DORC international B.V., NL). An automatic scissor (STORZ, Bausch & Lomb Surgical, Inc., San Dimas, CA, USA) was used to enlarge the retinotomy before the RPE was gently removed using a retinal scraper (1294, DORC international B.V., NL). The subretinal space was then washed with isotonic NaCl through a 21G needle (number 5021, Visitec, FL, USA) to ensure total removal of damaged RPE, and finally rupture to BM was made with the retinal perforator.

2.4. Transplantation Technique. AM was transplanted to the SRS in 15 pigs in addition to the CNV induction. DORC's Combined Spatula/Peeling Forceps (1297, DORC international B.V., NL) was used to deliver the AM to the SRS. The DORC hockeystick Microforceps (1286 LFT, DORC international B.V., NL) was then used to flatten the AM over the RPE lesion in the SRS (Figures 1(a) and 1(b)).

2.5. Followup. The observation period varied between 14 and 42 days. Prior to enucleation the pigs were examined by ophthalmoscopy and fundus photography. All pigs were hereafter euthanized by a lethal injection of 4 g pentobarbital with 400 mg of lidocaine hydrochloride (Veterinærapoteket Københavns Universitet, Copenhagen, Denmark).

2.6. Histopathology. Enucleated eyes were immediately fixed in 4% buffered formaldehyde (Lilly's fluid, Bie & Berntsen, Rødovre, Denmark) overnight at room temperature and paraffin embedded according to routine procedures. Sections of 4 μm were cut and stained with haematoxylin and eosin. Haematoxylin/phloxine/saffron staining was used to identify transplanted amnion membrane. Induced inflammation in the adjacent retina and choroid was scored semiquantitatively based on the number of lymphocytes per visual field ($\times$10 magnification) (0 = 0–10; 1 = 10–100; 2 = 100–1000; 3 >1000). In the analysis of the data the groups could be reduced further to 0: no increase and 1: inflammation (>100/field view).

2.7. Measurement of CNV. All sections were examined with a light microscope, Axioplan 2 (Carl Zeiss, Jena, Germany); digital images were obtained with an Axiocam HRC (Carl Zeiss). Areas of interest were demarcated on digital images and their sizes were computed with the software package Axiovision 3.1 (Carl Zeiss). Average CNV thickness was preferred as a size measurement because it has proved to be the most reproducible size measurement at our disposal in this model [12]. Kruskal-Wallis one-way analysis of variance on ranks was performed. Statistics and graphs were made in SigmaStat/SigmaPlot (Systat Software Inc., San Jose, CA).

3. Results

In this study, a total number of 24 pigs were induced with CNV. 15 pigs were transplanted with AM after mechanical removal of RPE and rupture of BM. 9 pigs served as a control group. The control group has been described histologically in a previous study [13].

The lesion in BM and the induced CNV could be identified in all 24 eyes. In 7 eyes, AM was found to completely cover the BM lesion. In 8 eyes, AM did not cover the entire lesion, and in 3 of these cases AM was not in contact with the induced defect in BM. The measurements of the CNV are given as mean +/− SD in Figure 2.

3.1. Surgery. The lens protrudes far back into the vitreous body of pigs making the lens vulnerable to peroperative damage. However, surgical complications after transplantation of amniotic membranes were limited. Four pigs had localised cataracts close to upper nasal sclerotomy most likely induced by the retinal perforator. No pigs were excluded due to surgical complications.

3.2. Inflammatory Response. The induction of CNV in the pig induces a huge inflammatory response in the main choroid but also the retina. This inflammation in the choroid is seen in 100% of the control group. The transplanted AM reduced the number of inflammatory cells in the tissue close to the transplanted membrane material (data not shown). In the cases with successful placed AM and minimal CNV no increase in number of inflammatory cells was observed. This difference was significant ($P < 0.005$, Fischer's exact test). Inflammation in the neuroretina was, however, comparable between the two groups (control: 70%, AM: 34%, $P = 0.28$).

3.3. RPE Response. The transplanted amniotic membranes were completely or partly covered with RPE cells. The RPE

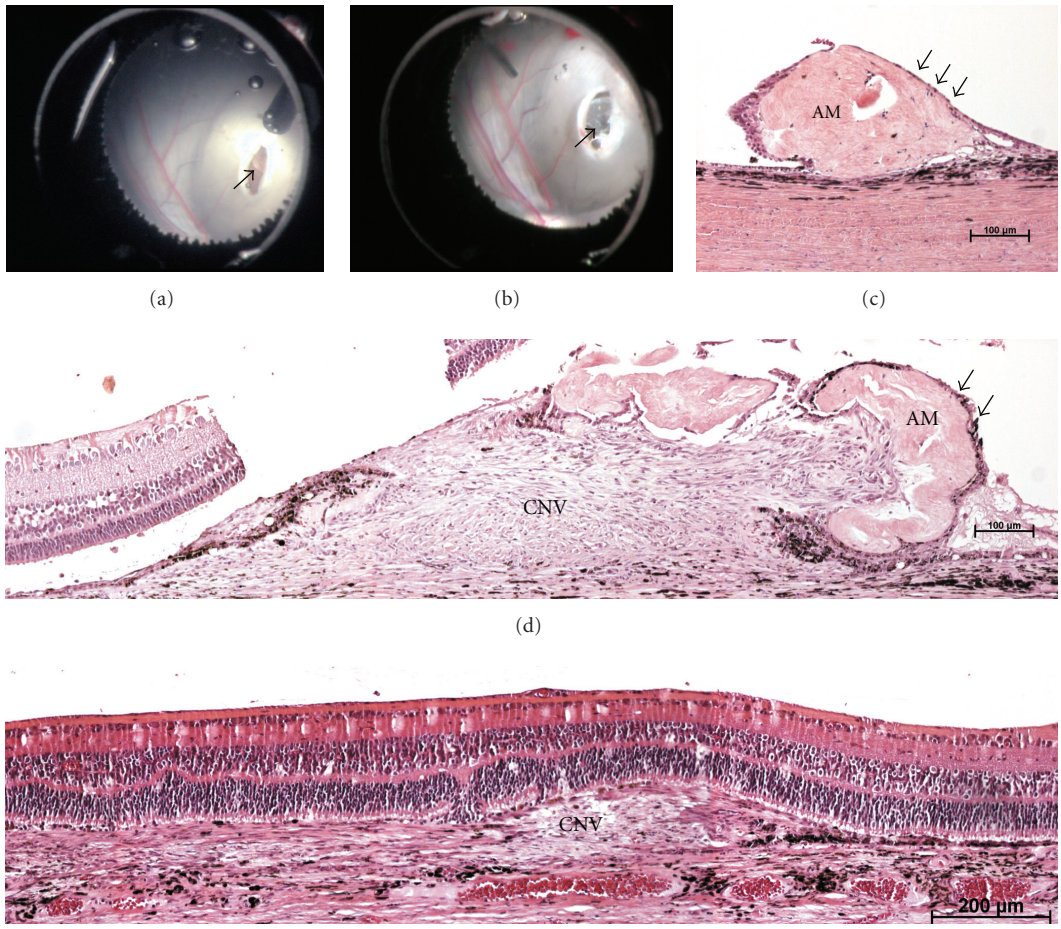

Figure 1: (a) Peroperative photo of the bleb with the retinotomy. Arrow points at the lesion in the retinal pigment epithelium trough the retinotomy. (b) Peroperative photo from the same operation as (a). The arrow points now at transplanted amniotic membrane (AM) covering the induced lesion. (c) Micrograph of the subretinal space (SRS) in a pig after transplantation of AM. The AM is in close contact with the RPE and covers the lesion completely. AM is totally covered with RPE cells similar to the normal host RPE and no CNV is observed. (d) Micrograph of the SRS in a pig after transplantation of AM. AM covers in this case only partly the induced lesion. Formation of a choroidal neovascularisation (CNV) is seen. AM is in contact with the RPE at one side and the RPE has covered the retina near side of the AM. We have not observed CNV penetrate the AM, but the CNV rather tends to "crawl under" the membrane out into the SRS. (e) Micrograph of a control eye that received mechanical damage to RPE/Bruch's membrane, but did not receive any AM. A large CNV is seen in the SRS. The peripheral part is covered with RPE, whereas the central part is in close contact with the photoreceptors. The scale bars are: (a) 100 μm, (b) 100 μm, and (c) 200 μm.

was always observed as a monolayer on the inner surface of AM. The pigmentation of the RPE varied from completely depigmented to normal pigmentation with cigar-shaped granules. Depigmented RPE cells on the AM were always found in combination with a zone of depigmented RPE cells on normal-looking BM surrounding the AM. Such a zone with depigmented RPE cells on BM was never observed in cases where normal pigmented RPE cells had covered the AM.

4. Discussion

In this paper we demonstrate that isolated amniotic membrane can modify the formation of choroidal neovascularisation in a porcine model of subretinal wound healing. Amniotic membrane is a well-known inhibitor of neovascularisation on the ocular surface [14], and anti-inflammatory and antiangiogenic proteins have not only been shown to be synthesised in the amniotic epithelium, but they have also been identified in the compact layer of the AM stroma [15]. We do observe a few new vessels within the membrane, but these vessels are only found in the space beneath the membrane and are never observed to penetrate the AM. The fact that we only used AM without epithelium for transplantation and the observed short radius of action makes it likely that the anti-inflammatory and antiangiogenic effect of the AM are dependent on factors in the stroma, and that these factors are immobilised in the membrane. Decreased, or lack of, inflammation was also observed in tissue in close contact to the AM.

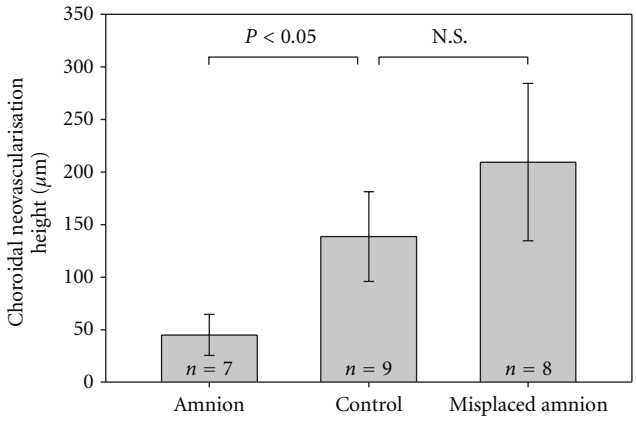

Figure 2: Graph of maximal height in induced choroidal neovascularisation measured in um. Experiments were divided in successful (amnion), unsuccessful (misplaced amnion), and control (no amnion). Data are presented as mean +/− SD. Kruskal-Wallis one-way analysis of variance on ranks was performed.

The idea of delivery of active drugs together with cellular transplants is a major objective in the construction of synthetic scaffolds [16], but AM may happen to be a natural reservoir for relevant growth factors for the optimal survival for stem cells. Increased attention on AM as a basement membrane support for cultured RPE is therefore seen in vitro [17, 18] and in vivo [10, 11].

AM is, in contrast to the anterior les capsule (ALC), another basement membrane [19], very easy to handle and flatten in vitro. In vivo we succeeded to flatten the AM in the subretinal space during surgery (Figure 1(b)), but unfortunately, histology show that we were not able to maintain the AM flattened in the SRS (Figures 1(c) and 1(d)). We are currently evaluating different techniques that could circumvent the problem. The use of gas or silicone oil could as well keep retina and the underlying AM flat, but may also cause increased glial reaction on the naked AM as seen when neuroretina gets into contact with naked ALC [19]. Use of photocoagulation to weld the AM to the underlying BM might be another possibility. However, scar formation takes time and photocoagulation may therefore need to be used in combination with a method that keeps the AM in place while scarring occurs. Bioadhesives like the types used to glue retinal prosthesis to the retina are being developed [20] and might be a more suitable solution.

The orientation of the AM in the SRS might be important, but we did not test for this in this study. The AM is part of an organised structure and is in itself a polarised membrane. Only the surface toward the foetus is covered with epithelium. We did not harvest from a specific part of the yolk sack and we did not check the orientation of the transplanted membranes. More careful harvesting procedures and storage of the membranes on filter paper to allow orientation of the membrane could answer these questions in future studies.

The ingrowths of RPE on the membrane support our previous observations in both ALC transplantations and RPE removal experiments [10, 19]. RPE cells covering denuded BM become more and more flat and depigmented the farther away they are from intact RPE whereas RPE covering the AM maintains morphology similar to adjacent RPE. Therefore, it seems important not only to cover the rupture itself in BM, but also to cover the denuded BM placing the AM in immediate contact with healthy RPE.

The AM seems to be a good candidate for future studies, since this membrane can be handled surgically and has anti-inflammatory and antiangiogenic properties that enable the correctly placed AM to inhibit the formation of CNV. Finally, the AM is an excellent growth support for cells whatever host RPE cells, new RPE cells, or stem cells are needed in the SRS.

Abbreviations

AM: Amniotic membrane
ALC: Anterior lens capsule
BM: Bruch's membrane
CNV: Choroidal neovascularisation
H&E: Haematoxylin and eosin
RPE: Retinal pigment epithelium
SD: Standard deviation.

Acknowledgments

A part of this study was presented as a poster at the ARVO in 2001. This paper is supported by grants from the Danish Eye Foundation, Landsforeningen Værn om synet, Civilingenør Lars Andersens Legat, Novo Nordic Foundation, and Svend H.A. Schrøders og Hustru L.L. Schrøders Fond.

References

[1] H. Klassen, K. Warfvinge, P. H. Schwartz et al., "Isolation of progenitor cells from GFP-transgenic pigs and transplantation to the retina of allorecipients," *Cloning and Stem Cells*, vol. 10, no. 3, pp. 391–402, 2008.

[2] F. D. Rodriguez and E. Vecino, "Stem cell plasticity, neuroprotection and regeneration in human eye diseases," *Current Stem Cell Research & Therapy*, vol. 6, no. 1, pp. 73–81, 2011.

[3] L. V. Del Priore, H. J. Kaplan, T. H. Tezel, N. Hayashi, A. S. Berger, and W. R. Green, "Retinal pigment epithelial cell transplantation after subfoveal membranectomy in age-related macular degeneration: clinicopathologic correlation," *American Journal of Ophthalmology*, vol. 131, no. 4, pp. 472–480, 2001.

[4] H. E. Grossniklaus, A. K. Hutchinson, A. Capone, J. Woolfson, and H. M. Lambert, "Clinicopathologic features of surgically excised choroidal neovascular membranes," *Ophthalmology*, vol. 101, no. 6, pp. 1099–1111, 1994.

[5] H. E. Grossniklaus and J. D. M. Gass, "Clinicopathologic correlations of surgically excised type 1 and type 2 submacular choroidal neovascular membranes," *American Journal of Ophthalmology*, vol. 126, no. 1, pp. 59–69, 1998.

[6] C. W. Spraul, G. E. Lang, H. E. Grossniklaus, and G. K. Lang, "Histologic and morphometric analysis of the choroid, Bruch's membrane, and retinal pigment epithelium in postmortem eyes with age-related macular degeneration and histologic

examination of surgically excised choroidal neovascular membranes," *Survey of Ophthalmology*, vol. 44, supplement 1, pp. S10–S32, 1999.

[7] L. V. Del Priore, T. H. Tezel, and H. J. Kaplan, "Maculoplasty for age-related macular degeneration: reengineering Bruch's membrane and the human macula," *Progress in Retinal and Eye Research*, vol. 25, no. 6, pp. 539–562, 2006.

[8] M. Tomita, E. Lavik, H. Klassen, T. Zahir, R. Langer, and M. J. Young, "Biodegradable polymer composite grafts promote the survival and differentiation of retinal progenitor cells," *Stem Cells*, vol. 23, no. 10, pp. 1579–1588, 2005.

[9] S. Cai, M. E. Smith, S. M. Redenti, G. E. Wnek, and M. J. Young, "Mouse retinal progenitor cell dynamics on electrospun poly(varepsilon-caprolactone)," *Journal of Biomaterials Science, Polymer Edition*. In press.

[10] J. F. Kiilgaard, J. U. Prause, M. Prause, E. Scherfig, M. H. Nissen, and M. La Cour, "Subretinal posterior pole injury induces selective proliferation of RPE cells in the periphery in in vivo studies in pigs," *Investigative Ophthalmology and Visual Science*, vol. 48, no. 1, pp. 355–360, 2007.

[11] N. Lassota, J. F. Kiilgaard, J. U. Prause, and M. la Cour, "Correlation between clinical and histological features in a pig model of choroidal neovascularization," *Graefe's Archive for Clinical and Experimental Ophthalmology*, vol. 244, no. 3, pp. 394–398, 2006.

[12] N. Lassota, J. F. Kiilgaard, J. U. Prause, K. Qvortrup, E. Scherfig, and M. la Cour, "Surgical induction of choroidal neovascularization in a porcine model," *Graefe's Archive for Clinical and Experimental Ophthalmology*, vol. 245, no. 8, pp. 1189–1198, 2007.

[13] J. F. Kiilgaard, M. V. N. Andersen, A. K. Wiencke et al., "A new animal model of choroidal neovascularization," *Acta Ophthalmologica Scandinavica*, vol. 83, no. 6, pp. 697–704, 2005.

[14] A. Jiang, C. Li, Y. Gao, M. Zhang, J. Hu, and W. Kuang, "In vivo and in vitro inhibitory effect of amniotic extraction on neovascularization," *Cornea*, vol. 25, no. 10, supplement 1, pp. S36–S40, 2006.

[15] Y. Hao, D. H. K. Ma, D. G. Hwang, W. S. Kim, and F. Zhang, "Identification of antiangiogenic and antiinflammatory proteins in human amniotic membrane," *Cornea*, vol. 19, no. 3, pp. 348–352, 2000.

[16] S. R. Hynes and E. B. Lavik, "A tissue-engineered approach towards retinal repair: scaffolds for cell transplantation to the subretinal space," *Graefe's Archive for Clinical and Experimental Ophthalmology*, vol. 248, no. 6, pp. 763–778, 2010.

[17] R. D. Hamilton, A. J. Foss, and L. Leach, "Establishment of a human in vitro model of the outer blood-retinal barrier," *Journal of Anatomy*, vol. 211, no. 6, pp. 707–716, 2007.

[18] R. D. Hamilton and L. Leach, "Isolation and properties of an in vitro human outer blood-retinal barrier model," *Methods in Molecular Biology*, vol. 686, pp. 401–416, 2011.

[19] J. F. Kiilgaard, A. K. Wiencke, E. Scherfig, J. U. Prause, and M. La Cour, "Transplantation of allogenic anterior lens capsule to the subretinal space in pigs," *Acta Ophthalmologica Scandinavica*, vol. 80, no. 1, pp. 76–81, 2002.

[20] E. Margalit, G. Y. Fujii, J. C. Lai et al., "Bioadhesives for intraocular use," *Retina*, vol. 20, no. 5, pp. 469–477, 2000.

Hindawi Publishing Corporation
Stem Cells International
Volume 2012, Article ID 685901, 12 pages
doi:10.1155/2012/685901

Research Article

Assessment of Hereditary Retinal Degeneration in the English Springer Spaniel Dog and Disease Relationship to an *RPGRIP1* Mutation

Kristina Narfström,[1,2] Manbok Jeong,[3] Jennifer Hyman,[4] Richard W. Madsen,[5] and Tomas F. Bergström[6]

[1] *Department of Veterinary Medicine and Surgery, College of Veterinary Medicine, University of Missouri, Columbia, MO 65211, USA*
[2] *Department of Ophthalmology, Mason Eye Institute, University of Missouri, Columbia, MO 65211, USA*
[3] *Department of Veterinary Medicine and Surgery, College of Veterinary Medicine and BK21 Program for Veterinary Science, Seoul National University, Seoul 151-742, Republic of Korea*
[4] *Eye Care For Animals, VA, 20176-3367, USA*
[5] *Biostatistics, School of Medicine, University of Missouri, Columbia, MO 65211, USA*
[6] *Department of Animal Breeding and Genetics, Swedish University of Agricultural Sciences, 750 07 Uppsala, Sweden*

Correspondence should be addressed to Kristina Narfström, narfstromk@missouri.edu

Received 12 September 2011; Revised 9 November 2011; Accepted 15 November 2011

Academic Editor: Henry J. Klassen

Intensive breeding and selection on desired traits have produced high rates of inherited diseases in dogs. Hereditary retinal degeneration, often called progressive retinal atrophy (PRA), is prevalent in dogs with disease entities comparable to human retinitis pigmentosa (RP) and Leber's congenital amaurosis (LCA). Recent molecular studies in the English Springer Spaniel (ESS) dog have shown that PRA cases are often homozygous for a mutation in the RPGRIP1 gene, the defect also causing human RP, LCA, and cone rod dystrophies. The present study characterizes the disease in a group of affected ESS in USA, using clinical, functional, and morphological studies. An objective evaluation of retinal function using electroretinography (ERG) is further performed in a masked fashion in a group of American ESS dogs, with the examiner masked to the genetic status of the dogs. Only 4 of 6 homozygous animals showed clinical signs of disease, emphasizing the need and importance for more precise studies on the clinical expression of molecular defects before utilizing animal models for translational research, such as when using stem cells for therapeutic intervention.

1. Introduction

The domestic dog has a unique population history with bottlenecks that has shaped the diversity and structure of the canine genome. The first bottleneck can be traced back about 7,000–50,000 generations [1] and reflects the early domestication of dogs from wild populations of wolves 15,000–100,000 years ago [2–4]. When dog breeds were established in the 1800s (about 50–100 generations ago) more genetic variation was lost, and this second population bottleneck resulted in relatively large genetic differences between breeds and little genetic variation within breeds. The two bottlenecks left distinctive signatures in the canine genome with long-range linkage disequilibrium (LD) and long haplotype blocks of 500 kb–1 Mb within breeds and short-range LD across breeds [1, 5]. Intensive breeding and selection on desired traits have also produced high rates of inherited diseases with genetic causes that are breed-specific or nearly so. The domestic dog has therefore emerged as an important animal model for comparative genome analysis and for characterization of inherited disease. Other uses for dog models are in translational research such as gene therapy or stem cell transplantation for treatment strategies in conjunction with hereditary retinal blinding diseases.

Hereditary retinal degeneration, often called progressive retinal atrophy (PRA) in dogs and also in cats, is a group of diseases of the photoreceptors that exists in various forms. Rods and cones are usually primarily affected, with time leading to bilateral blindness. More than 100 dog breeds are on the list for those that may be affected, in which at least 15 mutations are prevalent in 34 specific dog breeds [6]. For cats, PRA is observed less frequently, although recently, a mutation in the CEP290 gene was shown to be causative of hereditary retinal degeneration in a large number of cat breeds, primarily Abyssinian and Siamese cats [7].

Through advancement in the understanding of hereditary disease processes affecting the outermost portion of the retina, PRA has been further characterized biochemically, electrophysiologically, morphologically, and genetically. Using molecular methods, including the elucidation of causative mutant genes for several hereditary retinal disorders, much knowledge has been gained especially in regards to disease mechanisms [8]. The availability of the canine genome sequence [1] (http://www.genome.gov/12511476) has simplified the task of identifying genes responsible for diseases and traits in dogs. Similarly, a full genome sequence (10X) of the cat has recently been completed (Wes Warren, Washington University, personal communication, 2010). A number of the PRAs have been designated gene symbols reflecting either the specific cells involved in the hereditary retinal dystrophy or the protein involved in the retinal degenerative condition.

Although PRA is usually manifested with a breed specific phenotype, the same allelic mutation may be shared by several different breeds, such as for the *prcd* mutation [9]. In other instances, different but allelic mutations causative of PRA have been documented in related breeds [10]. Importantly, breeds may also express more than one form of PRA. For example, in golden retrievers at least three different genes and mutations are responsible for PRA. Two of the genes are known, prcd and slc4a3, but at least one more gene remains to be characterized [11]. The presence of more than one causative mutation for PRA in some breeds is complicating the understanding and interpretation of phenotype-genotype relationships and thus the results of DNA testing procedures [12]. Due to these factors, phenotypic heterogeneity is often found when studying various forms of retinal degenerative diseases of dogs. This has also been observed in similar retinal disease processes of humans, such as in retinitis pigmentosa (RP) or in Leber's congenital amaurosis (LCA). In these diseases, significant phenotypic heterogeneity is found including age of onset, clinical findings, and progression of disease [8, 13]. This is especially true for RP in which at least 140 mutations have been described only in the rhodopsin gene [14, http://omim.org/entry/268000].

Classical PRA has been described as a generalized disease of the fundus, affecting the rod photoreceptors primarily and with later involvement of cones. Clinically night blindness is an early sign but with progression of disease, affection of both night and day vision occurs. Ophthalmoscopically early changes have been noted as a generalized diffuse change in coloration and reflectivity of the tapetal fundus with vascular attenuation in later stages, the changes being most severe in the peripheral parts but with later involvement of the entire fundus [15].

PRA in the English Springer Spaniel dog was originally described in USA [16]. There were some unusual findings in the disease in that there was an increased granularity of the fundus or a slightly patchy discoloration as the earliest clinical sign observed in the very far periphery of the tapetal fundus. The disease had a variable time of onset and progression, leading to blindness in most of the affected dogs.

Mutations in the RPGRIP1 gene have been identified as causative to human RP, LCA, and cone-rod dystrophies [17–19]. The RPGRIP1 protein was shown to be involved in transport mechanisms that occur through the photoreceptor connecting cilium by interaction with another protein, RPGR [20]. Defects in the latter gene are responsible for the X-linked retinopathy of humans and also in X-linked PRA in Samoyed and Siberian husky dogs [21]. Further, a mutation in NPHP4, another gene known to interact with RPGRIP1, was shown to be causative of cone/rod dystrophy of the wire-haired Dachshund [22, 23]. Another such gene working in concert with RPGRIP1 is CEP290, and when mutated it was found to cause hereditary retinal degeneration in cats [24]. The protein is also an important component of the transport mechanism, whereby specialized proteins critical for phototransduction are transferred from their site of synthesis in the inner segment through the connecting cilium to the outer segment [25]. A number of normal genes are thus necessary for normal function and structure of the entire photoreceptor cell and, especially, for outer segment disc morphogenesis [26].

Mellersh and collaborators recently mapped the cone rod locus (cord1) to a 14.5 Mb region on dog chromosome 15 (16.54–30.68 Mb: coordinates as in CanFam2.0), which contained the RPGRIP1 gene. A 44 bp insertion in exon 2 was further identified in the RPGRIP1 gene, truncating the protein. This defect segregated completely with the cord1 phenotype of cone rod dystrophy in the Animal Health Trust (United Kingdom) research colony of miniature dachshunds. It was concluded that the mutation was responsible for cord1 disease, due to a mutation in the RPGRIP1 gene. It was further emphasized that dogs with this disease are valuable animal models for exploring disease mechanisms and potential therapies for the human counterpart, LCA [27].

The *RPGRIP1* mutation in cone rod dystrophy (cord1) was further evaluated as a candidate gene for PRA in ESS dogs using DNA collected at the University of Missouri (Columbia, USA), from a large number of dogs, unaffected and affected by bilateral, generalized retinal degeneration. The mutation was observed in exon 2 of RPGRIP1 in all of the affected dogs (Gary Johnson and Liz Hansen, personal communications, 2007).

This paper describes the results of a research project that was thereafter initiated, in order to characterize the clinical signs of retinal degeneration in the ESS breed and to evaluate the genotype-phenotype correlation in USA in family-owned ESS, in regards to the mutation in the RPGRIP1 gene. Recently, the study was further expanded to also include blood samples from a group of Swedish ESS dogs, with and

Table 1: Swedish ESS dogs with genotype-phenotype correlation in regards to the RPGRIP1 mutation. The sex of the dogs is indicated as M for males and F for females. The age of diagnosis is shown as years (y) and months (m) when dogs were first examined and diagnosed with PRA. For the dogs without PRA (normal), the most recent examination dates were used for age at examination. The genotypes are given as −/− for genetically affected, +/− for carriers, and +/+ for genetically clear individuals of the 44 bp deletion in exon 2 of the RPGRIP1 gene.

Dog number	Sex	Age at examination	Phenotype	RPGRIP1 genotype
ESS-008	M	2 y 4 m	PRA	−/−
ESS-014	F	3 y 8 m	PRA	−/−
ESS-004	F	5 y 9 m	PRA	+/−
ESS-006	M	5 y 7 m	PRA	+/−
ESS-016	M	7 y 3 m	PRA	+/−
ESS-020	M	9 y 8 m	PRA	+/−
ESS-003	F	5 y 4 m	PRA	+/+
ESS-005	F	3 y 1 m	PRA	+/+
ESS-007	M	11 y 4 m	PRA	+/+
ESS-009	M	4 y 6 m	PRA	+/+
ESS-015	F	8 y 3 m	Normal	+/+
ESS-017	F	5 y 11 m	Normal	+/+
ESS-018	F	12 y 1 m	Normal	+/+
ESS-019	M	7 y 10 m	Normal	+/+

without clinical signs of PRA and the correlation in regards to the *RPGRIP1* mutation.

2. Materials and Methods

2.1. Animals and Clinical Examinations. ESS dogs from USA were included in the characterization of disease. They were privately owned dogs for which owners or breeders had requested eye examinations, according to eye scheme routines, since their dogs or their close relatives were used for breeding. Twelve cases with clinical signs of retinal degeneration in 1.5- to 12-year-old ESS dogs were discovered during the two-year study period. All of the affected dogs were homozygous for the *RPGRIP1* mutation.

Informed consent was obtained from the owners of participating dogs. The clinical study included evaluation of retinal and vision based responses and reflexes: menace, dazzle, and examination of the pupillary light reflexes as well as visual testing by behavior and visual reactions to falling cotton balls [28]. Pupils were dilated with short-acting mydriatics 20 minutes before examination of the internal structures, using 1-2 drops of 1% tropicamide in each eye (Mydriacyl, Bausch and Lomb Inc., Tampa, FL). Standard ophthalmic examination of the interior of the eye was then performed using indirect ophthalmoscopy (Welch-Allyn Distributors, Medical Device Depot, Inc., MD, USA) and slit lamp biomicroscopy (SL14, KOWA Co. Ltd., Tokyo, Japan). Fundus appearance was documented with a digital fundus camera (Nidek NM-100, Nidek Co. Ltd., Freemont, CA).

2.2. DNA Samples. DNA samples from ESS dogs previously collected by Dr. Gary Johnson's laboratory, University of Missouri, Columbia, USA, were utilized. All samples were collected as surplus from blood specimens submitted for routine *cord1* test or for clinical biochemistry under the condition of anonymity of the individuals and their owners. DNA was extracted from blood samples and genotyping for the *cord1* disease causing allele of the mutated gene RPGRIP1 gene was performed as described by Mellersh et al., 2006 [27].

In addition, to investigate whether the cord1 genotype was prevalent among ESS dogs in Sweden, and especially in ESS dogs diagnosed with PRA, blood samples from a total of 14 normal and affected dogs were tested for the 44 bp insertion in exon 2 of the RPGRIP1 gene (Table 1). The blood from the Swedish dogs was collected into EDTA tubes and genomic DNA was extracted manually from peripheral blood leukocytes using QIAamp DNA Blood Midi Kit (Qiagen, Hilden, Germany) or automatically on a QIA symphony SP/AS instrument (Qiagen, Hilden, Germany).

Primers for genotyping the 44 bp insertion in exon2 of RPGRIP1 gene were designed using the software Primer3 [29]. PCR amplification was performed using the primers Cfa_Cord1-F (5′-6FAM-CCCTTTCCTGGGACTTTAGG-3′) and Cfa_Cord1-R (5′-CCCTCTGCCTATGTCTCTGC-3′). 10–20 ng of genomic DNA was used in a 10 uL PCR-reaction with 0.5 mM of each primer, 50 mM KCl, 10 mM Tris-HCl pH 8.3, 2.5 mM $MgCl_2$, 0.2 mM of each dNTP and 0.5 units of Taq polymerase (AmpliTaq Gold; Applied Biosystems, Foster City, CA, USA; DNA polymerase). A total of 35 PCR cycles was performed, each with denaturation at 94°C for 1 minute, annealing at 60°C for 40 s and a primer extension at 72°C for 40 s. The fragment length polymorphism was then determined using an ABI 3100 DNA Analyzer and GeneMapper Software (Applied Biosystems, Inc., (ABI), Foster City, CA).

2.3. Masked Electroretinography Study. Fourteen American dogs were included in a masked electroretinography (ERG) study for objective evaluation of retinal function (for ERG see details below). Blood from these dogs, age between 7 y 9 m and 13 y 10 m, had previously been genotyped by Dr. Johnson's laboratory, as described above. Dogs were

Table 2: Details in regards to dogs in the masked ERG study. The genotypes are given as −/− for genetically affected, +/− for carriers, and +/+ for genetically clear individuals of the 44 bp deletion in exon 2 of the RPGRIP1 gene. The age at the time for ophthalmic and ERG examinations is given as years (y) and months (m).

Dog number	RPGRIP1 genotype	Age at ERG	ERG results	Other clinical findings
1	−/−	9 y 2 m	Abnormal	Normal vision, fundus normal
2	+/−	8 y 7 m	Normal	Normal vision, fundus normal
3	+/−	7 y 9 m	Normal	Normal vision, fundus normal
4	+/−	7 y 9 m	Normal	Normal vision, fundus normal
5	+/−	13 y 10 m	Normal	Normal vision, fundus normal
6	+/−	11 y 11 m	Normal	Normal vision, fundus normal
7	−/−	9 y 2 m	Abnormal	Normal vision, fundus abnormal
8	−/−	9 y 2 m	Abnormal	Normal vision, fundus abnormal
9	−/−	8 y 4 m	Normal	Normal vision, fundus normal
10	+/−	9 y 4 m	Normal	Normal vision, fundus normal
11	+/−	8 y	Normal	Normal vision, fundus normal
12	+/+	9 y 3 m	Normal	Normal vision, fundus normal
13	−/−	12 y 4 m	Abnormal	Reduced vision, fundus abnormal
14	−/−	7 y	Normal	Normal vision, fundus normal

chosen for retinal functional evaluation in accordance with the owner's consent and availability. The genetic status of each dog in regards to the *RPGRIP1* mutation was unknown to the investigator (K. Narfström) at the time of the ERG recordings: 6 dogs were homozygous (affected); *RPGRIP*−/−, 7 were heterozygous (normal); *RPGRIP*−/+, and 1 was homozygous (normal); *RPGRIP1*+/+ (Table 2). Before the ERG was performed in each dog, they underwent a routine ophthalmic examination as previously described.

2.4. Electroretinography. Unilateral electroretinographic (ERG) evaluations were performed using a portable ERG unit (HMsERG model 1000, RetVet Corp., Columbia, MO), with a mini-Ganzfeld dome positioned approximately 1 cm from the right tested eye (Figure 1). For practical reasons it was deemed sufficient to perform the evaluation in only one eye since both eyes are usually affected in hereditary retinopathies and the eyes are usually at the same stage of the retinal degenerative process [15]. Dogs were deeply sedated by using medetomidine IV (Domitor, Novartis, Pfizer Animal Health, Exton, PA), up to 150 micrograms/kg, equivalent to 0.15 mL/kg, and prepared for the ERG session in ordinary room light. Heart and respiratory rates were closely monitored before and throughout the procedure and the dogs were temperature controlled. The dog's head was positioned on a cushion for stabilization. Maximal pupillary dilation was provided for by the use of short-acting mydriatics (see above) and the eye was further topically anesthetized using 0.5% proparacaine hydrochloride (Alcaine, Alcon, Fort Worth, TX). A lid speculum was inserted to ensure that the nictitating membrane as well as the upper and lower eyelids did not interfere with light exposure to the maximally dilated pupils. Platinum subdermal needle electrodes (model E2, Grass Instrument Division, Astro-Med, Inc., West Warwick, RI) were used for the ground electrode, positioned on the occipital crest, and for the reference electrode, positioned 3 cm from the lateral canthus, close to the base of the right ear. An active contact lens electrode (ERG-Jet, Universo Plastique, LKC Technologies Inc., Gaithersburg, Md) was placed on the cornea after instillation of one drop of 2% methylcellulose (Methocel, Ciba Vision, Munich, Germany). The electrodes were connected to a preamplifier and the signals were amplified with a bandpass filter between 0.3 and 300 Hz.

Figure 1: An English Springer Spaniel (ESS) dog deeply sedated and prepared for functional evaluation of the retina. The handheld multispecies electroretinograph (HMsERG) unit is used together with a preprogrammed protocol for evaluation of rod and cone function.

Each ERG session consisted of scotopic and photopic ERGs in accordance with the "Dog Diagnostic Protocol," recommended by the European College of Veterinary Ophthalmologists, primarily for evaluation and separation of rod and cone function [30]. This protocol is preprogrammed on the ERG unit and is executed automatically upon initiation of the ERG session by the examiner. During 20 minutes

of dark adaptation, scotopic-low intensity rod responses were elicited every 4 minutes at a stimulus intensity of 0.01 cd·s/m^2; responses were averaged after 10 flashes given at 2 seconds interval and rod responses were recorded at each time point (test #1–5). The light stimulus intensity was then increased to 3 cd·s/m^2 for scotopic standard intensity stimulation and responses averaged and recorded after 4 flashes at 10-second intervals (test #6). Thereafter scotopic high-intensity responses were elicited using 10 cd·s/m^2; responses were averaged to 4 flashes administered at 20-second intervals (test #7). The latter two recordings depict a mixture of responses from both rods and cones. After 10 minutes of light adaptation with a background luminance of 30 cd/m^2, photopic single flash responses were recorded, using 3 cd·s/m^2 of flash stimulus, averaging 32 flashes at an interval of 0.5 seconds (test #8), followed by evaluation of 30 Hz photopic flicker at the same light intensity stimulation (test #9). The latter two recordings were performed in order to evaluate cone and cone pathways, respectively. Data were collected automatically on the compact flash card of the ERG unit, transferred to a computer, printed, and stored for further analysis. ERGs were evaluated and the amplitudes and implicit times for the a- and b-waves were measured as previously described [30].

After termination of the ERG session an injection of atipamazole hydrochloride (Antisedan, Pfizer Inc., St Louis, MO) was administered intramuscularly to reverse the deep sedation (at a dosage 5-times higher than that given of the medetomidine, i.e., similar volumes were injected).

2.5. Morphology. Upon the owner's request due to unrelated medical problems, three American ESS dogs were euthanized and the eye tissue made available for the present study. Advanced PRA had been diagnosed in two of the dogs (9 and 6 years old, resp.), while the third dog, 3 years old, had a normal fundus appearance. Euthanasia was performed by intravenous infusion of Beuthanasia-D-Special (Schering Plough Animal Health, Omaha, NE.). The eyes of each dog were enucleated immediately after death and the posterior segment of each eye placed in fixative solution for examination using light and electron microscopy (LM and EM). The fixative included 2.0% glutaraldehyde, 1.12% paraformaldehyde, 0.13 M sodium cacodylate, 0.13 mM $CaCl_2$, pH 7.40. Eyecups were incubated with gentle agitation for at least 2 hours at room temperature. The eyecups were then gross sectioned to obtain 2 × 3 mm pieces from the following regions: the central part of the fundus, temporal to the optic nerve head (the area centralis-like region), superior midperiphery and periphery, and inferior midperiphery and periphery. Samples from these regions were postfixed in 1% osmium tetroxide and embedded in epoxy resin. They were washed with 0.17 M sodium cacodylate, pH 7.4, followed by secondary fixation in 1% osmium tetroxide. Subsequently, the samples were dehydrated via sequential incubation in increasing concentrations of acetone and embedded in epoxy resin. Sections of the embedded samples were cut for both LM and EM examinations. For LM, 1-micron-thick sections were mounted on glass slides and stained with toluidine blue. For EM, sections were mounted on copper grids and were stained with uranyl acetate and lead citrate. LM was performed using a Zeiss Axiophot microscope and EM was performed using a JEOL 1200 EX transmission electron microscope.

Figure 2: A composite of fundus pictures from a two-year-old ESS dog affected with cone rod dystrophy and homozygous for the *RPGRIP1* mutation. The central fundus is mainly normal appearing while an increase in granularity is observed in the midperipheral and peripheral fundus (star). There is also slight vascular attenuation with variable diameter of retinal vasculature (arrows).

2.6. Statistical Evaluations. Descriptive statistics were performed in relation to the masked ERG study using the SAS v9 (SAS Institute Inc. Cary, NC, USA) of the dogs classified as normal (including homozygous normal and heterozygous dogs) and affected dogs by DNA analysis for the *RPGRIP1* mutation. Due to the small sample size in the affected group and the fact that the data did not show any extreme outliers, two-sample t-tests with the Satterthwaite approximation for degrees of freedom allowing for unequal variances between the groups were utilized. Due to the marked differences between the groups, results were considered significant at the 0.01 significance level.

3. Results

3.1. Clinical Characterization of Retinal Degeneration due to the RPGRIP1 Mutation. A 10-year-old dog was examined due to severe visual problems reported by the owner, first noted at the age of 8 years. Advanced signs of retinal degeneration were observed by ophthalmoscopy in this dog. None of the other 11 dogs examined with clinical signs of retinal disease (ophthalmoscopic changes or reduced ERG responses) had shown visual problems until the age of 6–9 years, according to the owners.

The earliest ophthalmoscopic signs of disease were observed in a 1.5- and a 2-year-old ESS dog, respectively. Both showed increased granularity in the far peripheral tapetal fundus, with minute hyporeflective brown to gray spots in the far periphery of the tapetal fundus (Figure 2). With increasing age (in 3–8-year-old dogs) these abnormalities became more generalized with diffuse mottling

of the tapetal fundus and changes in fundus coloration. There was also generalized changes in tapetal reflectivity (hyporeflectivity and with movement of the lens used for indirect ophthalmoscopy, some of these areas became hyperreflective). At this later stage there was also severe attenuation of retinal vasculature. At 9-10 years of age, a generalized, end-stage type of retinal degeneration was observed in most affected dogs with a marked hyperreflective tapetal area, severe attenuation of retinal vasculature with few vessels still visible, mainly in the central parts of the fundus. At this stage there was also decoloration interspersed with hyperpigmentation of the nontapetal fundus. One 9-year-old dog had a mainly normal fundus appearance although ERG examination showed reduced responses for both the cone and the rod system. Bilateral, secondary cataracts (complete and immature types) were observed at age 12 years in one of the clinically affected dogs described in the present study.

3.2. Genotype-Phenotype Evaluation in Swedish ESS. Blood from 14 dogs was included in the study in which ten of the dogs had been diagnosed with PRA. Two cases of PRA were found to be homozygous for the disease causing RPGRIP allele (−/−), four were genotyped as heterozygous (+/−) and four of the cases had the homozygous genotype for the normal allele (+/+) (Table 1).

3.3. Masked ERG Study. A marked reduction of ERG responses was observed in 4 of 6 of the dogs that had been diagnosed as homozygous for the *RPGRIP1* mutation through blood testing (Table 2). Three of the 4 dogs evaluated as affected by ERGs had not shown any apparent deficiency in vision as evaluated by the owner or by the examiner. Two of these dogs had normal fundus appearances, while the other two dogs had early and moderately advanced retinal degenerative changes, respectively. The two dogs, homozygous for the *RPGRIP* mutation that had normal ERGs, were also ophthalmoscopically normal.

Results of ERG recordings in a normal 8-year-old ESS and in two affected dogs, 9 and 12 year olds, respectively, are shown in Figure 3. Evaluation of a-wave amplitudes showed significant differences between the affected group and the heterozygous and homozygous normal group, at the 0.01 significance level, when scotopic and photopic standard intensity responses were compared ($P < 0.0004$ and $P < 0.0007$, resp.). For the b-wave these differences were also significant at the same level for 4 of the 5 scotopic low-intensity responses evaluated (#2–5) ($P < 0.0084$, 0.0003, 0.0005, and 0.0020, resp.) and for the photopic flicker response ($P < 0.0032$). For a- and b-wave implicit times there were no significant differences for the former while for the latter a significant longer implicit time was found for the affected group of dogs in comparison to the normal group for scotopic standard intensity stimulation ($P < 0.0066$). For ERG amplitude and implicit time details see Table 3.

Two dogs in the group, found to be homozygous for the *RPGRIP1* mutation by blood testing, had a- and b-wave amplitude and implicit time values that were in complete accordance with the normal group of dogs.

In order to evaluate if the cone system was more affected than the rod system by the disease, the percentage reduction for each was calculated. This was performed through comparison of the median response from affected and normal dogs, respectively, using photopic standard intensity (test #8) and photopic flicker responses (test #9) for the cone system and scotopic low-intensity stimulation (test #5) for the rod system. It was found that the cone system was more affected than the rod system: 46% and 58% reduction, respectively, for the cones and 44% reduction for the rods in the affected group when compared with the normal ESS group of dogs.

3.4. Morphology. Light and electron microscopies were performed using retinal sections from 3 dogs. The two older dogs had ophthalmoscopic signs of severe bilateral generalized retinal degeneration while the younger, a 3-year-old ESS dog, exhibited a granular but otherwise normal fundus appearance. DNA from the youngest dog only was obtained, and showed homozygocity for the *RPGRIP1* mutation.

In the 9-year-old dog, bilaterally atrophic retinas with no residual photoreceptor cells and sporadic remnants of cells from inner nuclear and ganglion cell layers were observed, with marked retinal gliosis (Figures 4 and 5).

The retinas of the second dog, 6-years-old, showed signs of bilateral generalized retinal degeneration, with complete atrophy of the inferior retina, and a lack of photoreceptor cells in this area, while in the superior retina 1-2 layers of photoreceptor nuclei could be observed.

The 3-year-old dog, however, demonstrated mainly normal retinal morphology except for changes in the photoreceptor cell layer at all retinal locations examined: cone cell nuclei appeared slightly abnormal, with dense chromatin and with photoreceptor inner segments condensed and shrunken (Figure 6). Photoreceptor outer segments could not be clearly visualized in the thin sections obtained, and thus their ultrastructure was not possible to fully evaluate.

4. Discussion

The present study indicates that a majority of the American ESS dogs with hereditary retinal degeneration can be associated with homozygosity for the disease causing allele of the *RPGRIP1* gene. However, four of the 6 dogs homozygous for the *RPGRIP1* mutation had clinical signs of disease while 2 were completely normal appearing both by ophthalmoscopic examination and by ERG. Thus, a clear genotype-phenotype discordance was observed in regards to this group of ESS dogs.

A large proportion of the genetically and/or clinically affected dogs did not show signs of visual impairment until comparably late in life and 2 were clinically completely normal. The reason for the latter finding is unclear. It could be that the *RPGRIP1* insertion by itself is not sufficient to cause retinal degeneration. It appears likely that additional factors are warranted for initiation of photoreceptor cell death such as additional loci involved as modifiers of the disease, as have been described for various forms of PRA, for example, prcd and X-linked PRA [9, 31]. It could possibly also be that there is not full penetrance for the mutation [32].

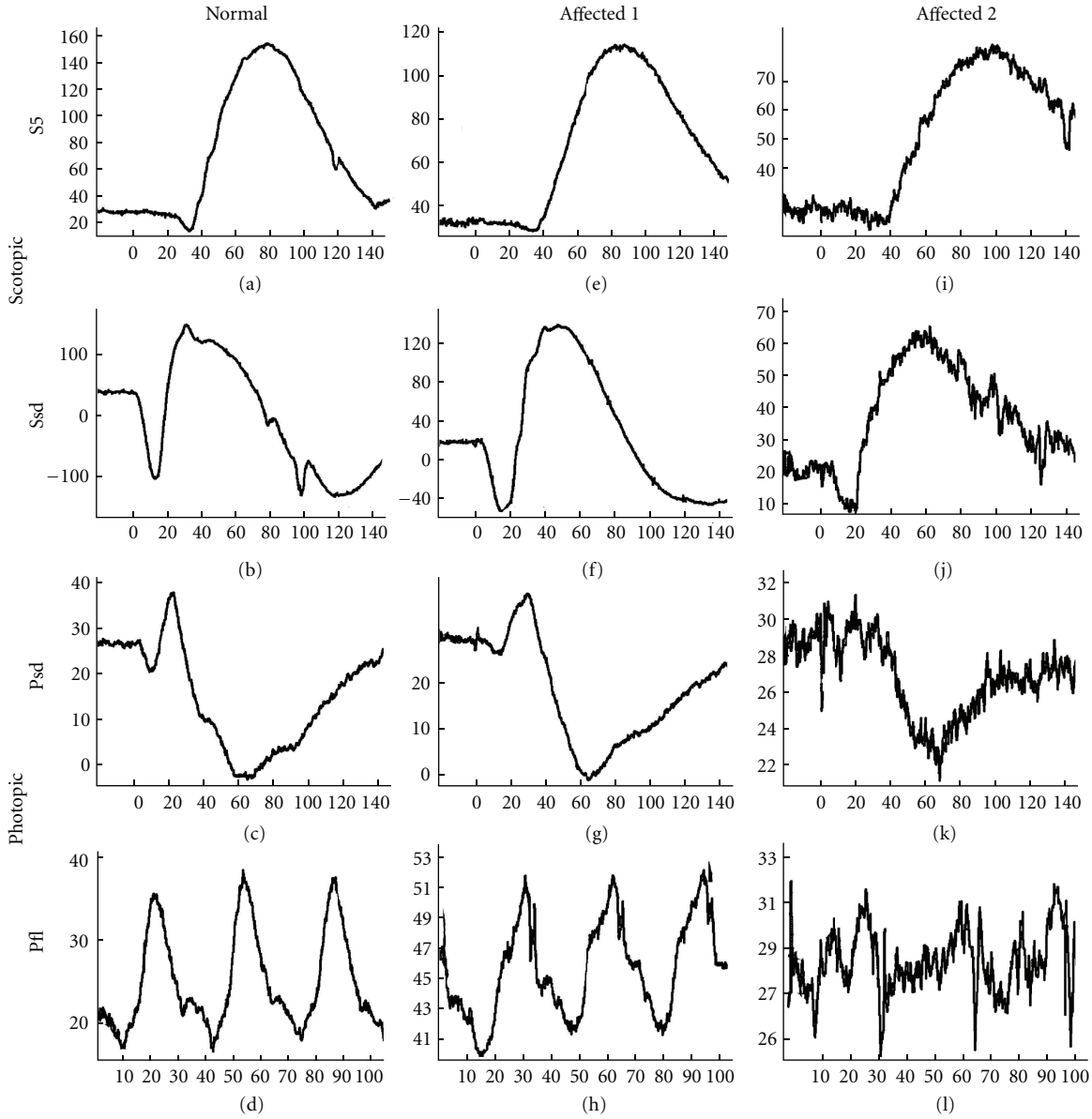

Figure 3: Scotopic and photopic ERGs from a normal 8-year-old ESS dog and two RPGRIP1−/− affected ESS dogs at the age of 9 (affected 1) and 12 years (affected 2), respectively. The latter affected dog was normal at ophthalmoscopic examination when it was 9 years old. At the age of 12 years it was only slightly visually compromised, and in a moderately advanced stage of retinal degeneration as seen by ophthalmoscopy. S5: scotopic ERG response using 10 mcd·s/m^2 of light stimuli after 20 minutes of dark adaptation, Ssd: scotopic ERG response using 3 cd·s/m^2 of light stimuli in the dark, Psd: photopic ERG response using 3 cd·s/m^2 in the light after 10 minutes of light adaptation (with 30 cd/m^2 of background light), Pfl: photopic ERG flicker response after 30 Hz flickering light stimuli in the light adapted state.

Similar findings have been observed in comparable human clinical studies in cone rod dystrophies and degenerations. A phenotypic variation between clinical signs in affected individuals and in the onset of hereditary retinal dystrophies has been observed, also by functional testing in human cone rod dystrophies [33]. The variation in clinical signs and time for initial symptoms is especially true for retinopathies caused by the *RPGRIP1* mutation, on a variable genetic background, such as is the case in the human population. In purebred dogs, however, a more uniform phenotype is usually expressed, due to a more homogenous background. This fact is true for most forms of PRA; however, for the cone-rod dystrophies observed in the longhaired and shorthaired Dachshund breeds, with the *RPGRIP1* and *NPHP4* mutations, respectively, severe heterogeneity has been described for both [22, 27, 34].

In retinal degeneration of the ESS dog clinical signs most often appear comparably late in life and are often difficult to evaluate by the owner. For most of the affected dogs observed in the present study the owners had not noted any visual impairment. The owner of an 11-year-old dog from the present study described that the dog could still play with

Table 3: ERG amplitude and implicit time for normal and affected ESS dogs in the masked study. Median, 5th and 95th percentiles are given for ERG a- and b-wave amplitudes (a) in microvolts and in (b) for implicit times in milliseconds, for normal and affected ESS dogs. Scotopic ERGs consisted of scotopic low-intensity responses (S: 0.01 cd·s/m^2), which were elicited 4, 8, 12, 16, and 20 minutes after dark adaptation designated: S1, S2, S3, S4, and S5, scotopic standard intensity responses, Ssd: 3 cd·s/m^2, and scotopic higher intensity responses, Sh: 10 cd·s/m^2. Photopic ERGs consisted of a photopic single flash response: Psd, and 30 Hz flicker responses: Pfl, using 3 cd·s/m^2 for both, after at least 10 minutes of light adaptation using 30 cd/m^2 of background light.

(a)

Response	Wave	Normal			Affected		
		Median	5th	95th	Median	5th	95th
S1	b	29.8	16.7	53.1	20.4	15.0	34.0
S2	b	61.6	40.2	101.3	37.7	35.4	45.0
S3	b	98.4	73.9	116.3	52.1	39.4	61.2
S4	b	122.8	78.8	146.4	56.2	50.9	71.2
S5	b	137.3	86.5	185.0	75.0	53.4	85.8
Ssd	a	128.1	102.1	181.9	29.0	16.9	64.9
	b	196.5	138.7	261.6	146.5	72.5	186.0
Sh	a	162.3	137.4	236.8	38.1	23.5	86.9
	b	240.5	171.7	307.7	169.4	77.6	230.8
Psd	a	8.3	3.9	11.5	3.0	2.5	3.6
	b	30.8	13.8	35.0	15.4	6.6	24.9
Pfl	b	34.1	15.4	47.5	15.0	6.9	22.6

(b)

Response	Wave	Normal			Affected		
		Median	5th	95th	Median	5th	95th
S1	b	63.5	57.2	87.1	81.0	65.7	87.7
S2	b	75.8	69.2	92.4	84.5	78.5	91.7
S3	b	78.7	75.0	92.3	81.4	76.9	89.8
S4	b	82.3	73.6	95.3	80.3	76.3	96.0
S5	b	80.6	74.8	94.9	86.2	77.3	94.3
Ssd	a	14.3	12.5	15.4	13.5	12.3	15.7
	b	32.7	31.3	59.5	196.5	138.7	261.6
Sh	a	12.6	11.3	13.7	13.3	10.1	15.0
	b	46.9	32.6	52.4	240.5	171.7	307.7
Psd	a	10.6	10.0	12.0	10.0	9.0	12.8
	b	21.6	20.0	23.5	30.8	13.8	35.0
Pfl	b	21.5	20.4	24.8	34.1	15.4	47.5

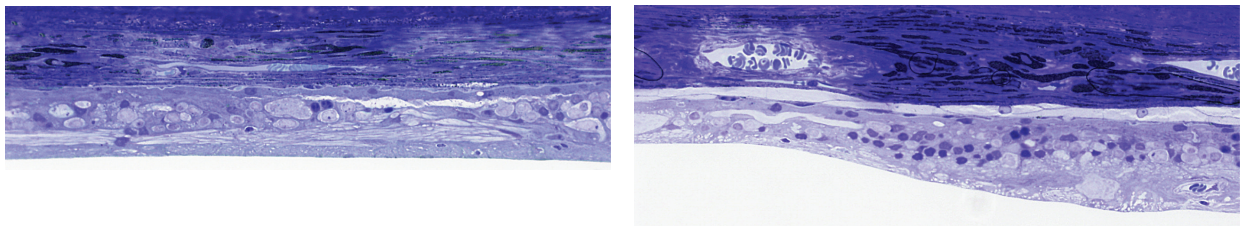

(a) (b)

Figure 4: (a) Light microscopy (LM) of the inferior nontapetal retina of the 9-year-old ESS dog. Severe thinning of the entire retina is seen with complete degeneration of photoreceptor cells and inner retinal degeneration, disorganization, and gliosis. (b) LM of superior tapetal retina. A variation in retinal thickness is observed and some areas with a single row of photoreceptor nuclei that are still present. Toluidine blue staining; ×40.

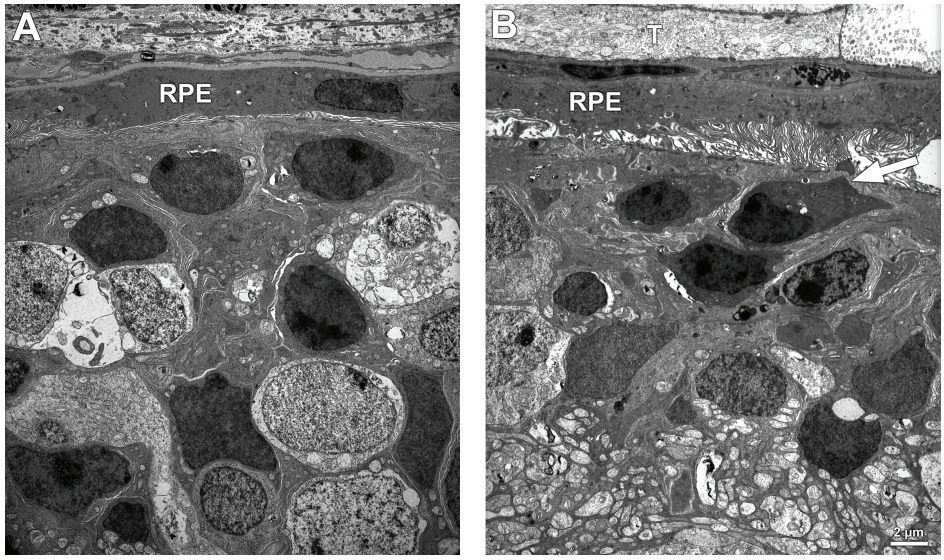

(a) (b)

Figure 5: Ultrastructure of nontapetal (a) and tapetal retina (b) from the same dog shown in Figure 4. Note the severely disorganized outer and inner retinal cell layers and structures. The RPE cell layer appears preserved, however. In (b) there is relative sparing of the retina with some minor remnants of photoreceptor nuclei with inner segments (arrow) and an abundance of RPE apical microvilli. RPE: retinal pigment epithelial cells, T: tapetal cells. Bar depicts magnification which is the same for (a) and (b).

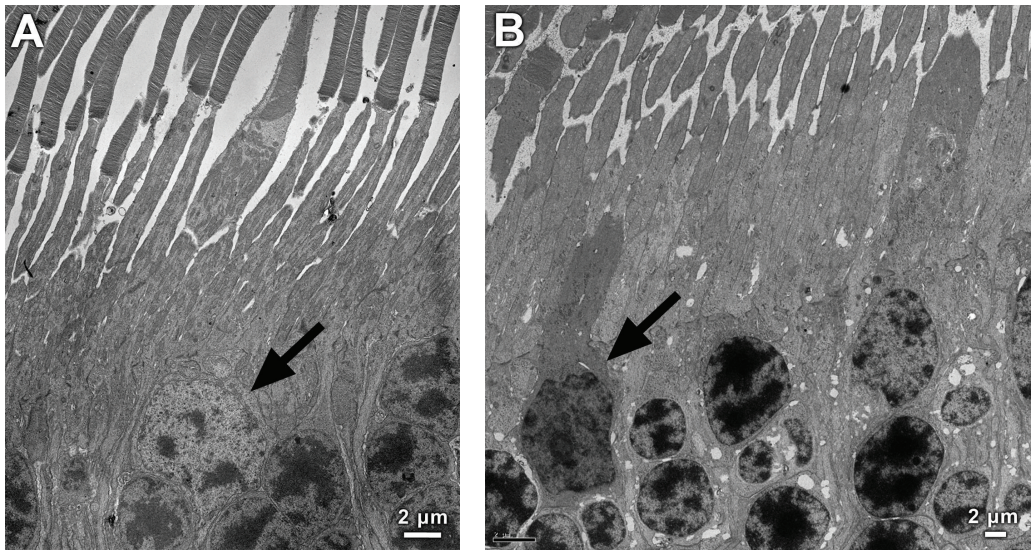

(a) (b)

Figure 6: Ultrastructure of the outer retina of a normal 2-year-old dog (a) and that of the affected 3-year-old dog (b). Note the condensed configuration of the cone nuclei in the retina of the affected animal (arrow) in comparison to that of the normal one (in (a), arrow) and the dark appearance of the inner segments in the retina of the affected animal. Bar depicts magnification which is the same for (a) and (b).

a transparent frisbee and could easily walk down an indoor stairway in low-lighting conditions. This dog had moderately advanced retinal degeneration with ophthalmoscopically visible changes and was homozygous for the *RPGRIP1* mutation. Another dog showing clinical signs of retinal degeneration had been diagnosed as ophthalmoscopically normal by a veterinary ophthalmologist one year previously, at the age of 7 years. ERGs showed, however, severely reduced retinal function in accordance with a cone rod dystrophy.

It is likely that the cone affection in the disease is early onset, and a defect the dog learns to live with as long as its rod function is normal. Morphology of one 3-year-old ESS dog, homozygous for the *RPGRIP1* mutation, showed ultrastructural changes specifically in cones, while rod photoreceptors were still normal appearing. It is possible that the visual problems become apparent clinically later in life when also the rods start to degenerate. Further, this second phase appears to occur at a variable time point, but

most often not until late in life, then leading to a rather fast generalized severe retinal degeneration (retinal atrophy).

ERG recordings proved to be useful in the masked study of the present investigation for objectively detecting reduced photoreceptor function in accordance with cone rod dystrophy due to the *RPGRIP1* mutation. In two cases, however, function in genetically affected individuals was found to be within normal limits. These discordant clinical results could be consistent with incomplete penetrance for the mutation, but other factors previously outlined may also be involved.

Other affected genes or other mutations in *RPGRIP1* may also be present in the ESS breed. One mutated gene, prevalent in at least 32 canine breeds, is prcd, (http://www.optigen.com/, 2011). This could also be a candidate gene since it is known to affect the English and American Cocker Spaniel dog breeds, distant relatives to the ESS dog (Liz Hansen, personal communication 2006). Some of the other mutations causing primary photoreceptor degenerations in dogs are ADAM9 [35], CCDC66 [36], CNGB3 [37], RD3 [38], RHO [39], RPE65 [40], VMD2 [41], PDE6beta [42], PDE6A [43], and PDC [44].

Among the ten PRA cases in ESS dogs previously diagnosed in Sweden, from which DNA was available for the current study, only two individuals were homozygous for the disease causing allele at the *RPGRIP1* locus. Four were found to be heterozygous and four were homozygous for the normal wild-type allele (Table 1). The two cases being homozygous for the RPGRIP1 insertion were diagnosed with PRA at two and four years of age, respectively. Although the number of cases is small there appears to be a tendency for a later onset of PRA among the other eight cases. None of the normal dogs were found to be homozygous for the RPGRIP1 insertion in the Swedish samples, but to make any inferences about the penetrance, a much larger data set would be needed. Taken together, the study of the Swedish samples suggests that at least one more gene is responsible for PRA in the Swedish population.

The complete association between *RPGRIP1* and PRA observed in the ESS thus remains to be fully elucidated. There are strong indications that the *RPGRIP1* gene is involved in the cone rod dystrophy described herein, but the genotype-phenotype discordance observed shows that the genetic background most probably is more complex than previously suspected. In conclusion, there are strong indications that other mutations or modulating genes may be involved in cone rod dystrophy of ESS dogs and could also be causative to other types of hereditary retinal degenerations in the breed. Further investigations in regards to additional loci or genes required for development of cord1 are therefore warranted.

An important goal for vision research is to provide effective treatments for the millions of people affected with retinal blinding disorders. Therapeutic intervention using large animal models such as dogs and cats are effective and necessary methods to utilize before proceeding with human treatment trials. Proof of principle was obtained through therapeutic studies using gene therapy in a dog model of LCA [45], resulting in successful restoration of vision. Similar procedures were performed in human patients with successful outcome [46, 47]. Another promising therapeutic method for retinal blinding disease is stem cell therapy, with or without combination of gene therapy [48]. In preparation for such studies it is, however, of utmost importance that the animal model with its specific retinal disease is precisely characterized clinically beforehand, and with molecular methods, for maximal outcome in the translational process.

Acknowledgments

The authors would like to thank the breeders and owners of English Springer Spaniel dogs for participation in eye examinations with their dogs, which made this study possible. Dr. Gary S. Johnson and Liz Hansen provided DNA from ESS dogs from their genetics department data bank for the masked study, which is gratefully acknowledged. They would also like to thank Leilani Castaner, Howard Wilson and Davida Myrby for outstanding technical assistance. This paper has been financed by the American Kennel Club, the joint research fund of Agria and the Swedish Kennel Club, and the English Springer Spaniel breeding clubs in Sweden and in USA.

References

[1] K. Lindblad-Toh, C. M. Wade, T. S. Mikkelsen et al., "Genome sequence, comparative analysis and haplotype structure of the domestic dog," *Nature*, vol. 438, no. 7069, pp. 803–819, 2005.

[2] J. A. Leonard, R. K. Wayne, J. Wheeler, R. Valadez, S. Guillén, and C. Vilà, "Ancient DNA evidence for old world origin of New World dogs," *Science*, vol. 298, no. 5598, pp. 1613–1616, 2002.

[3] P. Savolainen, Y. P. Zhang, J. Luo, J. Lundeberg, and T. Leitner, "Genetic evidence for an East Asian origin of domestic dogs," *Science*, vol. 298, no. 5598, pp. 1610–1613, 2002.

[4] B. M. Vonholdt, J. P. Pollinger, K. E. Lohmueller et al., "Genome-wide SNP and haplotype analyses reveal a rich history underlying dog domestication," *Nature*, vol. 464, no. 7290, pp. 898–902, 2010.

[5] E. K. Karlsson, I. Baranowska, C. M. Wade et al., "Efficient mapping of mendelian traits in dogs through genome-wide association," *Nature Genetics*, vol. 39, no. 11, pp. 1321–1328, 2007.

[6] S. Petersen-Jones, "Advances in the molecular understanding of canine retinal diseases," *Journal of Small Animal Practice*, vol. 46, no. 8, pp. 371–380, 2005.

[7] M. Menotti-Raymond, V. A. David, A. A. Schäffer et al., "Mutation in CEP290 discovered for cat model of human retinal degeneration," *Journal of Heredity*, vol. 98, no. 3, pp. 211–220, 2007.

[8] A. I. den Hollander, R. Roepman, R. K. Koenekoop, and F. P. M. Cremers, "Leber congenital amaurosis: genes, proteins and disease mechanisms," *Progress in Retinal and Eye Research*, vol. 27, no. 4, pp. 391–419, 2008.

[9] B. Zangerl, O. Goldstein, A. R. Philp et al., "Identical mutation in a novel retinal gene causes progressive rod-cone degeneration in dogs and retinitis pigmentosa in humans," *Genomics*, vol. 88, no. 5, pp. 551–563, 2006.

[10] G. Dekomien, M. Runte, R. Gödde, and J. T. Epplen, "Generalized progressive retinal atrophy of Sloughi dogs is due to an 8-bp insertion in exon 21 of the PDE6B gene,"

Cytogenetics and Cell Genetics, vol. 90, no. 3-4, pp. 261–267, 2000.

[11] L. M. Downs, B. Wallin-Håkansson, M. Boursnell et al., "A frameshift mutation in Golden Retriever dogs with progressive retinal atrophy endorses SLC4A3 as a candidate gene for human retinal degenerations," *PLoS ONE*, vol. 6, no. 6, article e21452, 2011.

[12] M. B. Jeong, C. H. Han, K. Narfström et al., "A phosducin (PDC) gene mutation does not cause progressive retinal atrophy in Korean miniature schnauzers," *Animal Genetics*, vol. 39, no. 4, pp. 455–456, 2008.

[13] E. M. Stone, "Leber congenital amaurosis—a model for efficient genetic testing of heterogeneous disorders. LXIV Edward Jackson Memorial Lecture," *American Journal of Ophthalmology*, vol. 144, no. 6, pp. 791–811, 2007.

[14] E. M. Stone, "Finding and interpreting genetic variations that are important to ophthalmologists," *Transactions of the American Ophthalmological Society*, vol. 101, pp. 437–484, 2003.

[15] K. Narfström and S. Petersen-Jones, "Diseases of the canine ocular fundus," in *Veterinary Ophthalmology*, K. N. Gelatt, Ed., vol. 2, pp. 944–1025, Blackwell Publishing, 4th edition, 2007.

[16] J. Hyman, S. A. Koch, J. P. Pickett, and S. Estep, "A unique retinal degenerative disease in the English Springer Spaniel; a continued prospective study," in *Proceedings of the European College of Veterinary Ophthalmology Stockholm Meeting*, p. 34, 2001.

[17] T. P. Dryja, S. M. Adams, J. L. Grimsby et al., "Null RPGRIP1 alleles in patients with Leber congenital amaurosis," *American Journal of Human Genetics*, vol. 68, no. 5, pp. 1295–1298, 2001.

[18] A. Hameed, A. Abid, A. Aziz, M. Ismail, S. Q. Mehdi, and S. Khaliq, "Evidence of RPGRIP1 gene mutations associated with recessive cone-rod dystrophy," *Journal of Medical Genetics*, vol. 40, no. 8, pp. 616–619, 2003.

[19] J. C. Booij, R. J. Florijn, J. B. ten Brink et al., "Identification of mutations in the AIPL1, CRB1, GUCY2D, RPE65, and RPGRIP1 genes in patients with juvenile retinitis pigmentosa," *Journal of Medical Genetics*, vol. 42, no. 11, p. e67, 2005.

[20] R. Roepman, N. Bernoud-Hubac, D. E. Schick et al., "The retinitis pigmentosa GTPase regulator (RPGR) interacts with novel transport-like proteins in the outer segments of rod photoreceptors," *Human Molecular Genetics*, vol. 9, no. 14, pp. 2095–2105, 2000.

[21] Q. Zhang, G. M. Acland, W. X. Wu et al., "Different RPGR exon ORF15 mutations in Canids provide insights into photoreceptor cell degeneration," *Human Molecular Genetics*, vol. 11, no. 9, pp. 993–1003, 2002.

[22] E. O. Ropstad, K. Narfström, F. Lingaas, C. Wiik, A. Bruun, and E. Bjerkas, "Functional and structural changes in the retina of wirehaired dachshunds with early onset cone-rod dystrophy," *Investigative Ophthalmology & Visual Science*, vol. 49, no. 3, pp. 1106–1115, 2008.

[23] A. C. Wiik, C. Wade, T. Biagi et al., "A deletion in nephronophthisis 4 (NPHP4) is associated with recessive cone-rod dystrophy in standard wire-haired dachshund," *Genome Research*, vol. 18, no. 9, pp. 1415–1421, 2008.

[24] K. Narfström, K. Holland Deckman, and M. Menotti-Rymond, "The domestic cat as a large animal model for characterization of disease and therapeutic intervention in hereditary retinal blindness," *Journal of Ophthalmology*, vol. 2011, Article ID 906943, 8 pages, 2011.

[25] G. J. Pazour, S. A. Baker, J. A. Deane et al., "The intraflagellar transport protein, IFT88, is essential for vertebrate photoreceptor assembly and maintenance," *Journal of Cell Biology*, vol. 157, no. 1, pp. 103–113, 2002.

[26] Y. Zhao, D. H. Hong, B. Pawlyk et al., "The retinitis pigmentosa GTPase regulator (RPGR)-interacting protein: subserving RPGR function and participating in disk morphogenesis," *Proceedings of the National Academy of Sciences of the United States of America*, vol. 100, no. 7, pp. 3965–3970, 2003.

[27] C. S. Mellersh, M. E. G. Boursnell, L. Pettitt et al., "Canine RPGRIP1 mutation establishes cone-rod dystrophy in miniature longhaired dachshunds as a homologue of human Leber congenital amaurosis," *Genomics*, vol. 88, no. 3, pp. 293–301, 2006.

[28] K. Narfström, E. Bjerkås, and B. Ekesten, "Visual impairment," in *Small Animal Ophthalmology, a Problem Oriented Approach*, R. L. Peiffer and S. M. Petersen-Jones, Eds., pp. 85–165, Saunders, 2nd edition, 2000.

[29] S. Rozen and H. Skaletsky, "Primer3 on the WWW for general users and for biologist programmers," *Methods in Molecular Biology*, vol. 132, pp. 365–386, 2000.

[30] K. Narfström, B. Ekesten, S. G. Rosolen, B. M. Spiess, C. L. Percicot, and R. Ofri, "Guidelines for clinical electroretinography in the dog," *Documenta Ophthalmologica*, vol. 105, no. 2, pp. 83–92, 2002.

[31] R. Guyon, S. E. Pearce-Kelling, C. J. Zeiss, G. M. Acland, and G. D. Aguirre, "Analysis of six candidate genes as potential modifiers of disease expression in canine XLPRA1, a model for human X-linked retinitis pigmentosa," *Molecular Vision*, vol. 13, pp. 1094–1105, 2007.

[32] N. Udar, S. Yelchits, M. Chalukya et al., "Identification of GUCY2D gene mutations in CORD5 families and evidence of incomplete penetrance," *Human Mutation*, vol. 21, no. 2, pp. 170–171, 2003.

[33] K. Yagasaki and S. G. Jacobson, "Cone-rod dystrophy. Phenotypic diversity by retinal function testing," *Archives of Ophthalmology*, vol. 107, no. 5, pp. 701–708, 1989.

[34] K. Miyadera, K. Kato, J. Aguirre-Hernández et al., "Phenotypic variation and genotype-phenotype discordance in canine cone-rod dystrophy with an *RPGRIP1* mutation," *Molecular Vision*, vol. 15, pp. 2287–2305, 2009.

[35] O. Goldstein, J. G. Mezey, A. R. Boyko et al., "An *ADAM9* mutation in canine cone-rod dystrophy 3 establishes homology with human cone-rod dystrophy 9," *Molecular Vision*, vol. 16, pp. 1549–1569, 2010.

[36] G. Dekomien, C. Vollrath, E. Petrasch-Parwez et al., "Progressive retinal atrophy in Schapendoes dogs: mutation of the newly identified CCDC66 gene," *Neurogenetics*, vol. 11, no. 2, pp. 163–174, 2010.

[37] D. J. Sidjanin, J. K. Lowe, J. L. McElwee et al., "Canine CNGB3 mutations establish cone degeneration as orthologous to the human achromatopsia locus ACHM3," *Human Molecular Genetics*, vol. 11, no. 16, pp. 1823–1833, 2002.

[38] A. V. Kukekova, O. Goldstein, J. L. Johnson et al., "Canine *RD3* mutation establishes rod-cone dysplasia type 2 (rcd2) as ortholog of human and murine rd3," *Mammalian Genome*, vol. 20, no. 2, pp. 109–123, 2009.

[39] J. W. Kijas, A. V. Cideciyan, T. S. Aleman et al., "Naturally occurring rhodopsin mutation in the dog causes retinal dysfunction and degeneration mimicking human dominant retinitis pigmentosa," *Proceedings of the National Academy of Sciences of the United States of America*, vol. 99, no. 9, pp. 6328–6333, 2002.

[40] A. Veske, S. E. G. Nilsson, K. Narfström, and A. Gal, "Retinal dystrophy of Swedish briard/briard-beagle dogs is due to a 4-bp deletion in RPE65," *Genomics*, vol. 57, no. 1, pp. 57–61, 1999.

[41] K. E. Guziewicz, B. Zangerl, S. J. Lindauer et al., "Bestrophin gene mutations cause canine multifocal retinopathy: a novel animal model for best disease," *Investigative Ophthalmology and Visual Science*, vol. 48, no. 5, pp. 1959–1967, 2007.

[42] M. L. Suber, S. J. Pittler, N. Qin et al., "Irish setter dogs affected with rod/cone dysplasia contain a nonsense mutation in the rod cGMP phosphodiesterase β-subunit gene," *Proceedings of the National Academy of Sciences of the United States of America*, vol. 90, no. 9, pp. 3968–3972, 1993.

[43] S. M. Petersen-Jones, D. D. Entz, and D. R. Sargan, "cGMP phosphodiesterase-α mutation causes progressive retinal atrophy in the Cardigan Welsh corgi dog," *Investigative Ophthalmology and Visual Science*, vol. 40, no. 8, pp. 1637–1644, 1999.

[44] Q. Zhang, G. M. Acland, C. J. Parshall, J. Haskell, K. Ray, and G. D. Aguirre, "Characterization of canine photoreceptor phosducin cDNA and identification of a sequence variant in dogs with photoreceptor dysplasia," *Gene*, vol. 215, no. 2, pp. 231–239, 1998.

[45] G. M. Acland, G. D. Aguirre, J. Ray et al., "Gene therapy restores vision in a canine model of childhood blindness," *Nature Genetics*, vol. 28, no. 1, pp. 92–95, 2001.

[46] A. M. Maguire, K. A. High, A. Auricchio et al., "Age-dependent effects of RPE65 gene therapy for Leber's congenital amaurosis: a phase 1 dose-escalation trial," *The Lancet*, vol. 374, no. 9701, pp. 1597–1605, 2009.

[47] F. Simonelli, A. M. Maguire, F. Testa et al., "Gene therapy for leber's congenital amaurosis is safe and effective through 1.5 years after vector administration," *Molecular Therapy*, vol. 18, no. 3, pp. 643–650, 2010.

[48] R. Ofri and K. Narfström, "Light at the end of the tunnel? Advances in the understanding and treatment of glaucoma and inherited retinal degeneration," *Veterinary Journal*, vol. 174, no. 1, pp. 10–22, 2007.

Hindawi Publishing Corporation
Stem Cells International
Volume 2012, Article ID 675805, 10 pages
doi:10.1155/2012/675805

Research Article

Characterization of Progenitor Cells during Canine Retinal Development

Mallely Ávila-García,[1] Gustavo García-Sánchez,[2] Esmeralda Lira-Romero,[1] and Norma Moreno-Mendoza[1]

[1] *Departamento de Biología Celular y Fisiología, Instituto de Investigaciones Biomédicas, Universidad Nacional Autónoma de México, Ciudad Universitaria, Apartado Postal 70228, Ciudad de México, DF 04510, Mexico*
[2] *School of Veterinary Medicine, Louisiana State University, Baton Rouge, LA 70803, USA*

Correspondence should be addressed to Norma Moreno-Mendoza, angelica@biomedicas.unam.mx

Received 29 September 2011; Revised 28 November 2011; Accepted 28 November 2011

Academic Editor: Henry J. Klassen

We identify the presence of progenitor cells during retinal development in the dog, as this species represents a natural model for studying several breed-specific degenerative retinal disorders. Antibodies to detected progenitor cells (Pax6, C-kit, and nestin) and ganglion cells (BDNF, Brn3a, and Thy1) were used in combination with H3 for the purpose of identifying proliferating cells. Pax6, nestin, C-kit, and H3 were localized mainly in the neuroblastic layer of the retina during the embryonic stage. During the fetal stage, proteins were expressed in the inner neuroblastic layer (INL) as well as in the outer neuroblastic layer; BDNF, Thy1, and Brn3a were also expressed in the INL. During the neonatal stage only C-kit was not expressed. Proliferating cells were present in both undifferentiated and differentiated retina. These results suggest that, during canine retinogenesis, progenitor cells are distributed along the retina and some of these cells remain as progenitor cells of the ganglion cells during the first postnatal days.

1. Introduction

Progressive retinal cell death is a common phenomenon observed in human or animal degenerative eye diseases such as progressive retinal atrophy, age-related macular degeneration, retinal detachment, and glaucoma [1]. Different treatment strategies directed towards medically slowing the progression of retinal degenerative diseases with oral supplements have been considered including preservation of affected retinas with specific neurotrophic growth factors and the implantation of retinal pigment epithelial cells (RPEs) in affected eyes. Currently stem cells are being investigated as a potential cellular source for replacing damaged RPE or photoreceptor cells [2]. Both adult bone-marrow-derived stem cells and embryonic stem cells are being used in animal models with the goal of investigating how to induce appropriate cell integration and differentiation.

Single pigmented ciliary margin cells which are able to differentiate into retinal-specific cell types have been identified in the adult mouse retina [3]. Stem cells derived from the pars plicata and pars plana of the retinal cell margin of human eyes produced all of the different cell types, demonstrating multipotentiality [4]. Based on these data, it was suggested that the sphere-forming cells in the mammalian ciliary epithelium (CE) are retinal stem cells. However, it was revealed that the clonogenic spheres derived from the mouse and human CE originate from differentiated pigmented CE cells rather than the stem cell population harbored in the CE [5]. Fetal cat retinal sheets incubated with BDNF microspheres were transplanted to the subretinal space to investigate whether it is possible for sheets of fetal retinal allograft to integrate into the dystrophic Abyssinian cat retina where progressive rod cone degeneration is taking place [6]. To the authors knowledge there is a lack of

information regarding generation, proliferation, and differentiation of progenitor cells during embryonic and fetal stages in other mammals, particularly in the dog where progressive retinal degeneration associated with different ocular diseases is frequently observed.

Multipotent progenitor cells are stem cells which preserve their capacity and potential for self-renewal, giving rise to cells from multiple lineages; however, these are limited in number [1, 7–9]. During the optic cup stage of the developing embryonic eye, a group of multipotent progenitor cells exist which manifest the ability to differentiate into neurons and glial cells. In some species, these cells are able to differentiate into adult stages of development. The retina of many fish and amphibians grows throughout life, roughly matching the overall growth of the animal. The new retinal cells are continually added at the anterior margin of the retina, in a circumferential zone of cells, known as the ciliary marginal zone, or CMZ. In chickens, has been found that new neurons are added to the retina via proliferation and subsequent differentiation of neurons and glia at the retinal margin in a zone highly reminiscent of the CMZ of lower vertebrates [10]. Likewise, other researchers have reported that it may be possible to isolate putative retinal stem cells from the ciliary margin of the adult mouse [11]. In some birds this capacity is apparently only evident during the embryonic stage, and the types of cells produced by progenitors at the retinal margin can be altered by exogenous growth factors although normally the microenvironment imposes limitations on the types of neurons produced [12–14].

Retinal neurogenesis is largely determined intrinsically. Many genes have been identified in order to determine the fate of specific types of retinal neurons [15]. Some of the genes involved in the fate and maintenance of the progenitor cells at the ciliary margin zone include Shh, Notch, and Wnt as well as Chx10, Pax6, Rx1, Six3, and Six6. Their activation either induces the formation or modifies the presence of specific cell types whereas their loss induces important ocular malformations such as anophthalmia, microphthalmia, cyclopia, coloboma, aphakia, among others [16–18].

A series of genes express themselves early during ocular development, responsible for determining specific eye fields, critical to the development of the retina [19]. Within this group of genes, the transcription factor Pax6 is considered of utmost importance during eye development, as it has been observed that this actively participates in the differentiation of the lens and retina during embryonic development, whereas in the adult eye its expression is maintained in the lens, cornea, ganglion, and amacrine cells [20]. Mutation of this gene induces the formation of ectopic structures in *Xenopus* and *Drosophila* [21, 22]. The expression of Pax6 in retinal progenitor cells has also been observed in mice where its limited expression leads to a reduction in mitotic activity with delayed differentiation of neurons, and when absent the differentiation of progenitor cells is restricted to the generation of amacrine cells only [23–29]. Recently, the expression of Pax6 was detected in a small number of cell progenitors in the inner neuroblastic layer (INBL) of the chicken [30].

Nestin has also been described as a marker of neural progenitor cells [31]. Specifically it is expressed both in neural and glial cells, as well as in their common precursors [32]. In foetal human retina, nestin expression has been shown to occur in Müller cells [33]. Likewise, cells positive to nestin have been found in adult human retina [34, 35].

Retinal ganglion cells are the first mature retinal cells to differentiate from the immature retinal progenitors. Certain genes such as BDNF, Thy1, and Brn3a have been used as markers of differentiated ganglion cells [36]. Particularly, different authors have reported the expression of BDNF and TrkB in the ganglion cell layer and inner nuclear layer of different species of vertebrates [37–39].

Presently, few reports provide evidence indicating the existence of retinal progenitor cells in adult mammals. In this study, we identify the presence of progenitor cells during retinal development in the dog. This species represents a potential, natural, animal model for studies focusing on a number of degenerative retinal disorders.

2. Materials and Methods

2.1. Animals. Embryos, fetus, and neonatal dogs were provided by the Canine Control Center at Ecatepec, State of Mexico, and the Department of Surgical Teaching of the Faculty of Veterinary Medicine and Animal Science at the National Autonomous University of Mexico (UNAM). All experiments were approved by and under the supervision of the Norma Oficial Mexicana NOM-062-ZOO-1999. Before enucleation the animals were euthanized with a lethal dose of sodium pentobarbital (50 mg/kg). Eyes were immediately fixed in 4% cold paraformaldehyde in 0.1 M phosphate-buffered saline (PBS) for immunofluorescence analysis.

2.2. Histological Analysis. For histological paraffin sections, enucleated eyes were fixed in 4% paraformaldehyde solution (PFA, Sigma, USA) in PBS (phosphate-buffered saline, pH 7.1, Gibco) for 24 h. at 4°C. Later, ocular samples were dehydrated in a gradual alcohol series, embedded in paraffin (Paraplast, McCormick Scientific), and cut into serial sections (15 μm). The sections were mounted on glass slides, dewaxed, rehydrated, and stained with Hematoxylin and eosin. For sections embedded in plastic resin, the collected eyes were fixed in the Karnovsky solution (glutaraldehyde 2.5% in 0.1 M phosphate buffer, pH 7.4) [40] for 12 h. at 4°C. These were then washed with sodium cacodylate buffer and postfixed with 1% osmium tetroxide (OsO_4) in Zetterqvist's buffer for 1 h., washed again with distilled water, and dehydrated in a gradual alcohol series and acetronile; to be finally embedded in Epon 812 resin. Semithin sections (1 μm) were obtained with an ultra microtome and then dyed with toluidine blue. Fine sections (60 to 90 nm) were contrasted by applying uranyl acetate and lead citrate for transmission electron microscopy.

2.3. Immunofluorescence. Ocular tissue samples were removed, fixed for 20 min. With 4% paraformaldehyde solution

Table 1: Antibodies and dilutions.

Antibody	Brand	Dilution
Rabbit polyclonal to PAX6	Abcam, MA, USA (ab5790)	1 : 250
Rabbit polyclonal to Nestin	Abcam, MA, USA (ab5968)	1 : 250
Rabbit polyclonal to C-kit	Santa Cruz Biotechnology, CA, USA (sc-168)	1 : 200
Rabbit polyclonal to BDNF	Santa Cruz Biotechnology, CA, USA (sc-546)	1 : 250
Rabbit polyclonal to BRN3A	Abcam, MA, USA (ab23579)	1 : 50
Mouse monoclonal to Thy1.1	Abcam, MA, USA (ab65193)	1 : 200
Rabbit polyclonal to Histone 3 (H3)	Upstate, Temecula CA, USA (06–570)	1 : 200
Anti-rabbit IgG TRITC conjugate	Zymed, San Francisco, CA, USA (81–6114)	1 : 100
Anti-rabbit IgG Cy 5 conjugate	Zymed, San Francisco, CA, USA (81–6116)	1 : 100
Anti-rabbit IgG FITC conjugate	Zymed, San Francisco, CA, USA (81–611)	1 : 100
Anti-mouse IgG TRITC conjugate	Zymed, San Francisco, CA, USA (81–6714)	1 : 100
Anti-mouse IgG FITC conjugate	Zymed, San Francisco, CA, USA (61–6511)	1 : 100

Primary and secondary antibodies used for immunofluorescence. All dilutions were prepared in *bovine serum albumin*.

in PBS and cryoprotected with 30% sucrose in PBS at 4°C overnight. Later tissues were embedded in OCT medium (Tissue-Tek, Sakura Finetek, Torrance, CA) and frozen in hexane (J. T. Baker) on dry ice. Serial frozen transversal sections of approximately 15 μm were obtained to be used for immunofluorescence using conventional techniques. Sections were then incubated with the primary antibodies and treated with the secondary corresponding antibody. As a positive control, one day postnatal and adult mouse CD1 eyes were employed. As a negative control, samples without primary antibody were incubated. Subsequently, these were washed with PBS and double consecutive immunofluorescences were carried out, in order to simultaneously detect different proteins. Finally these were mounted in Dako paramount aqueous mounting medium (Dako North America, INC. USA). The antibodies and dilutions used are presented in Table 1. Sections were analysed in a confocal microscope (LSM 5 Pascal, Zeiss) equipped with Argon-Kripton and Helium-Neon laser using filters BP 450–490 and 546/12. Double immunofluorescences were detected simultaneously.

3. Results

The presence and distribution of retinal progenitor cells during embryonic stages (up to 25 days of gestation: dg), fetal (30–60 dg), and neonatal (1 day postnatal: dp) was studied for canine development. These stages were determined according to criteria established by Aguirre et al. [41], Simoens and Budras [42], and Cook [43, 44], and corroborated by histological examination of the retina.

3.1. Morphogenesis of Canine Retina

3.1.1. Embryonic Stage. At 25 days of embryonic development, taking histological sections of the eye, there appear to be primary fibers in the lens which are completely separate from the surface ectoderm (Figure 1(a)). At the back of the eye, the retina was found to consist of a neuroblastic layer (NBL) which in turn divided into two parts: an inner marginal area (not nuclear) and another outer nuclear zone (Figure 1(b)). The retinal pigmented epithelium (RPE) consists of several rows of cells with pigment (Figure 1(c)). At electron microscope level, mitotic figures are evident in the inner neuroblastic layer (INBL, Figure 1(d)).

3.1.2. Fetal Stage. Fetuses between 35 and 55 days of gestation manifested clear development of various structures which make up the retina (Figure 1(e)). Histologically, it was observed that cells from the nuclear area migrated to the internal marginal zone, forming two nuclear layers: the inner neuroblastic layer (INBL), and the outer neuroblastic layer (ONBL, Figure 1(f)). Both layers were separated by the transient layer of Chievitz, evidently a space with no cell content (Figure 1(h)). In the innermost part of the INBL some ganglion cells project their axons in order to initiate the formation of the optic nerve, forming the nerve fiber layer (NFL). The retinal pigmented epithelium (RPE) manifests several layers of cells and in some areas the presence of rudimentary photoreceptor precursor cells (Figure 1(g)).

3.1.3. Postnatal Stage. In the last stage analyzed, corresponding to 1 day postnatal puppies, the development of the layers is more evident (Figure 1(i)). The retina is formed by the NFL, and a greater number of ganglion cells and axons can be observed directed towards the brain in order to form the optic nerve. The ganglion cell layer (GCL) was shown to be separated from the INBL by the inner plexiform layer (IPL, Figures 1(j) and 1(i)). The RPE manifested a row of cubic cells, and in some of these the microvillus was evident (Figure 1(k)).

3.2. Identification of Retinal Progenitor Cells

3.2.1. Embryonic Stages. At this stage, the expression of C-kit, Nestin, and Pax6 markers were detected located in the lens and the NBL. The expression of C-kit (Figures 2(a) and 2(d)) and Pax6 (Figures 2(b) and 2(e)) was very marked in the cell nuclei. For its part, Nestin (Figures 2(c) and 2(f)) was observed in the filaments of the progenitor cells. The

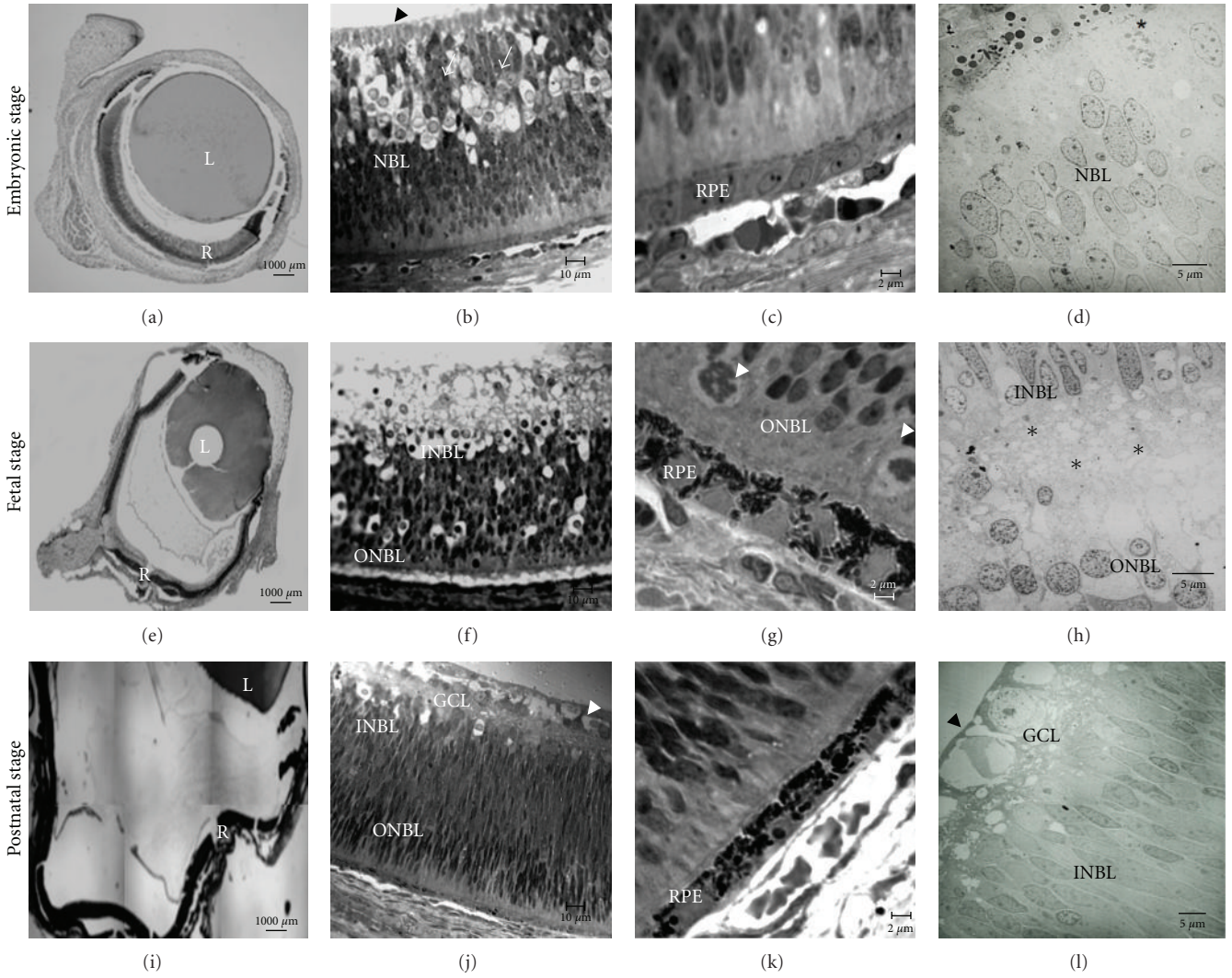

Figure 1: Histological analysis of the retina in embryos ((a)–(d)), fetuses ((e)–(h)) and neonatal ((i)–(l)) dogs. (a) Transversal section of the eye showing the retina (R) and lens (L). (b) In longitudinal section, retina consists of a neuroblastic layer (NBL) formed by an inner marginal (arrow head) and outer nuclear zone (arrows). (c) The retinal pigment epithelium (RPE) is observed to consist of a single layer with oval shaped melanosomes on the apical surface. (d) Electron micrograph showing cells with mitotic activity (*) localized in the NBL. (e) Eye from the fetal stage where retina (R) and lens (L) are evident. (f) Cell migration has formed the inner neuroblastic layer (INBL) and outer neuroblastic layer (ONBL). (g) Some rudimentary photoreceptors were evident at the fetal stage (arrow head). (h) The INBL and ONBL are separated by the transitional space of Chievitz where high resolution exposes a space between the INBL and ONBL without any cells (*). (i) Eye from the postnatal stage where part of the lens (L) and the retina (R) are visible. (j) During the postnatal stage the ganglion cell layer (GCL) was apparent. (k) The RPE was observed as a row of cubic cells. (l) Electron micrograph showing the GCL where the axons (arrow head) are forming the nerve fiber.

proliferative activity of cells takes place due to the presence of the histone 3 (H3) protein. Thus, we identified an increasing level of expression of H3 in the proliferative zone, both in the central region as well as at the side of the retina. There were also some proliferating cells, located in the marginal layer of the NBL co-localized with cells positive to the C-kit marker (Figures 2(g), 2(h), and 2(i)).

3.2.2. Fetal Stage. During this stage, cells positive to the C-kit (Figure 3(a)), Pax6 (Figure 3(b)), and Nestin (Figure 3(c)) proteins were detected. The marker is primarily located in the INBL, but positive cells were also observed in the ONBL, although they were less intense. Proliferating cells were detected in the proliferative zone located in the ONBL (data not shown). For the identification of progenitor cells with proliferative activity, double immunofluorescence tests were performed using C-kit and Pax6 in combination with H3. Proliferating cells were found in both the INBL as well as in the proliferative zone ONBL. Cells positive both to C-kit and H3 were located in the INBL (Figures 2(g) and 2(h)). Beside this, cell positive to Pax6 demonstrating proliferative activity were located in the INBL (Figure 3(j)).

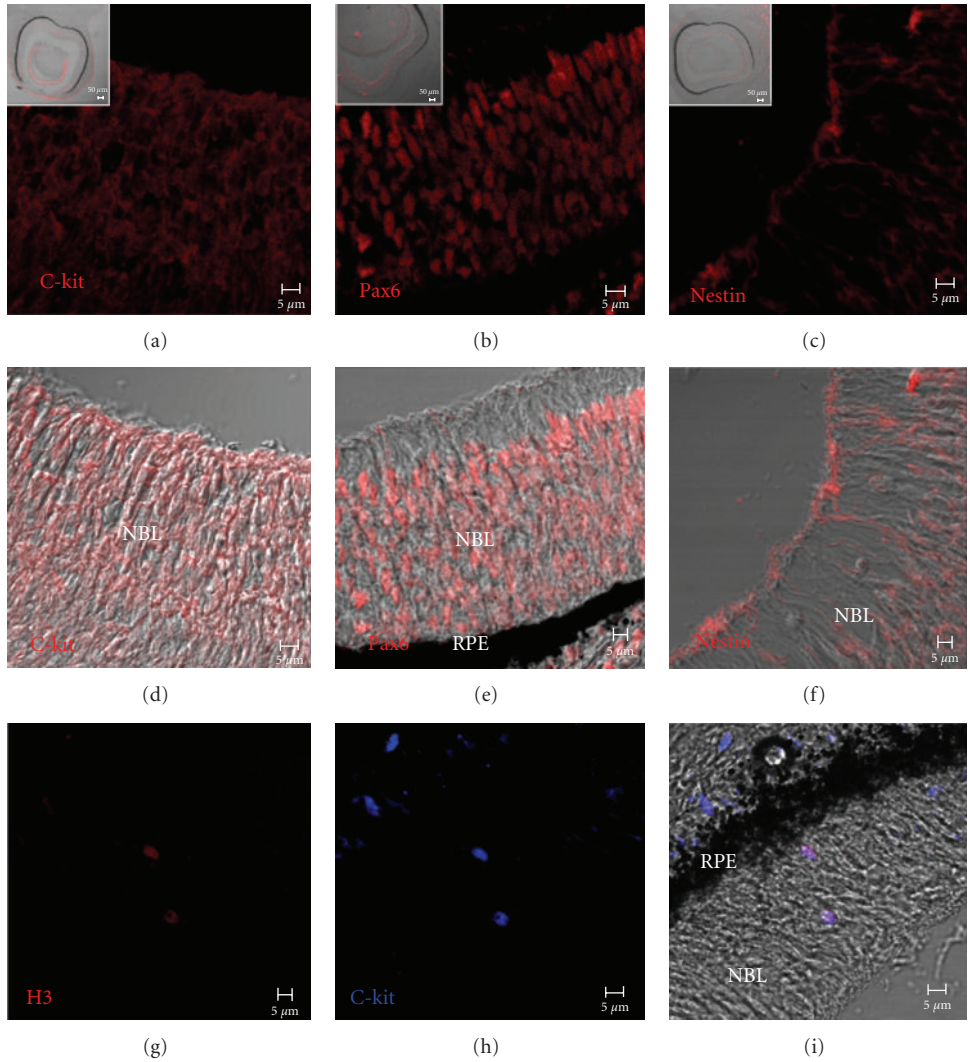

Figure 2: Immunofluorescent staining of C-kit (a and d), Pax6 ((b) and (e)) and Nestin ((c) and (f)) in the retina from dog embryos. The expression was observed in the NBL, examined in combination with Nomarski optics. Inserts present a panoramic view of the pattern of expression for the C-kit, Pax6 and Nestin. (g) Confocal image showing the proliferation of cells stained with H3. (h) The same figure presented in (g) but here the C-kit positive cells are evident. (i) Merged image showing cells expressing both C-kit (blue) and H3 (red) proteins in combination with Nomarski optics.

Ganglion cell differentiation was evident at this stage of retinogenesis, with the identification of cells positive to BDNF (Figure 3(d)) and Thy1 (Figure 3(e)). The presence of this signal is localized in the cytoplasm of ganglion cells located in the INBL. Contrastingly, only a slight expression of Brn3a in some ganglion cells (Figure 3(f)) was identified. Implementing double immunofluorescence tests using antibodies Thy1/H3 (Figures 3(g), 3(h), and 3(i)) and BDNF/H3 (Figure 3(k)), we observed that certain cells located in the INBL co-localized, and it may prove that these are ganglion cells. The combination of Brn3a/BDNF perfectly delineated the presence of ganglion cells located in the INBL; Brn3a was expressed in the nucleus, whereas BDNF was located in the cytoplasm (Figure 3(l)).

3.2.3. Postnatal Stage. At this stage of retinal development, the expression of C-kit was not observed however the expression of Nestin (Figure 4(a)) and Pax6 (Figure 4(b)) was evident mainly in the ganglion cell layer, whereas limited expression was detected in the both INBL and ONBL. Some cells located in the GCL presented proliferative activity made evident by the positive expression of H3 (Figure 4(c)). BDNF, Thy1 and Brn3a were evident in the GCL, both in the central and peripheral area of the retina (Figures 4(d), 4(c), and 4(f)). The presence of proliferating ganglion cells is also indicated by the colocalization of BDNF/H3 protein (Figures 4(g), 4(h) and 4(i)) and Thy1/H3 (Figures 4(j), 4(k), and 4(l)).

4. Discussion

4.1. Histological Analysis. The light and electron microscopy in the embryonic stage showed that the retina had a neuroblast layer, perfectly delimited into two zones: inner

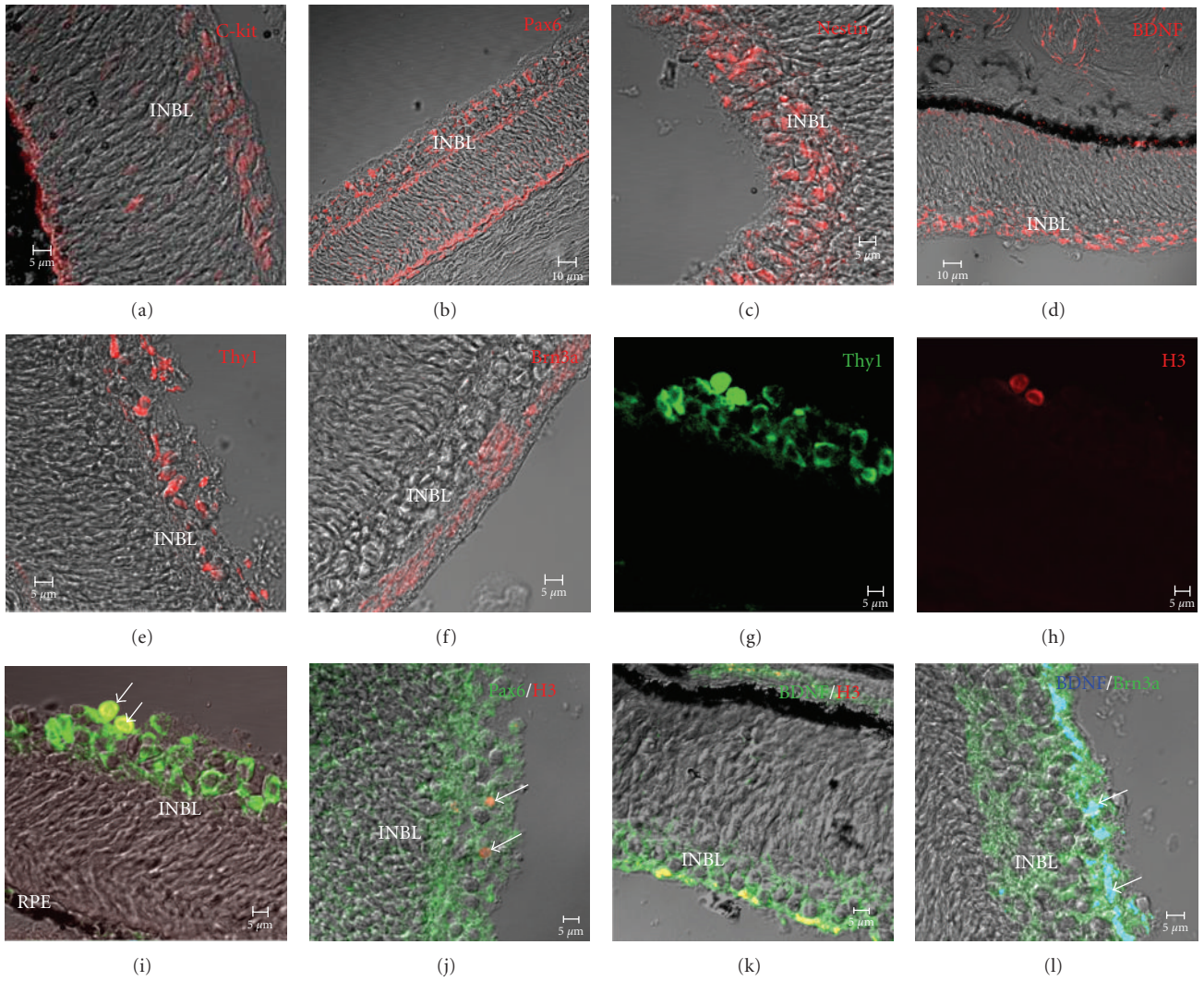

Figure 3: C-kit (a), Pax6 (b) and Nestin (c) expression in the retina from fetal stage. The expression pattern was evident in the INBL. At this stage the differentiation of ganglion cells was evident as were the markers BDNF (d), Thy1 (e) and Brn3a (f). (g) Confocal image showing the Thy1 positive cells. (h) The same image was presented in (g) but made evident with H3. (i) Merged image, but the proliferation of Thy1 cells is evident, localized in INBL (arrows). (j) Merged image illustrates the colocalization of Pax6 positive cells with H3 positive cells (arrows). (k) Merged image illustrating proliferation of BDNF positive cells in the INBL made evident by H3 (yellow stained). (l) Colocalization of BDNF and Brn3a proteins distributed along the INBL (arrows).

marginal and outer nuclear zone. The cells exhibited a distinct pattern: prophase and metaphase profiles were similar to those previously described by J. W. Hinds and P. L. Hinds [45]; these findings suggest interkinetic nuclear migration, where cells migrate from the apical side to the basement of the neuroretina, as the cell cycle progresses [46, 47]. The retinal pigment epithelium appeared as a single layer with melanosomes of oval-shape near the apical surface. Taking into account these findings and comparing them with those reported by Aguirre et al. [41] and Cook [43, 44], it was determined that embryos included in this stage had completed 25 days of gestation.

During the fetal stage, as a result of cell migration in the retina, there were two neuroblastic layers, inner and outer, separated from each other by a cell-free space called the transitional space of Chievitz. At this stage the initiation of cellular differentiation was evident; some cells, in the inner neuroblastic layer (INBL) had differentiated into ganglion cells and their axons established the layer of nerve fibers and the optic nerve. Beside this, some rudimentary photoreceptors became apparent in the outer neuroblastic layer, adjacent to the pigmented epithelium. These findings are consistent with the histological work done by Aguirre et al. [41] and Cook [43, 44] for the fetal embryonic stage in this species. Using electron microscopy, it has been noticed a difference between the nuclei of the inner and outer neuroblastic layers [48]. In the current study these differences were also apparent: in the outer neuroblastic layer the nuclei were oval, in contrast to those of the inner neuroblastic layer where the nuclei were spherical.

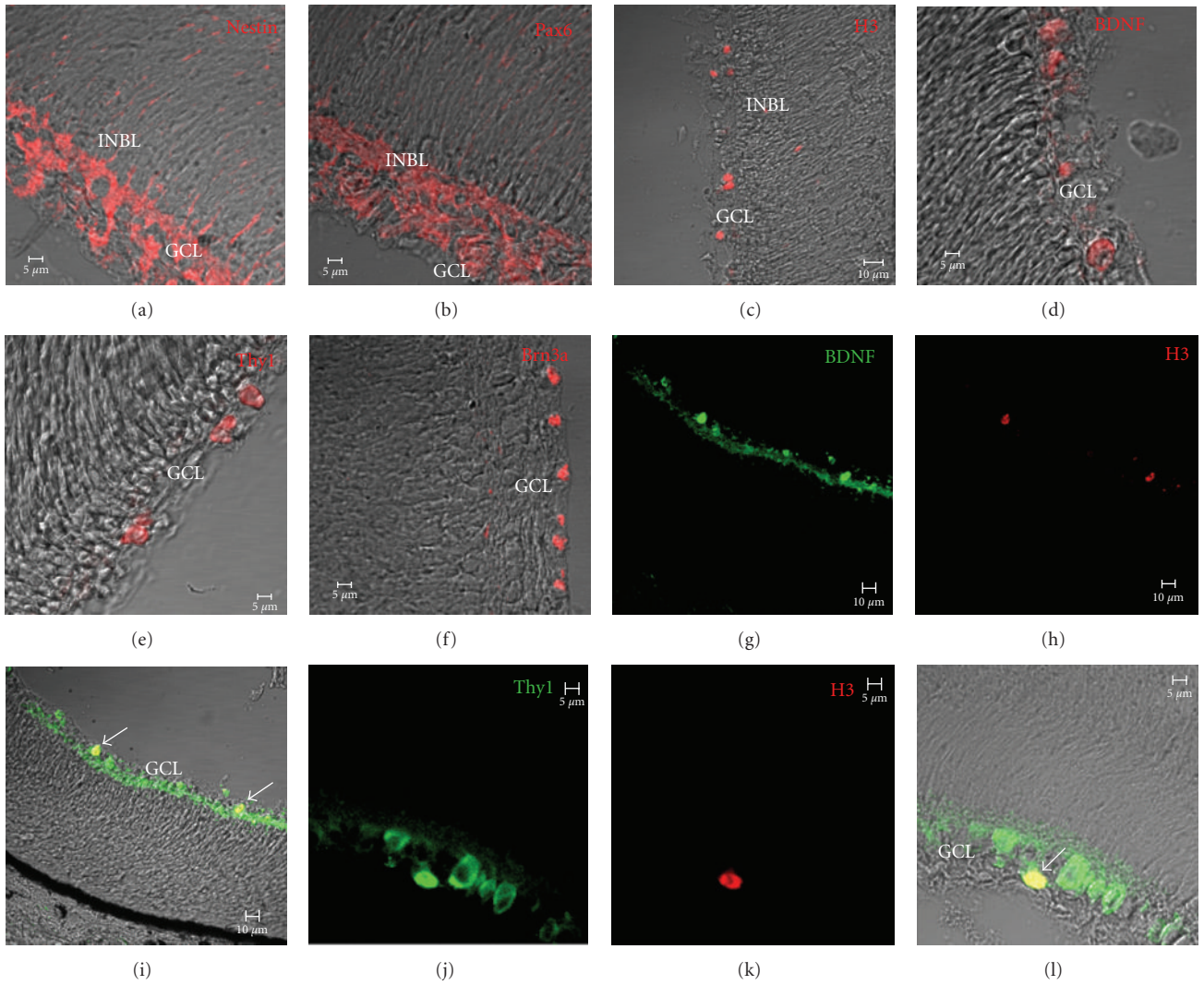

Figure 4: Immunofluorescent staining of Nestin (a) and Pax6 (b) during neonatal stage was observed in the INBL. (c) H3 only revealed in the GCL and did not co-localize with stem cell markers. BDNF (d), Thy1 (e) and Brn3a (f) staining showed the typical morphology of ganglion cells localized in the GCL (red cells). A number of cells marked with BDNF ((g)–(i)) and Thy1 ((j)–(l) were evidently proliferating as they were positive to H3 protein (arrows).

At the neonatal stage, histologically the canine retina presents the same characteristics as those described for the fetal stage; however, there are a greater number of ganglion cells. The structure of the ganglion cells was observed using electron microscopy: these cells have very large nuclei which cover the greater part of the cell body and their axons form the nerve fiber layer. At this stage, the retinal pigment epithelium consists of a row of cuboidal cells. These findings were similar to those described by Spira and Hollenberg [48] and Cook [43].

4.2. Characterization of Stem Cells. Different markers of progenitor cells have been used with great success for the purpose of identifying these cell types. Pax6 is a key gene during development of the eye, and is actively involved in the differentiation of the lens and retina in different species of vertebrates. Mutations in this gene lead to the presence of different disorders during development, resulting in anomalies of the iris, retina, lens, and cornea. During adulthood, expression continues in lens and cornea, as well as in amacrine cells and retinal ganglion cells [24, 27]. During these three stages, we observed that Pax6 presented a similar pattern covering both the central retina and the peripheral area however its expression was higher in the INBL during the fetal and neonatal stages, similar to findings reported by Doh et al. [30] who noted the expression of Pax6 in chicken embryos; this gene was detected in progenitor cells in the INBL during E4, and, as development advanced, its increase was evident in the inner nuclear layer (CNI). Finally, during late stages of development, both ganglion and amacrine cells expressed this gene.

Nestin is a protein made up of intermediate filaments which can be employed as a marker of neural progenitor cells.

It plays an important role in cell movement, including displacement, contraction and cytokinesis [49]. During chicken embryonic development, transitin, which is a homology of Nestin, may be induced in the Müller cells by acute retinal damage. Transitin-positive cells were observed mainly in the ganglion cell layer (GCL) and nerve fiber layer (NFL), possibly marking the endings of the Müller glia; however, intense immunoreactivity was presented in the ciliary margin zone (CMZ) and the ciliary body. Downregulation was restricted to the CMZ prior to hatching. The expression of Nestin in the retina of the dog had a pattern similar to that reported by Ghai et al. [50] in the chicken, where the immunoreactivity was higher in the GCL and NFL. There was, however, a higher expression near the ciliary body, ruling out the existence of a niche as occurs in the chicken. Thus it appears that this niche does not appear in the dog and that the expression of stem cell markers decreases during development.

Another marker of retinal progenitor cells is C-kit, whose participation is widely studied in gametogenesis, hematopoiesis, melanogenesis, and neurogenesis, where this gene has been observed to be involved in the establishment of neural connections. Likewise, C-kit promotes survival, proliferation, and cell differentiation [51, 52]. C-kit has been localized in the neural retinal, pigmented epithelium and ciliary body; yet the expression pattern during retinogenesis is not well known. It has been reported the presence of C-kit in the NBL and GCL during the embryonic stage of the mouse [53]. During the postnatal stage they observed a dramatic decrease, which is consistent with exit from the cell cycle and the initiation of differentiation. In this study we looked at the expression of C-kit protein during embryonic and fetal stages, where positive cells were localized mainly in the inner neuroblast layer (IN); however, it was not found during the neonatal stage. These results are consistent with those described by Koso et al. [53].

An important feature associated with the presence of stem cells is mitotic activity: stem cells in the adult are capable of mitotic activity but are frequently quiescent, whereas progenitors are often very mitotically active. In the case of the retina, it has proposed a model of nuclear migration during the development of the retina, where the nuclei of neuroepithelial cells migrate from apical to basal and basal to apical as the cell cycle progresses [47]. This places cells in G1, G2, and M in the apical zone, adjacent to the pigmented epithelium, whereas cells in phase S remain in the basement zone. It has observed that the expression of H3 starts during the G2 phase and peaks during the metaphase of mitosis [54]. In the present study, we found the presence of proliferating cells located near the retinal pigmented epithelium, confirming that cell migration occurs as part of progression in the cell cycle. In the embryonic stage, proliferating progenitor cells were observed in the germinal zone located near the pigmented epithelium.

4.3. Ganglion Cell Differentiation. During cell differentiation, retinal progenitor cells begin to express genes such as Brn3a, Thy1, and BDNF, the exact role of which is imperfectly understood, however, they may all play an important role during the differentiation of progenitor cells to become retinal ganglion cells. In this study, we discovered the expression of three markers in GCC during the fetal stage, by applying immunofluorescence. Although it has been reported that ganglion cells are abundant in the central zone, we observed the presence of ganglion cells in the peripheral and central zones.

Schlamp et al. [55] commented that in the case of marker ganglion cells in both the mouse and rat with damage to the retina, when expression diminished, damage increased. On the other hand, it has been detected Thy1 and Brn3a in the adult mouse which are identified in the CGL of the ganglion cell body as well as in their dendrites on the inner plexiform layer [56]. Recently, Germanà et al. [39] revealed the presence of BDNF in zebrafish by applying peroxidase immunohistochemistry. They detected the expression of this antibody between 10 dpf and 180 dpf in the outer nuclear, outer plexiform, and inner plexiform layer, observing an increase of similar intensity advancing with development. The expression of Brn3a was observed too in the retina of the chicken which progressed with development, observing that this label was clearly evident in the inner nuclear layer, ganglion cell layer and nerve fiber layer [30].

The expression of ganglion cells was only detected in the fetal and neonatal stage, a result similar to that described by Schlamp et al. [55] and Raymond et al. [56]. Germanà et al. [39] and Doh et al. [30] marked the ganglion cells with the same antibodies used in this work, and likewise we observed the colocalization of ganglion cells with H3. These data suggest that ganglion cells undergo proliferating activity during development.

5. Conclusions

Canine retinal progenitor cells express the markers Pax6 and nestin in the neuroblastic layer during pre- and postnatal stages. However, the expression of C-kit was limited to the embryonic and fetal stage probably due to cellular differentiation. Cells manifesting mitotic activity were detected in the embryonic and fetal stages in combination with cells expressing C-kit and Pax6, in contrast to the newborn stage, where the mitotic activity was observed in ganglion cells marked with BDNF and Thy1. The presence of the Brn3a, Thy1 and BDNF proteins were all detected during the fetal stage corresponding to the beginning of cell differentiation. Therefore, we suggest that a small group of progenitor cells localized in the GCL are in fact ganglion cells which are present in the retina of the dog during the first days after birth.

Acknowledgment

This work was supported by CONACyT (no. 81269) and PAPIIT-UNAM (no. IN205011).

References

[1] I. Ahmad, "Stem cells: new opportunities to treat eye diseases," *Investigative Ophthalmology and Visual Science*, vol. 42, no. 12, pp. 2743–2748, 2001.

[2] I. Klimanskaya, "Retinal pigment epithelium derived from embryonic stem cells," in *Stem Cell Anthology: Stem Cell Biology, Tissue, Engineering, Cloning, Regenerative Medicine and Biology*, B. C. Carlson, Ed., pp. 335–346, Elsevier, San Diego, Calif, USA, 1st edition, 2010.

[3] V. Tropepe, B. L. K. Coles, B. J. Chiasson et al., "Retinal stem cells in the adult mammalian eye," *Science*, vol. 287, no. 5460, pp. 2032–2036, 2000.

[4] B. L. K. Coles, B. Angénieux, T. Inoue et al., "Facile isolation and the characterization of human retinal stem cells," *Proceedings of the National Academy of Sciences of the United States of America*, vol. 101, no. 44, pp. 15772–15777, 2004.

[5] S. A. Cicero, D. Johnson, S. Reyntjens et al., "Cells previously identified as retinal stem cells are pigmented ciliary epithelial cells," *Proceedings of the National Academy of Sciences of the United States of America*, vol. 106, no. 16, pp. 6685–6690, 2009.

[6] M. J. Seiler, R. B. Aramant, M. W. Seeliger, R. Bragadottir, M. Mahoney, and K. Narfstrom, "Functional and structural assessment of retinal sheet allograft transplantation in feline hereditary retinal degeneration," *Veterinary Ophthalmology*, vol. 12, no. 3, pp. 158–169, 2009.

[7] E. A. McCulloch and J. E. Till, "Perspectives on the properties of stem cells," *Nature Medicine*, vol. 11, no. 10, pp. 1026–1028, 2005.

[8] L. Li and T. Xie, "Stem cell niche: structure and function," *Annual Review of Cell and Developmental Biology*, vol. 21, pp. 605–631, 2005.

[9] H. K. Salem and C. Thiemermann, "Mesenchymal stromal cells: current understanding and clinical status," *Stem Cells*, vol. 28, no. 3, pp. 585–596, 2010.

[10] A. J. Fischer and T. A. Reh, "Identification of a proliferating marginal zone of retinal progenitors in postnatal chickens," *Developmental Biology*, vol. 220, no. 2, pp. 197–210, 2000.

[11] H. Xu, I. D. D. Sta, J. L. Kielczewski et al., "Characteristics of progenitor cells derived from adult ciliary body in mouse, rat, and human eyes," *Investigative Ophthalmology and Visual Science*, vol. 48, no. 4, pp. 1674–1682, 2007.

[12] T. A. Reh and E. M. Levine, "Multipotential stem cells and progenitors in the vertebrate retina," *Journal of Neurobiology*, vol. 36, no. 2, pp. 206–220, 1998.

[13] A. J. Fischer, B. D. Dierks, and T. A. Reh, "Exogenous growth factors induce the production of ganglion cells at the retinal margin," *Development*, vol. 129, no. 9, pp. 2283–2291, 2002.

[14] A. J. Fischer, J. J. Stanke, K. Ghai, M. Scott, and G. Omar, "Development of bullwhip neurons in the embryonic chicken retina," *Journal of Comparative Neurology*, vol. 503, no. 4, pp. 539–549, 2007.

[15] X. Mu and W. H. Klein, "A gene regulatory hierarchy for retinal ganglion cell specification and differentiation," *Seminars in Cell and Developmental Biology*, vol. 15, no. 1, pp. 115–123, 2004.

[16] T. Marquardt and P. Gruss, "Generating neuronal diversity in the retina: one for nearly all," *Trends in Neurosciences*, vol. 25, no. 1, pp. 32–38, 2002.

[17] N. A. Zaghloul, B. Yan, and S. A. Moody, "Step-wise specification of retinal stem cells during normal embryogenesis," *Biology of the Cell*, vol. 97, no. 5, pp. 321–337, 2005.

[18] P. A. Raymond, L. K. Barthel, R. L. Bernardos, and J. J. Perkowski, "Molecular characterization of retinal stem cells and their niches in adult zebrafish," *BMC Developmental Biology*, vol. 26, pp. 1–17, 2006.

[19] M. E. Zuber, G. Gestri, A. S. Viczian, G. Barsacchi, and W. A. Harris, "Specification of the vertebrate eye by a network of eye field transcription factors," *Development*, vol. 130, no. 21, pp. 5155–5167, 2003.

[20] C. Walther and P. Gruss, "Pax-6, a murine paired box gene, is expressed in the developing CNS," *Development*, vol. 113, no. 4, pp. 1435–1449, 1991.

[21] R. L. Chow, C. R. Altmann, R. A. Lang, and A. Hemmati-Brivanlou, "Pax6 induces ectopic eyes in a vertebrate," *Development*, vol. 126, no. 19, pp. 4213–4222, 1999.

[22] G. Halder, P. Callaerts, and W. J. Gehring, "New perspectives on eye evolution," *Current Opinion in Genetics and Development*, vol. 5, no. 5, pp. 602–609, 1995.

[23] J. C. Grindley, D. R. Davidson, and R. E. Hill, "The role of Pax-6 in eye and nasal development," *Development*, vol. 121, no. 5, pp. 1433–1442, 1995.

[24] T. Strachan and A. P. Read, "PAX genes," *Current Opinion in Genetics and Development*, vol. 4, no. 3, pp. 427–438, 1994.

[25] J. C. Quinn, J. D. West, and R. E. Hill, "Multiple functions for Pax6 in mouse eye and nasal development," *Genes and Development*, vol. 10, no. 4, pp. 435–446, 1996.

[26] R. Ashery-Padan, T. Marquardt, X. Zhou, and P. Gruss, "Pax6 activity in the lens primordium is required for lens formation and for correct placement of a single retina in the eye," *Genes and Development*, vol. 14, no. 21, pp. 2701–2711, 2000.

[27] T. Marquardt, R. Ashery-Padan, N. Andrejewski, R. Scardigli, F. Guillemot, and P. Gruss, "Pax6 is required for the multipotent state of retinal progenitor cells," *Cell*, vol. 105, no. 1, pp. 43–55, 2001.

[28] A. M. Hever, K. A. Williamson, and V. van Heyningen, "Developmental malformations of the eye: The role of PAX6, SOX2 and OTX2," *Clinical Genetics*, vol. 69, no. 6, pp. 459–470, 2006.

[29] N. Osumi, H. Shinohara, K. Numayama-Tsuruta, and M. Maekawa, "Concise review: Pax6 transcription factor contributes to both embryonic and adult neurogenesis as a multifunctional regulator," *Stem Cells*, vol. 26, no. 7, pp. 1663–1672, 2008.

[30] S. T. Doh, H. Hao, S. C. Loh et al., "Analysis of retinal cell development in chick embryo by immunohistochemistry and in ovo electroporation techniques," *BMC Developmental Biology*, vol. 10, article 8, 2010.

[31] J. Dahlstrand, M. Lardelli, and U. Lendahl, "Nestin mRNA expression correlates with the central nervous system progenitor cell state in many, but not all, regions of developing central nervous system," *Developmental Brain Research*, vol. 84, no. 1, pp. 109–129, 1995.

[32] S. Fukuda, F. Kato, Y. Tozuka, M. Yamaguchi, Y. Miyamoto, and T. Hisatsune, "Two distinct subpopulations of nestin-positive cells in adult mouse dentate gyrus," *Journal of Neuroscience*, vol. 23, no. 28, pp. 9357–9366, 2003.

[33] J. C. Walcott and J. M. Provis, "Müller cells express the neuronal progenitor cell marker nestin in both differentiated and undifferentiated human foetal retina," *Clinical and Experimental Ophthalmology*, vol. 31, no. 3, pp. 246–249, 2003.

[34] E. J. Mayer, D. A. Carter, Y. Ren et al., "Neural progenitor cells from postmortem adult human retina," *British Journal of Ophthalmology*, vol. 89, no. 1, pp. 102–106, 2005.

[35] H. Kohno, T. Sakai, and K. Kitahara, "Induction of nestin, Ki-67, and cyclin D1 expression in Müller cells after laser injury in adult rat retina," *Graefe's Archive for Clinical and Experimental Ophthalmology*, vol. 244, no. 1, pp. 90–95, 2006.

[36] B. Jagatha, M. S. Divya, R. Sanalkumar et al., "In vitro differentiation of retinal ganglion-like cells from embryonic stem cell derived neural progenitors," *Biochemical and Biophysical Research Communications*, vol. 380, no. 2, pp. 230–235, 2009.

[37] E. Caminos, E. Becker, D. Martin-Zanca, and E. Vecino, "Neurotrophins and their receptors in the normal and regenerating tench retina. An in situ hybridisation and immunoreactivity study," *Journal of Comparitive Neurology*, vol. 404, no. 3, pp. 321–331, 1999.

[38] A. J. Weber and C. D. Harman, "BDNF preserves the dendritic morphology of α and β ganglion cells in the cat retina after optic nerve injury," *Investigative Ophthalmology and Visual Science*, vol. 49, no. 6, pp. 2456–2463, 2008.

[39] A. Germanà, C. Sánchez-Ramos, M. C. Guerrera et al., "Expression and cell localization of brain-derived neurotrophic factor and TrkB during zebrafish retinal development," *Journal of Anatomy*, vol. 217, no. 3, pp. 214–222, 2010.

[40] M. J. Karnovsky, "A formaldehyde-glutaraldehyde fixative of high osmolality for use in electron microscopy," *Journal of Cell Biology*, vol. 27, no. 137, 1965.

[41] G. D. Aguirre, L. F. Rubin, and S. I. Bistner, "Development of the canine eye," *American Journal of Veterinary Research*, vol. 33, no. 12, pp. 2399–2414, 1972.

[42] P. Simoens and K. D. Budras, "The eye," in *Anatomy of the Dog*, K.-D. Budras, P. H. McCarthy, W. Fricke, and R. Richter, Eds., pp. 118–119, Schlütersche, Frankfurt, Germany, 5th edition, 2007.

[43] C. S. Cook, "Embryogenesis of congenital eye malformations," *Veterinary and Comparative Ophthalmology*, vol. 5, no. 2, pp. 109–1211, 1995.

[44] C. S. Cook, "Ocular embryology and congenital malformations," in *Veterinary Ophthalmology*, K. N. Gelatt, Ed., pp. 3–30, Blackwell, Ames, Iowa, USA, 4th edition, 2007.

[45] J. W. Hinds and P. L. Hinds, "Early ganglion cell differentiation in the mouse retina: an electron microscopic analysis utilizing serial sections," *Developmental Biology*, vol. 37, no. 2, pp. 381–416, 1974.

[46] L. M. Baye and B. A. Link, "Interkinetic nuclear migration and the selection of neurogenic cell divisions during vertebrate retinogenesis," *Journal of Neuroscience*, vol. 27, no. 38, pp. 10143–10152, 2007.

[47] L. M. Baye and B. A. Link, "Nuclear migration during retinal development," *Brain Research*, vol. 1192, no. C, pp. 29–36, 2008.

[48] A. W. Spira and M. J. Hollenberg, "Human retinal development: ultrastructure of the inner retinal layers," *Developmental Biology*, vol. 31, no. 1, pp. 1–21, 1973.

[49] K. Michalczyk and M. Ziman, "Nestin structure and predicted function in cellular cytoskeletal organisation," *Histology and Histopathology*, vol. 20, no. 2, pp. 665–671, 2005.

[50] K. Ghai, J. J. Stanke, and A. J. Fischer, "Patterning of the circumferential marginal zone of progenitors in the chicken retina," *Brain Research*, vol. 1192, pp. 76–89, 2008.

[51] T. Hirata, E. Morii, M. Morimoto et al., "Stem cell factor induces outgrowth of c-kit-positive neurites and supports the survival of c-kit-positive neurons in dorsal root ganglia of mouse embryos," *Development*, vol. 119, no. 1, pp. 49–56, 1993.

[52] A. V. Das, J. James, X. Zhao, J. Rahnenführer, and I. Ahmad, "Identification of c-Kit receptor as a regulator of adult neural stem cells in the mammalian eye: interactions with Notch signaling," *Developmental Biology*, vol. 273, no. 1, pp. 87–105, 2004.

[53] H. Koso, S. Satoh, and S. Watanabe, "c-kit marks late retinal progenitor cells and regulates their differentiation in developing mouse retina," *Developmental Biology*, vol. 301, no. 1, pp. 141–154, 2007.

[54] C. Prigent and S. Dimitrov, "Phosphorylation of serine 10 in histone H3, what for?" *Journal of Cell Science*, vol. 116, no. 18, pp. 3677–3685, 2003.

[55] C. L. Schlamp, E. C. Johnson, Y. Li, J. C. Morrison, and R. W. Nickells, "Changes in Thy1 gene expression associated with damaged retinal ganglion cells," *Molecular Vision*, vol. 7, pp. 192–201, 2001.

[56] I. D. Raymond, A. Vila, U. C. N. Huynh, and N. C. Brecha, "Cyan fluorescent protein expression in ganglion and amacrine cells in a thy1-CFP transgenic mouse retina," *Molecular Vision*, vol. 14, pp. 1559–1574, 2008.

Hindawi Publishing Corporation
Stem Cells International
Volume 2012, Article ID 263264, 7 pages
doi:10.1155/2012/263264

Research Article

The Influence of Brightness on Functional Assessment by mfERG: A Study on Scaffolds Used in Retinal Cell Transplantation in Pigs

A. T. Christiansen,[1] J. F. Kiilgaard,[1] M. Smith,[2] R. Ejstrup,[1] G. E. Wnek,[3] J. U. Prause,[4] M. J. Young,[5] H. Klassen,[6] H. Kaplan,[7] and M. La Cour[1]

[1] *Department of Ophthalmology, Glostrup Hospital, Copenhagen University Hospital, Nordre Ringvej 57, 2600 Glostrup, Denmark*
[2] *NuVention Solutions Inc., Valley View, OH 44125, USA*
[3] *Case Western Reserve University, Cleveland, OH 44106, USA*
[4] *Eye Pathology Institute, University of Copenhagen, 2100 Copenhagen, Denmark*
[5] *Schepens Eye Research Institute, Department of Ophthalmology, Harvard Medical School, Boston, MA 02114, USA*
[6] *The Gavin Herbert Eye Institute and Stem Cell Research Center, University of California, Irvine, CA 92697, USA*
[7] *Department of Ophthalmology and Visual Sciences, Kentucky Lions Eye Center, University of Louisville, Louisville, KY 40208, USA*

Correspondence should be addressed to J. F. Kiilgaard, jfkiilgaard@gmail.com

Received 16 August 2011; Accepted 7 November 2011

Academic Editor: Budd A. Tucker

To determine the effect of membrane brightness on multifocal electroretinograms (mfERGs), we implanted poly lactic-co-glycolic acid (PLGA) membranes in the subretinal space of 11 porcine eyes. We compared membranes with their native shiny white color with membranes that were stained with a blue dye (Brilliant Blue). Histological and electrophysiological evaluation of the overlying retina was carried out 6 weeks after implantation. Histologically, both white and blue membranes degraded in a spongiform manner leaving a disrupted outer retina with no preserved photoreceptor segments. Multifocal ERG revealed the white membranes to have a significantly higher P1-amplitude ratio than the blue ($P = 0.027$), and a correlation between brightness ratio and P1-amplitude ratio was found ($r = 0.762$). Based on our findings, we conclude that bright subretinal objects can produce normal mfERG amplitude ratios even when the adjacent photoreceptors are missing. Functional assessment with mfERG in scaffold implant studies should therefore be evaluated with care.

1. Introduction

Subretinal transplantation of stem cell-like cells, such as retinal progenitor cells (RPCs), has shown great restorative potential in a number of animal models of retinal degeneration [1]. Although these cells retain the ability to migrate to the outer retina, differentiate to mature photoreceptors, and generate synapses with existing cells [1], the number and the organization of surviving cells fall short of that needed to restore useful vision.

The use of scaffolds in subretinal transplantation has been shown to increase the number of delivered and surviving cells, to enable a more precise and localized delivery [2] and to promote differentiation and organization of grafted RPCs [2–4]. Furthermore, scaffolds can be loaded with regulatory and modulating drugs to further assist differentiation, function, and survival [5, 6].

As scaffold material, poly lactic-co-glycolic acid (PLGA) has shown good results for subretinal transplantation of RPC in mice [2, 5], rats [4], and pigs [3] and is among the more commonly used materials for generating scaffolds [7].

We wanted to use multifocal electroretinography (mfERG) to assess the functional impact of implantation of scaffolds made of PLGA and other polymers. To our surprise, we found that the mfERG amplitudes derived from retina apparently overlying the PLGA membranes were normal despite histologically verified destruction of the outer retina in the same area. We then hypothesized that the brightness of the white transplanted membranes caused the mfERG stimulus to be backscattered and so produced

a stray light-induced response. To test this hypothesis, we first implanted a batch of PLGA membranes stained with a blue dye, and therefore with reduced surface brightness. Hereafter, we compared the mfERG amplitude ratios derived from areas overlying white PLGA membranes with those derived from areas overlying blue PLGA membranes and furthermore correlated the mfERG amplitude ratios with the surface brightness ratios over the transplanted PLGA membranes.

2. Material and Methods

2.1. Animals. All experiments were performed in compliance with The Association for Research in Vision and Ophthalmology (ARVO) Statement for the Use of Animals in Ophthalmic and Vision Research. The Danish Animal Experiments Inspectorate granted permission for the use of the animals (permission 2007/561-768). Trained veterinary nurses and technicians carried out all handling of the animals.

A total of 21 female domestic pigs of Danish Landrace/Duroc/Hampshire/Yorkshire breed were used for these experiments (age 3-4 months; weight 23–30 kg). Only left eyes underwent membrane transplantation. The animals were premedicated with Tiletamine 1.19 mg/kg, Zolazepam 1.19 mg/kg (Zoletil 50 Vet Virbac SA, Carros, France), Methadone 0.24 mg/kg (Nycomed, Roskilde, Denmark), Ketamine 1.43 mg/kg (Intervet, Skovlunde, Denmark), and Xylazine 1.24 mg/kg (Intervet, Skovlunde, Denmark). Thereafter, anesthesia was maintained with continuous intravenous infusion (i.v.) of propofol 15 mg/kg/h (Fresenius Kabi, Bad Homburg, Germany). The animals were endotracheally intubated and artificially ventilated on 34% O_2. During anesthesia, the animals were placed resting on their elbows to minimizing the impact on the cardiovascular system [8]. In order to avoid hypothermia, the animals were wrapped in a blanket during anesthesia.

2.2. Surgical Procedure. Eyes were anesthetized, dilated, and disinfected, and a standard three-port core vitrectomy was performed as previously described [9]. In brief, the infusion line was secured inferiorly (Ringer Lactate; SAD, Copenhagen, Denmark), and the vitreous was removed during endoillumination using a 20 gauge (G) vitrector (Karl Storz GmbH, Tuttlingen, Germany). The posterior hyaloid was meticulous removed in the visual streak and optic disc area. A subretinal bleb in the visual streak area was raised by injection of Ringer Lactate (SAD, Copenhagen, Denmark) through a 41 G cannula (ref. 1270; DORC International BV, Zuidland, the Netherlands). To gain access to the subretinal space, a retinotomy was performed in the temporal aspect of the bleb using endodiathermy (Storz Premiere, Bausch and Lomb; energy set 15%, output range 7.5 Watts nominal at 100 ohms) and automated scissors (Storz Premiere, automatic scissors). This allowed a large piece of membrane (approx. 12 mm^2) to be inserted in the visual streak area. DORC's combined spatula/peeling forceps (Ref. 1297, DORC, Netherlands) were used for this process. In order to secure the membrane, a partial fluid-air-exchange with drainage at the retinotomy site was performed after the membrane was placed subretinally. Sclera and conjunctiva were sutured with 7–0 coated vicryl (Ethicon, Norderstedt, Germany). After the procedure, intraocular pressure was evaluated with bimanual palpation, and indirect ophthalmoscopy was performed to ensure correct placement of the membrane and absence of bleeding and retinal detachment. Finally, topical application of chloramphenicol ointment was given, and the eye was patched (Kloramfenikol "DAK"; Nycomed, Roskilde, Denmark). In order to ensure reliable mfERG recordings, animals with any surgical complication, such as bleeding, surgical lens damage or retinal detachment as well as animals with significant opacities in the media were excluded from the study.

2.3. Follow-Up Procedure. Six weeks after-surgery, animals were reanesthetized as previously described [8] with addition of a neuromuscular blocker to avoid eye movement, 2 mg/h i.v. Pancurium Bromide (Oss, Organon, Holland). Infrared (IR) fundus imaging with an external IR light source was used as previously described [8]. Color fundus photos obtained with a Zeiss fundus camera just prior to euthanasia (Zeiss FF450 plus-IR). Multifocal ERG was recorded on both eyes. Recordings were conducted in an electrically shielded room under standardized lighting conditions, and dilated eyes were adapted to room light for 15 minutes. A Burian-Allen bipolar contact lens electrode (VERIS Infrared Illuminating Electrode, EDI, Inc., Red Wood, CA) was placed on the cornea with a gel (Viscotears, Novartis, Copenhagen, Denmark) as contact fluid. A reference electrode was placed behind the right ear, and the animal was electrically grounded. To minimize the effect of anesthesia on the mfERG recording, the left membrane-implanted eye was always recorded within the first two hours of anesthesia [8], and the two eyes were recorded within a timeframe of 30 min.

At completion of follow-up studies, animals were euthanized by a lethal injection of 20 mL pentobarbital 200 mg/mL (Royal Veterinary and Agricultural University, Copenhagen, Denmark). Eyes were then enucleated and prepared for histology as previously described [8].

2.4. mfERG Settings. Recordings were obtained using VERIS Science 5.0.1 with visual stimulus displayed on a 1.5 inch cathode ray tube monitor integrated in the stimulus-camera (EDI Inc., Redwood City, CA, USA). A stimulus pattern of 241 unscaled white (200 cd/m^2) and black (2 cd/m^2) hexagons with a frame rate of 75 Hz and 16 samples per frames was used to obtain the best spatial resolution with a reasonable signal-to-noise ratio [8]. The m-sequence exponent was 15 and the durations of recordings were 7.17 minutes. The signals were band-pass filtered outside 10–300 Hz. There was no spatial averaging and only 1st order kernels were used.

2.5. mfERG Analysis. To identify hexagons representing retina with an underlying membrane, an alignment of the IR fundus photo of the left eye with the stimulus grid from the VERIS system and the corresponding Zeiss color fundus photo was performed using Photoshop (version 10.0, Adobe

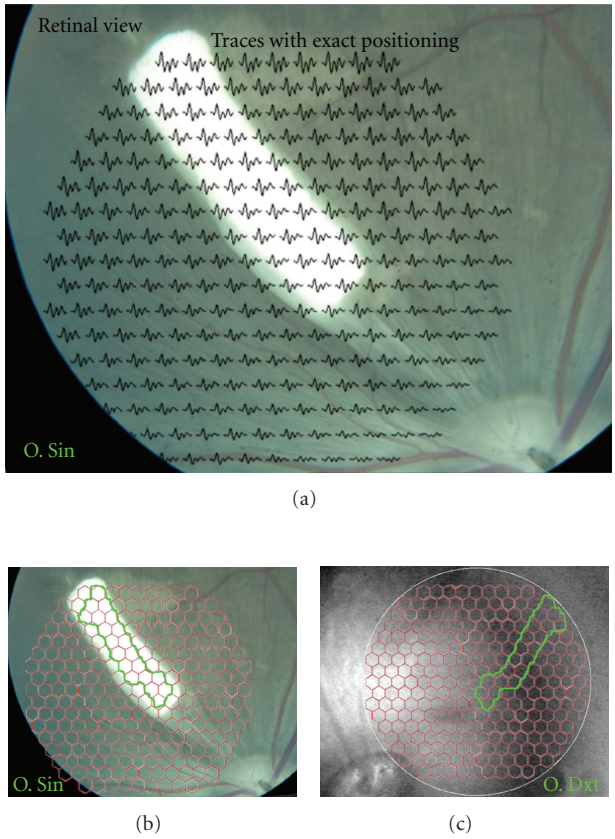

Figure 1: Fundus photos of both eyes 6 weeks after white PLGA transplantation. (a) Color fundus photo aligned with multifocal electroretinographic (mfERG) traces of the 241 unscaled stimulated hexagons. The bright reflective properties of the membranes are clearly visible. (b) Color fundus photo of the left membrane-transplanted eye aligned with hexagon grid used for mfERG recording. Area included as membrane is marked with a green line. (c) Infrared fundus photo of fellow right untouched eye with hexagon grid used for mfERG recording. The green line marks area included at membrane corresponding area for calculation of P1-amplitude ratio.

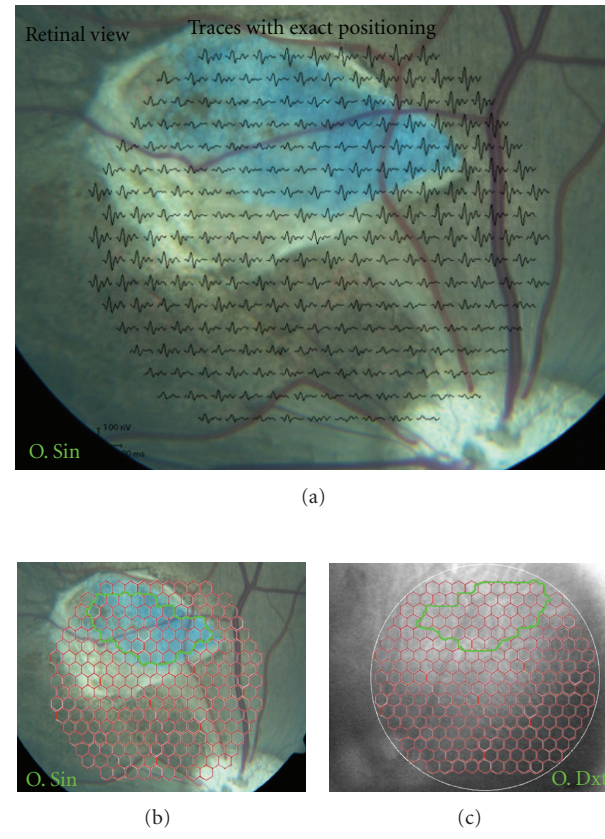

Figure 2: Fundus photos of both eyes 6 weeks after blue PLGA transplantation. (a) Color fundus photo aligned with multifocal electroretinographic (mfERG) traces of the 241 unscaled stimulated hexagons. The membrane is surrounded by choroidal neovascularization but does not appear to reflect light in the manner of the white PLGA. (b) Color fundus photo of the left membrane-transplanted eye aligned with hexagon grid used for mfERG recording. Area included as membrane is marked with a green line. (c) Infrared fundus photo of fellow right untouched eye with hexagon grid used for mfERG recording. The green line marks area included at membrane corresponding area for calculation of P1-amplitude ratio.

Systems Inc., San Jose, CA, USA). This was done for every individual left (experimental) eye in the study, and the hexagons completely within the membrane-affected area were labeled. The corresponding area in the right (control) eye was delineated from the VERIS IR fundus photo (Figures 1(b), 1(c), 2(b), 2(c)). The averages of the P1-amplitudes derived from hexagons within the membrane-affected area were calculated. The averages of P1-amplitudes in the right eye derived from the corresponding retinal area were also calculated as well as the ratios between these P1 amplitudes from the two eyes. Independent-samples t-test was used to test for equality of means between the two membrane color ratios (SPSS Statistics, version 17.0).

To control the comparability of the right and left eye, the visual streak was localized using the 3D multiplot of the Veris program, and mfERG for the entire visual streak was recorded and compared.

2.6. Brightness Analysis. Color fundus photos were used to evaluate the brightness of the subretinally transplanted membranes. Area of interest was marked and measured in Photoshop on a scale ranging from 0 (black point) to 255 (white point) as described by Hubbard et al. [10]. The ratio between the membrane area and the optic disc brightness was used to even out differences in the fundus photo flash intensity. The difference in brightness ratios between the two membrane colors and Pearsons correlation between brightness ratio and mfERG P1-amplitude ratio were calculated using SPSS (SPSS Statistics, version 17.0). Ratios were plotted in Figure 5 using SigmaPlot (SigmaPlot for Windows 11.0, Systat Software Inc., CA, USA).

2.7. Histology. The part of the formaldehyde (4%) fixated eye containing the PLGA membrane was cut out and embedded in paraffin. Sections of 5 micrometer through the membrane

Table 1: Distribution of complications after subretinal transplantation of white and blue PLGA membranes.

	Reaction in the vitreous body	Membrane dislocated to the vitreous body	Membrane implanted outside visual streak
White PLGA	2	3	1
Blue PLGA	2	1	1

were then stained with haematoxylin and eosin (HE) and evaluated by light microscopy.

2.8. Membranes. White (undyed) membranes were constructed by transferring a solution of 15 weight percent (wt%) PLGA in CHCl3 to a 5 mL syringe attached to a blunt tipped 18 G stainless steel needle. Hereafter, electrospinning was carried out through the application of a 15 kV positive voltage to the polymer solution. The solution was then fed via a syringe pump at a constant mass flow rate of 1 mL/h. Fibers were collected on a stainless steel grounded rotating drum until a nonwoven mat was formed. For the blue PLGA membranes, 2 wt% of Brilliant Blue FCF was added to the 15 wt% PLGA solution.

3. Results

A total of 21 pigs underwent PLGA-membrane transplantation surgery, whereof 12 had white membranes transplanted. Ten pigs, 4 with blue and 6 with white membranes, were excluded due to postoperative complications shown in Table 1. Included in the study were 11 pigs, 6 with white membranes, and 5 with blue membranes. The high modulus of the used PLGA membranes eased the insertion into the subretinal space. Contrarily the lack of compliance complicated the precise delivery within the bleb.

It was possible to obtain good mfERGs with acceptable signal-to-noise ratios in both the left and right eye in all included pigs. Evaluation of the recorded mfERGs shows that the visual streak of the fellow eyes is comparable. Further the ratios reveal a tendency for the right visual streak to produce a lower mfERG signal than the fellow left visual streak (Table 2). Multifocal ERG of the membrane and the membrane-corresponding areas revealed a significant difference between mean P1-amplitude ratios from white and blue membrane areas ($P = 0.027$, Table 3).

Histological examination showed, however, no major differences between blue and white membranes. Both membranes were associated with spongiform degeneration of the overlying retina, together with a giant cell foreign body reaction. No severe inflammation was seen in either retina or choroid. The retina adjacent to the membrane was intact but the overlying retina had complete loss of photoreceptor outer and inner segments. The outer nuclear layer (ONL) was marginally more preserved over the blue PLGAs but was generally either flattened, disorganized, or completely missing whereas the inner nuclear layer (INL) seemed relatively intact over both white and blue membranes (Figures 3 and 4).

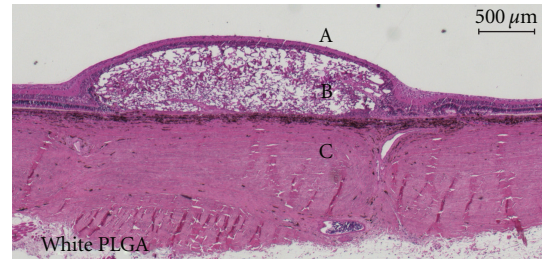

Figure 3: Micrograph of Hematoxylin- and Eosin-stained porcine retina after subretinally transplanting white PLGA membrane (B). The membrane is degrading in a spongiform manner disrupting and partly destroying the outer retina with no preserved photoreceptor segments and a flattened, disrupted, or completely missing outer nuclear layer. The inner nuclear layer is relatively intact and there is no sign of severe inflammation in either retina or choroid. Retina adjacent to the membrane appears intact. Vitreous body is indicated by "A" and sclera by "C".

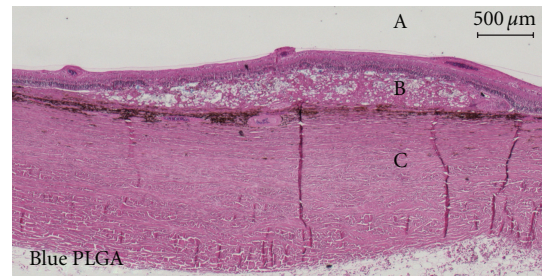

Figure 4: Micrograph of Hematoxylin- and Eosin-stained porcine retina after subretinally transplanting blue PLGA membrane (B). The membrane is degrading in a spongiform manner disrupting and partly destroying the outer retina. The disruption seems to vary, but no photoreceptor segments are preserved. The outer nuclear layer is relatively well preserved in a few places but generally flattened and disorganized or missing. The inner nuclear layer is relatively intact. No sign of severe inflammation in retina or choroid. Retina adjacent to the membrane appears intact. Vitreous body is indicated by "A" and sclera by "C".

In spite of the similar outer retinal destruction seen histologically (Figures 3 and 4), mfERG traces over the membranes differed between the two colors with near-normal P1-amplitudes over the white membranes and reduced P1-amplitudes over the blue membranes (Figures 1(a) and 2(a), Table 3).

Brightness ratios from all included animals were obtained and showed a significant difference between white and blue membranes (Figure 5). A correlation between brightness ratio and P1-amplitude ratio could be demonstrated ($r = 0.762$; $P = 0.006$) and is given in Figure 5.

MfERG recordings made prior to white PLGA membrane transplantation showed retinal responses in the visual streak to be identical in the left and right eyes and comparable with previously obtained baseline recordings [8] (data not shown). No preimplantation recordings were obtained for the blue membranes.

Table 2: Mean P1-amplitude values and ratios of visual streak obtained by multifocal electroretinogram before and 6 weeks after membrane implantation.

	White PLGA Week 0 ($n = 6$)	White PLGA Week 6 ($n = 6$)	Blue PLGA Week 6 ($n = 5$)
Mean P1-amplitude, nV/deg^2			
SIN visual streak, excl. memb. (SD)	12,08 (3,58)	8,05 (2,18)	11,18 (1,56)
DXT visual streak (SD)	11,37 (4,46)	7,18 (1,74)	9,80 (2,60)
Mean P1-amplitude ratio for visual			
streak (Sin/Dxt) (SD)	1,12 (0,19)	1,12 (0,13)	1,20 (0,28)

SD = standard deviation; Memb. = area of retina with underlying implanted membrane or scarring hereafter; Sin = Left membrane implanted eye; Dxt = right untouched corresponding eye.

Table 3: Effect of color of subretinally implanted membranes upon the multifocal electroretinogram 6 weeks after implantation.

	White PLGA ($n = 6$)	Blue PLGA ($n = 5$)	
Mean P1-amplitude, nV/deg^2			
Memb. (SD)	5,23 (1,70)	5,92 (1,72)	
Memb.-corresp. (SD)	4,75 (1,72)	10,00 (3,72)	
Mean P1-amplitude ratio.			
(Memb./memb.corresp.) (SD)	1,17(0,35)	0,65 (0,26)	($P = 0.027$)

SD = standard deviation; Memb. = membrane-supported area of retina;
Memb.-corresp. = membrane corresponding area in contralateral control eye.

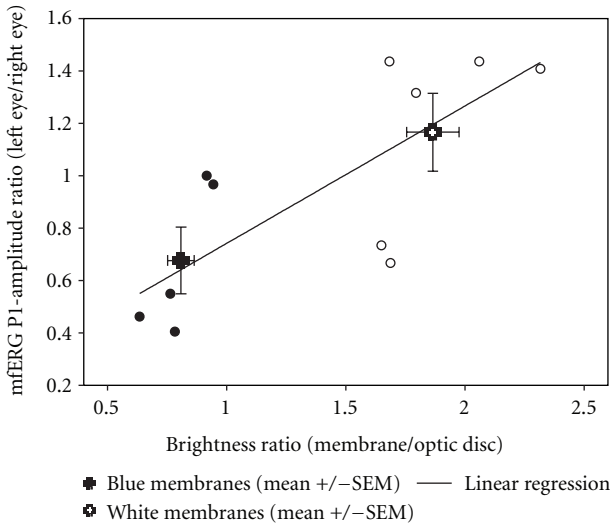

Figure 5: Mean values of white and blue membranes and correlation between brightness ratio (membrane/optic disc) and P1-amplitude ratio (left/right). Large symbols represent mean ± SEM for white and blue membranes and show a significant difference in P1-amplitude ratio ($P = 0.027$) and brightness ratio ($P < 0.001$). When observed together, the blue (•) and white (◦) membranes show a significant correlation ($r = 0.762$; $P = 0.006$).

4. Discussion

In this study, we show that the color of a subretinally transplanted membrane has an effect on the recorded mfERG. We further show a correlation between the brightness of the membrane and the effect on the P1-amplitude ratios in the mfERG. This is to our knowledge the first study that shows correlation of brightness and mfERG.

The optic disc has no photoreceptors and should therefore not be able to produce an electrical signal when illuminated. Nevertheless, focal illumination of the optic disc is well known to produce an ERG response [11]. This effect has been explained by stray light [11]. Shimada and Horiguchi substantiate this finding in a patient with an optic disc coloboma and show that increased light intensities increase the responses and can even induce a weak full field ERG-response [11]. Photoreceptors adjacent to the disc have been argued to contribute to the recorded response from the optic disc due to limited spatial resolution, eye movements, and forward scatter [12]; Shimada and Horiguchi do not discuss the influence of the color of the coloboma, but the effect of the increased light intensity indicates that color is important, since white surfaces reflect more light than dark surfaces. The membranes implanted in this study have a size of approx 12 mm^2 and are similar in size to the discussed optic disc coloboma. We show that the P1-amplitude ratio is linearly correlated to the brightness of the membrane, even when we correct for the fundus photo illumination (Figure 5).

The histological examination showed a low-grade inflammatory degeneration of the outer retina, foreign body giant cell reaction, and formation of choroidal neovascularisation, consistent with the fast degradation of the PLGA membranes with acidic byproducts found by others [13, 14]. We could not demonstrate any histological differences between the white and the blue membranes, and we do not suspect toxicity from the blue dye as it is normally used as

an approved food and drug additive [15]. The destruction of the outer retina and complete lack of photoreceptors in all experiments indicated that the membrane-affected areas indeed were without function. We used the highest possible number of hexagons to ensure the highest spatial resolution [16]. This allowed us to use only hexagons from retina completely within the membrane-affected area. The P1-amplitude originates primarily from the bipolar cells and to lesser degree photoreceptors, as has been shown in both pigs [17] and rhesus monkeys [18]. However, with a heavily destroyed outer retina, including photoreceptors, no activation of bipolar cells should take place, and P1-amplitudes should therefore be extinct from within the membrane-affected retinal area [19].

The interindividual variation of the mfERG in the pig is pronounced [8]. Furthermore the mfERG is very susceptible to the depth and length of the anesthesia [20], which accentuates the interindividual and interobservational variation of the mfERG measurements. In addition, the porcine retina is described as having areas of higher cone density within the visual streak [21], which alone could affect the differences found. To overcome the interindividual and interobservational variance, we chose to normalize the data using an identical area in the right, untouched eye. As membrane implanted left eyes were always recorded before the contralateral right control eye, the calculated P1-amplitude ratios of the membrane areas will be too high as it is demonstrated for the corresponding visual streak ratios in Table 2. Both eyes were recorded within a timeframe of 25 minutes and always within the first 2 hours of anesthesia, which should minimize the effect of the anaesthesia on the mfERG-measurements. The difference in mean P1-amplitudes for visual streak between week 0 and 6 combined with the consistency in left/right ratios supports the choice of using the fellow right eye as baseline when evaluating the membrane responses. Regarding the membrane corresponding areas, we found a significant difference in the P1-amplitudes between the control eyes for the blue and white groups. This is most likely due to a higher number of blue implanted membranes centered in the visual streak. Maybe because of the experimental surgical experience gained. Apart from giving higher amplitudes due to a corresponding area completely within the visual streak, the time of anesthesia will also be shorter as it was easier to locate areas near the centered vessels and optic disc prior to mfERG recordings.

In conclusion, brightness and therefore perceived color of a subretinal element influences the P1-amplitude of the mfERG. This should be taken in to account when using mfERG on retinal areas with altered reflective properties. Especially in future retinal tissue engineering studies, mfERG should be used with caution when evaluating local retinal function.

Abbreviations

RPC: Retinal progenitor cell
PLGA: Poly lactic-co-glycolic acid
mfERG: Multifocal electroretinogram
ARVO: The Association for Research in Vision and Ophthalmology
i.v.: Intravenous
IR: Infrared
HE: Hematoxylin and eosin
wt%: Weight percent
ONL: Outer nuclear layer
INL: Inner nuclear layer.

Conflict of Interests

The authors of this paper have no conflict of interests to disclose.

Acknowledgments

The authors would like to thank Lincy Foundation (H. K., M. J. Young), the Andrei Olenicoff Memorial Foundation (H. K.), Polly and Michael Smith Foundation (H. K.), and The Danish Agency for Science, Technology and Innovation (A. T. Christiansen).

References

[1] H. Klassen and B. Reubinoff, "Stem cells in a new light," *Nature Biotechnology*, vol. 26, no. 2, pp. 187–188, 2008.

[2] M. Tomita, E. Lavik, H. Klassen, T. Zahir, R. Langer, and M. J. Young, "Biodegradable polymer composite grafts promote the survival and differentiation of retinal progenitor cells," *Stem Cells*, vol. 23, no. 10, pp. 1579–1588, 2005.

[3] K. Warfvinge, J. F. Kiilgaard, E. B. Lavik et al., "Retinal progenitor cell xenografts to the pig retina: morphologic integration and cytochemical differentiation," *Archives of Ophthalmology*, vol. 123, no. 10, pp. 1385–1393, 2005.

[4] E. B. Lavik, H. Klassen, K. Warfvinge, R. Langer, and M. J. Young, "Fabrication of degradable polymer scaffolds to direct the integration and differentiation of retinal progenitors," *Biomaterials*, vol. 26, no. 16, pp. 3187–3196, 2005.

[5] B. A. Tucker, S. M. Redenti, C. Jiang et al., "The use of progenitor cell/biodegradable MMP2-PLGA polymer constructs to enhance cellular integration and retinal repopulation," *Biomaterials*, vol. 31, no. 1, pp. 9–19, 2010.

[6] J. Yao, B. A. Tucker, X. Zhang, P. Checa-Casalengua, R. Herrero-Vanrell, and M. J. Young, "Robust cell integration from co-transplantation of biodegradable MMP2-PLGA microspheres with retinal progenitor cells," *Biomaterials*, vol. 32, no. 4, pp. 1041–1050, 2011.

[7] S. R. Hynes and E. B. Lavik, "A tissue-engineered approach towards retinal repair: scaffolds for cell transplantation to the subretinal space," *Graefe's Archive for Clinical and Experimental Ophthalmology*, vol. 248, no. 6, pp. 763–778, 2010.

[8] M. V. Kyhn, J. F. Kiilgaard, A. G. Lopez, E. Scherfig, J. U. Prause, and M. la Cour, "The multifocal electroretinogram (mfERG) in the pig," *Acta Ophthalmologica Scandinavica*, vol. 85, no. 4, pp. 438–444, 2007.

[9] R. Ejstrup, E. Scherfig, and M. la Cour, "Electrophysiological consequences of experimental branch retinal vein occlusion in pigs and the effect of dorzolamide," *Investigative Ophthalmology and Visual Science*, vol. 52, no. 2, pp. 952–958, 2011.

[10] L. D. Hubbard, R. P. Danis, M. W. Neider et al., "Brightness, contrast, and color balance of digital versus film retinal images in the age-related eye disease study 2," *Investigative*

Ophthalmology and Visual Science, vol. 49, no. 8, pp. 3269–3282, 2008.

[11] Y. Shimada and M. Horiguchi, "Stray light-induced multifocal electroretinograms," *Investigative Ophthalmology and Visual Science*, vol. 44, no. 3, pp. 1245–1251, 2003.

[12] D. C. Hood, "Assessing retinal function with the multifocal technique," *Progress in Retinal and Eye Research*, vol. 19, no. 5, pp. 607–646, 2000.

[13] L. Lu, M. J. Yaszemski, and A. G. Mikos, "Retinal pigment epithelium engineering using synthetic biodegradable polymers," *Biomaterials*, vol. 22, no. 24, pp. 3345–3355, 2001.

[14] A. C. R. Grayson, G. Voskerician, A. Lynn, J. M. Anderson, M. J. Cima, and R. Langer, "Differential degradation rates in vivo and in vitro of biocompatible poly(lactic acid) and poly(glycolic acid) homo-and co-polymers for polymeric drug-delivery microchip," *Journal of Biomaterials Science, Polymer Edition*, vol. 15, no. 10, pp. 1281–1304, 2004.

[15] EFSA Panel on Food Additives and Nutrient Sources added to Food (ANS), "Scientific opinion on the re-evaluation of Brilliant Blue FCF (E 133) as a food additive," *EFSA Journal*, vol. 8, no. 11, p. 1853, 2010.

[16] M. V. Kyhn, J. F. Kiilgaard, E. Scherfig, J. U. Prause, and M. la Cour, "The spatial resolution of the porcine multifocal electroretinogram for detection of laser-induced retinal lesions," *Acta Ophthalmologica*, vol. 86, no. 7, pp. 786–793, 2008.

[17] Y. F. Ng, H. H. L. Chan, P. H. W. Chu et al., "Pharmacologically defined components of the normal porcine multifocal ERG," *Documenta Ophthalmologica*, vol. 116, no. 3, pp. 165–176, 2008.

[18] D. C. Hood, L. J. Frishman, S. Saszik, and S. Viswanathan, "Retinal origins of the primate multifocal ERG: implications for the human response," *Investigative Ophthalmology and Visual Science*, vol. 43, no. 5, pp. 1673–1685, 2002.

[19] D. C. Hood, J. G. Odel, C. S. Chen, and B. J. Winn, "The multifocal electroretinogram," *Journal of Neuro-Ophthalmology*, vol. 23, no. 3, pp. 225–235, 2003.

[20] P. Tanskanen, T. Kylma, B. Kommonen, and U. Karhunen, "Propofol influences the electroretinogram to a lesser degree than thiopentone," *Acta Anaesthesiologica Scandinavica*, vol. 40, no. 4, pp. 480–485, 1996.

[21] A. Hendrickson and D. Hicks, "Distribution and density of medium-and short-wavelength selective cones in the domestic pig retina," *Experimental Eye Research*, vol. 74, no. 4, pp. 435–444, 2002.

Hindawi Publishing Corporation
Stem Cells International
Volume 2012, Article ID 128732, 11 pages
doi:10.1155/2012/128732

Research Article

Adult-Brain-Derived Neural Stem Cells Grafting into a Vein Bridge Increases Postlesional Recovery and Regeneration in a Peripheral Nerve of Adult Pig

Olivier Liard,[1] Stéphanie Segura,[2] Emmanuel Sagui,[1] André Nau,[1] Aurélie Pascual,[1] Melissa Cambon,[3] Jean-Luc Darlix,[4] Thierry Fusai,[1] and Emmanuel Moyse[2]

[1] *Unité de Chirurgie et Physiologie Expérimentale (UCPE), Institut de Médecine Tropicale, 58 boulevard Charles Livon, 13007 Marseille, France*
[2] *Unité Physiologie de la Reproduction et des Comportements, UMR 85, Centre INRA de Tours, 37380 Nouzilly, France*
[3] *Laboratoire d'Ecologie fonctionnelle, Bâtiment 4R3, 118 route de Narbonne, 31062 Toulouse cedex 9, France*
[4] *Unité de Rétrovirologie, U421 INSERM, Ecole Normale Supérieure de Lyon, 46 Allée d'Italie, 69364 Lyon cedex 07, France*

Correspondence should be addressed to Emmanuel Moyse, moyseemmanuel@yahoo.fr

Received 15 August 2011; Revised 6 October 2011; Accepted 7 October 2011

Academic Editor: Henry J. Klassen

We attempted transplantation of adult neural stem cells (ANSCs) inside an autologous venous graft following surgical transsection of *nervis cruralis* with 30 mm long gap in adult pig. The transplanted cell suspension was a primary culture of neurospheres from adult pig subventricular zone (SVZ) which had been labeled *in vitro* with BrdU or lentivirally transferred fluorescent protein. Lesion-induced loss of leg extension on the thigh became definitive in controls but was reversed by 45–90 days after neurosphere-filled vein grafting. Electromyography showed stimulodetection recovery in neurosphere-transplanted pigs but not in controls. Postmortem immunohistochemistry revealed neurosphere-derived cells that survived inside the venous graft from 10 to 240 post-lesion days and all displayed a neuronal phenotype. Newly formed neurons were distributed inside the venous graft along the severed nerve longitudinal axis. Moreover, ANSC transplantation increased CNPase expression, indicating activation of intrinsic Schwann cells. Thus ANSC transplantation inside an autologous venous graft provides an efficient repair strategy.

1. Introduction

Nerve injuries which are frequent in civil practice [1, 2] and catastrophe-like earthquake [3, 4] or tsunami [5] combine associative lesion with crush syndrome. War improves the risk of gap and of treatment delay with ballistic wounds [6] because these ones are less prone to emergency than vascular injuries [7]. This risk pertains after war with remanent explosive [8]. The functional pronostic is dependent on the type of wound: transsection, crush, or gap, which has been further categorized according to the length of the gap, the type of nerve (sensitive, motor or mixed), localization, association of injuries, and patient's ageing, time of surgery, and vascular environment [9–12].

Neuroguides and especially vein grafts are regularly used to bridge small nerve gaps shorter than 3 cm; for long nerve gaps, autologous nerve graft has become the gold standard since the second war [13, 14]. But nerve repair outcome depends on fascicle concordance [15] and scar development, so expected alternatives for long nerve gaps remain a challenge to improve recovery after this type of lesion. Surgical trials to improve nerve repair have mainly targeted diversification of grafted neuroguides with resorbable materials [16]. The outcome has been improved by neuroguide preloading with extracellular matrix components [17–19], growth factors [20], or cultured regeneration-enhancing cells. The latter strategy, or cell therapy, has been attempted with primary cultures of Schwann cells [21, 22], olfactory bulb enshealting cells [23], or various types of stem cells [24]. In these studies, progenies of grafted stem cells mostly proved to be glial cells, which indirectly enhance axonal regeneration [24].

Neural stem cells from adult brain (ANSC) have been scarcely assayed to help postlesional repair of peripheral nerves, despite their strong potential of integration and

development into neurons [25]. The present study is based on the hypothesis that ANSC grafting inside a venous neuroguide might be efficient to bridge a long nerve gap in adult. We tested this hypothesis in the pig, which is the non-primate animal species most closely related to human and is prone to surgery and anesthesia conditions very close to human protocols in clinic [26]. To this aim, we have characterized primary cultures of neural stem cells from adult pig brain, by optimizing the neurosphere assay on subventricular zone explants [27]. In the present study, we labeled such primary expanded ANSC *in vitro* with either BrdU or lentiviral green fluorescent protein gene transfer, and we grafted labeled neurospheres into an autologous venous bridge after a surgical 30 mm long gap in adult pig *nervi cruralis*. We compared neurosphere-grafted and control pigs for functional recovery and assessed the fate of grafted cells inside the lesioned nerve at various post-lesion intervals.

2. Material and Methods

2.1. Animals. Twenty-four adults, 4-month-old Large White Landrace pigs were used in the present study. They were housed with *ad libitum* access to water and standard food pellets, in lodges that comprised one yard and one hard infrared-heated shelter. All *in vivo* experimental protocols were approved by the local Ethics Committee on the protection of animals used for scientific activities with the protocol number 31/2006/IMTSSA/UCPE. Personal protocol number for surgery and experimentation with pigs was 2007/29/DEF/DCSSA (to O. Liard). All efforts were made to minimize the number of animals used and their suffering.

2.2. Anesthesia. Deep anesthesia was initiated by intramuscular premedication with 30 mg/kg ketamine (Imalgene 1000, Merial, Lyon, France), 0.1 mL/kg acepromazine (Vetranquil, Calmivet, Bayer, Puteaux, France), and 25 μg/kg atropine sulphate (Meram, Melun, France). The animal was then equipped with a peripheral intravenous perfusion delivering Ringer-lactate-5% glucose serum at 5–7 mL/kg/h, with adhesive electrocardiographic electrodes in CM5-SpO2 (ECG monitor S5, Datex Ohmeda, Madison, WI, USA), and with an artificial oxygenator. Anesthesia induction was performed by intravenous injections of 2 mg/kg propofol (Diprivan, Bayer) during 30 sec slowly, and of sufentanil (Sufenta, Bayer) three times at 1.5 μg/kg. Local glottis anesthesia was made with 5% lidocaïne spray (Xylocaine, Bayer), before orotracheal intubation with a monolight cannula (internal diameter 6.5 mm). Ventilation of lung parenchyma was checked with a stethoscope and mechanically assisted. General anesthesia was sustained with electrically driven intravenous infusion of propofol 2 mg/kg/h (Diprivan, DCI), sufentanil 1 μg/kg/h (Sufenta, DCI) and rocuronium bromide 0.15 mg/kg/h (Esmeron, DCI); curarisation was supervised by means of a S5 monitor (Entropie module) but was not released for EMG. Antibioprophylaxy was administered. All along surgery, the cardioventilatory parameters (heart and ventilation rates, electrocardiogram, blood oxygenation, ventilation pressure and volume, MAC, temperature, hemoglucotest) as well as the sleep threshold were constantly watched with the S5 monitor.

2.3. Brain Tissue Sampling for Primary Neural Stem Cell Culture from Adult Pig. Separate animals were dedicated for primary culture and *in vitro* expansion of neural stem cells from brain subventricular zone (SVZ) as previously described [27]. On each deeply anesthetized pig, the dorsal face of the skull was cut with an electric saw and removed. A 15 mm thick coronal slice of the brain was performed with a scalpel at the commissural level of midbrain, manually explanted and transferred at 4°C on ice bed-laid sterile metal plate, beside a Bunsen flame for atmosphere sterilization. The experimental animal was thus alive until the explantation of the brain tissue slice. Each pig was sacrificed immediately after brain tissue sampling by intravenous injection of Dolethal (R) pentobarbital (DCI) at 1.5 mL/kg.

2.4. Primary Culture of SVZ Neural Stem Cells ("Neurosphere Assay"). As previously described [27], SVZ pieces were quickly microdissected from the thick midbrain slice (above) along the ventrolateral floor of lateral brain ventricles in low-calcium artificial cerebrospinal fluid (aCSF: 124 mM NaCl, 5 mM KCl, 3.2 mM $MgCl_2$, 0.1 mM $CaCl_2$, 26 mM $NaHCO_3$, 100 mM glucose, and pH 7.38). Tissue samples were rinsed twice with aCSF and digested first in 40 U cystein-EDTA-β-mercaptoethanol-preactivated papain (Sigma, L'Isle D'Abeau, France) for 10 min at 37°C, then in 250 μL undiluted TrypLE Express solution (heat-resistant, microbially produced, purified trypsinlike enzyme, Gibco # 12604-013, Invitrogen, Cergy-Pontoise, France) for 10 min at 37°C. After the addition of 750 μL of fresh aCSF and centrifugation for 8 min at 400 g at room temperature, the cell pellet was resuspended in 1 mL culture medium (DMEM (Sigma), 1x B27 (Gibco Invitrogen), 200 U/mL penicillin, and 200 μg/mL streptomycin (Gibco Invitrogen)) containing 20 ng/mL Epidermal Growth Factor (EGF, Gibco Invitrogen) and 20 ng/mL basic Fibroblast Growth Factor (bFGF, Gibco Invitrogen). The cells were dissociated gently with a 26 G steel needle on a sterile disposable 1 mL syringe, counted on a Malassez slide, and seeded at 20,000 cells per mL in 6-well plates (Falcon, BD Biosciences, Bedford, USA). Cultures were monitored daily to follow the morphological growth of the neurospheres; passage was performed when the majority of spheres were 100–120 μm in diameter. For passage, the primary spheres were collected in sterile tubes, incubated for 45–60 min at 37°C in 250 μL undiluted TrypLE Express solution (Gibco Invitrogen) per 6 mL culture-derived pellet, and dissociated gently with a 26 G steel needle on a 1 mL sterile syringe; dispersed cells were centrifuged, counted, and seeded as above. All culture media were renewed by the replacement of 2 mL of medium per 4 mL well every 2-3-days. For immunocytochemistry, coverslips bearing differentiated spheres were rinsed in PBS, fixed in 4% paraformaldehyde-containing PBS for 20 min at 4°C, and kept in PBS at 4°C until the assay.

2.5. In Vitro Labelling of Neurosphere Cells. In the first set of experiments, tertiary neurospheres were incubated with

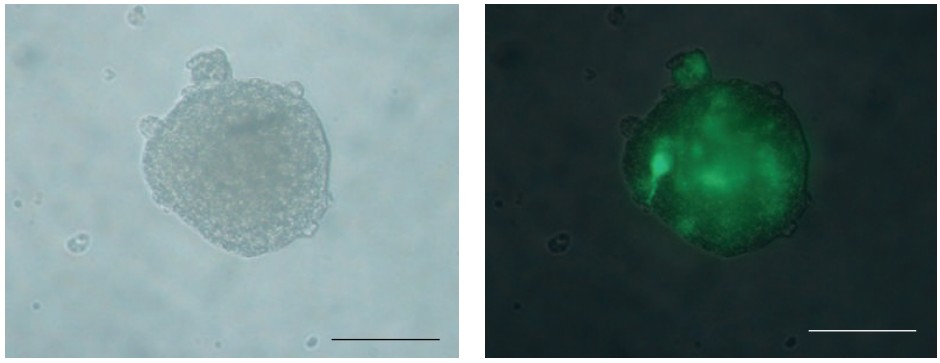

(a) (b)

Figure 1: LV-GFP-labeled secondary neurosphere from adult pig SVZ, just before transplantation and 3 days after *in vitro* infection with the lentiviral vector of GFP, as observed under a photonic microscope with natural light (a) or GFP fluorescence (b). Scale bars: 50 μm.

the DNA synthesis precursor bromo-2-deoxy-uridine at 30 μM (BrdU, Sigma) from 2 DIV after passage up to 8–10 DIV, BrdU being added fresh daily from concentrated stock.

In a second set of experiments, lineage labelling was performed by infection of secondary neurospheres with a lentiviral vector of green fluorescent protein gene (LV-GFP) at 4-5 DIV after passage. LV-GFP was freshly synthetized, titrated, and tested as previously described [28], stored at -80°C and unfrozen just before use. Neurosphere cultures were preincubated 30 min in the presence of 1 mM polybrene (Sigma) and void lentiviral particles (VLP, 29) at 0.1x M.O.I., and further incubated 2 h with fresh culture medium containing 1 mM polybrene and LV-GFP at 0.3x M.O.I.; incubation medium was then replaced by fresh standard culture medium. LV-GFP-infected neurospheres were allowed 3 days culture in standard conditions for optimal lineage labelling (Figure 1); [28].

After optimal culture period (5-6 days for BrdU, 3 days for LV-GFP) and just before transplantation on the nerve lesion site (see below), neurospheres were collected, centrifuged 4 min at 800 g, and resuspended in fresh culture medium at 3×10^3 spheres per mL.

2.6. Postlesional Grafting Surgery. The surgical approach was realized on the median face of thigh to isolate *nervis cruralis*. Nerve damage was established in the right *N. cruralis* by creating a 30 mm gap, which was then bridged with an autologous vein segment sampled from *v. mammelian externalis*. This venous neuroguide was sutured at both ends over the perinevre of the sectioned nerve. In some animals, once the venous shaft was sutured at the proximal end of the lesioned nerve, 300 μL of freshly prepared neurosphere suspension (10^3 spheres) were gently infused with a micropipet into the opposite end of the neuroguide, which was then sutured onto the distal lesioned nerve end. In other animals (controls), the venous neuroguide was sutured without any additional manipulation.

In the first set of experiments, lesioned pigs were thus grafted with autologous vein shafts which were either empty (controls, $N = 2$) or filled with BrdU-prelabeled neurospheres ($N = 4$). These animals were allowed 8 or 45 days survival after lesion.

In the second set of experiments, lesioned pigs were grafted with venous neuroguides which were either empty (controls, $N = 3$) or filled with LV-GFP-labeled neurospheres ($N = 6$). These animals were allowed 8 months survival after lesion.

2.7. Functional Analysis of Lesioned Animals. Animal behaviour was evaluated by assessing muscular atrophy, deficit of leg extension over the thigh. Each animal was examined before peripheral nerve lesioning and at days 45, 90, 180, and 240 following surgical bridging.

Motor function of the crural nerve was assayed by electromyography, using pregeled surface electrodes connected to a portable electromyographic recorder (Keypoint (R) v6.01, Medtronics, MN, USA). Bipolar concentric needles (diameter 0.47 mm) were applied on muscle *quadriceps femori* for stimulodetection analyses along *N. cruralis*. Stimuli were single 100 mA shocks, ranging from 0.1 to 1 msec durations. Electromyography was performed on animals before and at 45, 90, 180, and 240 days after transection. Values were recorded in terms of voltage, amplitude and time latency of detectable electromyographic activities.

2.8. Immunohistochemistry. At the end of postlesional survival, the operated region of *N. cruralis* of each experimental pig was dissected out of the thigh under anesthesia and fixed by immersion in a 4% paraformaldehyde solution in 0.05 M, pH 7.4, NaH_2PO_4/Na_2HPO_4 buffer for 24 h at 4°C, then rinsed for 24 h at 4°C in 0.1 M, pH 7.4 phosphate-buffered saline (PBS). It was then cryoprotected for 72 h in a 30% sucrose solution, flat-embedded in OCT mounting medium and snap-frozen in liquid isopentane at -40°C for storage at -80°C. Longitudinal 20 μm-thick sections were made in a cryostat (Leica 2800), mounted on commercial precoated slides (Superfrost-Plus, Fisher-Scientific, Canada), dried overnight at ambient air, and stored at -20°C.

For immunohistofluorescent labellings, these tissue sections were brought back to room temperature and permeabilized in 0.1 M PBS with 0.5% Triton-X-100. For nuclear

Table 1: List of primary antibodies used.

Antigen	Antibody	Supplier	Cell-type specificity	Dilution
BrdU	Rat polyclonal	ImmunologicalDirect.com	none	1/100
CNPase	Mouse monoclonal	Sigma, L'Isle-d'Abeau, France; C-5922, clone 11-5b	Schwann cells	1/200
GFAP	Rabbit polyclonal	Dako, Trappes, France; Z0334	Astrocytes, neural stem cells	1/1000
NeuN	Mouse monoclonal	Chemicon, MAB377	Mature neurons	1/100
NF-68	Mouse monoclonal	BD-Biosciences, Heidelberg, Germany	Mature neurons	1/400
S100β	Rabbit polyclonal	Dako, Trappes, France	Astrocytes, Schwann cells	1/500

antigens, tissue sections were also treated 15 min in 10 mM sodium citrate solution (pH 5.5) at 95°C. After a PBS rinse, all preparations were incubated in blocking buffer (0.1 M PBS, 0.1% Triton, 3% bovine serum albumin, 5% normal serum) for 1 h, then overnight at 4°C with one primary antibody (Table 1). After three 5-minute-rinses in fresh 0.1 M PBS, immunohistochemical labelings were revealed by 2 h incubation at room temperature in the dark with the appropriate Alexa-594-conjugated secondary antibodies (Molecular Probes, Eugene, OR, USA; 1/400). For double-staining experiments, Alexa-594-revealed slides were rinsed three times in fresh 0.1 M PBS and further incubated overnight at 4°C with another primary antibody, which was revealed with appropriate Alexa-488-conjugated secondary antibody (Molecular Probes; 1/200). After rinsing, fluorescent staining of cell nuclei was performed by 5 min incubation in the dark-with DAPI (0.5 μg/mL, Sigma). Labeled slides were coverslipped with aqueous mounting medium (Vectashield, Vector, Abcys, France) and photographed with a fluorescence microscope. CNPase immunohistochemical labeling was quantified on these photomicrographs by using the ImageJ software.

3. Results

3.1. Clinical Results. Before surgery, all experimental animals were healthy and displayed no walking deficit. After surgery, none of operated animals displayed any scar infection or host rejection response.

By clinical observation, loss of the right leg extension over the thigh was systematically observed after the surgical nerve transsection. This motor defect was maintained up to 240 days in animals which had crural nerve gap repaired by empty autologous venous bridge only. By contrast, lesioned leg extension over the thigh reappeared between 90 and 180 days in animals which had crural nerve gap repaired by the same type of autologous vein trunk filled with exogenous neurospheres.

3.2. Electromyography. Prior to surgery, electromyograms of m. quadriceps vast internal displayed amplitudes of 4.9 to 6.1 mV and poststimulus latencies of 0.89 to 3.7 ms. Immediately after surgical realization of *N. cruralis* substance loss, electromyograms of m. quadriceps were negative for all experimental animals, whatever their venous bridge had been filled or not with neurosphere suspension.

At 180 days (25 weeks) after lesion, neurosphere-transplanted pigs displayed positive electromyograms of m. quadriceps with 0.6 to 0.9 mV amplitudes and 0.96 to 2 ms latencies, whereas electromyograms of control animals remained negative (Figure 2).

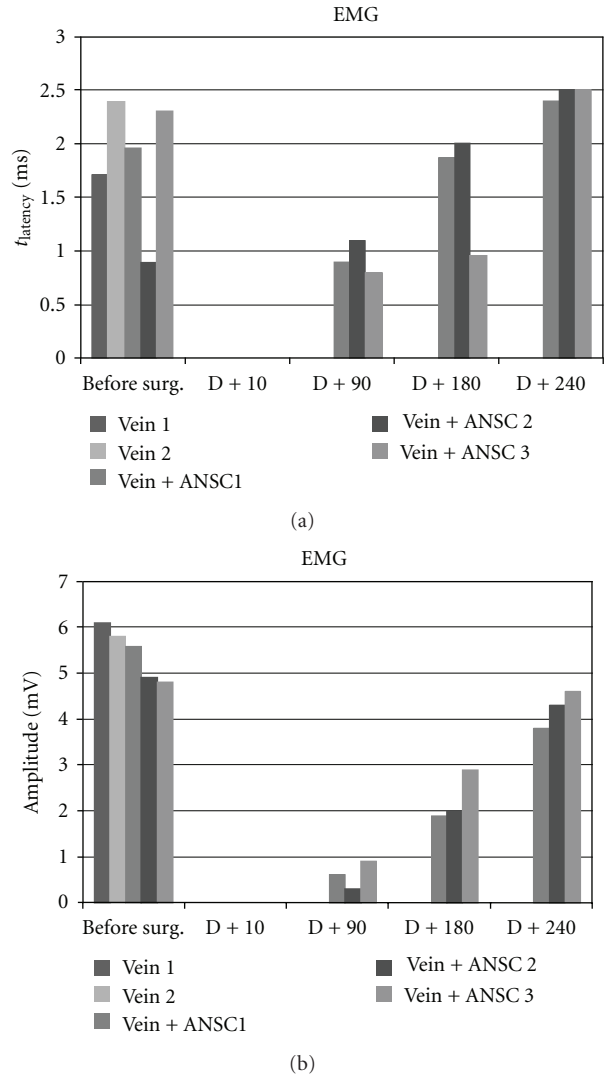

Figure 2: Electromyographic evaluation of muscle quadriceps femori at 90, 180, and 240 days following *N. cruralis* lesion and graft of GFP-labeled neurospheres inside a venous bridge before ("before surg.") or after ("D + 90", "D + 180", "D + 240") surgery.

At 240 days (34 weeks) after lesion, m. quadriceps electromyograms of neurosphere-transplanted pigs were improved up to 2.8–3.1 mV amplitudes with 2.4–2.5 ms

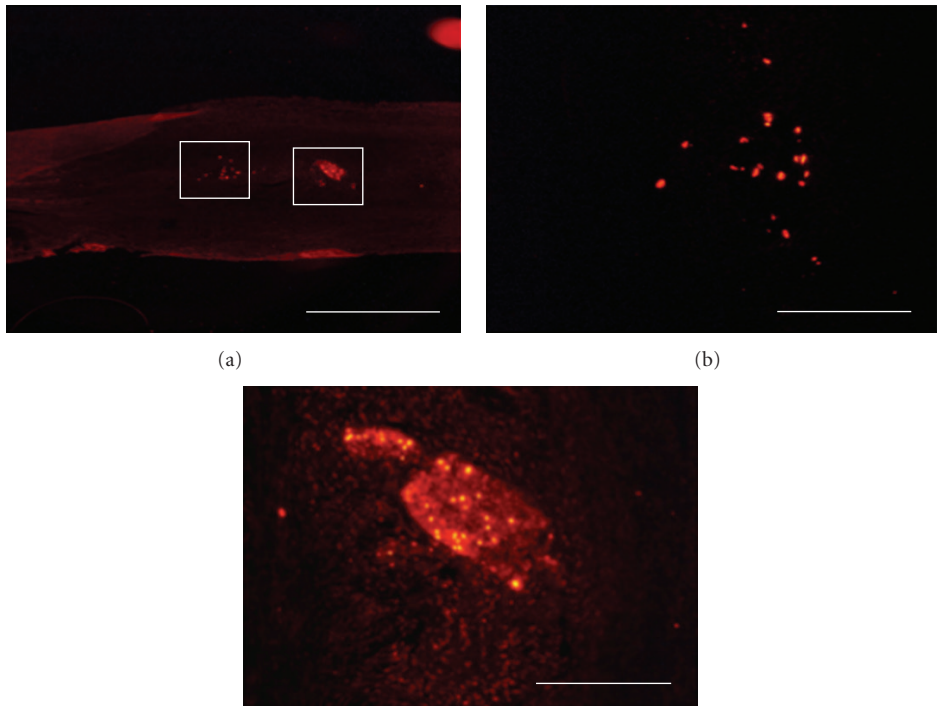

(a) (b)

(c)

Figure 3: Localization of transplanted BrdU-labeled neurospheres in the bridged nerve at 8 days after lesion, by postmortem immunohistochemistry. BrdU immunoreactivity is revealed by red Alexa-594 fluorescence on longitudinal postfixed graft sections at low (a) and high (b, c) magnifications. Enlarged fields (b, c) are localized as white forms in (a). Transplanted neurosphere cells are found either sparsed (b) or clustered (c) inside the venous bridge. Scale bars: 0.5 mm (a), 100 μm (b, c).

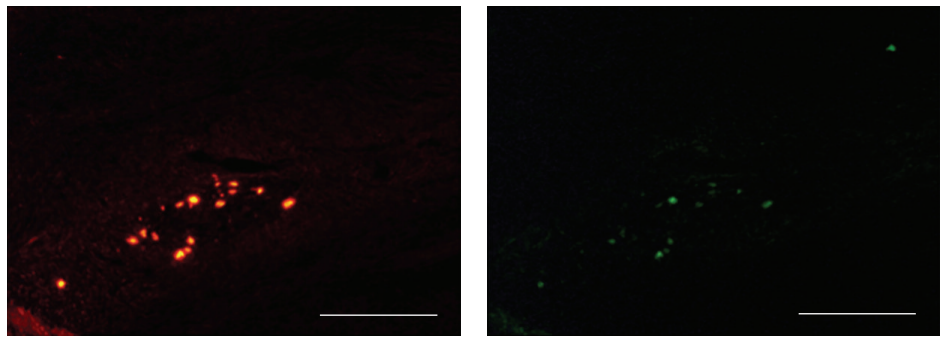

(a) (b)

Figure 4: Double BrdU-DCX immunohistochemistry on a sagittal section from a neurosphere-grafted bridged nerve at 8 days after lesion. One given field was sequentially photographed with fluorescent wavelengths revealing, respectively, Alexa-594-labeled BrdU immunoreactivity (a) and Alexa-488-DCX one (b). Note the extensive nuclear colocalization of the immature neuron marker DCX with BrdU (b). Scale bars 100 mm.

latencies, while electromyograms of controls were still negative (Figure 2).

3.3. In Situ Fate of Grafted Pig Neurosphere Cells. In the first experiment, grafted neurosphere cells had been labeled by *in vitro* BrdU incorporation prior to graft. By immunohistochemistry on postmortem venous grafts, groups of BrdU-immunoreactive cells were detected inside the venous tube (Figure 3). In grafts sampled at 8 days after surgery, most of these BrdU+ cells were clustered in sphere-like assemblies (Figures 3(a) and 3(c)) while some were sparsed inside the venous tube (Figure 3(b)). Most of BrdU+ cells were also immunoreactive for doublecortin (DCX) which is a specific marker of immature neurons (Figure 4). At 90 days after surgery, BrdU+ cells were still observed inside the venous tube and displayed immunoreactivity for NeuN, that is, a marker of differentiated neurons (Figure 5).

In the second experiment, expanded secondary neurospheres at 8 DIV had been stained by LV-GFP transfection just before collection and postlesional transplantation on

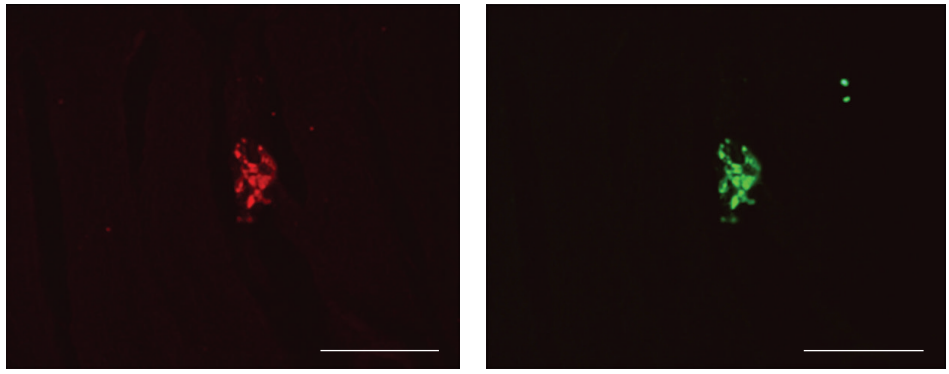

(a) (b)

Figure 5: Double BrdU-NeuN immunohistochemistry on a sagittal section from a neurosphere-grafted bridged nerve at 90 days after lesion. One given field was sequentially photographed with fluorescent wavelengths revealing, respectively, Alexa-594-labeled BrdU immunoreactivity (a) and Alexa-488-NeuN one (b). Note the extensive nuclear colocalization of the mature neuron marker NeuN with BrdU (b). Scale bars 100 mm.

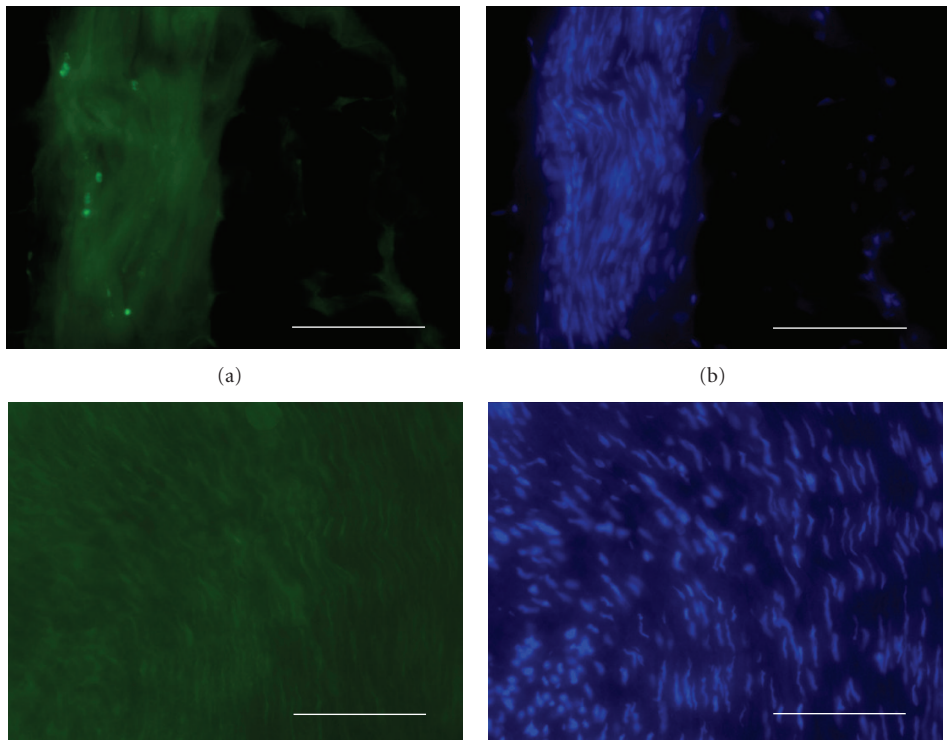

(a) (b)

(c) (d)

Figure 6: GFP lineage-labelling detection in DAPI-counterstained sagittal sections of venous bridges with (a, b) or without (c, d) transplantation of LV-GFP-labeled neurospheres, at 240 days after lesion. GFP-expressing neurosphere progeny (a, c) and DAPI-labeled tissue cell nuclei (b, d) are detected by fluorescence microscopy by using, respectively, adequate wavelengths. Scale bars: 0.5 mm (a, b), 100 μm (c, d).

the pig nerve gap. All neurospheres displayed fluorescent GFP labeling in most, but not all, cells (Figure 1). At either 45, 90, 180, or 240 days after lesion, sphere transplantation, each vein-bridged and LV-GFP sphere-transplanted nerve segment displayed a number of GFP-fluorescent cells which were exclusively localized inside the nerve fascicles (Figures 6(a) and 6(b)) and absent in nontransplanted control bridges (Figures 6(c) and 6(d)). Combined immunohistofluorescent labeling of either NeuN or neurofilament NF-68 revealed that most of GFP fluorescence was colocalized with these neuronal markers (Figures 7(a)–7(c)). By contrast, GFP fluorescence did not colocalize with either of the glial markers assessed: S-100b (Figures 7(d)–7(f)), GFAP, CNPase.

Interestingly, at 180 and 240 days after nerve lesion and GFP-expressing neurosphere transplantation, CNPase immunohistofluorescent labeling was much higher than in vein-bridged lesioned controls which had not received neurosphere transplantation (Figure 8). Both the number of

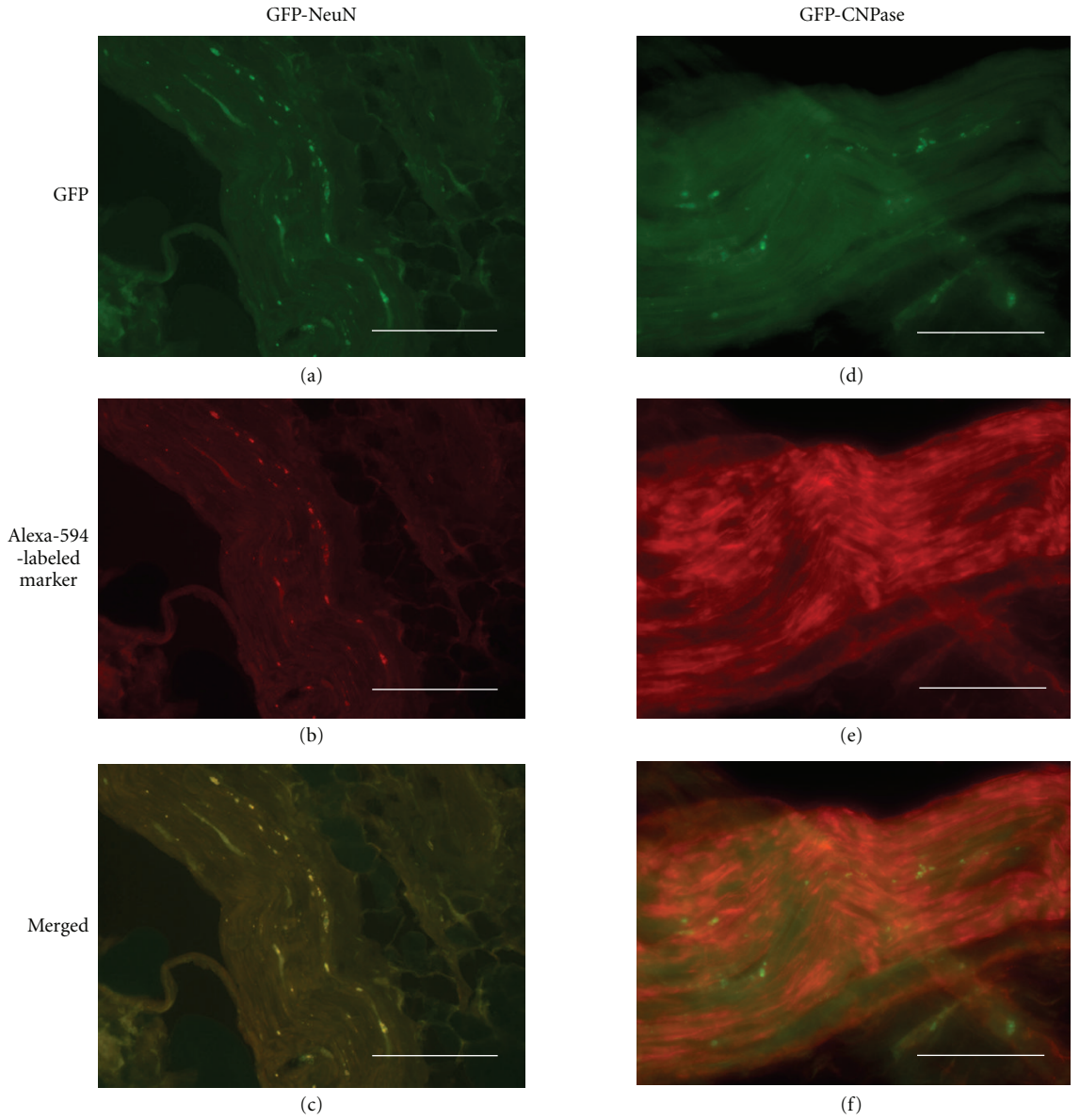

Figure 7: GFP detection and phenotypic marker immunohistofluorescence (NeuN on left column, Schwann cells' CNPase on right column) in sagittal sections of venous bridges which had been transplanted with LV-GFP-labeled neurospheres and were sampled at 240 days after lesion. (a, d) green endogenous fluorescence for detection of lineage-infected neurosphere progeny; (b, e) Alexa-594-revealed phenotypic marker immunoreactivities; (c, f) merged fluorescences. Note yellow-labeled colocalization of GFP-expressing neurosphere progeny with NeuN immunoreactivity (c) but not with CNPase (f). Scale bars: 0.5 mm.

CNPase-immunoreactive Schwann cell processes and their labeling intensities were higher in neurosphere-grafted nerves than in controls. By densitometric quantification with the ImageJ software, immunohistochemical CNPase labeling of neurosphere-grafted lesioned nerves, at 240 days after lesion, reached 276 ± 2% of the 100 ± 2.9% value of lesioned controls which were devoid of neurospheres; this difference being statistically significant at $P < 0.001$ by Anova.

4. Discussion

Degeneration of the distal axon segment is the consequence of axotomy and the challenge of nerve repair is to connect the proximal stump to this distal segment. For long nerve gap, it is a race between axon regeneration and distal degeneration with phenotypic change of Schwann cells [24]. Autologous nerve graft is the gold standard but results are not satisfactory [15]. Any alternative is currently believed to require a neuroguide, providing a permissive microenvironment to increase axonal regeneration and to preserve supportive cells and distal axons. Stem cells have already been studied but differentiation was mostly towards supportive cells. Neural stem cells have been reported to become integrated and provide new neurons after transplantation within central nervous system with permissive microenvironment [25]. In order to test the efficiency of this type of graft for postlesional repair

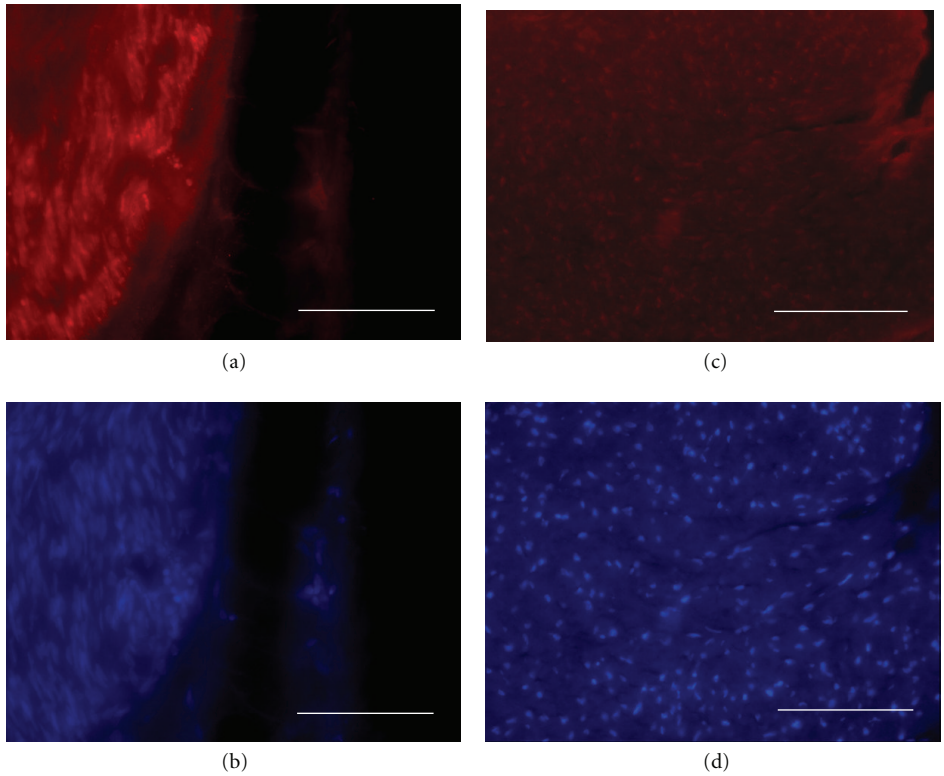

Figure 8: CNPase immunohistofluorescence on sagittal sections of venous bridges without (a, b) or with (c, d) transplantation of LV-GFP-labeled neurospheres, which had been sampled 240 days after lesion. Alexa-594 fluorescence-revealed CNPase immunoreactivity (a, c) is combined with histofluroescent DAPI counterstaining (b, d). Note that Schwann cell labelling density is strikingly higher in neurosphere-transplanted graft (c, d) than in void venous bridge (a, b). $\Sigma\chi\alpha\lambda\varepsilon\,\beta\alpha\rho\sigma$: 100 μm.

of peripheral nerves, we have established a primary culture of adult pig neural stem cells which generate neurons *in vitro* in our previous report [27]. In the present study, we show for the first time in adult pig that transplantation of *in vitro* preexpanded adult neural stem cells into a peripheral nerve gap inside a venous bridge both leads to genesis of longitudinally aligned neurons and improves functional recovery.

4.1. Methodological Considerations. The present experimental protocol of nerve lesion: transsection and 30 mm long nerve substance removal, has been chosen to mimic the common cases of long nerve injury in human clinics. In these cases indeed, whatever be the initial type of injury (section, tearing, crush), the surgical regularization of both nerve stumps corresponds to a model of transsection.

Autologous vein segment graft as a nerve conduit has been established as an effective treatment for the repair of nerve gaps less than 3 cm [29, 30]; it is used in hand surgery [31] and in pediatrics [32]. In a recent study [33], histomorphological examination of the sections proximal to, from, and distal to the repair zone over three months revealed less epineural scarring, a thinner epineurium, more regenerated axons and fewer inflammatory cells in groups where vein grafting was used, because the vein graft provided additional mechanical and chemical support in the size discrepancy of the nerve regeneration. A small vein graft keeps its property for end-to-side neurorrhaphy [34], but size discrepancy between the donor and recipient nerves and length of the bypass are another problem with the risk of collapse. Vein bridging also gives excellent results in secondary repair of neglected injuries [35]. The present protocol is routinely realized in adult pig, as a convenient training system for human-operating surgeons.

The present postlesional cell therapy attempt used an *in vitro* expanded primary culture of adult pig brain neurospheres which had been extensively characterized in a previous study [27]. We had indeed shown that the present protocols of adult pig subventricular zone sampling and neurosphere assay allow to purify and maintain true neural stem cells with unlimited proliferative potential, self-renewal capacity, and ability to generate all neural cell types [27]. In particular, these neurospheres from adult pig SVZ displayed the same proportions of neurons (25%), astrocytes (70%), and oligodendrocytes (5%) as neurospheres from various adult rodent brain structures [36–38].

The procedure for fluorescent lineage labeling of grafted neurospheres used a lentiviral vector of GFP which has been validated previously [28]. Freshly prepared lentiviral particles were quantified by multiplicity of infection (MOI) determination using routine virologist assays, for optimization of the neurosphere labeling. We checked that this *in vitro* procedure allowed extensive labeling of adult pig neurospheres without alteration of their cell dynamics. It allowed subsequent identification of grafted cell progenies *in situ*

merely by histofluorescence, which easily enabled to perform phenotype characterization by immunohistochemistry as revealed with different fluorophores.

4.2. Functional Recovery Enhancement by Vein-Guided Neurosphere Transplantation. Electromyographic evaluation of the muscle which is innervated by the lesioned nerve demonstrated that our protocol of venous-graft-assisted neurosphere transplantation strongly improved functional recovery at 6 months after lesion, as compared to controls. Our subsequent histofluorescent analyses provided putative cytological substrates for such positive influence of grafted ANSC-derived cells.

In the same time, clinical evaluation was based on a simple observation. The section of the crural nerve pulled a deficient flexion of the thigh on the pond. The only recoveries of normal step were observed on the transplanted animals. The main question was to know if this recovery was bound to accelerated axonal regrowth or to the creation of a functional intermediate neuronal bypass. In fact we have a double observation of neurons and regrowth of the axons of the host.

4.3. Neuronal Outcome of Grafted Neurospheres inside the Venous Bridge. In the present cell therapy attempt, the grafted neurospheres yielded exclusively neuronal progenies whatever be the postlesional delay. This outcome is striking since the neuronal yields from adult SVZ neural stem cells are known to reach only 25% neurons *in vitro* and 75% in the olfactory pathway *in vivo* [25, 37, 39]. The present *in vivo* result indicates that the venous graft provided an efficient proneurogenic environment for the transplanted neurospheres. It is in keeping with the recent demonstrations that vascular walls favor neurogenesis from adult neural stem cells [38, 40, 41], which is mediated in some rodent models by the vascular endothelium-derived growth factor (VEGF) [42]. Our results suggest that choosing a venous trunk versus an artificial neuroguide to bridge a nerve gap is an interesting solution because of intrinsic property. Furthermore, all surgeons are able to take a vein trunk on superficial vein network and this is much less expensive than neurotubes in emergency conditions. At the same time, to understand mechanism of interaction between endothelial cells and grafted neural stem cells will allow progress for the development of new artificial neurotubes. More generally, local tissue microenvironment has been formally demonstrated to be determinant on the phenotypic fate of stem-cell-derived progenies: for instance, nonneurogenic neural stem cells from the adult spinal cord generated neurons exclusively, once transplanted into the hippocampus [43].

These newly formed neurons survived at long delays after the original transplantation, which indicates they have been successfully integrated inside the severed nerve. Further, the linear distribution of these neuronal perikarya, parallel to the longitudinal axis of the lesioned nerve, suggests that the new neurons might be interconnected into multisynaptic nets bridging the lesional gap of preexisting nerve fibers. This multisynaptic nets have been described after neural stem cells graft [44, 45] This interpretation is also supported by the evolution of transplanted cell clusters across time inside the venous graft, that is, from spherical assemblies in the first week after lesion to linear chainlike successions of sparse cells at longer delays. Such outcome arises apart of the strategies for peripheral nerve repair which have been worked out thus far and consist in stimulating either axonal regrowth into the distal nerve end or remyelination with additional Schwann cells [24].

The present results contrast with previous ones using different kinds of transplanted cells, like fœtal neural stem cells, which triggered Schwann cell like proliferation in the lesioned peripheral nerve [46], promoting in turn myelinisation and indirectly regeneration [47]. In addition, transplantation of immortalized C17.2 cells from postnatal cerebellum, which were shown to be distinct of neural stem cells [48], has been reported to trigger tumor formation in a rat model of injured sciatic nerve [49]. Adult neural stem cells are especially relevant for cell therapy from this viewpoint, because they were demonstrated to display exceptionally high resistance to tumorigenesis and senescence [50].

4.4. Possibility to Graft New Neurons into a Peripheral Nerve Gap. There are two approaches, either to transplant neurons, or to transplant stem cells possessing neuronal differentiation potential. For primary neurons, dorsal root neurons can be prepared *in vitro* and their axons stretch-growth [20]. Moreover, engineered nervous tissue construct consisted of longitudinally aligned axonal tracts spanning two neuronal populations, embedded in a collagen matrix and inserted in a PGA tube [44] demonstrated neuronal survival during 112 days after surgical repair of the sciatic nerve in the rat. But only studies on the big animals allow the study of nerve gaps in good conditions.

4.5. High Survival Rate of Allogenic Transplants. In our study, adult neural stem cells were prepared *in vitro* after explantation of SVZ cells from another pig, and allogenic grafted cells were integrated without immunosuppressive therapy. The same observation was noted for embryonic rat progenitors for the adult rat sciatic nerve [44] and with xenograft of embryonic rat neural stem cells into a collagen conduit for the rabbit facial nerve injury model [51]. In these attempts, grafted cells were expanded *in vitro* before transplantation, like in the present study.

4.6. Activation of Intrinsic Schwann Cells by Neurosphere Transplantation. Phenotypic characterization of grafted cell progenies showed that our transplanted neurospheres generated no Schwann cell directly, but they triggered increases of the number and activity of this cell population as compared to controls. CNPase+ cells were observed along axonal regeneration but were always LV-GFP-. This result is in keeping with a previous report showing that venous graft favored Schwann cells proliferation after nerve lesion [52]. However, since in the present study controls have received a neurosphere-devoid venous graft, our results indicated that neurosphere cells emit diffusible signals that stimulate Schwann cells. Neurospheres have indeed been shown *in vitro* to secrete neurotrophic factors [53, 54].

5. Conclusion

The positive impact of the present cell therapy protocol can be attributed to genesis and integration of new neurons inside the lesioned nerve and/or to indirect activation of intrinsic Schwann cell population. However, Schwann cell activation was previously shown to occur after grafting a venous segment onto the lesioned nerve without neural stem cells inside. Therefore, the specific benefit of the present procedure is likely caused by the neurosphere transplantation, and hence by the genesis of new neurons inside the lesioned nerve. LV-GFP is confirmed to provide an excellent marker for grafted cells across long-time studies. Both new neuron genesis and host Schwann cell proliferation contributed to regenerate new axon fascicles in the host to bridge the long nerve gap, and the functionality of this histological repair was demonstrated in the same animals by electromyography and clinics. Large animals, and especially the pig, allow repair and study of long nerve gap with clinical conditions close to human. These results were obtained without adjunction of extracellular matrix or extrinsic growth factor. The present study thus provides a hope for improvement in human clinics.

Acknowledgments

These studies were supported by Délégation Générale pour l'Armement (DGA, France; REPAR Project, Grant 08co205). The authors express their gratitude to Professor Anne Duittoz (INRA Tours-Nouzilly) for precious advise about phenotypic marker immunohistochemistry in adult pig brain.

References

[1] J. Noble, C. A. Munro, V. S. S. V. Prasad, and R. Midha, "Analysis of upper and lower extremity peripheral nerve injuries in a population of patients with multiple injuries," *Journal of Trauma*, vol. 45, no. 1, pp. 116–122, 1998.

[2] J. A. Kouyoumdjian, "Peripheral nerve injuries: a retrospective survey of 456 cases," *Muscle and Nerve*, vol. 34, no. 6, pp. 785–788, 2006.

[3] M. N. Ahrari, N. Zangiabadi, A. Asadi, and A. Sarafi Nejad, "Prevalence and distribution of peripheral nerve injuries in victims of Bam earthquake," *Electromyography and Clinical Neurophysiology*, vol. 46, no. 1, pp. 59–62, 2006.

[4] M. Etienne, C. Powell, and B. Faux, "Disaster relief in Haiti: a perspective from the neurologists on the USNS COMFORT," *The Lancet Neurology*, vol. 9, no. 5, pp. 461–463, 2010.

[5] S. Charuluxananan, P. Bunburaphong, L. Tuchinda, P. Vorapaluk, and O. Kyokong, "Anesthesia for Indian Ocean tsunami-affected patients at a southern Thailand provincial hospital," *Acta Anaesthesiologica Scandinavica*, vol. 50, no. 3, pp. 320–323, 2006.

[6] M. O. Hansen, D. W. Polly, K. A. McHale, and L. M. Asplund, "A prospective evaluation of orthopedic patients evacuated from Operations Desert Shield and Desert Storm: the Walter Reed experience," *Military Medicine*, vol. 159, no. 5, pp. 376–380, 1994.

[7] J. Nanobashvili, T. Kopadze, M. Tvaladze, T. Buachidze, and G. Nazvlishvili, "War injuries of major extremity arteries," *World Journal of Surgery*, vol. 27, no. 2, pp. 134–139, 2003.

[8] M. E. Kett and S. J. Mannion, "Managing the health effects of the explosive remnants of war," *Journal of The Royal Society for the Promotion of Health*, vol. 124, no. 6, pp. 262–267, 2004.

[9] H. J. Seddon, "Three types of nerve injury," *Brain*, vol. 66, no. 4, pp. 237–288, 1943.

[10] S. Sunderland, "A classification of peripheral nerve injuries producing loss of function," *Brain*, vol. 74, no. 4, pp. 491–516, 1951.

[11] S. Sunderland, "The anatomy and physiology of nerve injury," *Muscle and Nerve*, vol. 13, no. 9, pp. 771–784, 1990.

[12] S. E. Mackinnon and A. L. Dellon, "A comparison of nerve regeneration across a sural nerve graft and a vascularized pseudosheath," *Journal of Hand Surgery*, vol. 13, no. 6, pp. 935–942, 1988.

[13] B. C. Cooley, "History of vein grafting," *Microsurgery*, vol. 18, no. 4, pp. 234–236, 1998.

[14] K. L. Colen, M. Choi, and D. T. Chiu, "Nerve grafts and conduits," *Plastic and Reconstructive Surgery*, vol. 124, no. 6 supplement, pp. 386–394, 2009.

[15] N. Lago and X. Navarro, "Correlation between target reinnervation and distribution of motor axons in the injured rat sciatic nerve," *Journal of Neurotrauma*, vol. 23, no. 2, pp. 227–240, 2006.

[16] W. Z. Ray and S. E. Mackinnon, "Management of nerve gaps: autografts, allografts, nerve transfers, and end-to-side neurorrhaphy," *Experimental Neurology*, vol. 223, no. 1, pp. 77–85, 2010.

[17] S. Yoshii and M. Oka, "Collagen filaments as a scaffold for nerve regeneration," *Journal of Biomedical Materials Research*, vol. 56, no. 3, pp. 400–405, 2001.

[18] D. F. Kalbermatten, P. J. Kingham, D. Mahay et al., "Fibrin matrix for suspension of regenerative cells in an artificial nerve conduit," *Journal of Plastic, Reconstructive and Aesthetic Surgery*, vol. 61, no. 6, pp. 669–675, 2008.

[19] Y. Zhang, H. Luo, Z. Zhang et al., "A nerve graft constructed with xenogeneic acellular nerve matrix and autologous adipose-derived mesenchymal stem cells," *Biomaterials*, vol. 31, no. 20, pp. 5312–5324, 2010.

[20] L. A. Pfister, M. Papaloïzos, H. P. Merkle, and B. Gander, "Nerve conduits and growth factor delivery in peripheral nerve repair," *Journal of the Peripheral Nervous System*, vol. 12, no. 2, pp. 65–82, 2007.

[21] M. Timmer, S. Robben, and F. Muller-Ostermeyer, "Axonal regeneration across long gaps in silicone chambers filled with Schwann cells overexpressing high molecular weight FGF-2," *Cell Transplantation*, vol. 12, no. 3, pp. 265–277, 2003.

[22] B. Hood, H. B. Levene, and A. D. Levi, "Transplantation of autologous Schwann cells for the repair of segmental peripheral nerve defects," *Neurosurgical Focus*, vol. 26, no. 2, article E4, 2009.

[23] E Verdu, X Narvarro, G Gudino-Cabrera et al., "Olfactory bulb ensheathing cells enhance peripheral nerve regeneration," *Neuroreport*, vol. 10, pp. 1097–1101, 1999.

[24] S. Walsh and R. Midha, "Use of stem cells to augment nerve injury repair," *Neurosurgery*, vol. 65, no. 4, pp. A80–A86, 2009.

[25] E. Moyse, S. Segura, O. Liard, S. Mahaut, and N. Mechawar, "Microenvironmental determinants of adult neural stem cell proliferation and lineage commitment in the healthy and injured central nervous system," *Current Stem Cell Research and Therapy*, vol. 3, no. 3, pp. 163–184, 2008.

[26] P. Vodicka, K. Smetana Jr., B. Dvorankova et al., "The miniature pig as an animal model in biomedical research," *Annals of the New York Academy of Sciences*, vol. 1049, pp. 161–171, 2005.

[27] O. Liard, S. Segura, A. Pascual, P. Gaudreau, T. Fusai, and E. Moyse, "In vitro isolation of neural precursor cells from the adult pig subventricular zone," *Journal of Neuroscience Methods*, vol. 182, no. 2, pp. 172–179, 2009.

[28] P. E. Mangeot, K. Duperrier, D. Nègre et al., "High levels of transduction of human dendritic cells with optimized SIV vectors," *Molecular Therapy*, vol. 5, no. 3, pp. 283–290, 2002.

[29] D. T. W. Chiu, I. Janecka, and T. J. Krizek, "Autogenous vein graft as a conduit for nerve regeneration," *Surgery*, vol. 91, no. 2, pp. 226–233, 1982.

[30] D. T. W. Chiu and B. Strauch, "A prospective clinical evaluation of autogenous vein grafts used as a nerve conduit for distal sensory nerve defects of 3 cm or less," *Plastic and Reconstructive Surgery*, vol. 86, no. 5, pp. 928–934, 1990.

[31] G. Risitano, G. Cavallaro, T. Merrino, S. Coppolin, and F. Ruggeri, "Clinical results and thoughts on sensory nerve repair by autologous vein graft in emergency hand reconstruction," *Chirurgie de la Main*, vol. 21, no. 3, pp. 194–197, 2002.

[32] Y. Kaufman, P. Cole, and L. Hollier, "Peripheral nerve injuries of the pediatric hand: issues in diagnosis and management," *Journal of Craniofacial Surgery*, vol. 20, no. 4, pp. 1011–1015, 2009.

[33] H. I. Acar, A. Comert, H. Ozer et al., "Femoral seating position of the EndoButton in single incision anterior cruciate ligament reconstruction: an anatomical study," *Surgical and Radiologic Anatomy*, vol. 30, no. 8, pp. 639–643, 2008.

[34] B. Manasseri, S. Raimondo, S. Geuna, G. Risitano, and F. S. D'Alcontres, "Ulnar nerve repair by end-to-side neurorrhaphy on the median nerve with interposition of a vein: an experimental study," *Microsurgery*, vol. 27, no. 1, pp. 27–31, 2007.

[35] Y. H. Lee and S. J. Shieh, "Secondary nerve reconstruction using vein conduit grafts for neglected digital nerve injuries," *Microsurgery*, vol. 28, no. 6, pp. 436–440, 2008.

[36] B. A. Reynolds and S. Weiss, "Generation of neurons and astrocytes from isolated cells of the adult mammalian central nervous system," *Science*, vol. 255, no. 5052, pp. 1707–1710, 1992.

[37] S. A. Louis, R. L. Rietze, L. Deleyrolle et al., "Enumeration of neural stem and progenitor cells in the neural colony-forming cell assay," *Stem Cells*, vol. 26, no. 4, pp. 988–996, 2008.

[38] L. Bennett, M. Yang, G. Enikolopov, and L. Iacovitti, "Circumventricular organs: a novel site of neural stem cells in the adult brain," *Molecular and Cellular Neuroscience*, vol. 41, no. 3, pp. 337–347, 2009.

[39] R. Belvindrah, F. Lazarini, and P. M. Lledo, "Postnatal neurogenesis: from neuroblast migration to neuronal integration," *Reviews in the Neurosciences*, vol. 20, no. 5-6, pp. 331–346, 2009.

[40] M. Tavazoie, L. Van der Veken, V. Silva-Vargas et al., "A specialized vascular niche for adult neural stem cells," *Cell Stem Cell*, vol. 3, no. 3, pp. 279–288, 2008.

[41] J. S. Goldberg and K. K. Hirschi, "Diverse roles of the vasculature within the neural stem cell niche," *Regenerative Medicine*, vol. 4, no. 6, pp. 879–897, 2009.

[42] A. Schänzer, F. P. Wachs, D. Wilhelm et al., "Direct stimulation of adult neural stem cells in vitro and neurogenesis in vivo by vascular endothelial growth factor," *Brain Pathology*, vol. 14, no. 3, pp. 237–248, 2004.

[43] L. S. Shihabuddin, P. J. Horner, J. Ray, and F. H. Gage, "Adult spinal cord stem cells generate neurons after transplantation in the adult dentate gyrus," *Journal of Neuroscience*, vol. 20, no. 23, pp. 8727–8735, 2000.

[44] J. H. Huang, D. K. Cullen, K. D. Browne et al., "Long-term survival and integration of transplanted engineered nervous tissue constructs promotes peripheral nerve regeneration," *Tissue Engineering A*, vol. 15, no. 7, pp. 1677–1685, 2009.

[45] J. F. Bonner, T. M. Connors, W. F. Silverman, D. P. Kowalski, M. A. Lemay, and I. Fischer, "Grafted neural progenitors integrate and restore synaptic connectivity across the injured spinal cord," *The Journal of Neuroscience*, vol. 31, no. 12, pp. 4675–4686, 2011.

[46] T. Murakami, Y. Fujimoto, Y. Yasunaga et al., "Transplanted neuronal progenitor cells in a peripheral nerve gap promote nerve repair," *Brain Research*, vol. 974, no. 1-2, pp. 17–24, 2003.

[47] T. B. Seo, M. J. Oh, B. G. You et al., "ERK1/2-mediated schwann cell proliferation in the regenerating sciatic nerve by treadmill training," *Journal of Neurotrauma*, vol. 26, no. 10, pp. 1733–1744, 2009.

[48] R. Mi, Y. Luo, J. Cai, T. L. Limke, M. S. Rao, and A. Höke, "Immortalized neural stem cells differ from nonimmortalized cortical neurospheres and cerebellar granule cell progenitors," *Experimental Neurology*, vol. 194, no. 2, pp. 301–319, 2005.

[49] T. S. Johnson, A. C. O'Neill, P. M. Motarjem, J. Nazzal, M. Randolph, and J. M. Winograd, "Tumor formation following murine neural precursor cell transplantation in a rat peripheral nerve injury model," *Journal of Reconstructive Microsurgery*, vol. 24, no. 8, pp. 545–550, 2008.

[50] C. Foroni, R. Galli, B. Cipelletti et al., "Resilience to transformation and inherent genetic and functional stability of adult neural stem cells ex vivo," *Cancer Research*, vol. 67, no. 8, pp. 3725–3733, 2007.

[51] H. Zhang, Y. T. Wei, K. S. Tsang et al., "Implantation of neural stem cells embedded in hyaluronic acid and collagen composite conduit promotes regeneration in a rabbit facial nerve injury model," *Journal of Translational Medicine*, vol. 6, article no. 67, 2008.

[52] C. Y. Tseng, G. Hu, R. T. Ambron, and D. T. W. Chiu, "Histologic analysis of Schwann cell migration and peripheral nerve regeneration in the autogenous venous nerve conduit (AVNC)," *Journal of Reconstructive Microsurgery*, vol. 19, no. 5, pp. 331–339, 2003.

[53] M. Xiao, K. M. Klueber, C. Lu et al., "Human adult olfactory neural progenitors rescue axotomized rodent rubrospinal neurons and promote functional recovery," *Experimental Neurology*, vol. 194, no. 1, pp. 12–30, 2005.

[54] S. R. Chirasani, A. Sternjak, P. Wend et al., "Bone morphogenetic protein-7 release from endogenous neural precursor cells suppresses the tumourigenicity of stem-like glioblastoma cells," *Brain*, vol. 133, no. 7, pp. 1961–1972, 2010.